Alma Mater Studiorum – Università di Bologna

DOTTORATO DI RICERCA IN
INGEGNERIA CIVILE, CHIMICA, AMBIENTALE E DEI MATERIALI

Ciclo XXXIV

Settore Concorsuale: 08/B3 - Tecnica delle Costruzioni
Settore Scientifico Disciplinare: ICAR09 – Tecnica delle Costruzioni

EVALUATION OF SEISMIC LOSSES OF RC BUILDINGS: THE CASE OF THE INDUSTRIAL AREAS AFTER THE 2012 EMILIA EARTHQUAKE

Presentata da: **Lucia Praticò**

Coordinatore Dottorato
Prof. Alessandro Tugnoli

Supervisore
Prof. Marco Savoia

Co-supervisori
Dott. Marco Bovo
Prof. Nicola Buratti

Esame finale anno 2022

Alla Donnola,
che è sempre con me.

ABSTRACT

The topic of seismic loss assessment of existing buildings not only incorporates many aspects of the earthquake engineering, but also entails social factors, public policies and business interests. Concerning the subject of the structural engineering, the evaluation of the seismic losses requires the integration of different broad fields including the characterization of the seismic hazard, the risk assessment and the seismic performance assessment of structural and non-structural systems. Because of its multidisciplinary character, the seismic loss assessment process may be complex to challenge, and sound discouraging to neophytes.

In this context, with the pace of progress in the field of loss assessment, there is an increasing need of deriving simplified methodologies to streamline the process and provide tools for decision-makers, but also practitioners. This dissertation investigates different possible applications both in the area of modelling and prediction of seismic losses, both in the analysis of observational seismic data.

Regarding the first topic, the PRESSAFE-disp method is proposed for the fast evaluation of the fragility curves of precast reinforced-concrete (RC) structures. The method allows a comprehensive explanation of the seismic in-plane behaviour of existing precast RC buildings and could be adopted effectively, for example, in seismic risk assessments and loss estimations of large industrial areas in Italy as well as in other seismic-prone territories of the Mediterranean area. Hence, a direct application of the method to the productive area of San Felice sul Panaro is studied to assess the seismic consequences in terms of number of collapsed buildings under a specific seismic scenario. In particular, with reference to the buildings subjected to the 2012 Emilia Romagna ground-motion, two large-scale stochastic models are outlined to predict the number of buildings collapsed in the area. The outcomes of the simplified framework applied at the large scale are promising, in good agreement with the observed damage scenario.

Furthermore, at the scale of a single RC building, a simplified displacement-based loss assessment methodology is outlined for the definition of quantitative performance metrics to be used in the decision-making phase of a seismic retrofit. The method is deemed suitable to evaluate the seismic performance of different feasible seismic retrofit options, for a comparative analysis of the effectiveness and the convenience of each solution.

Finally, a contribution to the analysis of the observational seismic losses of damaged buildings is presented in the last part of the dissertation. A specific database of loss data of precast RC buildings damaged by the 2012 Earthquake is created and investigated. A statistical analysis of the losses is performed, allowing deriving several consequence functions depending on the damage state and the structural typology. The outcomes presented may be implemented in probabilistic seismic risk assessment methodologies to forecast the losses of possible seismic events on precast buildings at a large scale. Furthermore, they may be adopted to guide the decision-making in establishing priorities and retrofit policies to prevent and reduce the consequences of future earthquakes in industrial areas.

Keywords: data analysis; fragility curve; large-scale assessment; loss assessment; precast building.

TABLE OF CONTENTS

1. INTRODUCTION

1.1. MOTIVATION

The evaluation of seismic losses is a wide field of research involving multi-criteria methodologies. The probabilistic process is inherently complex due to the large number of alternatives and the different criteria to be evaluated in order to provide a reliable estimation of the seismic consequences (see Silva et al. 2021 for an incisive description of this theme).

The need for a simplification of the procedure has been widely acknowledge by researchers (Cosenza et al. 2018, Pampanin 2017), paving the way for streamlined analytical applications of the seismic loss predictions. Indeed, the more robust methodologies for the seismic loss assessment, derived in the context of PEER-PBEE (Porter 2003, FEMA 2018), implement computationally expensive analyses to assess different loss metrics. The more sophisticated methods may not be suitable for handling rapid results for decision-makers, nor user friendly for the majority of nowadays engineers. The simplified models, instead, aim at adopting analytical or numerical approaches to evaluate the losses and identify the most vulnerable buildings due to either a possible earthquake scenario, or expected within a certain time-frame. To this aim, different levels of refinement may be achieved, to obtain diversified outcomes. Indeed, not only the direct losses can be determined, such as the number of damaged buildings, the repair costs of structural and non-structural components, or the reconstruction costs, but also the indirect ones, i.e., the business disruption, the supply chain interruption, and the number of fatalities, injuries and homeless.

To date, numerous methods are available for the evaluation of the seismic vulnerability and the losses of ordinary RC and masonry buildings. However, a minor attention has been oriented to precast RC buildings. As enhanced by Belleri et al. (2021), there is the need to develop risk assessment methodologies and collect data on this fragile structural category, to bridge the gap with the other typologies. Indeed, after the lesson learnt from the 2012 Earthquake in Emilia, reliable seismic design criteria have been established for the design of new precast structures, however, a large percentage of the existing precast buildings (in particular in the Italy) actually has not been object of interventions and remains in an unsafe condition with regard to the seismic actions.

In this context, the methods for a rapid seismic assessment can be very helpful both to estimate the current safety level of large precast building stocks, and to plan the necessary strengthening interventions possibly at the large scale of an industrial area. To this regard, this dissertation proposes a simplified methodology to evaluate the fragility curves of precast RC buildings, and offers a procedure to forecast possible damage scenarios in seismic prone industrial areas. Furthermore, a simplified displacement-based loss assessment methodology is outlined to explore the influence of different loss terms to guide the process of the decision-making.

The analysis of the damage and loss data offers the possibility to derive useful tools for seismic risk assessments and earthquake loss estimations in seismic prone territories. Concerning this aspect, an observational database specific for precast RC buildings damaged by the 2012 Earthquake is proposed in this thesis. The empirical losses are studied in a multifaceted framework of analysis, to highlight different aspects of the losses of industrial buildings and derive useful consequence functions to be adopted in prediction models.

1.2. OUTLINE OF THE DISSERTATION

This dissertation is divided into five chapters, including this introduction, **Chapter 1**.

Chapter 2 briefly summarizes the main principles of the loss assessment to provide a comprehensive panorama, from the framework of the PEER-PBEE approach to an insight on the recent Italian experiences.

Chapter 3 presents new diversified contributions to the modelling of seismic losses and consequences. Firstly, the attention is focused on the precast RC buildings to highlight the main causes of the seismic vulnerability of this structural category. Thus, the PRESSAFE-disp method is outlined for the fast evaluation of the fragility curves of precast RC structures. The principles and the steps of the procedure are explained, together with the main outcomes. Furthermore, the method is applied at the large scale on the productive area of San Felice sul Panaro to assess the seismic losses in terms of number of collapsed buildings under a specific seismic scenario. Considering a cluster of buildings damaged by the 2012 ground-motion in Emilia, two large-scale stochastic models are outlined to predict the number of collapses. Comparative considerations on the results of the two methods are discussed for different seismic intensities, including the directionality effect of the ground-motion, and the outcomes are compared with the actual data collected through in-situ surveys. In addition, a simplified displacement-based loss assessment methodology is described for applications at the scale of a single RC building, to define quantitative performance and loss metrics useful in decision-making. A real case study building with different seismic retrofit options is considered to test the application of the framework and perform a critical evaluation on the possibilities of the procedure.

Chapter 4 introduces new contributions in the collection of observational loss data. A database of empirical losses of damaged precast RC buildings after the 2012 Earthquake is created and analysed. The criteria for the creation of the database are illustrated in the first section. The following sections are devoted to the investigation of diversified aspects of the losses and the repair costs of the buildings, both for structural and non-structural components. Several consequence functions are derived at different damage levels and for the main structural typologies of industrial precast buildings in the territory. An insight on the main structural properties of the buildings is offered in the last section.

Chapter 5 summarizes the main findings of the previous sections and provides recommendations for the future development of the research.

Appendix A illustrates the main outcomes of an additional work aimed at the evaluation of the effectiveness of a seismic intervention with dissipative devices applied on a precast RC building, focused on the estimation of the seismic vulnerability.

2. BACKGROUND ON THE EVALUATION OF THE SEISMIC LOSSES

Natural disasters cause a wide range of possible physical and socio-economic impacts, with short to long-lasting effects. In particular, earthquakes represent one of the major threats for many countries in the world, especially for Italy as demonstrated by recent events (Dolce and Di Bucci, 2016). Whether a strong seismic event hit a densely populated area, the damage to the building stock, the infrastructure systems and the facilities generates cascading negative consequences such as the business disruption, the supply interruption, the stagnant economy, but also homeless, fatalities, injuries and the community disruption. All these terms constitute the broader concept of ‘losses’, which include a variety of different effects of the natural risk.

Seismic loss estimates can be performed by analysing the direct and indirect effects associated with the earthquake-induced structural damage, both at the local scale of a single building and at the territorial scale. Regarding the latter, the role of the indirect losses altering the business is reflected in the indicators of the economic health of a territory. Indeed, recent experiences have shown that the Gross Domestic Product (GDP) of a country can suffer a significant drop after a seismic event (Daniell et al. 2011). Moreover, the governments spend huge amount of funds in the post-earthquake phase to organize the whole reconstruction process of the built environment. In Italy, from the Belice earthquake in 1968 to the Central Italy earthquake in 2016 more than two hundred billion euros were spent by the State for direct and indirect losses such as assistance, recovery and reconstruction (Dolce et al. 2021).

Given the high criticality of this issue, the scientific community is deeply engaged in the research field of risk assessment, aimed at combining hazard, vulnerability and exposure models. The evaluation of seismic losses can be pursued following two main domains of the research: the first one is the modelling, and the second one is the empirical data collection. In the modelling/prediction area, the aim is to provide suitable approaches and methods to forecast the seismic losses in a probable scenario, or expected within a given time-frame, at different level of detail. The main question is whether it is possible to estimate the losses before natural distasters occur, in order to orient decision makers in defining suitable mitigation plans. In the field of the empirical data collection, the focus is on the analysis of diversified loss data collected after seismic events, in order to create repositories of sources to be used to calibrate the theoretical models. In particular, the analysis of the loss data allows deriving consequence functions to link the seismic damage to a different amount of losses.

The basis of the on-going research on seismic risk and loss assessment can be followed up in the context of the PBEE, Performance-Based-Earthquake-Engineering, which is a complete probabilistic framework aimed at the design of structures with predictable levels of performance. An overview of the main principles is offered in Section 2.1. Moreover, an insight on the Italian experience in the advancements of the scientific research upon seismic losses is reported in Section 2.2.

2.1. THE PEER'S - PBEE APPROACH

Performance-based earthquake engineering, PBEE, can be considered as a set of principles developed to achieve the desired structural performance objectives, under different levels of seismic intensity. This approach has been pursued since the development of the project Vision2000 (SEAOC 1995), following the Northridge earthquake of 1994, and with the following document of the Federal Emergency Management Agency, FEMA 273 (1997). These pioneering documents marked a shift from the concept of design based on prescriptive requirements, to the concept of design addressing a targeted performance, depending on the type of construction and the earthquake intensity. Each discrete performance level considered is linked to an exceedance probability in a specific life-period of the building. Other advancements in the definition of the method were brought by the FEMA 356 (2000) document, focusing on the seismic rehabilitation of existing buildings.
One of the most important upgrades achieved in this framework has been developed by the Pacific Earthquake Engineering Research Center, PEER (Porter 2003), proposing a comprehensive methodology to consider different loss measures in the evaluation of the performance of a building. The principal outputs of this approach are the repair costs, the economic losses, the downtime and the fatalities, evaluated in a probabilistic estimate (the so-called 3Ds "dollars, deaths, and downtimes"). In this light, by providing guidelines to define quantitatively the performance of a building, the engineers and the stakeholders are enabled to make informed decisions about seismic risk.
The PEER's PBEE approach features four main stages of analysis illustrated in the scheme in Figure 1 (Porter 2003, Mohele 2003): the ground-motion hazard analysis (IM, Intensity Measure), the structural response (EDP, Engineering Demand Parameter), the damage analysis (DM, Damage Measure), and the loss analysis (DV, Decision Variable); each of these results in a probabilistic distribution of the outputs, and allow considering uncertainties.

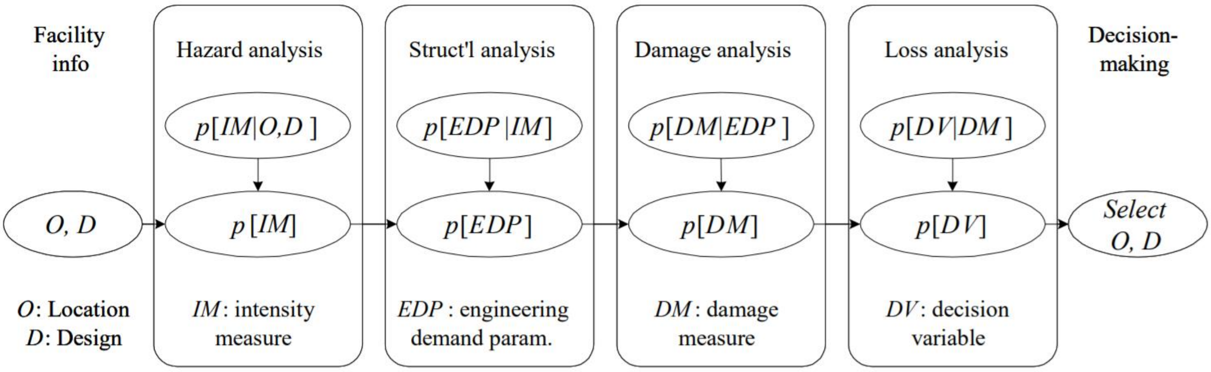

Figure 1. Main stages of the PBEE Procedure (from Mohele 2003).

The FEMA P-58 (FEMA 2018) is the actual reference document for the application of the procedure, defining both the theoretical basis and the applicative tools. The method can be applied to develop three different types of seismic performance assessments: intensity-based, scenario-based, and time-based. According to the guidelines, the first one allows evaluating the probable performance of a building under a specified ground-shaking intensity. The second one allows evaluating the probable performance of a building under an earthquake scenario, defined based on a specific magnitude occurring at a specific distance from the building site (indeed this is useful for buildings located close to one or more known active faults). The third assessment allows evaluating the probable performance of a building over a specified period of time (i.e., the building's life) considering all the events that could occur and the corresponding probability of occurrence. The first two methods of assessment are conditioned, meaning that they are associated with a specific earthquake, while the third one is unconditioned meaning that all the possible earthquakes are considered.

The aim of PEER is to describe the seismic performance with continuous variables, in particular defining the mean annual probability of exceedance of different loss terms in the time-based assessment. The mathematical expression of the procedure is represented by the following triple integral based on the Total Probability Theorem (Miranda and Aslani 2003):

$$\lambda(DV) = \iiint \mathrm{p}(DV/DM)\ \mathrm{p}(DM/EDP)\ \mathrm{p}(EDP/IM)\ \lambda(IM)\ \mathrm{d}IM\ \mathrm{d}EDP\ \mathrm{d}DM \tag{2.1}$$

Where: $\lambda(DV)$ is the mean annual frequency of exceedance for the DV, $\mathrm{p}(DV/DM)$ is the probability that the decision variables exceed specific values given that the DM are equal to particular thresholds; $\mathrm{p}(DM/IM)$ is the probability that the DM exceed these values given that the IM are equal to particular values; $\mathrm{p}(EDP/IM)$ is the probability that the EDP exceed specific thresholds given that the IM are equal to particular values; $\lambda(IM)$ is the mean annual frequency of the IM. In the Equation, IM, EDP, DM and DV are continuous random variables expressing a chain of conditional probabilities. Since the PEER-PBEE is an open framework, each stage of the process could be adapted to any level of refinement, from empirical or judgmental-based simplified models, to the latest and more comprehensive approaches available in the literature.

One of the most robust tools provided in FEMA P-58 (2018) is the Performance Assessment Calculation Tool (PACT), which is a software allowing the probabilistic estimation of losses through a Monte Carlo approach. The software allows performing seismic-induced loss computations, applying the PEER framework, for the most common structural systems and building occupancy types using component-based fragility data collected from multiple sources. All the three aforementioned typologies of loss assessments can be conducted with PACT.

In this complex field, there is a huge variability of possible loss assessment modelling procedures that can be developed, with different scopes. Considering a single building, the evaluation of losses can be pursued for the design of a new building or for the assessment of an existing one, focusing on the evaluation of the vulnerability of a specific structural (or non-structural) component, or for the identification of the most convenient possible seismic retrofit. At the territorial scale, the loss estimation may be conducted considering a seismic event shaking different areas, with the aim of identifying a prioritisation of intervention for the retrofit of the most vulnerable area (or the most vulnerable building typology), or for forecasting the effects of different seismic scenarios to allocate funds in a process of prevention policies decision. Clearly, a suitable approach defines the appropriate taxonomy of structural parameters, the damage metric, and the loss terms, depending on the scale of the problem and the data available. Accordingly, the methodology adopted for the loss assessment must be coherent with the degree of insight required.

2.2. THE ITALIAN EXPERIENCE AFTER RECENT EARTHQUAKES: REPOSITORIES AND METHODOLOGIES

The seismic activity of Italy is accredited by the long history of medium-strong earthquakes leaving traces from southern to northern regions. The seismic losses, both economic and social, registered in the past years have been considerably high and often unexpected. Since the devastating earthquake of Belice in 1968, after Friuli 1976, Irpinia 1980, and Umbria-Marche 1997, Italy has experienced losses of about 100 billion Euros (Di Ludovico et al. 2021). Eventually, considering Molise 2002, L’Aquila 2009, Emilia Romagna 2012 and Central Italy 2016, the amount almost doubled. Indeed, according to the National Risk Assessment, released by the Italian Civil Protection Department in 2018 (DPC 2018), in the last 50 years the earthquakes in Italy caused about 5000 fatalities and over 200 billion Euros of economic losses (Masi et al. 2021). These alarming numbers are likely to increase in the next decades if adequate measures of seismic retrofit are not planned, since one of the main issues in Italy is the high vulnerability of the existing building stock (Masi et al. 2021, Di Ludovico et al. 2021).

At the National scale, to estimate the seismic risk in Italy, the DPC supported by ReLUIS and Eucentre worked on the development of the so-called IRMA platform (Borzi et al. 2020). The aim of this project is to improve the vulnerability and the exposure models available in Italy, and adopt them, together with the hazard model, to foreseen possible conditioned and unconditioned losses in terms of expected repair or reconstruction costs (direct economic losses), number of unusable dwellings, homeless, dead and injured (Dolce et al. 2020). The seismic hazard in Italy is officially provided by the INGV Institute, with the latest probabilistic models defined in the works of Stucchi et al. (2011), which is implemented in IRMA and adopted also by the National codes (D.M. 2018). The most complete vulnerability model in Italy, even if it is not updated and it is affected by many uncertainties, is the ISTAT census database. A recently developed tool is the CARTIS database (Zuccaro et al. 2015), which is aimed at the typological and structural characterization of urban settlements in a more risk-oriented approach, even if it is not yet applied exhaustively at the National level. Nevertheless, some recent works dealing with the CARTIS data have been developed for the analysis of the vulnerability of different structural typologies at the territorial scale (for instance, see the ones of Polese et al. (2020), Basaglia et al. (2021), Tocchi et al. (2021) or Formisano et al. (2021)).

At the National level, it is worth mentioning a useful repository of seismic data created in past years: the web-based platform D.a.D.O. (Dolce et al. 2019) of the observed damage data collected after the main earthquakes in Italy, from 1976 to 2012. The database is a scientific heritage of data gathered with different seismic forms, from Friuli 1976 to AeDES 06/2008. The latter, is the recent version of the damage and usability evaluation form developed after the Umbria-Marche Earthquake in 1997. Nowadays, the AeDES survey form has become the official operational tool adopted by the DPC during the emergencies (Di Ludovico et al. 2021). A significant contribution to the analyses of the observational seismic data has been presented in the 'Libro Bianco' book following L'Aquila Earthquake (Di Ludovico et al. 2017a and 2017b). This offers comprehensive investigation of the repair and reconstructions costs under different damage levels (following the AeDES form) and for different structural typologies. Other inherent works are the ones of De Martino et al. (2016) estimating the repair costs from data collected by visual inspections after L'Aquila earthquake, and Mannella et al. (2017) analysing the process of the population assistance after the same earthquake. In addition, it is worth mentioning the works of Polese et al. (2018) discussing the factors influencing the demolition decisions in the analysis of the L'Aquila damage data, Di Ludovico et al. (2020) treating the complex issue of the reconstruction of historical centres after the same earthquake, and Del Gaudio et al. (2020) deriving observational fragility curves for RC buildings from D.a.D.O.

Another valuable Italian repository of seismic data is the so-called SFINGE-SISMA platform (Agenzia Regionale per la Ricostruzione 2018), collecting damage and loss data of buildings after the 2012 Earthquake in Emilia Romagna. Specifically, SFINGE has been devoted to the collection of seismic data regarding the business activities, resulting in an almost unique loss database of industrial long-span buildings. The first pioneering analyses of this data have been promoted by the works of Buratti et al. (2017) and Ongaretto et al. (2019), both focusing on the development of empirical fragility curves. Moreover, Rossi et al. (2019a, 2019b and 2020) proposed a first attempt of analysis of the economic loss data on long-span buildings, deriving consequence functions based on different damage levels. However, the disaggregation of the economic losses into different structural typologies has not been considered, thus there is not yet a comprehensive analysis such as the one available in 'Libro Bianco' for ordinary buildings.

Concerning the development of National risk maps in Italy, researchers in the literature have been working on this topic to a wide extent, to investigate the issue related with this multidisciplinary task. For instance, interesting results in the past have been developed by Lucantoni et al. (2001), deriving a map based on the Macroseismic (MCS) intensity scale, lately updated with the 2001 Census data available in Bramerini and Di Pasquale (2008). More recently, the researchers focused on the development of seismic risk mapping with the use of more refined quantitative intensity based estimates, using peak-ground acceleration (PGA) or spectral acceleration (PSA). Crowley et al. (2009) computed seismic risk maps adopting two analytical methods for the derivation of fragility curves based on PGA and PSA; Rota et al. (2011) investigated the seismic risk for different Italian building typologies, deriving typological maps in terms of average annual probability of loss. Moreover, Asprone et al. (2013) computed seismic risk maps with the aim of managing a seismic insurance model for Italy; Silva et al. (2012) presented the OpenQuake engine, a tool specifically developed for the creation of seismic risk maps for a given scenario or with the PSHA-based (Probabilistic Seismic Hazard Assessment) approach, allowing the computation of the loss-exceedance curve considering hazard, exposure and vulnerability. It is worth mentioning that the IRMA platform is implemented on the OpenQuake engine. More recently, Zanini et al. (2018)

proposed a framework for the development of risk maps aimed at the definition of a seismic risk reduction program for the Italian residential building stock.

In this rather complex field, various researchers recognized the need of outlying simplified solutions and methodologies for estimating the vulnerability of buildings and the seismic losses. Indeed, the more sophisticated and robust methods may not be convenient for handling rapid results for decision-makers, nor user friendly for the majority of engineers. A significant contribution in this process of simplification at the National scale in Italy is the development of the SismaBonus approach (Cosenza et al. 2018), to streamline the communication of the seismic risk of constructions to practitioners. This represent a first important attempt for the implementation of the loss assessment in the everyday work of engineers in Italy. Even if it is a simplified and empirical approach, the method can be applied to different typologies of buildings, and gives an estimate of the expected annual losses (EAL, or PAM in Italian) in an unconditioned approach, including both safety and economic loss considerations. Furthermore, it is worth mentioning the effort of different researchers in Italy to develop simplified methodologies for the assessment of the seismic vulnerability of buildings.

Just to mention some relevant contributions: the SP-BELA (Simplified-Pushover-Based-Earthquake-Loss-Assessment) method developed by Borzi et al. (2008a and 2008b) for the vulnerability assessment of Italian buildings, recently applied in the work of Borzi et al. (2021); the method RE.SIS.TO ("Resistenza Sismica Totale") for the rapid evaluation of the seismic vulnerability of both masonry and RC buildings (Mazzotti et al. 2013). Moreover, a simplified analytical method for the fragility assessment of RC buildings at the large scale has been proposed by Del Gaudio et al. (2015), which is the damage prediction model POST (PushOver on Shear Type models) applied in Del Gaudio et al. (2016) and Masi et al (2019). Lagormarsino and Cattari (2014) developed the model DBV-masonry (Displacement Based Vulnerability) for the derivation of fragility curves of masonry buildings, thus Ottonelli et al. (2020) implemented a comprehensive displacement-based loss estimation model. Pampanin (2017) proposed the SLaMA (Simplified Lateral Mechanism Analysis) methodology for the seismic assessment of buildings, lately refined by Gentile et al. (2018), and incorporated also in the New Zealand guidelines on seismic assessment of existing buildings. A review of different simplified analytical methods for the assessment of the vulnerability unreinforced masonry buildings can be found in Shabani et al. (2021).

Concerning the evaluation of seismic losses, in the Italian literature there are several important contributions to the analysis of the building performance under the seismic action. For instance, some valuable applications of the loss assessment at the scale of a single building can be found in the works of Ligabue et al. (2018) evaluating the relationship between the seismic performance of a building and the annualized probability of collapse, or in Bovo et al. (2020) exploring the time-based losses deriving from a new capacity design approach. Moreover, other inherent works are the ones of Perrone et al. (2020), assessing the seismic risk in school buildings computing the losses with both PACT and Italian SismaBonus, or D'Aragona et al. (2021), who developed a Stick-IT model for the prediction of the seismic economic losses of existing RC frame buildings.

Furthermore, the estimation of different seismic loss metrics has been frequently adopted to evaluate the convenience of different retrofit alternatives in a performance-based approach. Indeed, various methods, both simplified and rigorous, have been used to compare the effectiveness of different retrofit measures as well as different project solutions. For instance, Miano et al. (2019) proposed a nonlinear performance-based method to evaluate several seismic retrofit techniques for non-ductile frame buildings, and select the optimal strategy. Bosio et al. (2020) studied a displacement-based loss assessment to be applied to precast RC buildings and account for different interventions; Rossi et al. (2021) defined a new approach for the comparative evaluation of the economic convenience of different infill systems in RC buildings. Landi et al. (2020) implemented a simplified displacement-based method for the evaluation of losses in existing RC buildings, adopting it to evaluate the impact of the retrofit options; Del Vecchio et al. (2021) enhanced the convenience of the adoption of the FRP-based retrofit techniques for mitigation of risk at the large-scale, by analysing the data of the L'Aquila reconstruction process.

In addition, it is worth mentioning the effort of different researchers in the study of the economic losses not only at the scale of the entire building, but also at the scale of single components. In this light, losses and consequence functions have been derived considering the damage occurred to single structural or non-structural elements. For instance, Cardone and Perrone (2015) developed loss functions for masonry infill walls adopted in RC and steel frame buildings; Chiozzi and Miranda (2017) derived drift-based fragility functions for infill walls with in-plane loading. Moreover, Del Vecchio et al. (2018) analysed the predicted and actual losses of five buildings damaged by L'Aquila Earthquake, highlighting the need of deriving suitable consequence functions for components typical of the Mediterranean area. Eventually, Del Vecchio et al. (2020) derived the consequence functions for residential buildings and many different components at various damage levels, through the analysis of the data collected after L'Aquila Earthquake. Finally, De Risi et al. (2020) proposed a component-based method for the computation of the seismic losses of RC buildings considering infills and services, validated on a large data-set of Italian structures damaged by L'Aquila Earthquake, and Romano et al. (2021) evaluated the effect of the presence of different the masonry infills in RC buildings in the assessment of the expected annual losses.

3. CONTRIBUTIONS TO LOSS MODELLING: THE ASSESSMENT OF DIFFERENT EARTHQUAKE-INDUCED LOSSES

The seismic risk assessment of buildings is a diversified field of study, in which researchers developed a variety of methods to estimate and analyse fragility, vulnerability as well as potential losses caused by earthquakes. The main aim is to define appropriate modelling procedures to assess the expected performance of structures and the seismic-induced losses. Different approaches, both analytical and numerical, are available nowadays to define the performances of existing buildings under earthquakes (see the state of the art in Calvi et al. 2006, and Silva et al. 2019).

Nevertheless, until the 2012 Earthquake in Italy the research effort on the seismic fragility of precast RC structures was limited in comparison to the large amount of studies on cast-in-place or masonry buildings, as mentioned by Casotto et al. (2015). A recent impulse in the research field concerning precast structures arose after the seismic sequence that, in May 2012, hit several productive areas of the Emilia Romagna region in northern Italy, causing severe damage to structures, material stocks, industrial machineries and some human losses. After the lesson learnt from the earthquake, reliable seismic design criteria have been established for the design of new precast structures and for the strengthening of the existing ones. Despite this, a large percentage of the existing precast buildings in the Italian territories actually has not been object of interventions and remains in an unsafe condition with regard to the seismic actions. Section 3.1 offers an overview of the main structural deficiencies of this category of buildings, and the latest advancements in the research.

In this context, the methods allowing a rapid seismic assessment can be very helpful both to estimate the current safety degree of large building stocks, both to plan the necessary strengthening interventions at the large scale of an industrial area. In Section 3.2, a new methodology for the evaluation of fragility curves of precast RC buildings at large scale is presented, following the principles introduced in Bovo and Savoia (2021) and Bovo et al. (2022). The method allows a comprehensive evaluation of the seismic in-plane behaviour of existing precast RC buildings and could be adopted, for example, in earthquake loss estimations and seismic risk assessments of large Italian industrial areas, as well as of wide seismic-prone territories of the Mediterranean area. Moreover, an application of the method to a real production area for the estimation of the number of collapses likely to occur in a cluster of buildings under a specific scenario is illustrated in Section 3.3. This is a first application of the PRESSAFE-disp method to the industrial area of San Felice sul Panaro in Emilia. A large scale tool of assessment, based on simplified assumptions, has been outlined. The rapid methodology allowing the quantification of the number of damaged buildings in an industrial cluster may be used to drive the establishment of seismic risk mitigation policies, as well as prioritization measures for the retrofit of existing precast buildings in the seismic prone areas.

Concerning the scale of a single building, another contribution to the modelling of losses is presented in Section 3.4 referring to an existing RC building. Following the approach initially proposed in Ligabue (2015), a comprehensive extended methodology is presented to explore the influence of different loss metrics in a time-based assessment. In particular, the procedure allows comparing conceptually the effectiveness of different interventions based on few loss terms, which may be adopted to give indications in the decision-making process in the design phase of the seismic retrofit of an existing building.

3.1. THE SEISMIC VULNERABILITY OF THE PRECAST RC BUILDINGS

3.1.1. MAIN DAMAGE AND COLLAPSE MECHANISMS OBSERVED IN THE PRECAST RC BUILDINGS AFTER THE 2012 EMILIA EARTHQUAKE

The seismic events which shook the northern Italy in May 2012, as well as several past seismic events in the Mediterranean area, have caused significant damage to buildings realized with precast technologies. The earthquake represented a serious test bench for the existing precast reinforced concrete buildings since they were usually designed with non-redundant schemes to allow easy and fast assembling operations. In addition, even though the seismic activity of the Italian territory was well known since many years (INGV), wide areas of Italy, Emilia Romagna Region included, were considered non-seismic zones by national building codes until the re-classification proposed in 2003 (OPCM 2003). As a consequence, before 2003 the buildings were designed by means of static analyses by taking into account only vertical loads and the wind action (Savoia et al. 2017). Thus, several precast buildings, built in the Italy before 2003, feature simply-supported elements (beams and roof slab elements) with shear forces transmitted at the support level through friction resistance only. Indeed, steel connection devices, mandatory in seismic zones and fundamental to ensure the global safety of precast structures (Brunesi et al. 2015), usually were not adopted.

The 2012 Emilia earthquakes hit an area with many medium-to-large industrial and agrifood districts, causing extended damage to buildings (Liberatore et al. 2013, Bournas et al. 2014, Savoia et al. 2017). The two mainshocks, identified in many studies as the “Emilia Earthquake”, were registered on the 20th and 29th May: the second one, with a moment magnitude 5.9, had an epicentre 12 km east of the first one, characterized by a magnitude of 6.1 (Rovida et al. 2020, Rovida et al. 2021). Both were followed by a series of minor earthquakes, i.e., more than one thousand seismic shocks with magnitude higher than 2.0, many of these with a magnitude higher than 4.0 (Dolce et al. 2012).

A peculiar aspect of the seismic events is that they hit several production factories (agrifood, mechanics, biomedical, construction, as well as many smaller industries) located in precast concrete buildings not designed against seismic actions. According to the Region (Agenzia Regionale per la Ricostruzione 2018), almost 3000 productive buildings suffered structural damage and the 45 % of them either suffered severe damage or collapsed. To this regard, also past earthquakes in other countries caused widespread structural collapses or serious damage to this building typology (Tzenov et al. 1978, Tapan et al. 2013), highlighting the international character of this criticality.

As a result, the seismic vulnerability of the Italian precast RC buildings has been largely acknowledged by engineers and researchers after the 2012 seismic events. The surveys conducted in the aftermath of 2012 Emilia earthquake enabled researchers to collect a series of observations on the weaknesses and structural deficiencies of precast RC buildings (Liberatore et al. 2013, Belleri et al. 2014, Bournas et al. 2014, Magliulo et al. 2014, Minghini et al. 2016, Savoia et al. 2017, Batalha et al. 2019). All the studies agree in concluding that the precast RC buildings, built without seismic details and prescriptions, represent one of the most seismically vulnerable building typology (Savoia et al. 2012). Due to the regular layout and the simple static scheme usually adopted for these highly standardised buildings (i.e., simply-supported horizontal elements above cantilever RC columns, with infilled masonry walls or precast cladding panels along the perimeter (Savoia et al. 2012, Bellotti et al. 2014)), the damage mechanisms observed in Emilia can be collected within a few common types:

- the failure at the base of the columns due to the insufficient longitudinal and transverse reinforcement bars, resulting in inadequate flexural capacity (Figure 2a);
- the sliding of roof elements and, in several cases, even their fall, caused by the absence or inadequacy of steel connection devices between columns and beams or between beams and roof slab elements. Where the steel elements were absent, the sliding mechanism was even eased by the presence of neoprene pads between the precast RC elements (Figure 2b and 2c);
- the collapse of the non-structural walls along the perimeter of the buildings i.e., the detachment and the fall of the horizontal (Figure 2d) and vertical cladding panels (Figure 2e) and in-plane failure of masonry infills (Figure 2f).

It is evident that, when precast RC buildings are subjected to a horizontal ground-motion, the damage may affect both the structural and the non-structural elements, and all these aspects should be taken into account in a comprehensive structural model. Moreover, the non-linear contribution of the second order effects should be considered since it may increase the displacements and the corresponding damage in tall and flexible structures, like those considered here.

(a)

(b)

(c)

(d)

(e)

(f)

Figure 2. Details of the main damage typologies in precast RC buildings after the Emilia earthquake of 2012: (a) damage at the base of the columns; (b) sliding and (c) fall of the precast beams and the roof slab elements causing the collapse of the roof; collapse of the (d) horizontal and the (e) vertical cladding panels; (f) failure of the masonry infill walls.

3.1.2. STATE OF THE ART OF THE RESEARCH ON THE SEISMIC VULNERABILITY OF PRECAST RC BUILDINGS

The lesson learnt after the 2012 Emilia sequence represented an occasion for engineers and researchers both for collecting data concerning the structural damage on precast structures, both for developing reliable models to investigate the seismic behaviour of such buildings. Concerning the latter aspect, the possibility of disposing of a large amount of data on the structural deficiencies of precast buildings boosted the investigations of many international researchers (see Liberatore et al. 2013, Belleri et al. 2014, Bournas et al. 2014, Bovo and Savoia 2018, Ercolino et al. 2018b, Bovo and Savoia 2019). With specific reference to the seismic fragility functions, different authors focused on particular classes of precast buildings (e.g. considering specific types of connections or claddings, or considering only one type of collapse mechanism but neglecting the others). Consequently, the outcomes of the various studies (Casotto et al. 2015, Buratti et al. 2017) are not simple to compare, thus the results cannot be generalized to a widespread stock of buildings. Furthermore, in other cases, the seismic fragility functions have been obtained for stocks that collect structures with very different dynamic features. In this way, the fragilities represent an average evaluation of the seismic performances of a certain group of buildings but are not properly valid in general.

Concerning the seismic fragility of precast RC buildings, several recent studies proposed models using either observational damage data (Buratti et al. 2017, Ongaretto et al. 2019, Rossi et al. 2020) or the results of numerical simulations (Casotto et al. 2015, Babic et al. 2016). Fragility models are used in several probabilistic analyses, such as loss, damage and risk assessment (Ramirez and Miranda 2009, FEMA 2018), which can be performed with different levels of detail, spanning from small-scale analyses on single buildings, to large-scale assessments at regional or national level. The latter are particularly relevant in Civil Protection applications such as the development of National plans for the reduction of the seismic risk, the prediction of damage scenarios after possible future earthquakes, and the estimation of damage and casualties in the aftermath of an earthquake. To this regard, in the literature there are various examples of seismic assessments, at the territorial scale, of cast-in-situ RC and masonry buildings in urban areas (see for example Maio et al. 2015, Lestuzzi et al. 2016, Formisano et al. 2017, Villar-Vega et al. 2017, Anglade et al. 2020, Polese et al. 2020, da Porto et al. 2021). However, as enhanced by Belleri et al. (2021), there are few studies on precast RC buildings in productive areas (Petruzzelli 2016, Demartino et al. 2017, Ercolino et al. 2018a, Hofer et al. 2018, Rodriguez et al. 2018, Bosio et al. 2020, Bressanelli et al. 2021, Andreolli et al. 2022).

With the aim of providing a more uniform approach, Bovo and Savoia (2021) proposed a method for the fast seismic assessment of different classes of one-story precast RC buildings, selected on the basis of international reports and databases (Regione Emilia Romagna 2020).

3.2. THE PRESSAFE-DISP METHOD

The PRESSAFE (PRecast Existing Structure Seismic Assessment by Fast Evaluation) methodology aims at defining, through a simplified framework, the seismic fragility curves of different existing precast RC structures. The method, starting from the seismic deficiencies and weaknesses observed in the precast structures during past earthquakes, provides the fragility curves of different common building typologies of the Mediterranean area. By following the approach proposed in Bovo and Savoia (2021), an alternative method called PRESSAFE-disp (PRecast Existing Structure Seismic Assessment by Fast Evaluation-displacements) is outlined.

Starting from the information collected in the numerous building inspections conducted in the aftermath of the 2012 Emilia Earthquake, PRESSAFE-disp accounts for different damage mechanisms, taking into account the relative displacements and sliding between the precast elements. The damage criteria have been properly selected and modelled in order to reproduce the mechanisms observed during the building surveys. The main difference between the two methods, PRESSAFE and PRESSAFE-disp, relies in the definition of the collapse condition: in the first one, the attainment of the plastic strength capacity in one of the sliding hinges (adopting a force-based collapse criterion) is considered; while in the latter, the attainment of the displacement capacity in one of the sliding hinges (adopting a displacement-based collapse criterion) is considered. In both methods, under the hypothesis of flexible roof (i.e., no diaphragm effect), a frequent condition observed in many precast buildings in Emilia, the main frames of a building are studied separately. The horizontal force acting on a frame is considered to be proportional to its tributary vertical mass, thus the seismic in-plane behaviour is evaluated with dynamic analyses.

In this study, different precast frame typologies have been selected and investigated with incremental dynamic analyses (IDA) considering, for each building category, 8 vibrating periods ranging from 0.25 s to 3.0 s. The frames have been analysed by considering or excluding the presence of three common typologies of perimeter elements (i.e., RC horizontal cladding panels, RC vertical cladding panels and masonry infill walls), in order to simulate the perimeter frames or the internal bare frames of a precast building, respectively. Therefore, 120 different frame classes, 24 internal and 96 perimeter frames, have been analysed in the work. Two seismic fragility functions, related to severe damage and collapse state, have been obtained from the outcomes of the dynamic analyses. By interpolating the fragility functions over the set of the 8 periods of vibration, 3D fragility surfaces of each category have been derived, defining also the analytical expressions. The fragility surface provided in this work is a useful tool allowing defining the fragility curve of a precast frame starting from the knowledge of its structural category and the value of the first period of vibration T_1. Moreover, the fragility functions at failure of the different perimeter elements have been also obtained and reported. As confirmed in recent studies (Silva and Horspool 2019), the availability of mathematical functions associating the vibrating period to fragility curves represents a powerful tool, not commonly provided in other studies concerning fragility functions. Indeed, it could be adopted to perform statistical calculations based on vulnerability models, like seismic loss and damage assessments, considering the uncertainty in the period of vibration.

The simplified approach, introduced in the framework of this study, allows a fast evaluation of the fragility curves of a precast frame, starting from the knowledge of few structural information, which can be collected through a building survey with a visual inspection and non-destructive tests. Hence, the approach can be useful for performing rapid seismic risk evaluations. In particular, the methodology is deemed suitable for multiple applications at a territorial scale, for example in the case of large numbers of building stocks located in productive areas, and may be adopted for the identification of the most sensitive productive areas of a region. This may help to define specific economic measures for the seismic risk reduction, or may be considered as a tool to support decision, for instance in the context of the Civil Protection seismic plan definition.

3.2.1. DEFINITION OF THE METHODOLOGY

The aim of the methodology is to estimate the seismic vulnerability of existing one-story precast RC buildings, adopting simple mechanical models which capable of reproducing the in-plane damage and collapse mechanisms. The method is based on the main following steps:

- classification of the building stock to be investigated, starting from the data of reports and building surveys in the aftermath of May 2012. This is achieved by identifying the most important parameters which mainly influence the response of these buildings when hit by the ground-motion;
- analysis of the behaviour of the internal frames and perimeter frames identified in the previous step. Considering the hypothesis of flexible diaphragm for this class of buildings, internal frames and perimeter frames are studied separately, the latter being characterized by the presence of cladding panels or masonry infills;
- incremental dynamic (time-history) analyses with reference to the finite element models of internal and perimeter frames;
- definition of the fragility curves and the fragility surfaces for each class of internal and perimeter frames. The fragility surfaces are defined as a function of the first vibrating period of the frames. Obviously, internal and perimeter frames could have different values of the period of vibration.

3.2.1.1. SELECTION OF THE TAXONOMY AND DEFINITION OF THE CLASSIFICATION

The first step involves the identification and classification of the most widely used precast structural typologies, drawn from databases collecting the surveys of experts and engineers carried out after the Emilia 2012 seismic event (Bellotti et al. 2014, Ongaretto et al. 2019). The most common structural layout is constituted by cantilever columns supporting the horizontal roof elements, which are precast main beams bearing perpendicular precast floor slabs or secondary elements. The foundations are usually isolated socket foundations, not linked by beams as presently mandatory in seismic zones. More complex (and rare) layouts, such as multi-storey buildings or structures with shed roof, are not considered in this study.

The structure in elevation is quite slender since the typical height ranges from 6.0 to 9.0 m, and the square or rectangular column sectional dimensions are commonly 40 cm to 80 cm. Most of the building mass is concentrated at the roof level, where monolithic pre-stressed beams are inserted in top forks above the columns or placed on thick corbels, so behaving as simply-supported elements, with or without steel connectors. If the steel elements are absent, the support strength against the horizontal forces relies on the frictional resistance, which can be negatively influenced by the presence of interposed neoprene pads. The floor slab elements sustained by the main beams constitute the top roof level, providing a flexible in-plane behaviour due to the lack of continuity and the insufficiency of the connections. The features of the most common roof elements (i.e. main beams and roof slab elements) are presented in Bovo and Savoia (2021). In those few cases where mechanical devices connecting beams and columns were present, they were usually constituted by 2 steel dowels with Ø16 or Ø25 diameter, whereas the steel connections between slab elements and main beams were thin L-shaped plates. The connections proved to be stronger if compared with the friction-based support, since they have been able to prevent the horizontal sliding of the roof elements, as in many documented situations.

Masonry infill walls and precast cladding panels usually were the cladding elements on the perimeter of the buildings connected (or hanged) to the frames. In more recent buildings, horizontal or vertical precast cladding panels are directly connected to the structural frame elements (columns and/or perimeter beams), while the older buildings have masonry walls placed between consecutive columns. Among the connection typologies of the horizontal cladding panels, the two most frequently observed in the Emilia Romagna industrial areas are illustrated in Figure 3. The first one is constituted by strong steel brackets, both supporting the horizontal panels and providing the connection to the columns. These steel profiles are usually designed to sustain the weight of the panel, with a slope that allows preventing the out-of-plane displacement of the panel. The second type of panel-column connections consists of a steel channel placed in the column concrete cover and a hammer head strap fastened by means of a bolt in the panel (Colombo et al. 2016). In the case of a seismic action, this layout cannot guarantee the out-of-plane resistance of the panel because the shear deformation capacity of the connection is limited; as a result, this type of connection has proved to be very fragile during the Emilia seismic events. Finally, the vertical panels are usually connected to the perimeter upper beams through a bolted angular profile, as illustrated in Figure 4.

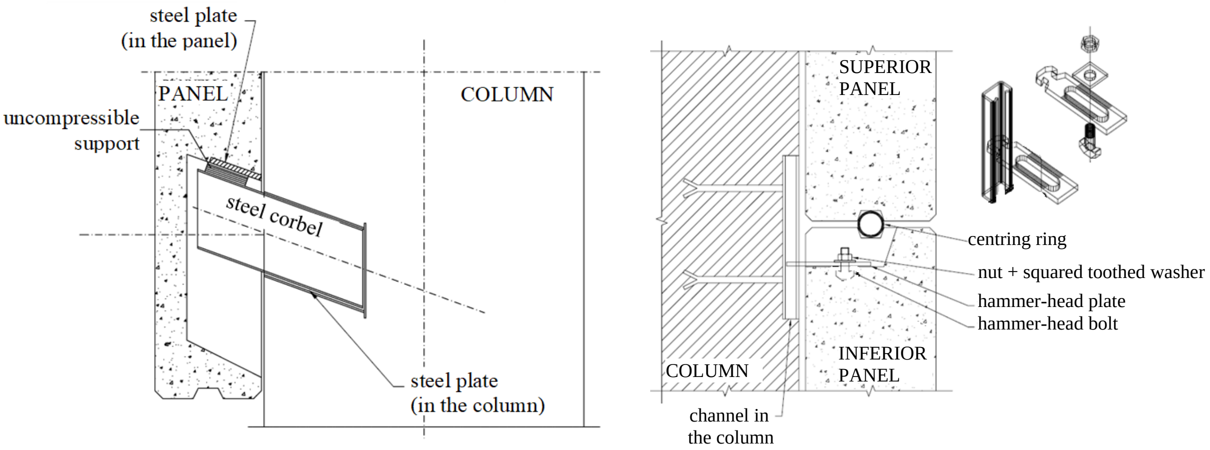

(a) *(b)*

Figure 3. Schemes of two typical connections for horizontal cladding panels, adapted from Reluis Report (Mandelli Contegni et al. 2007): connection adopted for (a) the (h1) frame class and (b) for the (h2) frame class.

All these characteristics have been selected from the in-situ surveys, and through the analysis of previous studies focused on the capacity of the frame elements and the different connections in precast buildings (Mandelli Contegni et al. 2007, Biondini et al. 2013a, Bournas et al. 2013, Magliulo et al. 2015, Zoubek et al. 2016, Belleri et al. 2018). Additional details are presented in Table 1.

Therefore, the most common existing precast buildings of the Emilia Romagna region can be classified according to the four main criteria schematized in Figure 5:

- The first criterion is the value of the yielding moment at the column's base, classified here through four reference values corresponding to four letters, from the lowest one (A) to the highest one (D). All the details for the calculation of the yielding moment values can be found in the paper of Bovo and Savoia (2021) and are not reported here for the sake of brevity.
- The second criterion is the beam-column connection, labelled with letters (L), (M) or (H), depending on the strength level of the typologies described above. This study concerns beams with tapered I cross-section.
- The third criterion is the roof slab-beam connection defined as low strength typology (L) or high strength typology (H). This study concerns roof slab elements with double tee cross-section.
- The fourth criterion is the type of perimeter panel, being one of the three aforementioned typologies, i.e. masonry infill walls (m), horizontal cladding panels (h) and vertical cladding panels (v). Two different types of connections for the horizontal cladding panels are considered in this study: the frames are labelled (h1) or (h2), when the steel corbel or the anchor channel connections are used, respectively.

Thus, 24 internal frame (I) categories and 96 perimeter frame (P) categories have been considered, the latter being further sub-classified according to the fourth criterion.

Each category for internal (bare frame) and perimeter frame of the buildings is thus labelled through 4 letters. The first 3 letters correspond to the first three criteria adopted. For example, one of the 24 internal frame categories is A-L-L-I, characterized by a column flexural capacity of 180 kNm (letter

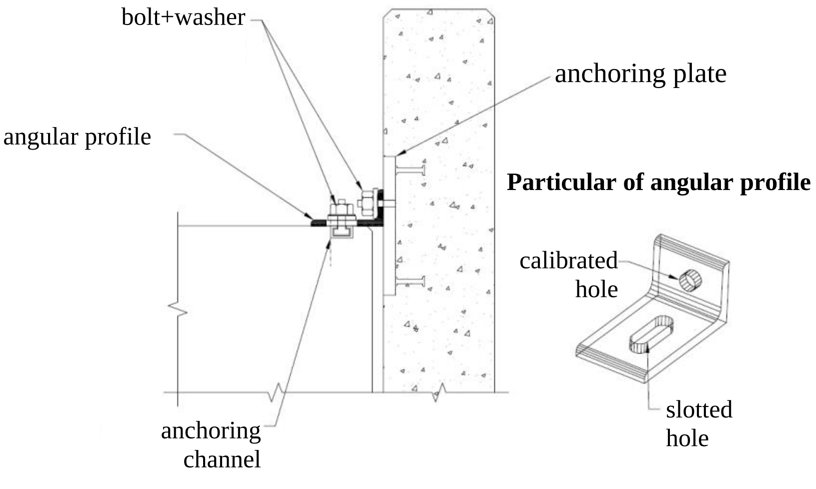

Figure 4. Scheme of a typical connection for vertical cladding panels, adapted from Reluis Report (Mandelli Contegni et al. 2007).

A), low strength of both beam-column and slab element-beam connections with neoprene pads (L-L). The final (I) stands for ‘internal frame’. Similarly, one of the 96 perimeter frames has the same first three letter classifications, plus a (P) that indicates a perimeter frame. For perimeter frames, the final letter defines the type of infill that can be (m) masonry wall, (h1) or (h2) horizontal cladding panels or (v) vertical cladding panels, according to the fourth criterion.

3.2.1.2. FINITE ELEMENT MODELLING

The seismic analyses of the frames belonging to the different categories have been performed on finite element (FE) models realized in OpenSees (OpenSees 2015) (see Figure 6). Figure 6a depicts the FE model of an internal frame (I), whereas Figures 6b, 6c and 6d show the models adopted for perimeter frames with the presence, respectively, of masonry infilled walls, horizontal and vertical precast RC cladding panels.

Table 1. Materials and geometries assumed for the four different flexural capacity levels of columns (f_{cm}: concrete mean cylindrical compressive strength; R_{ck}: concrete characteristic cubic compressive strength; f_{ym}: steel mean yielding stress; H: building height; L_b: beam spans; L_{fs}: span of the roof slab elements).

Base-column flexural capacity	f_{cm} [MPa]	R_{ck} [MPa]	Steel class	f_{ym} [MPa]	H [m]	L_b [m]	L_{fs} [m]
A	37.05	35.0	FeB32k	425.40	6.0	10.0	8.0
B	37.05	35.0	FeB32k	425.40	6.0	16.0	12.0
C	41.20	40.0	FeB44k	524.40	8.0	15.0	10.0
D	41.20	40.0	FeB44k	524.40	8.0	27.0	15.0

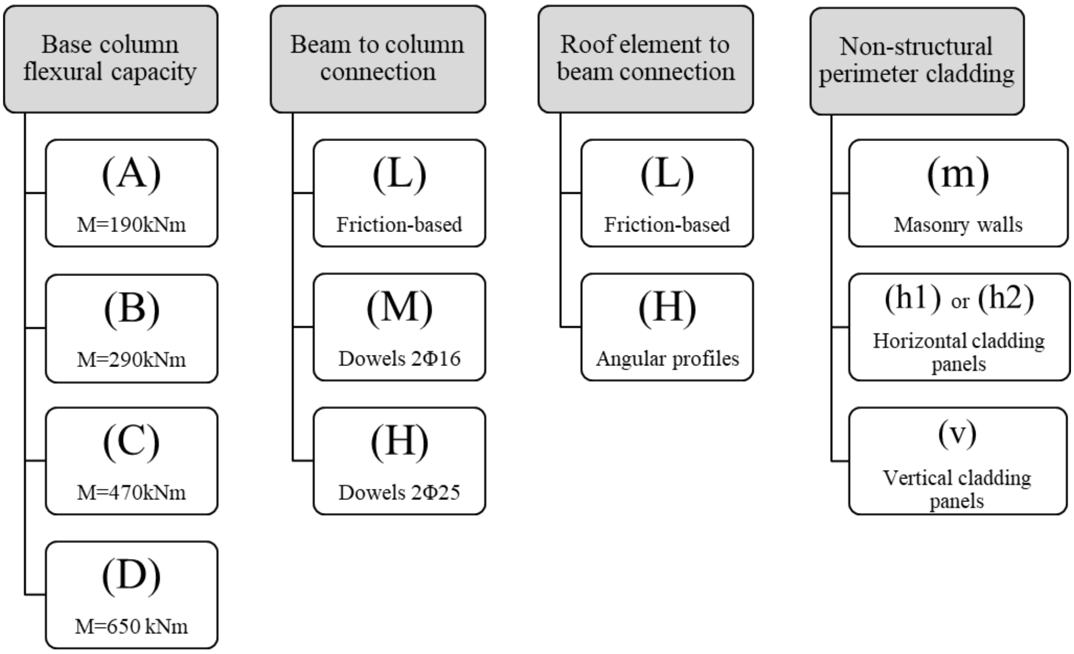

Figure 5. The four criteria adopted in the PRESSAFE-disp method for the classification of the frames.

3.2.1.2.1. FRAMES

The main elements of an internal frame (i.e. vertical columns and horizontal beams) have been modelled with 1-D elastic beam elements. The columns are fully clamped at the base and have pinned-pinned connections with upper beams.

The nonlinear behaviour of the columns has been accounted for by introducing plastic hinges at the column base, defined in terms of simplified trilinear moment-rotation laws (see sub-Figure a1 in Figure 7), where: M_y is the yielding moment depending on the flexural capacity level (i.e. A, B, C or D); M_u is the ultimate moment assumed equal to $1.05 \times M_y$; θ_y and θ_u are the corresponding rotations evaluated according to Eurocode 8 (CEN 2005). The plastic hinges have been defined by adopting the hysteretic uniaxial material in OpenSees (2015) with the following values for the damage parameters: pinchX=1.0, pinchY=1.0, damage1=0.0, damage2=0.08 and beta=0.12 in order to consider the hysteretic degradation of the RC elements when subjected to cyclic loadings (Kurtman 2007, Bovo and Buratti 2019). Moreover, the nonlinear behaviour of the beam-column connections has been modelled with a zero-length sliding hinge which is rigid-plastic if the connections are friction-based without mechanical devices (see sub-Figure a2 in Figure 7), or elastic-plastic if dowels are present (see sub-Figure a3 in Figure 7). In the friction-based connections, modelled with the

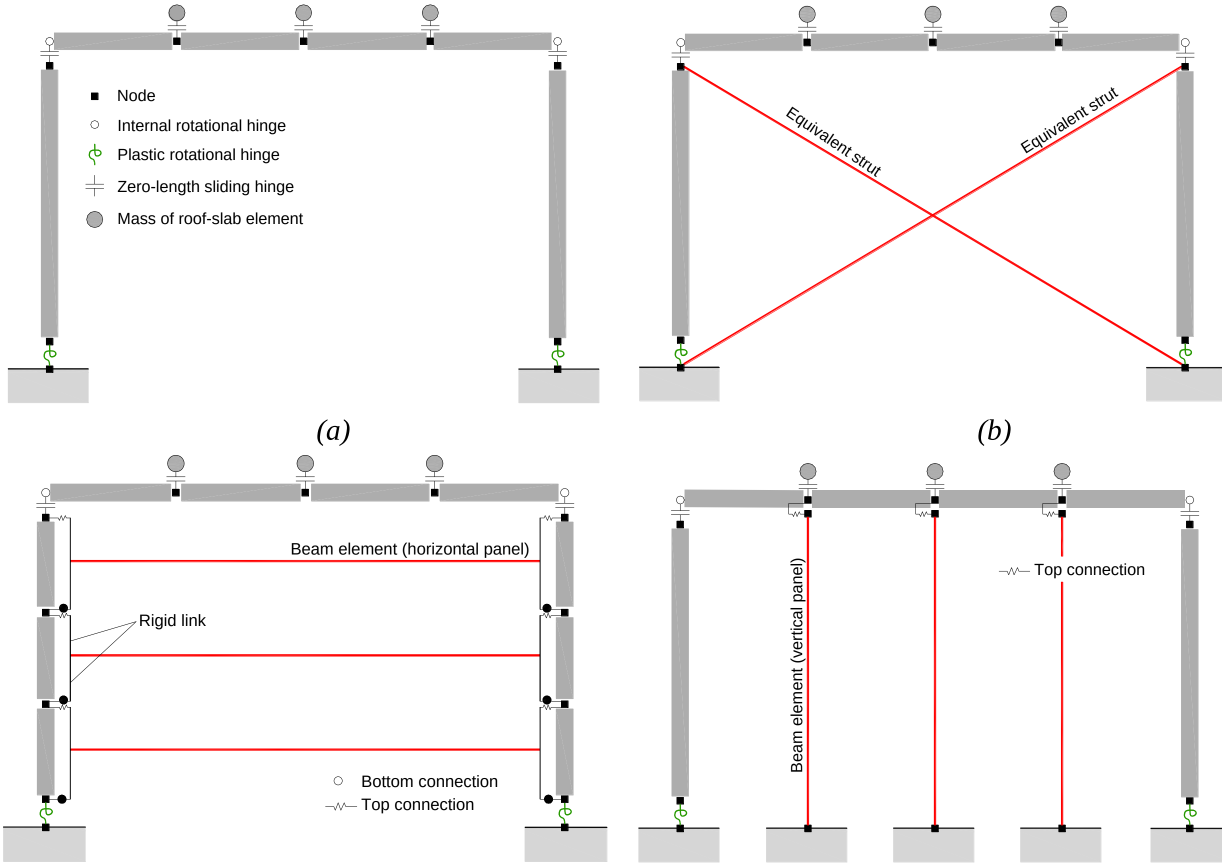

(a) (b)

(c) (d)

Figure 6. FE modelling of the different frame typologies: (a) Internal frame; Perimeter frame with (b) masonry infill walls, (c) horizontal cladding panels and (d) vertical cladding panels.

Coulomb friction model implemented in OpenSees, the strength capacity is calculated by considering the current vertical force on the connection (due to the self-weight of the precast elements added to the vertical seismic action) multiplied by the friction coefficient μ assumed equal to 0.1. The value selected is in accordance with the experimental tests reported in Magliulo et al. (2011) considering the presence of a neoprene pad between two precast elements.

The numerical parameters adopted to define the behaviour of the connections are summarized in Table 2. It is worth noting that the red circles in Figures 7a represent the attainment of a collapse condition of the structural frame. Finally, the column cross-sections have been selected, for each building category, in order to obtain specific values of the period of vibration of the frame (i.e. $\check{T}_1$ = 0.25, 0.5, 0.75, 1.0, 1.5, 2.0, 2.5 and 3.0 s).

Regarding the masses considered in the analyses, the mass of columns and beams has been considered as a consistent mass along the length of the element. The masses of the roof slab elements have been added as lumped masses connected by zero-length elements to the beams (see Figure 6). Moreover, the mass of the walls/panels in the plane of the perimeter frames has been introduced as a consistent mass along the finite elements simulating the panels or the struts. Finally, the mass of the walls/panels orthogonal to the plane of the internal and perimeter frames has been introduced as an equivalent consistent mass along the vertical finite elements of the columns.

Table 2. Parameters defining the mechanical properties of connections and equivalent masonry struts adopted in the numerical models (F=force; d=displacement).

<table>
<tr><td colspan="7">Numerical parameters adopted for perimeter and internal frames</td></tr>
<tr><td>Connection typology</td><td colspan="3">$F_{collapse}$ [kN]</td><td colspan="3">$d_{collapse}$ [mm]</td></tr>
<tr><td>Beam – column with neoprene pads</td><td colspan="3">0.1 × $F_{vertical}$</td><td colspan="3">100.0</td></tr>
<tr><td>Roof slab – beam with neoprene pads</td><td colspan="3">0.1 × $F_{vertical}$</td><td colspan="3">50.0</td></tr>
<tr><td>Beam – column with 2 Ø16 dowels</td><td colspan="3">70.0</td><td colspan="3">16.0</td></tr>
<tr><td>Beam – column with 2 Ø25 dowels</td><td colspan="3">180.0</td><td colspan="3">26.0</td></tr>
<tr><td>Roof slab – beam with steel plates</td><td colspan="3">30.0</td><td colspan="3">22.0</td></tr>
<tr><td colspan="7">Numerical parameters for perimeter frames only</td></tr>
<tr><td>Connection/strut typology</td><td>F_1 [kN]</td><td>d_1[mm]</td><td>F_2 [kN]</td><td>d_2[mm]</td><td>F_3 [kN]</td><td>d_3[mm]</td></tr>
<tr><td>Connection of horizontal panels (h1)</td><td>2.5</td><td>10.0</td><td>12.5</td><td>100.0</td><td>0.1</td><td>120.0</td></tr>
<tr><td>Connection of horizontal panels (h2)</td><td>2.5</td><td>10.0</td><td>4.0</td><td>50.0</td><td>0.1</td><td>70.0</td></tr>
<tr><td>Top connection of vertical panels</td><td>5.0</td><td>4.0</td><td>10.0</td><td>100.0</td><td>0.1</td><td>110.0</td></tr>
<tr><td>Masonry strut (A category)</td><td>300.0</td><td>2.2</td><td>360.0</td><td>17.6</td><td>3.6</td><td>68.9</td></tr>
<tr><td>Masonry strut (B category)</td><td>480.0</td><td>3.2</td><td>576.0</td><td>21.7</td><td>5.8</td><td>96.8</td></tr>
<tr><td>Masonry strut (C category)</td><td>450.0</td><td>3.14</td><td>540.0</td><td>24.2</td><td>5.4</td><td>99.0</td></tr>
<tr><td>Masonry strut (D category)</td><td>750.0</td><td>4.9</td><td>900.0</td><td>32.2</td><td>9.0</td><td>147.7</td></tr>
</table>

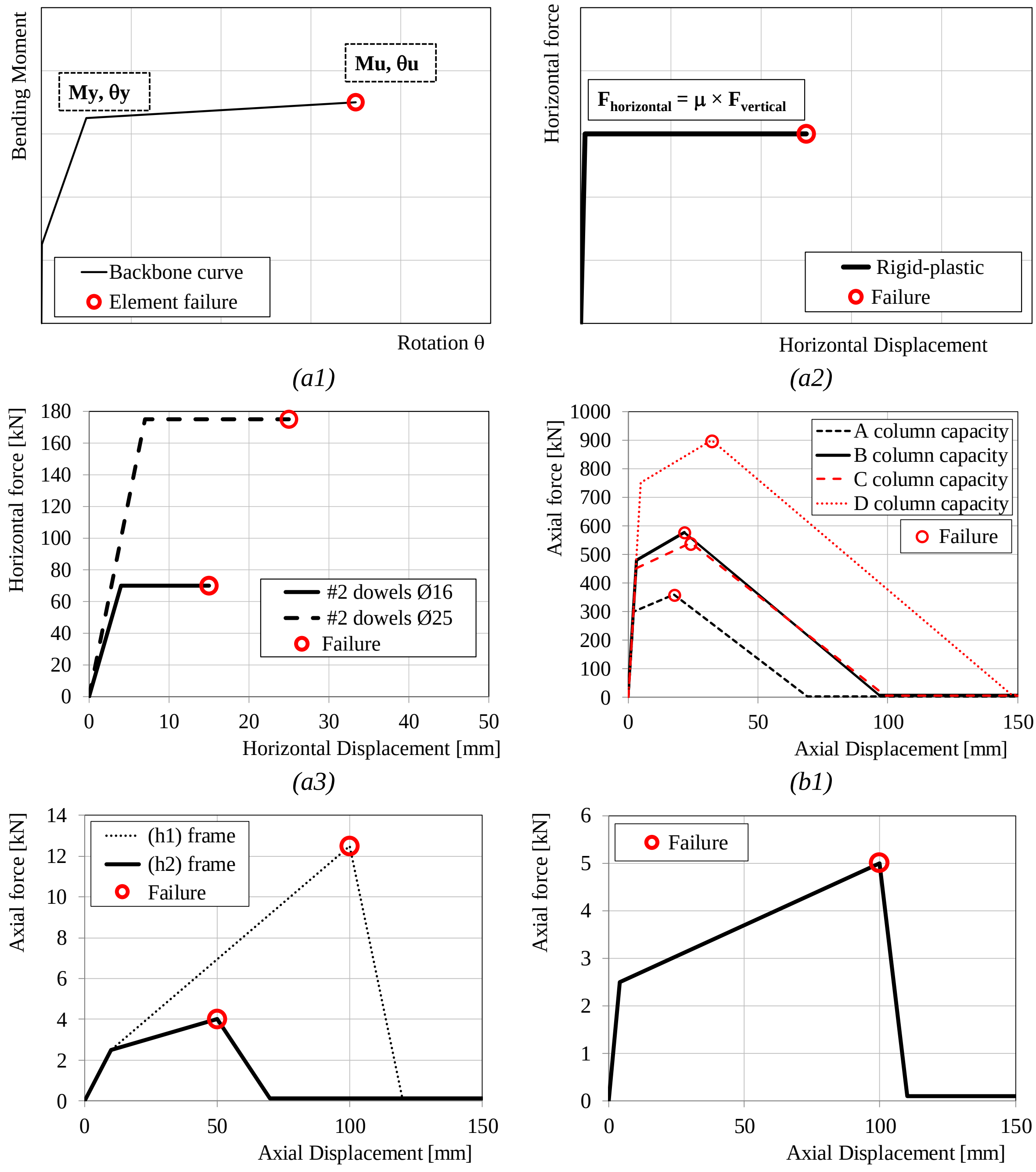

(a1) *(a2)*

(a3) *(b1)*

(b2) *(b3)*

Figure 7. Nonlinear laws adopted in the FE models. (a) Structural elements: (a1) Moment-rotation constitutive law for the plastic hinges at the base of the columns; (a2) Force-displacement shear law for zero-length sliding hinges simulating friction-based connections; (a3) Force-displacement shear law for zero-length sliding hinges simulating mechanical device-based connections. (b) Non-structural perimeter infill walls/panels: (b1) Force-displacement axial laws of the equivalent struts modelling the perimeter masonry infill walls; (b2) Force-displacement axial laws adopted for the column-panel connections of horizontal cladding panels; (b3) Force-displacement axial law adopted for the beam-panel connections of vertical cladding panels (top connection).

3.2.1.2.2. PERIMETER INFILL WALLS/PANELS

The infill walls considered in the study are 30 cm thick, and are unreinforced masonries with hollow clay bricks with mean compressive strength f_c = 3.5 MPa and hydraulic lime mortar with mean compressive strength f_c = 4.0 MPa. The masonry infill walls in the perimeter of the building have been modelled by means of two equivalent diagonal struts (see Figure 6b). This strategy provides a suitable approximation of the global response of the frame (Crisafulli et al. 2000, Asteris et al. 2011). The axial behaviour of the equivalent struts has been modelled in OpenSees as hysteretic elements by using the Hysteretic Material (OpenSees 2015) and assuming the values indicated in Table 2, as suggested in Fardis (1996) and Celarec et al. (2012). Since the strut behaviour is a function of the frame geometry, four different curves are obtained and reported in sub-Figure b1 in Figure 7, for the four aforementioned frame typologies (A), (B), (C) and (D). The failure for masonry infill walls has been assumed to be the crushing of the masonry struts. The results provided by these models are valid if the out-of-plane failure mechanisms of the masonry panels are prevented, or if these mechanisms are activated by higher horizontal accelerations than those causing the structural collapse. If the out-of-plane failure mechanisms of slender masonry panels are expected to happen before the structure collapse, the results of the model may not be realistic.

On the other hand, the perimeter elements of the more recent buildings are typically constituted by precast cladding panels, horizontally or vertically arranged. The former panels may typically assume in two main configurations. In the first solution (h1), the panels are hung at the columns in four points by means of mechanical steel devices: usually the lower ones (bottom connections) bear the self-weight of the panels, whereas the upper (top connections) prevent the outward overturning and the horizontal column-panel slip. In the second solution (h2), the lowest series of panels directly leans on the foundation beams and the outward overturning is prevented by two top connections realized as in Figure 3. Then, the upper series of panels directly leans on the lower one with analogous top connections. The FE model describing this typology of frames is reported in Figure 6c. The behaviour of the connections both for (h1) and (h2) typologies is shown in sub-Figure b2 in Figure 7. The values adopted in the FE models are reported in Table 2 and have been defined respectively for (h1) and (h2) connection typologies starting from the experimental outcomes reported in Belleri et al. (2016) and Del Monte et al. (2019). Three horizontal panel series have been considered in the models.

Lastly, the FE model simulating frames with vertical cladding panels is reported in Figure 6d. The vertical panel is clamped at the base and connected to the roof beam of the structure by means of the anchor–channel connections type HRC-U-M180 studied in Zoubek et al. (2016). The numerical law implemented for the top connection of the vertical panels is shown in sub-Figure b3 in Figure 7, and the corresponding parameters are reported in Table 2. For each vertical panel, two anchor-channel devices have been considered. It is worth noting that the red circles in Figures 7b correspond to the attainment of the failure of non-structural perimeter walls/panels. Since the dynamic analyses continue until the attainment of a collapse condition for the structural frame, also the post-failure behaviour of non-structural elements is defined. Considering that all these are 2D simplified models, the out-of-plane behaviour of walls and panels in the direction orthogonal to the frame has not been taken into account. It is worth noting that this could entail a modification of the seismic demand to the columns adjacent to the cladding elements.

3.2.1.3. DAMAGE AND COLLAPSE STATES

3.2.1.3.1. FRAMES

Following the indications reported in Section 3.1.1 regarding the observed damage, two limit states have been considered for the frames. They refer to a severe damage and a collapse condition of the main structural elements, respectively. The severe damage condition has been set at the attainment of one of the following sub-conditions: (i) the yielding bending moment of the base-section of a column; (ii) the strength capacity in a roof slab-beam connection or in a beam-column connection. The collapse condition has been defined at the attainment of one of the following sub-conditions: (i) the ultimate rotation for a column; (ii) the displacement capacity in one of the sliding hinges shown in Figure 6a, adopting a displacement-based collapse criterion for the connections.

The second criterion, in both conditions, has been properly added in order to simulate the common damage and collapse mechanisms observed in the aftermath of the Emilia earthquake, where the horizontal sliding of heavy beams or roof slab elements, in several cases, caused the complete unseating and the subsequent fall of the elements.

The attainment of the element or connection failure, indicated by the red circles in Figures 7a, identifies the collapse of the frame, at which the dynamic analyses have been interrupted. The possible attainment of a failure condition has been evaluated step-by-step during the dynamic time-history analysis. Moreover, in the IDA procedure, the second-order effects (P-Δ) have been also considered. In particular, in very flexible structures like those investigated here, in which cantilever columns support heavy masses, the non-linear second order effects may cause large displacements at the roof level and may increase the seismic damage anticipating the structural collapse.

3.2.1.3.2. PERIMETER INFILL WALLS/PANELS

It is worth highlighting that, in the aftermath of the Emilia earthquakes, the most commonly observed damage to non-structural elements concerned the perimeter walls/cladding panels (Savoia et al. 2012). Hence, the failure of perimeter infill walls and cladding panels has been also considered and recorded in the dynamic analyses. For the masonry infill walls, the failure of the panels has been identified at the attainment of the peak point in the strut axial behaviour (see sub-Figure b1 in Figure 7).

Analogously, the failure of the horizontal cladding panels has been identified with the attainment of the peak point in the behaviour of the connection supporting the panel (see sub-Figure b2 in Figure 7). To this regard, most of the precast buildings in the Emilia Romagna territories presents the (h2) connection typology illustrated in Figure 3b. The (h2) type of connections showed a very high sensitivity to seismic actions, whereas the (h1) one resulted to be significantly less weak.

Finally, the failure of the vertical panels has been identified with the failure of the mechanical devices (top connections in Figure 6d) connecting the panels to the structural elements (in this case the roof beam). Again, the failure of the connection has been registered at the attainment of the peak point of the constitutive law (see sub-Figure b3 in Figure 7).

After the attainment of the failure point for non-structural perimeter walls/panels, the analyses continue according to the post-peak behaviour shown in Figures 7b. Hence, the analyses have been interrupted at the attainment of one of the aforementioned collapse conditions related to the structural frames. In all cases, the non-structural walls/panels failure condition has been evaluated independently from the structural collapse condition of the whole frame.

3.2.2. INCREMENTAL DYNAMIC ANALYSES

In order to evaluate the seismic response of the frames, nonlinear time-histories analyses have been performed, considering as input the 30 ground-motion records selected in Vamvatsikos and Fragiadakis (2010). Both the horizontal and vertical components of the ground motions have been considered, covering a wide range of frequency, time, duration and amplitude. The free field records have been extracted from the PEER Strong Motion Database (accessed in 2020), following the criteria of selection adopted by Vamvatsikos and Fragiadakis (2010). The 5%-damped acceleration response spectra of the 30 horizontal ground motions are reported in Figure 8a. In the Figure, the 5% damped elastic spectra of the 30 recorded horizontal ground-motions are represented together with their average spectrum (in red). No scaling factor have been used in the selection phase. The distance from the source, between 15.1 km and 32.6 km, has been selected to avoid the directivity effects. The dataset adopted has an average value of horizontal over vertical peak ground acceleration ratio, i.e. PGA_h/PGA_v (see Figure 8b), comparable with that expected for seismic far fault records (PEER Strong Motion Database 2020). Following the criteria given in the PEER Report (2013), the vertical records considered do not present pulse-velocity shape.

The Incremental Dynamic Analyses (IDA) have been performed according to the methodology outlined by Vamvatsikos and Cornell (2002), to consider the record-to-record variability. The

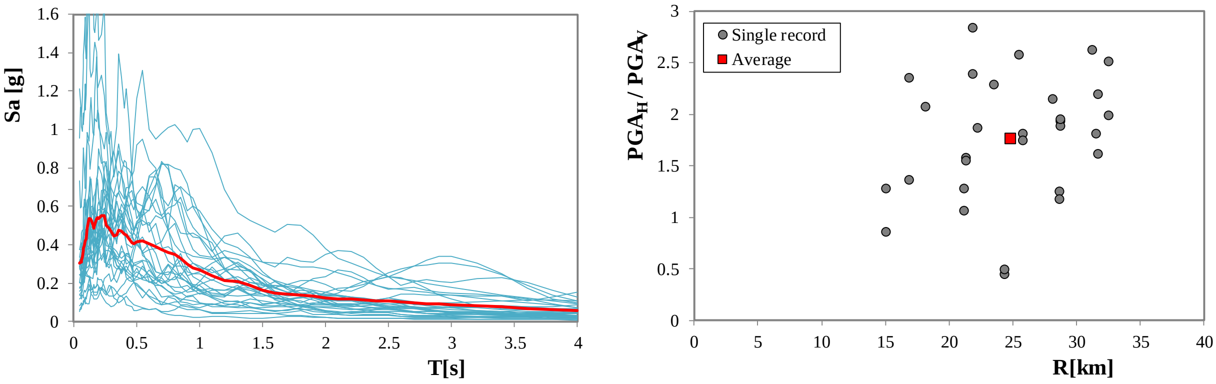

(a) *(b)*

Figure 8. Seismic inputs adopted for the dynamic analyses: (a) 5%-damped acceleration response spectra of the 30 horizontal ground motions and mean value (in red); (b) horizontal/vertical peak-ground acceleration vs. closest distance to fault rupture (R) for the records selected.

analyses have been carried out on 960 different FE models, considering, for each frame typology (i.e. 24 internal and 96 perimeter frames, for a total number of 120 frames), 8 different column cross-sections corresponding to 8 vibrating periods of the frames. The use of 8 periods of vibration allows to obtain a set with 8 fragility curves for each frame typology, which have been subsequently combined to determine one fragility surface considered as a function of the value of the first period of vibration (see the next Section). The intensity measure (IM) considered in the IDA procedure is the 5%-damped first mode spectral acceleration, $S_a(T_1,5\%)$ or S_a in the following, and the engineering demand parameter (EDP) adopted is the maximum horizontal displacement at the roof level. Rayleigh damping has been considered in the IDA analyses.

In the IDA procedure, each record has been scaled up to the attainment of at least one collapse condition, considering also the P-Δ effects.

The results of the time-history analyses have been 28800 IDA curves, statistically combined in order to generate 960 numerical fragility curves (see the procedures in Silva et al. 2019) and then 120

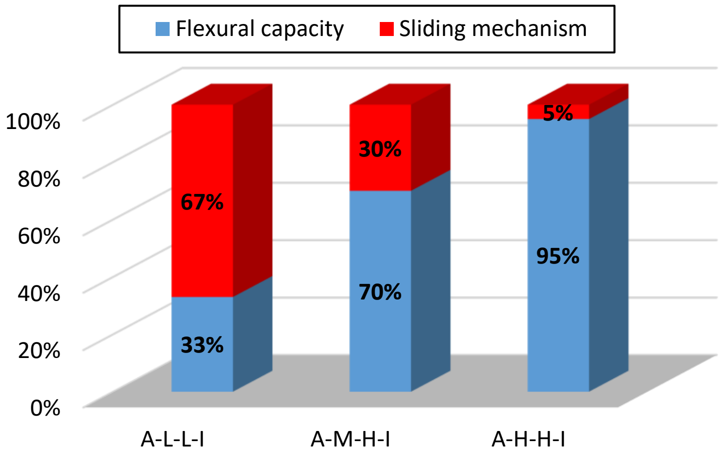

(a)

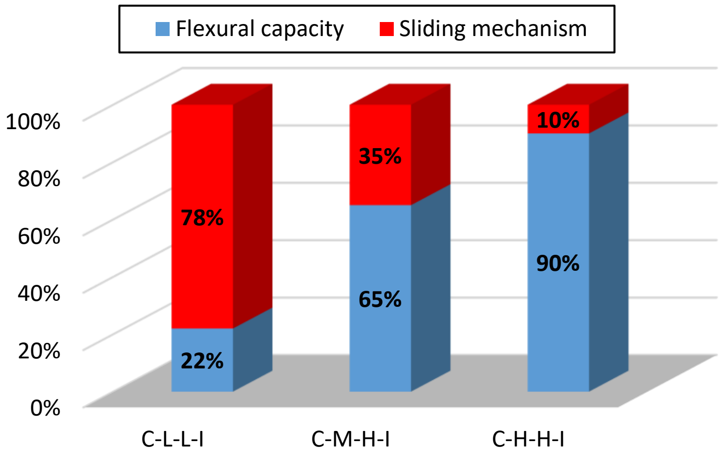

(b)

Figure 9. Percentage of attainment of the two collapse mechanisms for some frame typologies with two different base-column flexural capacity (for T_1*=1 s). (a) Level A; (b) Level C.*

fragility surfaces in which the value of the first vibrating period T_1 has been also considered as a variable (see Section 3.2.3).

The introduction of the cladding elements causes a significant stiffening of the perimeter frame with respect to the bare frame, changing the original elastic vibrating periods. Hence, for the sake of clarity and to avoid misleading, the outcomes presented in the following will be referred to the first period of vibration of the bare frame T_1 even if the record scaling has been performed with reference to $Sa(T_1^*,5\%)$ (where T_1^* is the elastic vibrating period of a perimeter frame with cladding elements and, obviously, $T_1^* < T_1$ for each category). Thus, the period of vibration for the perimeter frame has been calculated by removing the perimeter infills/panels from the FE model. Therefore, for the application of the method, the potential user should adopt the same procedure. This aspect makes the method more user-friendly since it simplifies considerably the procedure, especially for applications to existing buildings for which some structural parameters and details may be very complex to be determined through visual inspections only. Moreover, this allows a more direct comparison between frames with and without panels.

As an example, Figure 9 provides the percentage of attainment of the two different collapse mechanisms (failure of columns or sliding of roof elements). The results are reported for the sake of brevity for some representative frame categories only, i.e. A-L-L-I, A-M-H-I, A-H-H-I, C-L-L-I, C-M-H-I and C-H-H-I, for T_1 =1 s. The figure highlights that, for frames with friction-based support, i.e. A-L-L-I and C-L-L-I, most of the collapses can be attributed to sliding mechanisms. On the contrary, considering the frames with high-strength beam-column and roof slab element-beam connections, i.e. A-H-H-I and C-H-H-I, most of the collapses can be attributed to the failure of the columns. This confirms the reliability of the retrofitting criteria suggested by the Legislative Decree No. 74/2012 (2012) in the aftermath of the events. Indeed, the strengthening of the connections between precast elements has positive significant benefits preventing the fall of the roof elements, and can be considered the first effective retrofitting intervention to be introduced in order to reduce the vulnerability of these buildings.

3.2.3. DERIVATION OF FRAGILITY CURVES AND FRAGILITY SURFACES OF THE FRAMES

3.2.3.1. FRAGILITY FUNCTIONS AT COLLAPSE AND SEVERE DAMAGE

By means of the results of the IDA curves, for each frame typology, the cumulative fraction of structures reaching a specific damage state for the 30 accelerograms has been calculated, providing a set of points.

An empirical IM-based fragility function has been thus derived, by interpolating the so obtained set of points expressing the cumulative number corresponding to each IM. In particular, the set of points, representing the fragility for a given damage state of a frame with a specific period of vibration, has been fitted with a log-normal cumulative distribution function having the following form:

$$\mathrm{F}(s) = \Phi\left[\frac{\ln\left(\frac{s}{\mu}\right)}{\sigma}\right] \tag{3.1}$$

Where: s represents S_a , $\Phi\ [\cdot]$ is the standardized normal distribution function, μ and σ are the main descriptors of the fragility function (i.e., the mean and the standard deviation, respectively). These parameters have been calibrated through the maximum likelihood function (see Eq.(3.2)), imposing the maximisation of ln L (see Eq.(3.3)) in order to find the best fitting function for each numerical IDA dataset of points.

$$\mathrm{L} = \prod_{i=1}^{N} [\mathrm{F}(s_i)]^{x_i} \cdot [1 - \mathrm{F}(s_i)]^{1-x_i} \tag{3.2}$$

$$\frac{\partial \ln \mathrm{L}}{\partial\, \mu} = \frac{\partial \ln \mathrm{L}}{\partial\, \sigma} = 0 \tag{3.3}$$

Where: s_i represents the i-th S_a value, x_i the corresponding probability of failure, N is the total number of samples (i.e., 30 points) for a specific damage state, and a specific frame category.

In Figures 10 and 11, the (best fitting) fragility curves resulting from the regression procedure are shown for some building categories and for three periods of vibration (i.e. 0.5 s, 1.0 s and 2.0 s), at collapse and severe damage limit states, respectively. It is worth noting again, for the sake of the clarity, that the outcomes presented in the following, for perimeter frames, refer to the vibrating period of the bare frames T_1 (without the presence of non-structural walls/panels), in order to simplify the comparisons between the behaviour of different categories.

Considering a specific value of S_a (horizontal axis), the probability of exceedance (PoE) in both limit states (vertical axis of the fragility curves) increases with the increase of the period of vibration, meaning that the flexible frames (longer periods) are more likely to collapse or to be subjected to severe damage, due to large displacements and P-Δ effects. This effect is clearly visible for the internal frames, whereas it is not always valid for perimeter frames, in particular for those with masonry infill walls, which highly influence the structural behaviour (e.g. see sub-Figures a1, b1, c1 in Figure 10 and 11). Moreover, as expected, for a specific value of S_a for each category, all the severe damage fragility curves (see Figure 11) are characterized by higher PoE values with respect to the corresponding collapse fragility curves (see Figure 10). The increase of the flexural capacity at the base of the column, for instance from class C-L-L to class D-L-L, is reflected in a progressive decrease of the PoE for both limit states. Similarly, the benefit of having strong connections between the roof elements is evident by comparing the curves of frame category C-L-L and those of C-M-H.

For all frame categories, the presence of the perimeter elements on one hand has a positive effect in lowering the vulnerability of the frames if compared with that of the internal ones, on the other hand, it influences the shape of the fragility curves in a different way depending on the value of the period considered. This is only partially true for perimeter frames with vertical cladding panels, being the fragility curves very similar to those of the internal frames, due to the poor column-panel connections (see sub-Figures a3, b3, c3 in Figure 10 and 11).

As far as the different connection types of the horizontal cladding panels are concerned, the perimeter frame categories with the (h2) connections are significantly more vulnerable than those with (h1) connections. Indeed, the fragility curves of the frames with the (h1) connection typology have higher mean values than the ones with the (h2) typology (see sub-Figures a2, b2, c2 in Figure 10 and 11).

In addition, in order to perform some general comparisons, the collapse fragility curves are plotted in Figure 12 for the frame categories A-L-L, B-L-L and C-M-H, for various cladding typologies and different periods of vibration. The results obtained for the A-L-L category for frames with period of 1.5 s are shown in Figure 12a. For a specific S_a value, the masonry infilled frames (A-L-L-P(m)) show lower values of PoE at collapse, followed by those with horizontal cladding panels with (h1) connection (A-L-L-P(h1)). As mentioned before, horizontal cladding panels with (h2) connection (A-L-L-P(h2)) and vertical panels (A-L-L-P(v)) do not produce a relevant modification of the internal frame (A-L-L-I) fragilities, resulting in a very slight decrease of the PoE. The C-M-H frame category, characterized by higher strength of both columns flexural capacity and connections, exhibits an analogous behaviour (see Figure 12b).

With reference again to the perimeter frame category A-L-L-P, in Figure 12c the behaviour of frames with horizontal cladding panels and the (h2) connection (A-L-L-P(h2)) is compared with those with the (h1) connection typology (A-L-L-P(h1)). The figure confirms that the former frames are more vulnerable if compared with the latter, independently of the value of the vibrating period of the frames. Finally, the fragility curves for the 8 periods investigated are reported in Figure 12d for the frame typology B-L-L-P(h2). As expected, with the increase of the period, a general decrease in both the S_a value for a prescribed PoE (i.e. the collapse acceleration) and the S_a dispersion (i.e. scattered tendency of the collapse acceleration dataset) occurs.

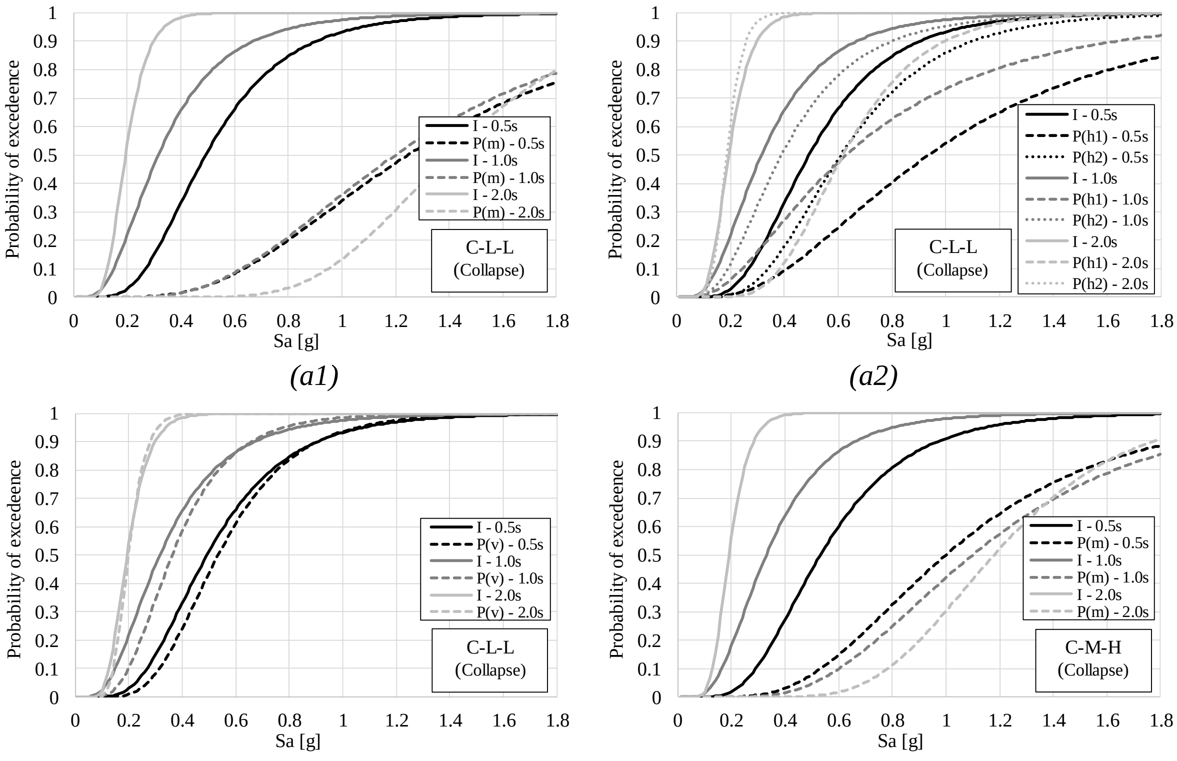

(a1) *(a2)*

(a3) *(b1)*

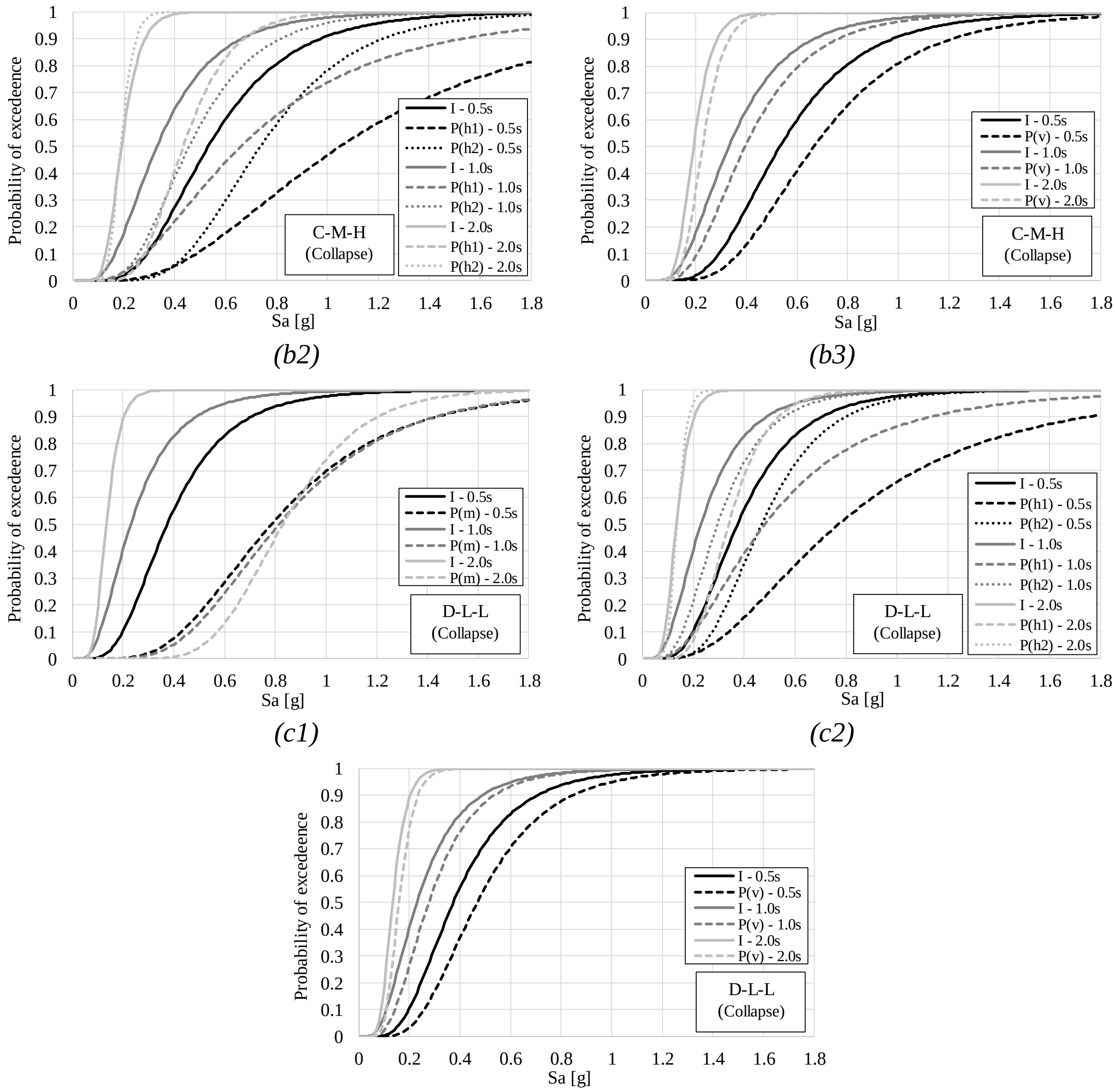

(b2) *(b3)*

(c1) *(c2)*

(c3)

Figure 10. Collapse fragilities for some relevant frame categories. I: internal frame; P(m), P(h1), P(h2) and P(v): perimeter frame with masonry infill walls, vertical and horizontal panels respectively.

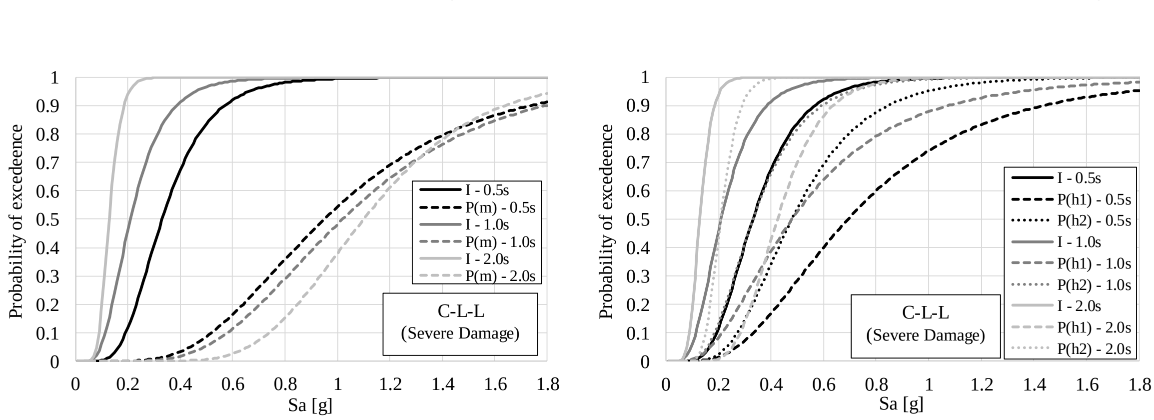

(a1) *(a2)*

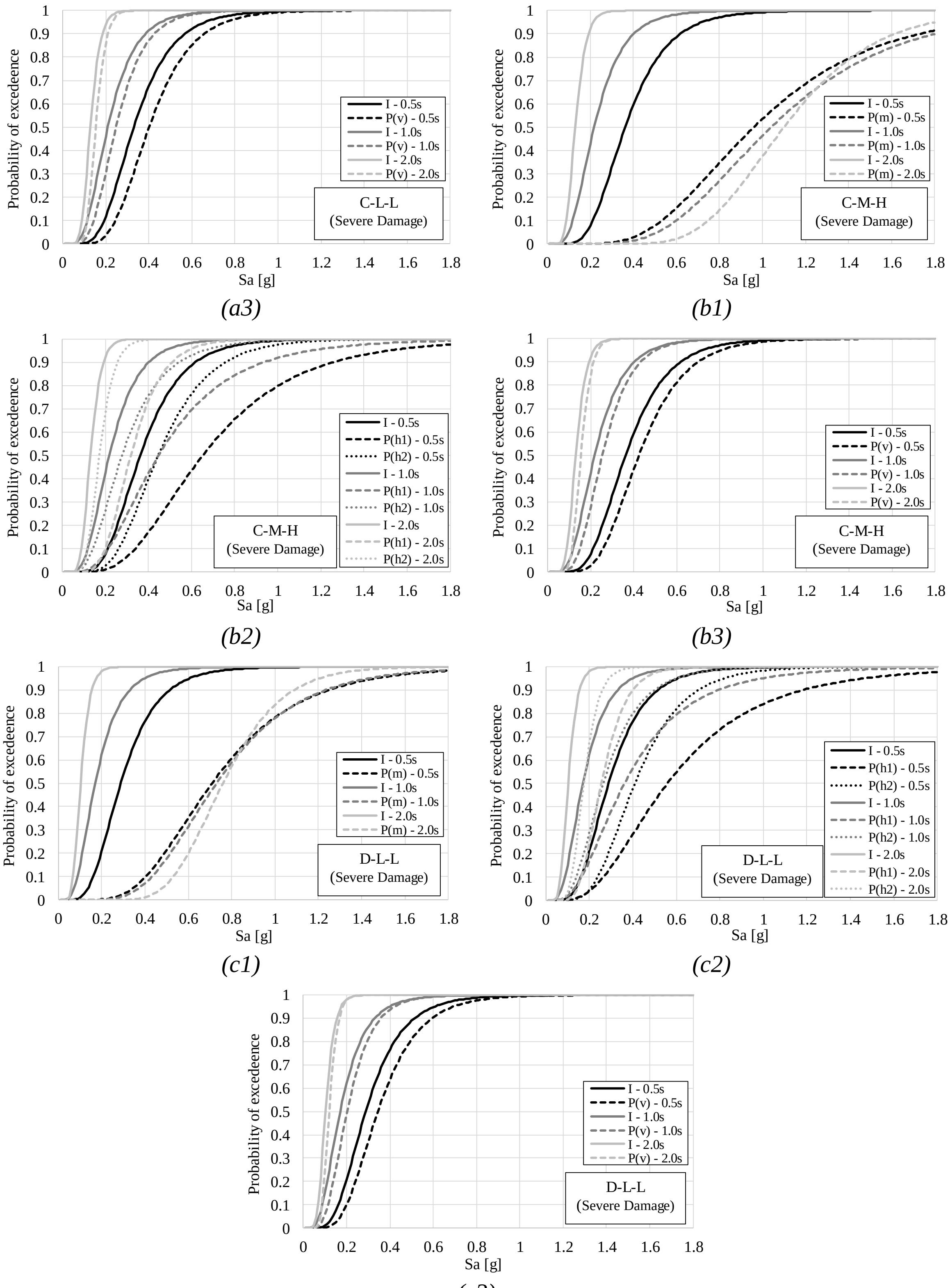

(a3) *(b1)*

(b2) *(b3)*

(c1) *(c2)*

(c3)

Figure 11. Severe damage fragilities for some relevant frame categories. I: internal frame; P(m), P(h1), P(h2) and P(v): perimeter frame with masonry infill walls, vertical and horizontal panels respectively.

3.2.3.2. FRAGILITY SURFACES AT COLLAPSE AND SEVERE DAMAGE

The fragility curves have been defined, for each structural typology, for 8 different periods of vibration T_1 and for the two limit states selected, i.e. structural collapse and structural severe damage. In order to provide the vulnerability of the frames as a function of T_1, the 2D fragility curves $F(S_a)$ have been assembled to create 3D smoothed fragility surfaces, expressed in the form $R(S_a,T_1)$. The mathematical functions expressing the variation of the statistical fragility curve parameters (μ, σ) with the value of the vibrating period have been firstly identified. In particular, the selected trend functions of the two fragility curve descriptors referring to collapse are the following:

for $0 < T_1 \leq 2.0$ s $\quad \mu^C(T_1) = a1 \cdot T_1^{\,2} + a2 \cdot T_1 + a3 \quad$ (3.4a)

for $2.0\text{ s} < T_1 < 3.0$ s $\quad \mu^C(T_1) = \mu^C(2.0) \quad$ (3.4b)

for $0 < T_1 < 3.0$ s $\quad \sigma^C = b1 \cdot T_1^{\,3} + b2 \cdot T_1^{\,2} + b3 \cdot T_1 + b4 \quad$ (3.4c)

Analogous functions for the severe damage limit state are:

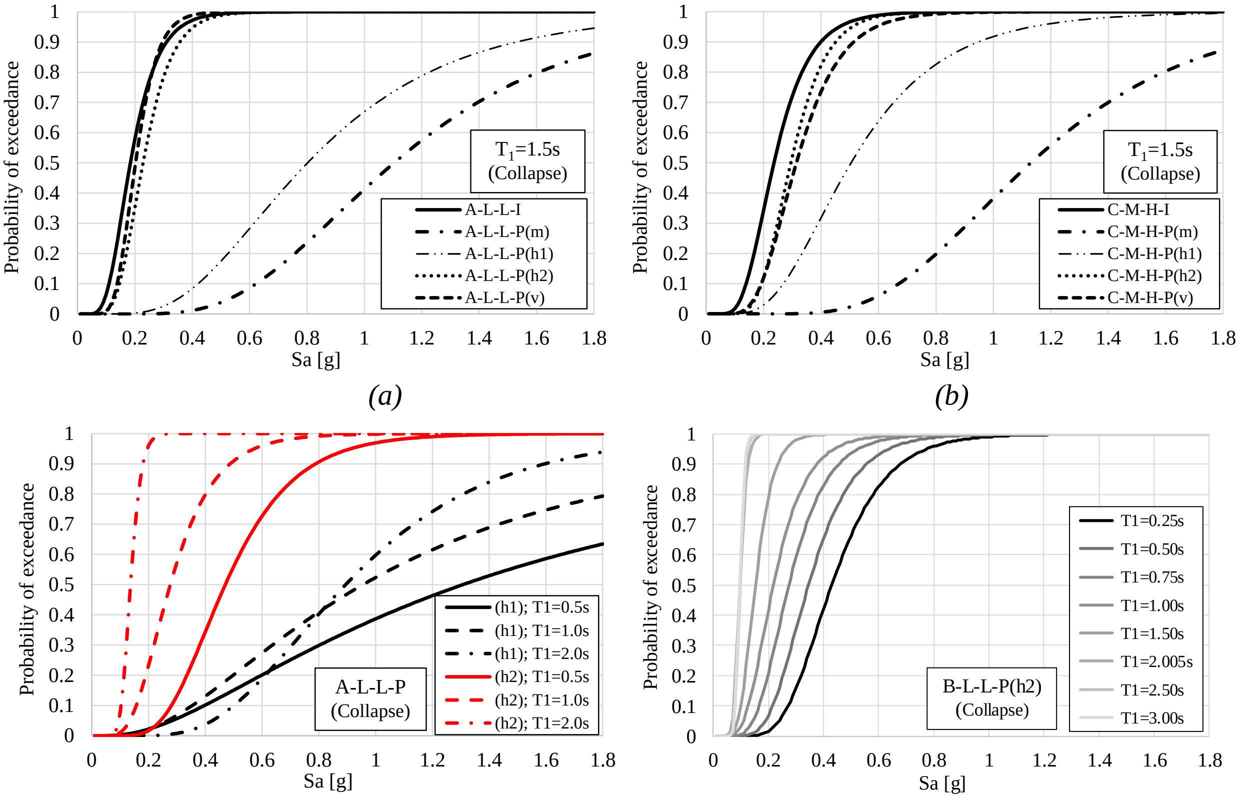

(a) *(b)*

(c) *(d)*

Figure 12. Collapse fragility functions of frames with perimeter walls. (a) Frame category with low flexural capacity and T_1*=1.5, A-L-L-I and A-L-L-P with different types of perimeter cladding elements; (b) frame category C-M-H-I and C-M-H-P with high flexural capacity and* T_1*=1.5 s; (c) frame category A-L-L-P with different horizontal cladding panels (h1) and (h2) at three vibrating periods; (d) frame category B-L-L-P(h2 at height vibrating periods.*

for $0 < T_1 \leq 2.0$ s $$\mu^{SD} = c1 \cdot {T_1}^2 + c2 \cdot T_1 + c3 \tag{3.5a}$$

for $2.0 \text{ s} < T_1 < 3.0$ s $$\mu^{SD}(T_1) = \mu^{SD}(2.0) \tag{3.5b}$$

for $0 < T_1 \leq 3.0$ s $$\sigma^{SD} = d1 \cdot {T_1}^3 + d2 \cdot {T_1}^2 + d3 \cdot T_1 + d4 \tag{3.5c}$$

Where: T_1 (in seconds) is the first period of vibration of the bare frame, and the coefficients a1-d4 have been obtained by fitting the IDA data through a nonlinear regression procedure based on the least squares' method. The effectiveness of the regression is proved by the value of the coefficient of determination, being R^2 always greater than 0.9 and frequently over 0.95. The coefficients are collected in five table, each with 24 structural typologies and 14 coefficients (a1-d4), for a total number of 1680 values. The coefficients can be found in Bovo et al. (2022), and are not reported here for the sake of clarity.

The fragility surfaces $R(S_a,T_1)$ allow to consider the uncertainties in the value of T_1 in the estimation of the vulnerability of a precast frame. Crowley et al. (2004) proposed a similar tool, with reference to ordinary RC buildings, for the derivation of relationships between the displacement capacity and the fundamental period of a building.

As a general example, a fragility surface for the category A-M-H-I is shown in Figure 13, together with the IDA data adopted in the fitting procedure: for a value of T_1 ranging between 0.25 s and 3.0 s, from the 3D fragility surface it is possible to extract the corresponding 2D fragility curve.

The plots of Equations (3.4) and (3.5) are illustrated for some relevant structural categories at collapse in Figure 14. While the trends related to μ are characterized by similar wavy shapes, the trend of σ presents some variations. In particular, for some categories (see sub-Figure a1, c1, d1 and e1 in Figure 14) it has have a reversed bell shape, differently from those of the perimeter frame categories with masonry infill walls (sub-Figure b1 in Figure 14). This seems to be linked to the strong influence of the latter cladding typology on the frame response, as masonry infill walls influence, in particular, the highest vibrating periods.

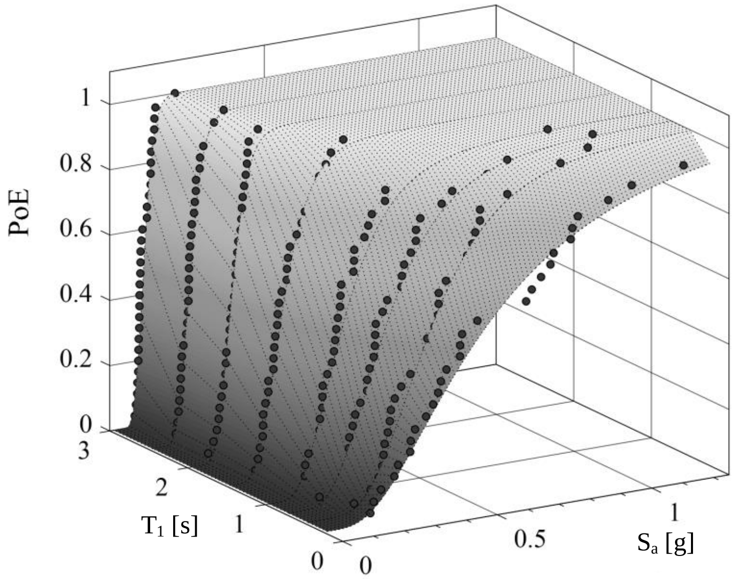

Figure 13. Example of a fragility surface (for A-M-H-I frame category). Points obtained from IDA and best fitting approximation for the different periods.

The poor behaviour of the (h2) type of connection for horizontal cladding panels, with respect to the (h1) ones, is once again highlighted by lower values of the μ functions for both limit states (see sub-Figures c1 and d1 in Figure 14). The σ functions, related to the frames with the two different horizontal cladding panel connections, have similar trends for high periods, whereas they are very different for low periods (see sub-Figures c2 and d2 in Figure 14). In particular, the (h1) connection typology results in higher σ values for the more sensitive structural categories, i.e. A-L-L and A-M-H, at the low period values (see sub-Figure c2 in Figure 14). These different trends are because the weak connection (h2), differently from the (h1) typology, is not able to modify considerably the seismic response and the collapse value of the perimeter frames with respect to the internal (bare) frames. Hence, for frames with (h2) connection type, in the whole range of periods, the σ value is very similar to the case of internal frames. This effect is no more visible at higher periods for the frames with (h1) connections, because of the presence of remarkable P-Δ effects (in flexible frames).

3.2.3.3. FRAGILITY SURFACES OF INFILL WALLS/PANELS AT FAILURE

Analogously to the procedure described in the previous Sections for the structural frames, the IDA outcomes related to the failure of perimeter infill walls and cladding panels have been elaborated to obtain the fragility curves (i.e. fragility functions) of the various types of building perimeter elements. The fragility curves for masonry infill walls have been defined considering the attainment of the peak point in the force-displacement curve of the equivalent struts (see sub-Figure b1 in Figure 7). For the precast RC cladding panels, instead, the failure condition has been set, conventionally, at the attainment of the peak point in the constitutive diagram of the connections hanging the panel (see the laws in sub-Figures b2 and b3 in Figure 7, and the red circles reporting the label "Failure").

For some frame classes, the structural collapse anticipates the failure of the perimeter elements and, in those cases, i.e. for panels largely more robust than the frame, the IM value causing the collapse is not available. In other cases, the structural collapse and the failure of non-structural elements have comparable values and the walls/panels failure data are available just for some seismic inputs over the whole set investigated. Assuming the fragility functions of the walls/panels to be independent from the frame class, the fragilities of a given cladding element have been obtained, irrespective of the frame typology, by considering all the collapse data available (i.e. when the wall failure anticipated the frame structural collapse).

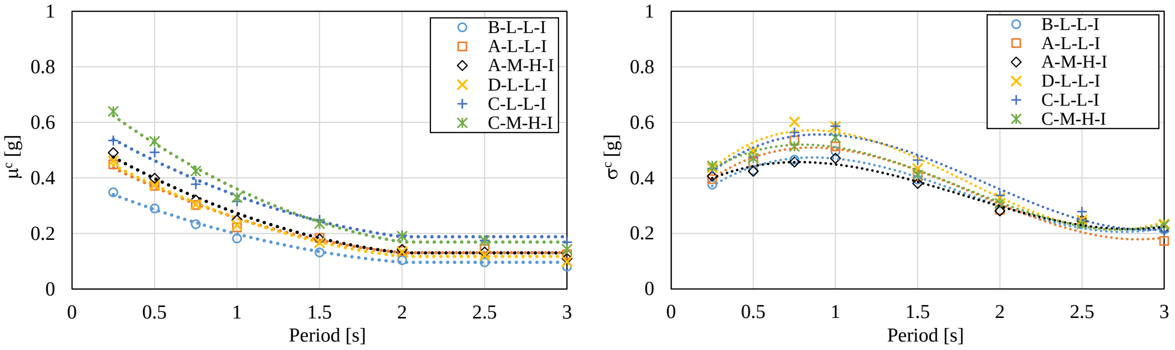

(a1) *(a2)*

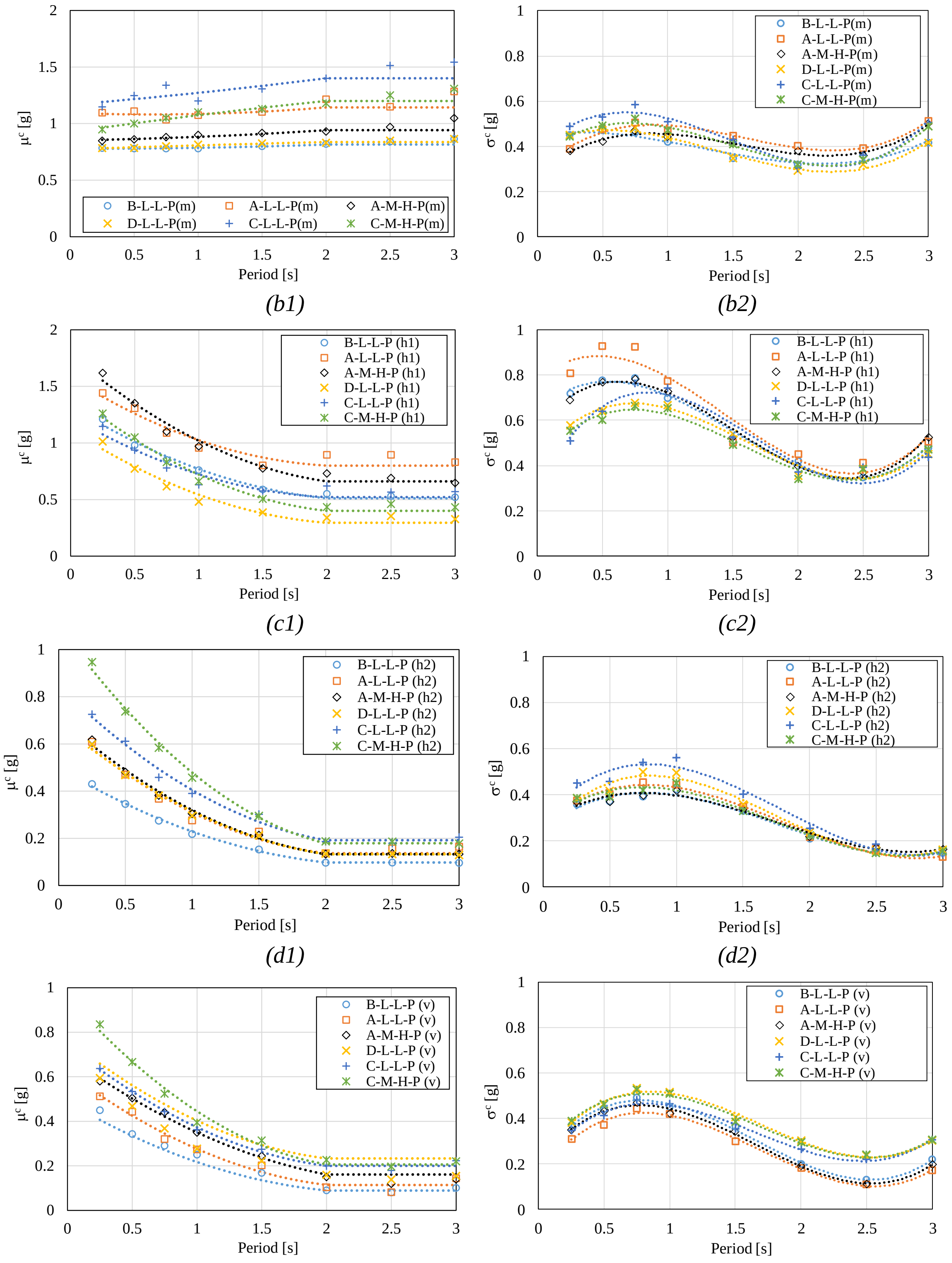

(b1) *(b2)*

(c1) *(c2)*

(d1) *(d2)*

(e1) *(e2)*

Figure 14. Trend of μ^C and σ^C of lognormal distributions at collapse for some relevant frame typologies (see Equations (3.4)), for (a) internal frames, perimeter frames with (b) masonry infills, (c) horizontal panels with (h1) connection, (d) horizontal panels with (h2) connection and (e) vertical panels.

In this way, it has been possible to establish, for the different cladding typologies and for each period investigated, the lognormal fragility functions. They have been provided assuming the same laws for the characteristic parameters of the distribution (i.e. μ and σ) as given in Equations (3.4).

The values of μ and σ of the curves of the various perimeter elements are shown in Figure 15 for the different periods of vibration. The equations of the fitting curves are reported directly in the Figures.

For masonry infill walls, a different trend has been obtained from the analyses of the different building categories, especially when comparing categories A-B and C-D. Hence, two different fitting procedures have been followed to obtain the parameters μ and σ of the lognormal collapse fragility surfaces, and the main results of the regression analyses are reported in sub-Figures a1 and a2 in Figure 15.

The results confirm a lower capacity, in terms of median S_a, for frame categories C and D with respect to categories A and B, with median collapse spectral acceleration around 0.5 g -0.6 g for C-D frames and 0.7 g-0.8 g for A and B frames. The difference is probably due to the different geometries of frames A-B and C-D (see Table 1). Indeed, due to the higher column's height of the C-D categories, top displacements are larger than those of A-B categories for analogous levels of horizontal forces. Anyway, the values of μ for a given category are quite similar as they seems to be rather insensitive to the period's variation.

Concerning σ, the values related to masonry infills in frame categories A-B and C-D have very similar trends, with the former having slightly bigger dispersion values (about 20% greater) than the latter.

The trends of μ for the two different horizontal cladding panel connections, at failure, are reported in sub-Figures b1 and c1 in Figure 15, respectively.

It is worth noting, as already emerged from the analyses at collapse of the structural frames, that the horizontal panel connections (h1) can sustain a higher acceleration before collapse with respect to connections (h2), being μ about twice in the whole range of the periods investigated. Both panel connections show that their median acceleration value at failure is strongly period-dependent: it changes significantly, for instance for (h1) connection, from about 1 g to 0.2 g by moving from 0.5 s to 2.0 s of periods. The trends of σ parameter are very similar but with higher variability for (h1) cladding panel system (see sub-Figures b2 and c2 in Figure 15).

The very different acceleration capacities between (h1) and (h2) types of cladding panel connections is in fully agreement with the in situ observations in the aftermath of the Emilia earthquakes (Savoia et al. 2017), confirming the extended damage detected in the buildings with (h2) panel connection type and, on the other hand, very few cases of failure observed for the (h1) type.

Lastly, the outcomes obtained for the vertical RC cladding panels are reported in sub-Figures d1 and d2 in Figure 15. For this type of panels, both μ and σ distributions are intermediate between those of the (h1) and (h2) typologies. Also in this case, the μ value is strongly period-dependent and σ, representing the dispersion of the outcomes basically depending on the record-to-record variability, has the usual wavy trend already observed for the other cladding typologies.

It is worth noting that the equations corresponding to the failure of the perimeter elements, reported in Figure 15, could result useful in the framework of a seismic performance and loss assessment of precast RC buildings subjected to probable seismic events (FEMA 2018).

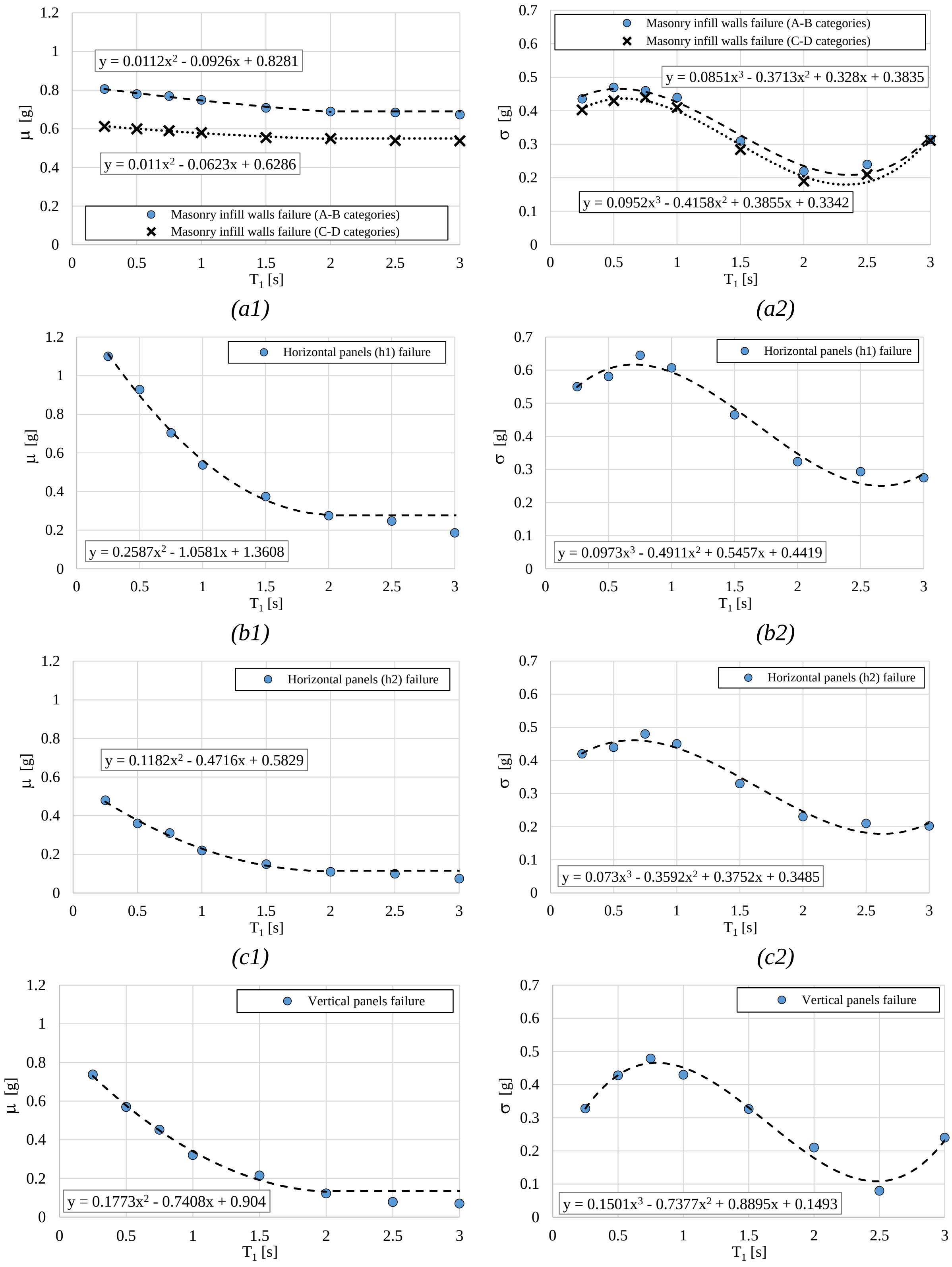

(a1) *(a2)*

(b1) *(b2)*

(c1) *(c2)*

(d1) *(d2)*

Figure 15. Trend of μ and σ of lognormal fragility curves at failure of non-structural elements for (a) masonry infilled walls, (b) horizontal cladding panels with (h1) connection, (c) horizontal cladding panels with (h2) connection and (d) vertical cladding panels.

Indeed, they represent the component fragility curves of perimeter walls/panels which are necessary, together with the fragility curves of the structural elements, in order to perform a reliable seismic loss estimation.

Moreover, while a wide literature already exists with regard to the component fragility of masonry infill panels in cast in-situ RC frames (for example see Del Gaudio et al. 2009, Rossetto et al. 2014), the component fragility of precast RC panels is not commonly provided.

3.2.4. CONCLUDING REMARKS

The aim of this study is to provide a fast procedure, named PRESSAFE-disp (PRecast Existing Structure Seismic Assessment by Fast Evaluation-displacement), for the definition of the fragility curves of one-story precast RC buildings, typical of the European areas. The methodology allows defining the seismic fragilities in a simplified framework, considering the hypothesis of flexible roof diaphragm, starting from the knowledge of few information that could be collected through a visual inspection or non-destructive tests.

A series of conclusive remarks may be highlighted. Firstly, the seismic in-plane performances of 120 different frame typologies of existing one-storey precast frames have been investigated, and the fragility curves have been obtained both for severe damage and collapse limit states. It is worth noting that the presence of the perimeter non-structural elements, typically, increases the in-plane seismic capacity of a precast frame and in general the perimeter frames result less vulnerable to the seismic action than the internal bare frames. This has been observed for almost all the frame categories at the severe damage state and, in several cases, also at the collapse state. Indeed, the increase of the collapse capacity is possible only if the non-structural walls/panels, at the attainment of the collapse of the frame, are still resisting. In general, the capacity increase is more evident for buildings with masonry infill walls.

Furthermore, the displacement-based collapse criteria significantly differentiate the results of the PRESSAFE-disp method from the results of the alternative PRESSAFE method. The analytical expressions of the fragility surfaces R(S_a ,T_1) have been obtained for each frame typology, providing the PoE as a function of S_a and T_1 for the limit state of interest. Moreover, the analytical expressions of the fragility curves defining the failure of different typologies of non-structural elements on the perimeter, i.e. masonry infill walls, horizontal precast cladding panels and vertical precast cladding panels, have been provided.

Finally, the method and the outcomes obtained allow a fast assessment of the fragilities which can be used for seismic risk analyses of large precast building stocks in seismic prone areas. It is worth saying that the results presented are representative of common typologies of precast buildings and elements observed in the Emilia Romagna territories, but they can be easily extended. Indeed, additional analyses following the same approach proposed here, but concerning other structural typologies of precast frames, or other damage mechanisms, can be conducted to widen the library of the categories included in the so-called PRESSAFE method.

3.3. SEISMIC SCENARIO ASSESSMENT OF THE INDUSTRIAL AREA OF SAN FELICE SUL PANARO

With the purpose of investigating the seismic risk of industrial areas, a simplified probabilistic large-scale methodology is presented herein. The procedure outlined is based on the PRESSAFE-disp method described in Section 3.2 (Bovo et al. 2022) for the definition of the fragility curves of precast RC buildings. Starting with the outcome made available in the previous Section, a simplified method for the estimation of the number of collapsed precast buildings in a given seismic scenario is outlined. PRESSAFE-disp offers the possibility to derive rapidly, for a high number of buildings classified into different structural typologies, the fragility surfaces that define the seismic fragility as a function of the natural period of vibration. In this context, the study presented in this Section consists in the first application of the PRESSAFE-disp method, allowing testing its feasibility in large scale analysis.

The methodology has been applied to the productive area of San Felice sul Panaro, Modena, Italy, for which detailed data on 91 precast buildings are available, together with careful descriptions of the effects of the 2012 earthquake. The structural characteristics and materials properties used in the application of the PRESSAFE-disp method are those of the pre-earthquake condition of the buildings, in order to simulate the seismic behaviour occurred at the time of the seismic shock. Through the analysis of the documents and survey data available, the pre-earthquake structural features have been established for each building, together with the damage caused by the seismic event. In particular, the latter has been derived from the documentation provided by the owners requesting for national funds for the post-earthquake reconstruction.

A Monte Carlo probabilistic simulation has been performed with the purpose of assessing the average number of collapsed buildings for the scenario selected. Moreover, the results observed are compared with those of an alternative direct simplified simulation, neglecting the effects of the uncertainties included in the Monte Carlo assessment. Finally, the outcomes of the two procedures are compared with the actual damage scenario observed after the 29th May 2012 earthquake, in order to test the reliability and accuracy of the methods.

Comparative considerations are provided and commented, showing the effect of considering different seismic inputs. In particular, the adoption of a seismic intensity including the directionality effects of the ground-motion is deemed to provide interesting results, since the outcomes of both large scale methods of simulation are in very good agreement, in terms of number of collapses, with the actual damage data observed in San Felice.

3.3.1. THE CASE-STUDY AREA

3.3.1.1. MAIN CHARACTERISTICS OF THE BUILDINGS

For the large-scale seismic damage scenario assessment, the productive area of San Felice sul Panaro (province of Modena, Emilia Romagna region, with average coordinates 44.835844°, 11.125078°) has been selected as case study, with reference to 91 precast RC buildings. These were severely damaged by the 29th May 2012 earthquake, which had an epicentre at 4 km from this area (see Figure 16), while they experienced nearly no damage from previous shocks. Furthermore, a ground-motion recording station was present nearby (SAN0, INGV). The perimeter of the area is highlighted in red in Figure 16.

The effects of the earthquake on the buildings are clearly visible in Figure 17; the first aerial picture was taken one year before the main shock and the second two years after the earthquake. From the pictures, it is possible to identify the different layouts of some clusters in the area, due to the demolition of few units. The aerial view in Figure 18 highlights the 91 buildings in the case-study area. The red markers indicate the 42 buildings collapsed (according to the criteria indicated in Section 3.2.1.3) during the 29th May 2012 main shock.

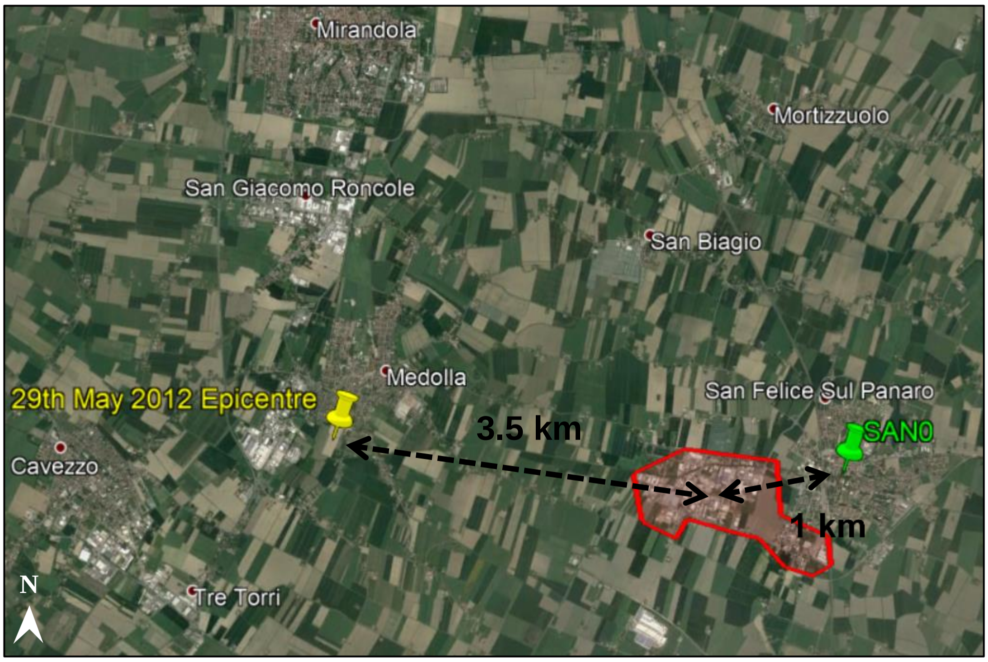

Figure 16. Google Earth (2020) aerial view: the 29th May 2012 main shock epicentre, the productive area of San Felice sul Panaro (the red polygon), and the ground-motion recording station SAN0.

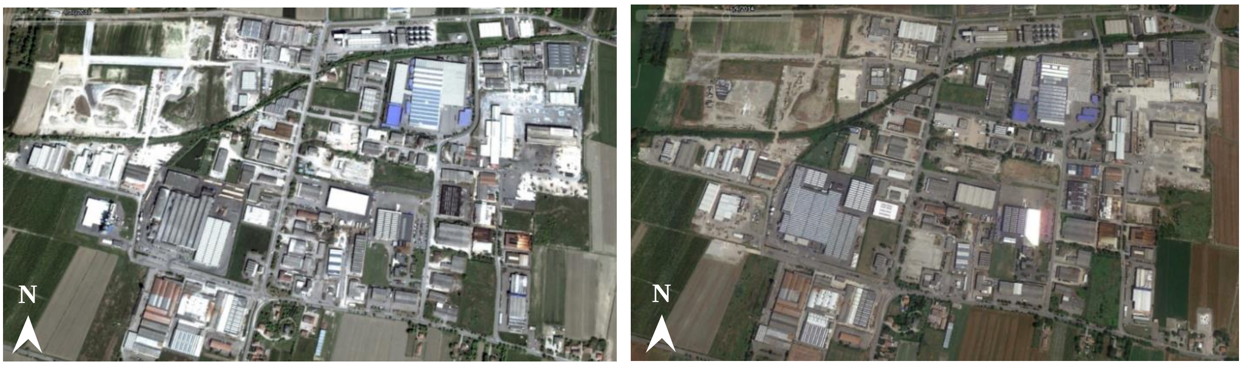

(a) *(b)*

Figure 17. Google Earth (2020) aerial views of the San Felice sul Panaro main productive area (a) before (21 April 2011), and (b) after (9 June 2014) the Emilia earthquake of 29th May 2012.

In 2012, all the 91 buildings featured one storey only and had a rectangular shape in plan, with dimensions ranging from 10.0 m to 150.0 m, and plan surfaces ranging from about 150 m^2 to 13700 m^2. The building heights varied from 3.0 m to 10.0 m. The column cross-section dimensions ranged between 25.0 cm and 70.0 cm, the beam spans between 6.0 m and 25.0 m, while the roofing elements length between 5.0 m and 30.0 m. The beam cross-sections were L-shaped, reverse T-shaped, tapered I-shaped, constant I-shaped, H-shaped, Y-shaped, Ω-shaped and shed beams. The floor slab element cross-sections were double tee shape, Y-shaped, rectangular box, hollow cored, channel shaped, wing shaped and shed elements.

3.3.1.2. OBSERVED DAMAGE IN THE AREA

The damage severity for each building was defined based on both accurate building inspections in the aftermath of the earthquake, and on information available from the technical documents issued for obtaining public funds for the post-earthquake reconstruction. The damage mechanisms reflect those identified in Section 3.1.1.

In many cases, the main frames of the buildings had significant horizontal relative displacements at the roof level, causing damage to the connections or the loss-of-support collapse of the horizontal beams and roof slab elements (see Figure 19a-c). In some buildings, the unseating failure of beams and roofing elements did not occur, but large residual displacements were visible (see Figure 19d). Another common damage mechanism was the formation of plastic hinges at base of columns, with concrete cover expulsion, wide cracks and considerable deformations of the longitudinal bars (see Figure 19e-f), sometimes with bar buckling. Moreover, damage to the cladding walls was also

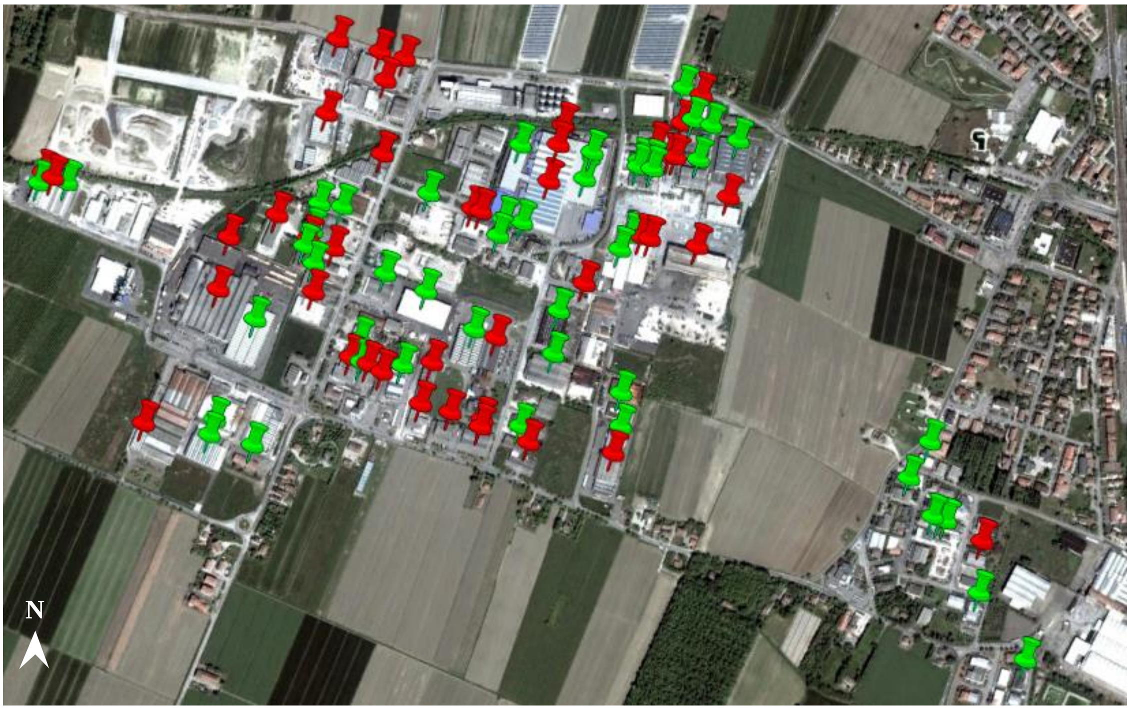

Figure 18. Google Earth (2020) aerial view with the position of the precast buildings. In red the buildings collapsed during the 29th May 2012 main shock.

common, involving cracks or overturning of infill masonry walls (see Figure 19g-h) or detachment of precast RC cladding panels (see Figure 19i-l) because of the failure of the connections.

3.3.1.3. CLASSIFICATION OF THE FRAMES

The first step for the application of the PRESSAFE-disp method is the attribution of a proper category to the frames of each building based on the taxonomy reported in Section 3.2.1.1. A frame class is to be considered representative of frames which share the same column capacity, type of structural connections and cladding type (if present), but which can have different natural periods of vibration. All the necessary structural details (e.g. geometry, dimensions, beam and roof element typology, column cross-section, material properties, connections, cladding etc.) were extracted from the documents available, or detected during the visual inspections.

The frame category selected for each of the 91 precast buildings are reported in Table 3. Three buildings did not have internal frames (due to their small dimensions) and three did not have perimeter frames since they were used as open storage areas. The symbols used for the classification are those adopted in PRESSAFE-disp.

In the few cases with incomplete documentation, the missing parameters were assumed by engineering judgements based on similarities with other buildings. Moreover, in some cases it was not possible to establish if the collapse occurred in the internal, perimeter or in both the frame types. This may influence the probabilistic calculation, which considers a separated seismic behaviour of the frames of the building, as further explained in the following Sections.

The internal and the perimeter frame categories, adopted for the 91 buildings in the case-study area, are illustrated in Figure 20a-d.

The disaggregation of the classification criteria of the frame categories is plotted in Figure 20e and 20f. The internal frames were classified into 13 categories, reported in the pie plot in Figure 20a. The values in this figure represent the number of frames belonging to each category.

Among the internal frames, 46 of them were associated to the lowest flexural capacity of columns (A), while 21, 20 and 1 were classified as (B), (C) and (D), respectively (see Figure 20e). On the other hand, 23 categories were used to classify the perimeter frames, which are represented in separated pie graphs based on the cladding typology (see Figure 20b-d). The majority of the perimeter frames, i.e. 42, had infill masonry walls (m), 29 frames had RC horizontal cladding panels (h2), and 17 frames had RC vertical cladding panels (v) (see Figure 20f).

Most of the frames had friction-based supports (code (L), meaning low strength). In particular, 67 frames featured this type of support in the beam-column connections and 79 frames in the roof-beam connections. Regarding the beam-column connections, 14 frames were classified as medium-strength connection type (M), whereas 7 frames as high strength connection type (H). Finally, only 9 frames had roof-beam connections classified as (H), i.e. high strength.

It is important to notice that the widespread adoption of friction-connections and the low moment-capacity of columns, is mainly due to the lack of seismic design of the buildings in the area under consideration. In fact, the area of interest was classified as non-seismic until 2003.

(a) *(b)* *(c)*

(e) *(f)* *(g)*

(g) *(h)*

(i) *(l)*

Figure 19. Collapse and damage mechanisms observed in the buildings in the case-study area of San Felice.

Table 3. Main parameters of the 91 precast RC buildings considered in the study.

#	Surface [m^2]	Column height [m]	Beam length [m]	T_1 [s] perimeter frame	T_1 [s] internal frame	Internal frame class	Perimeter frame class	Building collapsed
1	1276	7.2	21.1	1.07	0.76	C-L-L-I	C-L-L-P (m)	Y
2	389	5.0	19.7	0.92	0.65	A-M-L-I	A-M-L-P (v)	N
3	182	5.3	15.0	/	0.58	/	A-M-L-P (v)	N
4	387	5.3	15.0	0.70	0.50	A-M-L-I	A-M-L-P (v)	N
5	336	6.4	14.0	1.11	0.78	B-L-L-I	B-L-L-P (m)	Y
6	392	6.2	14.6	0.45	0.32	C-L-L-I	C-L-L-P (h2)	Y
7	140	4.5	9.4	0.45	0.32	B-M-L-I	B-M-L-P (h2)	Y
8	834	6.5	8.9	0.81	0.58	B-M-H-I	B-M-H-P (h2)	N
9	1617	6.0	16.4	1.04	0.73	B-M-H-I	B-M-H-P (m)	N
10	4958	8.6	19.5	1.88	1.83	B-M-L-I	B-M-L-P (h2)	N
11	1068	6.9	12.6	1.48	1.05	A-L-L-I	A-L-L-P (m)	Y
12	1280	7.0	16.0	1.56	1.10	A-L-L-I	A-L-L-P (m)	N
13	561	7.0	18.3	1.60	1.13	A-L-L-I	A-L-L-P (m)	Y
14	254	5.3	10.1	0.79	0.56	A-L-L-I	A-L-L-P (m)	N
15	714	5.0	17.0	0.60	0.43	A-M-L-I	A-M-L-P (m)	N
16	714	5.0	17.0	0.82	0.58	A-M-L-I	A-M-L-P (m)	N
17	3647	6.5	6.0	0.66	0.47	A-H-L-I	A-H-L-P (m)	N
18	1404	5.5	13.0	0.52	0.37	A-L-L-I	A-L-L-P (m)	Y
19	1855	5.9	20.3	0.85	0.60	A-L-L-I	A-L-L-P (m)	N
20	1115	3.8	20.4	0.44	0.31	A-L-L-I	A-L-L-P (v)	Y
21	896	4.5	10.5	0.46	0.33	A-M-H-I	A-M-H-P (v)	N
22	307	6.9	16.8	1.63	1.15	A-M-L-I	A-M-L-P (m)	N
23	1230	8.5	20.5	1.03	0.73	C-L-L-I	C-L-L-P (h2)	Y
24	820	8.5	20.5	1.03	0.73	C-L-L-I	C-L-L-P (h2)	Y
25	236	10.0	20.5	/	0.93	/	C-L-L-P (m)	N
26	2460	8.5	20.5	1.78	1.26	C-L-L-I	C-L-L-P (h2)	N
27	684	4.7	19.0	0.59	0.42	C-L-L-I	C-L-L-P (v)	Y
28	570	6.1	19.0	1.29	0.92	A-L-L-I	A-L-L-P (h2)	N
29	4104	7.1	18.0	1.61	1.14	A-L-L-I	A-L-L-P (m)	N
30	2687	8.0	11.0	1.47	1.04	B-L-L-I	B-L-L-P (h2)	Y
31	3514	8.0	17.5	1.25	0.88	B-L-L-I	B-L-L-P (h2)	Y
32	1464	6.0	15.0	1.08	0.76	A-L-L-I	A-L-L-P (h2)	Y
33	251	4.6	10.6	1.19	0.84	A-L-L-I	A-L-L-P (m)	N
34	627	5.0	14.0	0.54	0.38	B-L-L-I	B-L-L-P (m)	N
35	161	7.6	12.8	1.15	0.81	A-L-L-I	A-L-L-P (m)	N
36	384	6.7	12.8	1.17	0.82	A-L-L-I	A-L-L-P (m)	N
37	161	7.6	12.8	1.15	0.81	A-L-L-I	A-L-L-P (m)	N
38	384	6.7	12.8	1.17	0.82	A-L-L-I	A-L-L-P (m)	N
39	7378	8.9	13.0	1.07	0.75	C-L-L-I	C-L-L-P (v)	N
40	13750	4.5	15.7	0.50	0.35	A-L-L-I	A-L-L-P (m)	Y
41	2379	9.3	20.0	1.19	/	C-L-L-I	/	Y
42	7752	6.0	8.5	0.73	0.51	B-L-L-I	B-L-L-P (h2)	Y
43	1380	7.6	15.0	1.36	/	C-M-H-I	/	N
44	4484	8.0	5.9	0.83	0.59	B-L-L-I	B-L-L-P (h2)	Y
45	5400	7.6	8.5	1.76	1.24	C-M-H-I	C-M-H-P (v)	N
46	1596	8.0	8.0	0.89	0.63	B-L-L-I	B-L-L-P (v)	Y
47	2542	7.7	10.0	/	1.21	/	C-M-H-P (h2)	N
48	902	4.3	18.5	1.18	0.83	A-L-L-I	A-L-L-P (m)	Y
49	434	5.9	14.2	1.09	0.77	A-L-L-I	A-L-L-P (m)	N
50	337	5.9	14.1	1.07	0.76	A-L-L-I	A-L-L-P (m)	N
51	551	7.9	18.1	1.89	1.34	A-L-L-I	A-L-L-P (m)	Y
52	954	7.1	22.5	1.11	0.79	A-L-L-I	A-L-L-P (m)	N

53	827	3.6	18.6	0.63	0.44	A-L-L-I	A-L-L-P (h2)	N
54	2373	6.6	12.0	1.34	0.95	A-L-L-I	A-L-L-P (m)	Y
55	506	6.5	21.0	0.84	0.68	B-L-L-I	B-L-L-P (h2)	N
56	566	6.0	18.7	0.55	0.39	C-L-L-I	C-L-L-P (h2)	Y
57	756	6.5	14.0	0.92	0.65	A-L-L-I	A-L-L-P (h2)	N
58	675	7.0	22.2	1.22	0.86	A-H-L-I	A-H-L-P (m)	N
59	3986	8.1	10.0	1.48	1.04	C-H-H-I	C-H-H-P (v)	N
60	1952	5.8	16.0	0.66	0.47	B-L-L-I	B-L-L-P (m)	Y
61	1080	5.0	15.0	0.82	0.60	A-L-L-I	A-L-L-P (m)	Y
62	405	4.0	7.5	0.22	0.16	B-L-L-I	B-L-L-P (v)	Y
63	1088	5.3	20.0	0.57	0.40	B-L-L-I	B-L-L-P (v)	Y
64	935	5.8	8.7	0.58	0.41	B-L-L-I	B-L-L-P (h2)	Y
65	300	6.2	10.0	0.52	0.37	B-L-L-I	B-L-L-P (m)	Y
66	300	6.2	15.0	0.82	0.58	C-L-L-I	C-L-L-P (m)	N
67	880	4.5	11.0	0.65	0.46	C-L-L-I	C-L-L-P (h2)	Y
68	2442	5.9	9.3	0.86	0.61	A-L-L-I	A-L-L-P (h2)	Y
69	656	4.5	15.5	1.44	1.02	A-L-L-I	A-L-L-P (m)	N
70	419	6.5	17.2	1.03	0.73	A-L-L-I	A-L-L-P (h2)	Y
71	410	6.5	16.8	1.03	0.72	A-L-L-I	A-L-L-P (m)	Y
72	2604	6.7	10.0	1.04	0.74	C-H-H-I	C-H-H-P (h2)	N
73	750	6.0	15.0	1.09	0.77	B-H-H-I	B-H-H-P (m)	N
74	581	7.0	18.5	1.06	0.75	A-L-L-I	A-L-L-P (v)	N
75	1810	7.0	18.1	0.95	0.84	A-L-L-I	A-L-L-P (v)	N
76	1806	5.2	12.5	0.80	0.57	C-H-H-I	C-H-H-P (v)	Y
77	2020	7.0	19.0	1.38	0.96	B-M-L-I	B-M-L-P (h2)	N
78	1791	7.0	20.0	1.29	0.91	B-L-L-I	B-L-L-P (h2)	Y
79	1000	6.0	19.7	1.38	0.98	A-L-L-I	A-L-L-P (m)	Y
80	678	6.8	16.0	0.93	0.66	B-L-L-I	B-L-L-P (m)	Y
81	5971	10.0	23.0	1.52	1.08	D-L-L-I	D-L-L-P (h2)	Y
82	1909	9.1	16.5	1.32	0.93	A-L-L-I	A-L-L-P (m)	Y
83	3070	7.1	20.2	1.67	1.18	A-L-L-I	A-L-L-P (m)	N
84	263	4.2	6.2	0.42	/	A-L-L-I	/	Y
85	495	4.6	10.0	0.49	0.35	A-L-L-I	A-L-L-P (m)	N
86	2358	9.5	20.5	1.07	0.76	A-L-L-I	A-L-L-P (m)	Y
87	581	6.3	16.4	0.72	0.51	A-L-L-I	A-L-L-P (h2)	N
88	320	6.8	16.4	0.67	0.47	C-L-L-I	C-L-L-P (h2)	N
89	389	6.3	11.8	0.47	0.33	C-L-L-I	C-L-L-P (h2)	N
90	900	4.0	6.5	0.26	0.18	C-L-L-I	C-L-L-P (v)	Y
91	1350	4.0	6.5	0.26	0.18	C-H-L-I	C-H-L-P (v)	N

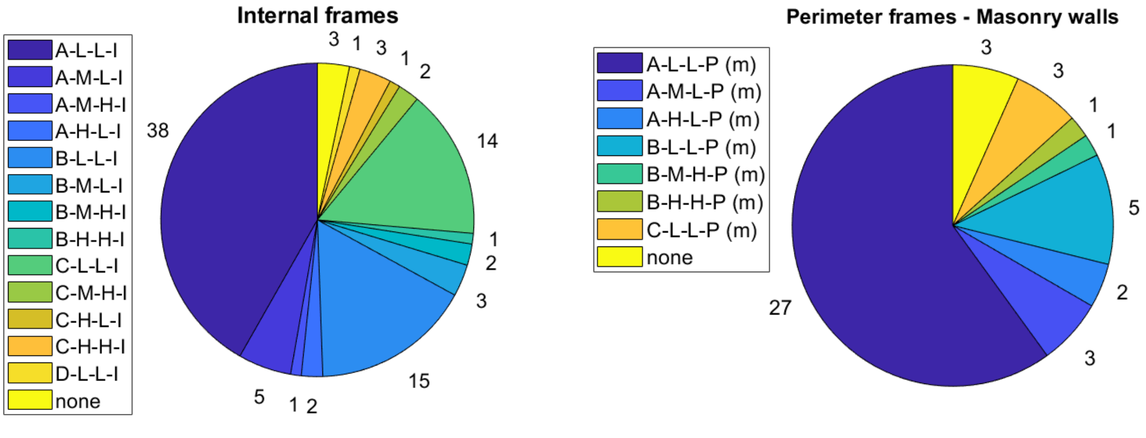

(a) *(b)*

3.3.1.4. DERIVATION OF THE FRAGILITY CURVES

The PRESSAFE-disp method defines the seismic fragility of each frame class as a function of the natural period of vibration, as discussed in Section 3.2.3. The first period of vibration is calculated for each frame considering the columns as cantilevers. This simple structural scheme is acceptable in one-storey precast RC buildings, in which usually the roof does not constitute a rigid diaphragm, as reported for example in Minghini et al. (2016). Therefore, the lateral stiffness K_f of each frame was:

$$K_f \;=\; \sum_i K_{c,i} = \sum_i 3E_c J_i / l_i^3 \tag{3.6}$$

where $K_{c,i}$, J_i, and l_i are the lateral stiffness, the second moment of the cross-section and the length of the *i*-th column, respectively, and E_c is the Young modulus of concrete.

The mass adopted to calculate the natural period was estimated from the load analysis. Table 3 reports the periods of the internal and the perimeter frames of all the buildings in the case-study area. Coherently with the method adopted, the periods of vibration are determined considering the bare frames, i.e., not considering the presence of the cladding elements. After the classification of the frames of the buildings and the calculation of their period of vibration, the parameters of the collapse

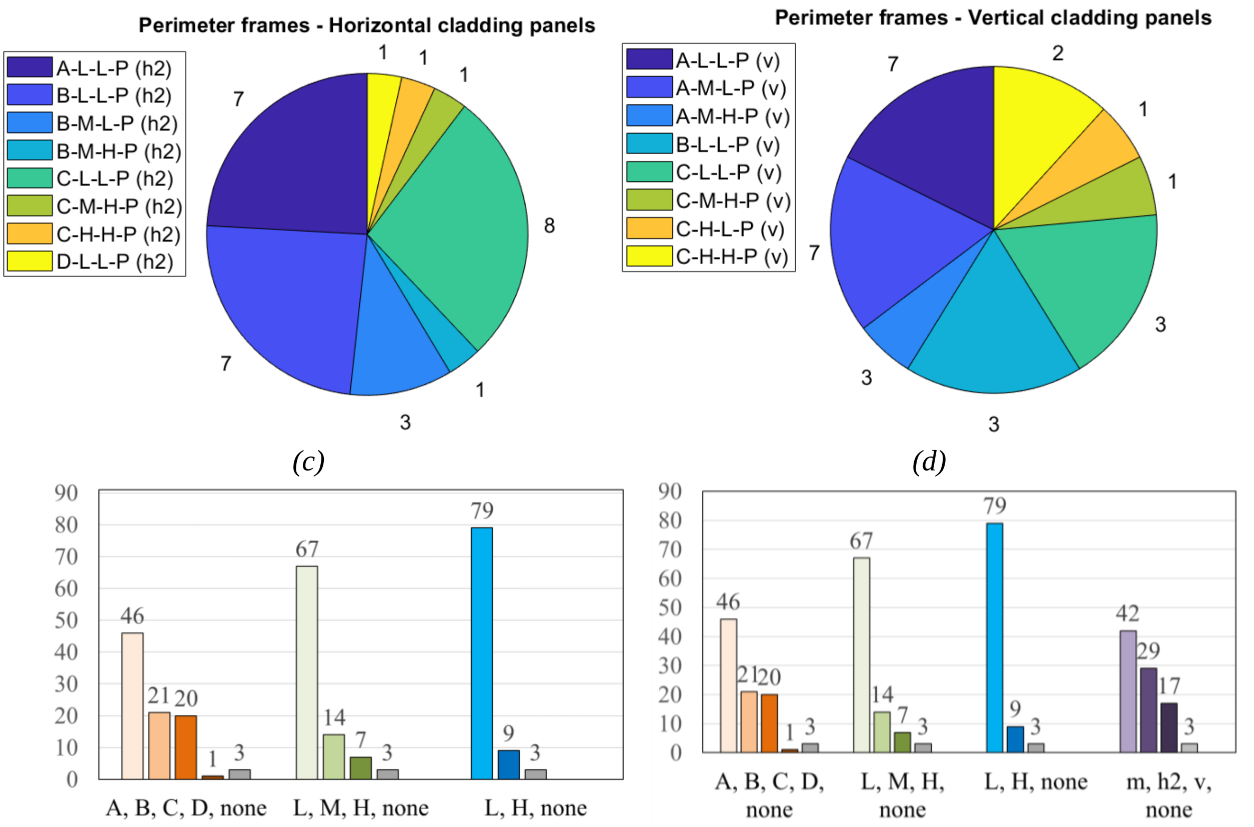

(c) *(d)*

(e) *(f)*

Figure 20. Classification of the frames of the 91 buildings following PRESSAFE-disp: (a) internal frames; (b) perimeter frames with masonry infills, (c) precast RC horizontal cladding panels, (d) precast RC vertical cladding panels. Disaggregation of the 91 categories of the (e) internal frames and (f) perimeter frames.

fragility curve for each frame (see Tables 4 and 5) were computed using Equations (3.4). The fragility curves obtained by means of the PRESSAFE-disp method are plotted in Figure 21a-b for the internal and perimeter frames, respectively. The Figures show that the fragility curves of the internal frames are less scattered than those of the perimeter frames. This is, in part, because there is a strong variability in the perimeter frames due to the different type of cladding, i.e., infill masonry walls, horizontal RC cladding panels and vertical RC cladding panels.

Moreover, in general, the fragility curves for the internal frames are characterized by lower median values (i.e. the values corresponding to PoE=0.5) than those for perimeter frames (e.g., ranging from 0.1 *g* to 0.5 *g* for the internal frames and from 0.25 *g* to 1.25 *g* for perimeter frames). The higher value of capacity (considering the median value) of the perimeter frames is due to the effect of cladding.

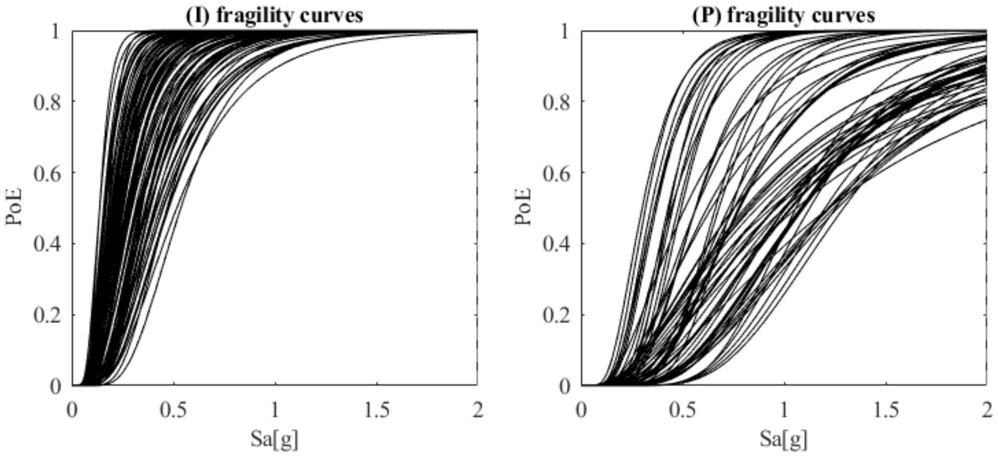

(a) *(b)*

Figure 21. Fragility curves obtained with the PRESSAFE-disp method for (a) internal frames and (b) perimeter frames, for the 91 buildings of the case-study area.

Table 4. PRESSAFE-disp coefficients (a1-b4) for the 91 internal frame fragility curves in San Felice; median value (μ^C) and standard deviation (σ^C) at the collapse limit state.

# building	μ^C (I)	σ^C (I)	a1	a2	a3	b1	b2	b3	b4
1	0.320	0.549	0.070	-0.358	0.624	0.086	-0.491	0.675	0.284
2	0.342	0.493	0.070	-0.306	0.564	0.078	-0.462	0.589	0.281
3	0.000	0.000	0.000	0.000	0.000	0.000	0.000	0.000	0.000
4	0.385	0.494	0.070	-0.306	0.564	0.078	-0.462	0.589	0.281
5	0.183	0.461	0.050	-0.252	0.400	0.079	-0.430	0.565	0.255
6	0.478	0.495	0.070	-0.358	0.624	0.086	-0.491	0.675	0.284
7	0.344	0.427	0.053	-0.237	0.440	0.073	-0.426	0.542	0.263
8	0.256	0.463	0.047	-0.265	0.440	0.076	-0.400	0.559	0.232
9	0.216	0.467	0.047	-0.265	0.440	0.076	-0.400	0.559	0.232
10	0.180	0.267	0.053	-0.237	0.440	0.073	-0.426	0.542	0.263
11	0.179	0.431	0.067	-0.325	0.513	0.084	-0.467	0.614	0.273
12	0.169	0.414	0.067	-0.325	0.513	0.084	-0.467	0.614	0.273
13	0.165	0.405	0.067	-0.325	0.513	0.084	-0.467	0.614	0.273
14	0.297	0.508	0.067	-0.325	0.513	0.084	-0.467	0.614	0.273
15	0.405	0.486	0.070	-0.306	0.564	0.078	-0.462	0.589	0.281
16	0.361	0.497	0.070	-0.306	0.564	0.078	-0.462	0.589	0.281
17	0.341	0.447	0.069	-0.322	0.523	0.084	-0.504	0.589	0.254

18	0.361	0.479	0.067	-0.325	0.513	0.084	-0.467	0.614	0.273
19	0.285	0.509	0.067	-0.325	0.513	0.084	-0.467	0.614	0.273
20	0.383	0.460	0.067	-0.325	0.513	0.084	-0.467	0.614	0.273
21	0.409	0.438	0.072	-0.359	0.560	0.059	-0.316	0.385	0.322
22	0.253	0.352	0.070	-0.306	0.564	0.078	-0.462	0.589	0.281
23	0.328	0.552	0.070	-0.358	0.624	0.086	-0.491	0.675	0.284
24	0.328	0.552	0.070	-0.358	0.624	0.086	-0.491	0.675	0.284
25	0.000	0.000	0.000	0.000	0.000	0.000	0.000	0.000	0.000
26	0.209	0.415	0.070	-0.358	0.624	0.086	-0.491	0.675	0.284
27	0.436	0.529	0.070	-0.358	0.624	0.086	-0.491	0.675	0.284
28	0.205	0.467	0.067	-0.325	0.513	0.084	-0.467	0.614	0.273
29	0.164	0.402	0.067	-0.325	0.513	0.084	-0.467	0.614	0.273
30	0.138	0.408	0.050	-0.252	0.400	0.079	-0.430	0.565	0.255
31	0.163	0.444	0.050	-0.252	0.400	0.079	-0.430	0.565	0.255
32	0.240	0.497	0.067	-0.325	0.513	0.084	-0.467	0.614	0.273
33	0.220	0.483	0.067	-0.325	0.513	0.084	-0.467	0.614	0.273
34	0.278	0.448	0.050	-0.252	0.400	0.079	-0.430	0.565	0.255
35	0.228	0.489	0.067	-0.325	0.513	0.084	-0.467	0.614	0.273
36	0.225	0.487	0.067	-0.325	0.513	0.084	-0.467	0.614	0.273
37	0.228	0.489	0.067	-0.325	0.513	0.084	-0.467	0.614	0.273
38	0.225	0.487	0.067	-0.325	0.513	0.084	-0.467	0.614	0.273
39	0.322	0.550	0.070	-0.358	0.624	0.086	-0.491	0.675	0.284
40	0.368	0.473	0.067	-0.325	0.513	0.084	-0.467	0.614	0.273
41	0.297	0.537	0.070	-0.358	0.624	0.086	-0.491	0.675	0.284
42	0.244	0.469	0.050	-0.252	0.400	0.079	-0.430	0.565	0.255
43	0.271	0.460	0.092	-0.467	0.735	0.085	-0.447	0.553	0.321
44	0.225	0.473	0.050	-0.252	0.400	0.079	-0.430	0.565	0.255
45	0.199	0.371	0.092	-0.467	0.735	0.085	-0.447	0.553	0.321
46	0.216	0.473	0.050	-0.252	0.400	0.079	-0.430	0.565	0.255
47	0.000	0.000	0.000	0.000	0.000	0.000	0.000	0.000	0.000
48	0.224	0.486	0.067	-0.325	0.513	0.084	-0.467	0.614	0.273
49	0.239	0.497	0.067	-0.325	0.513	0.084	-0.467	0.614	0.273
50	0.242	0.498	0.067	-0.325	0.513	0.084	-0.467	0.614	0.273
51	0.138	0.331	0.067	-0.325	0.513	0.084	-0.467	0.614	0.273
52	0.234	0.494	0.067	-0.325	0.513	0.084	-0.467	0.614	0.273
53	0.336	0.495	0.067	-0.325	0.513	0.084	-0.467	0.614	0.273
54	0.197	0.459	0.067	-0.325	0.513	0.084	-0.467	0.614	0.273
55	0.223	0.473	0.050	-0.252	0.400	0.079	-0.430	0.565	0.255
56	0.448	0.521	0.070	-0.358	0.624	0.086	-0.491	0.675	0.284
57	0.270	0.508	0.067	-0.325	0.513	0.084	-0.467	0.614	0.273
58	0.234	0.376	0.069	-0.322	0.523	0.084	-0.504	0.589	0.254
59	0.360	0.456	0.088	-0.434	0.809	0.081	-0.425	0.531	0.337
60	0.255	0.464	0.050	-0.252	0.400	0.079	-0.430	0.565	0.255
61	0.291	0.509	0.067	-0.325	0.513	0.084	-0.467	0.614	0.273
62	0.347	0.359	0.050	-0.252	0.400	0.079	-0.430	0.565	0.255
63	0.273	0.452	0.050	-0.252	0.400	0.079	-0.430	0.565	0.255
64	0.271	0.453	0.050	-0.252	0.400	0.079	-0.430	0.565	0.255
65	0.282	0.444	0.050	-0.252	0.400	0.079	-0.430	0.565	0.255
66	0.377	0.555	0.070	-0.358	0.624	0.086	-0.491	0.675	0.284
67	0.420	0.539	0.070	-0.358	0.624	0.086	-0.491	0.675	0.284
68	0.283	0.509	0.067	-0.325	0.513	0.084	-0.467	0.614	0.273
69	0.184	0.440	0.067	-0.325	0.513	0.084	-0.467	0.614	0.273
70	0.250	0.502	0.067	-0.325	0.513	0.084	-0.467	0.614	0.273
71	0.249	0.501	0.067	-0.325	0.513	0.084	-0.467	0.614	0.273
72	0.451	0.521	0.088	-0.434	0.809	0.081	-0.425	0.531	0.337
73	0.195	0.563	0.050	-0.249	0.408	0.087	-0.387	0.582	0.275
74	0.243	0.499	0.067	-0.325	0.513	0.084	-0.467	0.614	0.273

75	0.265	0.507	0.067	-0.325	0.513	0.084	-0.467	0.614	0.273
76	0.517	0.532	0.088	-0.434	0.809	0.081	-0.425	0.531	0.337
77	0.213	0.393	0.053	-0.237	0.440	0.073	-0.426	0.542	0.263
78	0.158	0.438	0.050	-0.252	0.400	0.079	-0.430	0.565	0.255
79	0.192	0.451	0.067	-0.325	0.513	0.084	-0.467	0.614	0.273
80	0.208	0.472	0.050	-0.252	0.400	0.079	-0.430	0.565	0.255
81	0.166	0.446	0.067	-0.339	0.527	0.113	-0.610	0.780	0.274
82	0.201	0.463	0.067	-0.325	0.513	0.084	-0.467	0.614	0.273
83	0.157	0.387	0.067	-0.325	0.513	0.084	-0.467	0.614	0.273
84	0.388	0.455	0.067	-0.325	0.513	0.084	-0.467	0.614	0.273
85	0.369	0.472	0.067	-0.325	0.513	0.084	-0.467	0.614	0.273
86	0.241	0.498	0.067	-0.325	0.513	0.084	-0.467	0.614	0.273
87	0.313	0.504	0.067	-0.325	0.513	0.084	-0.467	0.614	0.273
88	0.415	0.542	0.070	-0.358	0.624	0.086	-0.491	0.675	0.284
89	0.472	0.501	0.070	-0.358	0.624	0.086	-0.491	0.675	0.284
90	0.537	0.426	0.070	-0.358	0.624	0.086	-0.491	0.675	0.284
91	0.469	0.411	0.063	-0.383	0.563	0.083	-0.479	0.547	0.301

Table 5. PRESSAFE-disp coefficients (a1-b4) for the 91 perimeter frame fragility curves in San Felice; median value (μ^C) and standard deviation (σ^C) at the collapse limit state.

# building	μ^C (P)	σ^C (P)	a1	a2	a3	b1	b2	b3	b4
1	1.245	0.548	0.012	0.093	1.167	0.119	-0.525	0.546	0.384
2	0.429	0.368	0.095	-0.426	0.667	0.132	-0.645	0.689	0.156
3	0.452	0.364	0.095	-0.426	0.667	0.132	-0.645	0.689	0.156
4	0.478	0.355	0.095	-0.426	0.667	0.132	-0.645	0.689	0.156
5	0.783	0.442	0.011	-0.004	0.779	0.043	-0.160	0.090	0.449
6	0.773	0.529	0.120	-0.510	0.922	0.135	-0.664	0.788	0.342
7	0.536	0.807	0.083	-0.354	0.640	0.130	-0.495	0.422	0.719
8	0.303	0.376	0.069	-0.347	0.480	0.069	-0.385	0.397	0.262
9	0.727	0.455	0.011	-0.004	0.724	0.039	-0.150	0.097	0.449
10	0.270	0.630	0.083	-0.354	0.640	0.130	-0.495	0.422	0.719
11	1.086	0.491	0.034	-0.044	1.095	0.087	-0.411	0.527	0.290
12	1.088	0.488	0.034	-0.044	1.095	0.087	-0.411	0.527	0.290
13	1.089	0.486	0.034	-0.044	1.095	0.087	-0.411	0.527	0.290
14	1.081	0.472	0.034	-0.044	1.095	0.087	-0.411	0.527	0.290
15	1.005	0.469	0.033	-0.045	1.018	0.079	-0.386	0.569	0.290
16	1.003	0.506	0.033	-0.045	1.018	0.079	-0.386	0.569	0.290
17	1.217	0.504	0.033	-0.041	1.229	0.086	-0.351	0.521	0.329
18	1.083	0.433	0.034	-0.044	1.095	0.087	-0.411	0.527	0.290
19	1.081	0.477	0.034	-0.044	1.095	0.087	-0.411	0.527	0.290
20	0.494	0.332	0.091	-0.435	0.620	0.120	-0.606	0.744	0.156
21	0.564	0.382	0.077	-0.420	0.693	0.124	-0.617	0.729	0.205
22	1.010	0.554	0.033	-0.045	1.018	0.079	-0.386	0.569	0.290
23	0.613	0.616	0.120	-0.510	0.922	0.135	-0.664	0.788	0.342
24	0.613	0.616	0.120	-0.510	0.922	0.135	-0.664	0.788	0.342
25	1.264	0.533	0.012	0.093	1.167	0.119	-0.525	0.546	0.384
26	0.470	0.551	0.120	-0.510	0.922	0.135	-0.664	0.788	0.342
27	0.565	0.406	0.099	-0.470	0.744	0.115	-0.571	0.713	0.200
28	0.658	0.688	0.097	-0.393	0.936	0.149	-0.631	0.482	0.661
29	1.089	0.486	0.034	-0.044	1.095	0.087	-0.411	0.527	0.290
30	0.451	0.672	0.083	-0.337	0.711	0.127	-0.550	0.440	0.666
31	0.478	0.713	0.083	-0.337	0.711	0.127	-0.550	0.440	0.666
32	0.693	0.728	0.097	-0.393	0.936	0.149	-0.631	0.482	0.661
33	1.082	0.494	0.034	-0.044	1.095	0.087	-0.411	0.527	0.290
34	0.779	0.462	0.011	-0.004	0.779	0.043	-0.160	0.090	0.449

35	1.082	0.494	0.034	-0.044	1.095	0.087	-0.411	0.527	0.290
36	1.082	0.494	0.034	-0.044	1.095	0.087	-0.411	0.527	0.290
37	1.082	0.494	0.034	-0.044	1.095	0.087	-0.411	0.527	0.290
38	1.082	0.494	0.034	-0.044	1.095	0.087	-0.411	0.527	0.290
39	0.446	0.462	0.099	-0.470	0.744	0.115	-0.571	0.713	0.200
40	1.084	0.428	0.034	-0.044	1.095	0.087	-0.411	0.527	0.290
41	0.000	0.000	0.000	0.000	0.000	0.000	0.000	0.000	0.000
42	0.560	0.764	0.083	-0.337	0.711	0.127	-0.550	0.440	0.666
43	0.000	0.000	0.000	0.000	0.000	0.000	0.000	0.000	0.000
44	0.541	0.760	0.083	-0.337	0.711	0.127	-0.550	0.440	0.666
45	0.362	0.466	0.138	-0.653	0.960	0.115	-0.576	0.714	0.247
46	0.301	0.471	0.071	-0.341	0.487	0.130	-0.643	0.764	0.213
47	0.426	0.547	0.121	-0.544	0.907	0.131	-0.650	0.838	0.252
48	1.082	0.494	0.034	-0.044	1.095	0.087	-0.411	0.527	0.290
49	1.081	0.492	0.034	-0.044	1.095	0.087	-0.411	0.527	0.290
50	1.081	0.491	0.034	-0.044	1.095	0.087	-0.411	0.527	0.290
51	1.097	0.468	0.034	-0.044	1.095	0.087	-0.411	0.527	0.290
52	1.081	0.493	0.034	-0.044	1.095	0.087	-0.411	0.527	0.290
53	0.782	0.764	0.097	-0.393	0.936	0.149	-0.631	0.482	0.661
54	1.084	0.494	0.034	-0.044	1.095	0.087	-0.411	0.527	0.290
55	0.519	0.750	0.083	-0.337	0.711	0.127	-0.550	0.440	0.666
56	0.741	0.556	0.120	-0.510	0.922	0.135	-0.664	0.788	0.342
57	0.721	0.748	0.097	-0.393	0.936	0.149	-0.631	0.482	0.661
58	1.218	0.572	0.033	-0.041	1.229	0.086	-0.351	0.521	0.329
59	0.567	0.504	0.132	-0.607	1.056	0.110	-0.547	0.685	0.259
60	0.780	0.460	0.011	-0.004	0.779	0.043	-0.160	0.090	0.449
61	1.081	0.477	0.034	-0.044	1.095	0.087	-0.411	0.527	0.290
62	0.436	0.317	0.071	-0.341	0.487	0.130	-0.643	0.764	0.213
63	0.361	0.425	0.071	-0.341	0.487	0.130	-0.643	0.764	0.213
64	0.587	0.763	0.083	-0.337	0.711	0.127	-0.550	0.440	0.666
65	0.371	0.414	0.071	-0.341	0.487	0.130	-0.643	0.764	0.213
66	1.225	0.547	0.012	0.093	1.167	0.119	-0.525	0.546	0.384
67	0.712	0.577	0.120	-0.510	0.922	0.135	-0.664	0.788	0.342
68	0.733	0.754	0.097	-0.393	0.936	0.149	-0.631	0.482	0.661
69	1.085	0.492	0.034	-0.044	1.095	0.087	-0.411	0.527	0.290
70	0.702	0.735	0.097	-0.393	0.936	0.149	-0.631	0.482	0.661
71	1.081	0.489	0.034	-0.044	1.095	0.087	-0.411	0.527	0.290
72	0.531	0.614	0.116	-0.522	0.853	0.126	-0.631	0.922	0.227
73	0.775	0.426	0.011	-0.004	0.771	0.040	-0.176	0.082	0.449
74	0.344	0.424	0.091	-0.435	0.620	0.120	-0.606	0.744	0.156
75	0.318	0.424	0.091	-0.435	0.620	0.120	-0.606	0.744	0.156
76	0.754	0.492	0.132	-0.607	1.056	0.110	-0.547	0.685	0.259
77	0.377	0.783	0.083	-0.354	0.640	0.130	-0.495	0.422	0.719
78	0.473	0.706	0.083	-0.337	0.711	0.127	-0.550	0.440	0.666
79	1.084	0.494	0.034	-0.044	1.095	0.087	-0.411	0.527	0.290
80	0.781	0.451	0.011	-0.004	0.779	0.043	-0.160	0.090	0.449
81	0.381	0.596	0.129	-0.566	0.841	0.133	-0.637	0.745	0.367
82	1.084	0.495	0.034	-0.044	1.095	0.087	-0.411	0.527	0.290
83	1.091	0.482	0.034	-0.044	1.095	0.087	-0.411	0.527	0.290
84	0.000	0.000	0.000	0.000	0.000	0.000	0.000	0.000	0.000
85	1.084	0.428	0.034	-0.044	1.095	0.087	-0.411	0.527	0.290
86	1.081	0.491	0.034	-0.044	1.095	0.087	-0.411	0.527	0.290
87	0.761	0.762	0.097	-0.393	0.936	0.149	-0.631	0.482	0.661
88	0.707	0.581	0.120	-0.510	0.922	0.135	-0.664	0.788	0.342
89	0.767	0.535	0.120	-0.510	0.922	0.135	-0.664	0.788	0.342
90	0.662	0.311	0.099	-0.470	0.744	0.115	-0.571	0.713	0.200
91	0.742	0.312	0.104	-0.442	0.818	0.107	-0.565	0.684	0.206

3.3.2. ASSESSMENT OF THE DAMAGE SCENARIO

Starting from the outcomes discussed in the previous Section, a large-scale seismic damage scenario assessment was performed. In particular, the reference parameter considered for the application of the PRESSAFE-disp method was the number of collapsed buildings resulting from the calculation, in comparison with the actual number of collapsed buildings in the area, i.e. 42.

Generally, for the definition of the seismic damage assessment of a building, two input models must be established: (i) the fragility model and (ii) the seismic input model. The former has been already discussed and derived from the application of the PRESSAFE-disp method, whereas the latter is described in detail in the following.

In this study, the seismic input was assumed deterministic, due to the availability of the ground motion recordings of the station SAN0, located very close to the industrial area (about 1 km, see Figure 16). Two procedures have been adopted in this work to combine statistically the fragility model and the seismic input model. The first procedure adopted was based on Monte Carlo simulation (MC), while the second approach is Direct Simplified (DS) calculations, aimed at the fast evaluation of the number of collapsed buildings.

3.3.2.1. GROUND-MOTION INTENSITY

The industrial area under consideration was selected not only because of the availability of data on the precast buildings, but also because there was a ground motion recording station (SAN0) at a distance shorter than 1 km, allowing to reduce strongly the uncertainty on the ground-motion intensity during 29th May 2012.

Nevertheless, some uncertainties remain because of: (i) the attenuation of the ground-motion which can be fast in the near field region; (ii) the directionality of the ground motion, which was relevant for the earthquake under consideration (Savoia et al. 2017). The first uncertainty source was neglected in the present study, thus assuming that the ground motion recorded by the SAN0 station corresponds to that at the base of the buildings. The second uncertainty source was considered with different levels of approximation. In particular, starting from the accelerations registered during the 29th May 2012 main shock at the recording station SAN0 (Itaca database 2021), three seismic inputs (SIN) models were considered:

- SIN1: pseudo-acceleration response spectrum S_a with 5% damping, calculated as the maximum value between the two SAN0 ground-motion spectra in the North-South and East-West directions;
- SIN2: pseudo-acceleration response spectrum S_a with 5% damping, calculated as the geometric mean of the two SAN0 ground-motion spectra in the North-South and East-West directions;
- SIN3: pseudo-acceleration response spectrum S_a with 5% damping, in the direction of the main frames of each building; in this third approach the response spectrum can be different for each building.

The three different seismic input SIN1-SIN3 would represent a series of progressive refinements and improvements of the seismic input model, which is adopted to calculate the probability of collapse from the fragility curves of the frames. Theoretically, the SIN3 should provide the best assessment among the three approaches considered, because the behaviour of precast RC buildings tends to be very different in their longitudinal and transverse directions. To this regards, it is worth noting that the PRESSAFE-disp method is a simplified method which considers only the behaviour in the plane of the main frames.

The pseudo-acceleration response spectra adopted in the models SIN1 and SIN2 are plotted in Figure 22. To show the directionality of the ground-motion, considered in the model SIN3, Figure 23a reports the pseudo-spectral accelerations for *T*=0 s, *T*=0.5 s, *T*=1.0 s, *T*=1.5 s and *T*=2.0 s, along different orientations. Angles are measured with respect to the East direction, and increase towards North.

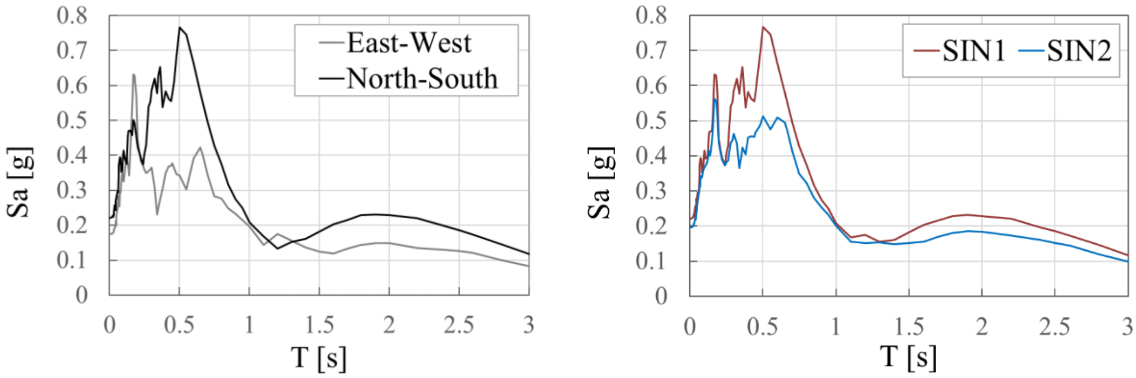

(a) *(b)*

Figure 22. Acceleration response spectra: (a) East-West and North-South spectra obtained from the recording station SAN0 during the 29th May 2012 main shock; (b) SIN1 and SIN2 response spectra calculated as the maximum and the geometric mean of the two recorded spectra, respectively.

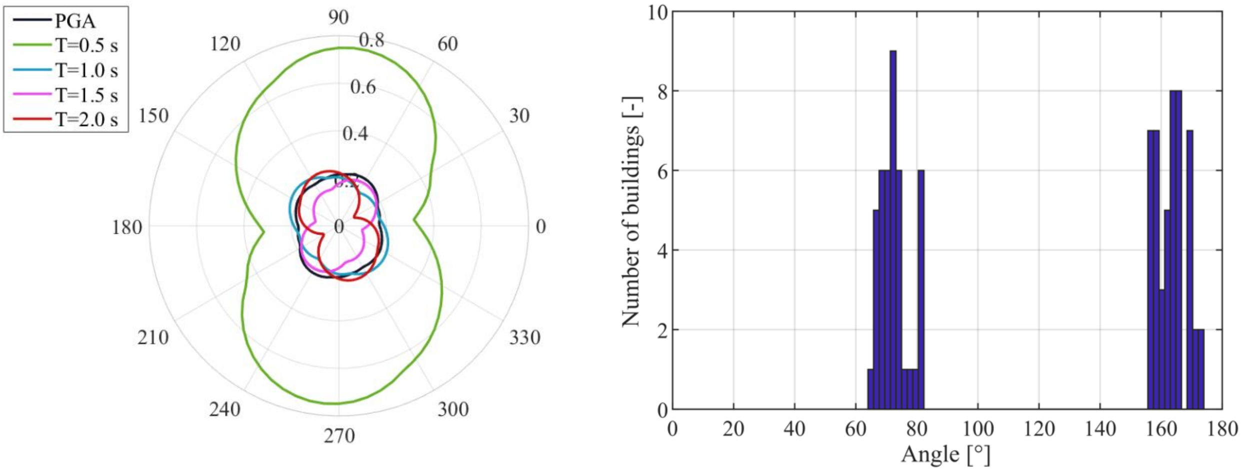

(a) *(b)*

Figure 23. (a) Pseudo-spectral accelerations in units of g at T=0 s, T=0.5 s, T=1.0 s, T=1.5 s, T=2.0 s, in different directions, and (b) orientation of the main frames for the 91 buildings considered. Angles are measured from East and 90° correspond to North.

In Figure 23a, the values at $T=0$ s correspond to the Peak Ground Acceleration (PGA), with maximum equal to 0.226 *g* and minimum equal to 0.170 *g*. Considering $T=0.5$ s, the maximum pseudo-spectral acceleration among all the horizontal directions is 0.750 *g*, while the minimum is 0.317 *g*; for $T=2.0$ s the maximum and minimum spectral accelerations are 0.236 *g* and 0.073 *g*, respectively.
The orientation of the main frames of the 91 buildings under consideration is reported in Figure 23b. Clearly, there are two clusters of buildings, one with main frames with orientation of about 70° from East and one at 160° from East. It should be noticed that, in the prediction of damage scenarios, the directionality of the ground motion is normally not considered since reliable predictive models are not yet available.

3.3.2.2. MONTE CARLO (MC) SIMULATION

The Monte Carlo simulation is a highly repetitive process in which the result, in this case the number of collapsed buildings, is calculated for a large number of numerical simulations (Grigoriu 2002). This method is used to estimate a range of possible outcomes based on a set of random input data; it results in a rather complex procedure which is computationally expensive because of the need of a large number of simulations. On the other hand, the Monte Carlo simulation is very powerful because it can be applied to different types of uncertainty models (e.g. parametric, non-parametric, continuous variables, discrete variables, etc.) and to non-linear models.

3.3.2.2.1. SIMULATION OF DAMAGE SCENARIOS

In the present case, in order to consider the epistemic uncertainty on the behaviour of the buildings (e.g., the uncertainties in selecting an appropriate structural model, as well as uncertainties in the measurement of physical quantities or lack of sufficient data, see Sections 3.3.1), the natural period of the perimeter and the internal frames was considered uncertain.
To this aim, a uniform probability distribution in the interval $[(1-\alpha)T_1, (1+\alpha)T_1]$ was used, where T_1 indicates the estimate of the period reported in Table 1 and α is a building-dependent parameter, set to either 0.1, 0.2 or 0.3, based on the quality and amount of data available. In the simulations, the periods of the internal and perimeter frame of the same building were considered uncorrelated.
As already mentioned in Section 3.2, since the precast buildings are conceived as systems of independent frames when designed without seismic provisions, the seismic behaviour of the two frame typologies was analysed separately, and then the results were combined in a later stage. When a frame typology (either internal or perimeter) was not present in a building, its fragility was based on the characteristics of the only frame type in the structure.
The following steps summarize the calculations performed in each of the MC simulations. The procedure was implemented in a Matlab (MathWorks 2020) script:

1. For each frame of each building, a value of the natural period is randomly sampled from a uniform distribution in the interval $[(1-\alpha)T_1, (1+\alpha)T_1]$, where T_1 is the estimate of the natural period reported in Table 1, and α is a building-dependent parameter, set to either 0.1, 0.2 or 0.3, based on the quality and amount of data available;

2. Given the period of each frame, the corresponding S_a value is determined from the seismic input model (i.e., either SIN1, SIN2 or SIN3);
3. Given the period of each frame, the corresponding fragility curve is determined using the parametric fragility surfaces of the PRESSAFE-disp method;
4. For each frame, the probability of collapse is calculated combining its fragility curves (step 3) with the spectral acceleration computed at step 2;
5. To determine if a frame collapses, a random value is sampled from a continuous uniform distribution in the interval [0;1] and compared with the probability of collapse computed at the step 4. If this random number is smaller than or equal to the probability of collapse (step 4), the frame is considered collapsed. This approach follows the recommendations given in FEMA (2018); considering the event "frame collapse" as a discrete Bernoulli random variable;
6. A building collapses if either the internal frame or the perimeter frame collapses;
7. The total number of collapsed buildings is computed.

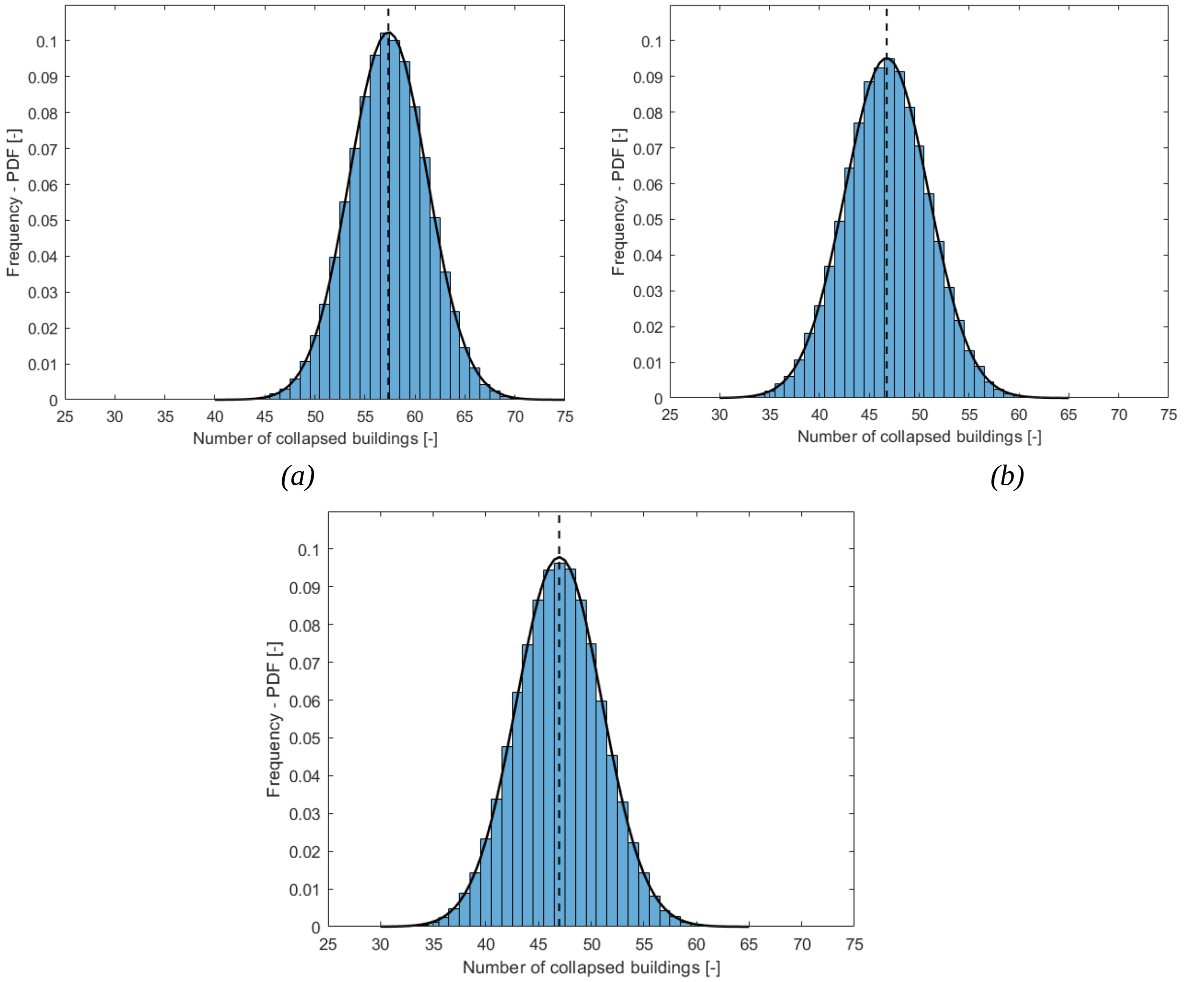

(a) *(b)*

(c)

Figure 24. Prediction of the number of collapsed buildings and best fitting normal distributions for 100'000 Monte Carlo simulations, for three different seismic inputs: (a) SIN1, (b) SIN2 and (c) SIN3.

In the present work, a total number of 100’000 simulations were performed. Figure 24 shows the results obtained, in terms of number of collapsed buildings, for the different seismic input models, i.e. SIN1, SIN2 and SIN3. The vertical axis of the plot indicates the relative frequency of the different numbers of collapsed buildings in the simulations, normalized in order to have a unitary total area of the histogram. From the literature (Benjamin and Cornell 1970), the central limit theorem indicates that the distribution of the sum of a large number of uniformly distributed independent random variables approaches the normal distribution. Thus, the fitting functions adopted in Figure 24 are normal distributions, represented with a continuous black line, characterized by the parameters of Table 6.

As visible in Figure 24, the dispersions of the distributions are essentially equivalent, whereas the expected (i.e. mean) value of collapsed building is about 57 for SIN1, 47 for SIN2 and 47 for SIN3. The parameters of the best fitting normal distributions are given in Table 6 for the three seismic input models considered, together with the relative prediction error (E_R), in percentage, computed as:

$$E_R\ [\%] = (N_{c,est} - N_{c,act})/N_{c,act} \times 100 \tag{3.7}$$

Where: $N_{c,est}$ is the number of collapsed buildings estimated and $N_{c,act}$ is the actual number of collapsed buildings occurred during the seismic event, i.e. 42 in the present case. The MC simulations with the three different seismic input models resulted in a slightly higher number of collapses if compared with the actual effect of the earthquake. This result could be somehow expected, due to the simplifying conservative assumptions introduced in the numerical simulations of the PRESSAFE-disp method (for instance the strength of some non-structural elements was neglected). Nevertheless, the rather small errors indicate that the fragility surfaces proposed, in this application at the territorial scale, offers a reliable representation of the seismic behaviour of precast RC buildings. The most accurate outcomes were obtained by adopting the seismic inputs SIN2 and SIN3, i.e. considering the geometric mean of the two SAN0 spectra and the spectra in the direction of the main frame of each building, respectively.

Other interesting results can be drawn considering the geographical orientation of the buildings. Indeed, as mentioned before, the buildings of the case-study area can be sorted in two groups according to their main frame orientations, with average values of about 70° and 160° respectively, measured from East (see Figure 23b). The mean values of the spectral accelerations for the two groups of buildings, for each seismic input, are represented in Table 7, for both internal and perimeter frames. The S_a values are strongly dependent on the frame orientations, and the SIN2 and SIN3 models are

Table 6. Main descriptors of best fitting normal distribution illustrated in Figure 11, for three different seismic inputs.

	Mean [-]	Median [-]	Standard deviation [-]	E_R [%]
SIN1	57.3	57	3.9	+36.5
SIN2	46.7	47	4.2	+11.2
SIN3	46.9	47	4.1	+11.7

on average in good agreement for both type of frames, featuring lower values compared to SIN1, as expected. Moreover, the average spectral accelerations of the perimeter frames are higher compared to the ones of the internal frames for all seismic inputs, due to the different values of natural periods (see Table 3).

Table 8 reports the average number of collapses in the 100’000 Monte Carlo simulations, for both groups of buildings. The sum of the number of collapses provided in Table 8, corresponds to the mean values reported in Table 6, for each seismic input considered. As mentioned before, the adoption of SIN1 leads to a higher number of collapses with respect to the other two seismic inputs. It is worth noticing that there is not a remarkable difference between the outcomes of the two groups of buildings in terms of number of collapses, since a mixed population of frame categories, with a significantly different seismic behaviour, is included in both groups.

All these results, on one hand, suggests that the seismic input SIN1, calculated as the maximum between the two spectra recorded in SAN0, is too conservative, on the other hand, they prove that the adoption of the PRESSAFE-disp fragilities, together with an appropriate seismic input, could represent a reliable tool for the damage scenario assessment of precast RC buildings. Even though the seismic input SIN2 is obtained through a rather simple calculation, the MC outcomes show that it could be effectively adopted to obtain a realistic assessment of the number of collapsed buildings, even if precise data on the directionality effects of the ground motion was not taken into account.

3.3.2.2.2. DISAGGREGATION OF THE RESULTS

Figure 25 shows the disaggregation of the outcomes of the MC simulations considering the seismic input model SIN3. In particular, the histograms represent the frequency of occurrence of the collapse

Table 7. Mean values of the spectral accelerations of internal (I) and perimeter (P) frames, for the two groups of frames with different average orientations, for the three seismic inputs.

	Average orientation 70°		**Average orientation 160°**	
	S_a (I) [g]	S_a (P) [g]	S_a (I) [g]	S_a (P) [g]
SIN1	0.287	0.440	0.354	0.438
SIN2	0.241	0.356	0.288	0.340
SIN3	0.262	0.402	0.264	0.300

Table 8. Number of collapses of the precast buildings estimated in the Monte Carlo simulation, for the two groups of frames with different average orientations, for the three seismic inputs.

	Average orientation 70°	**Average orientation 160°**
	$N_{c,est}$ [-]	$N_{c,est}$ [-]
SIN1	26.4	30.9
SIN2	21.5	25.2
SIN3	24.5	22.4

condition in the 100’000 simulations, of internal and perimeter frames, and of the whole buildings. With reference to the steps of analysis described before, Figure 25a illustrates the disaggregation of the outcomes obtained at step 5, whereas Figure 25b shows the ones obtained at step 6. On average, the perimeter frames showed a lower collapse attitude than internal frames, because they can benefit from the presence of non-structural walls/panels.

It is worth noticing that each histogram in Figure 25b, representing the frequency of occurrence of collapse for the 91 precast buildings, is at least as high as the highest histogram representing the collapse of the corresponding frames (see Figure 25a), in accordance with the hypothesis of the calculation defined at step 6.

In Figure 26 the outcomes of the MC simulation are disaggregated for each building, for the seismic input SIN3. The coloured cylinder, located in correspondence of each building position in the map, represents the collapse attitude of the precast structure out of the whole set of simulations. The collapse occurrence is graphically represented by means of the height and the colour of the cylinder: the red cylinders represent the buildings with a frequency of occurrence of collapse higher than 75%; the green cylinders a frequency lower than 25%; yellow cylinders a frequency from 25% to 50% and orange cylinders in the range 50% to 75%.

The results of Figure 26 can be qualitatively compared with the map in Figure 18, in which the red marks indicate the exact positions of the collapsed buildings in the seismic event considered. This

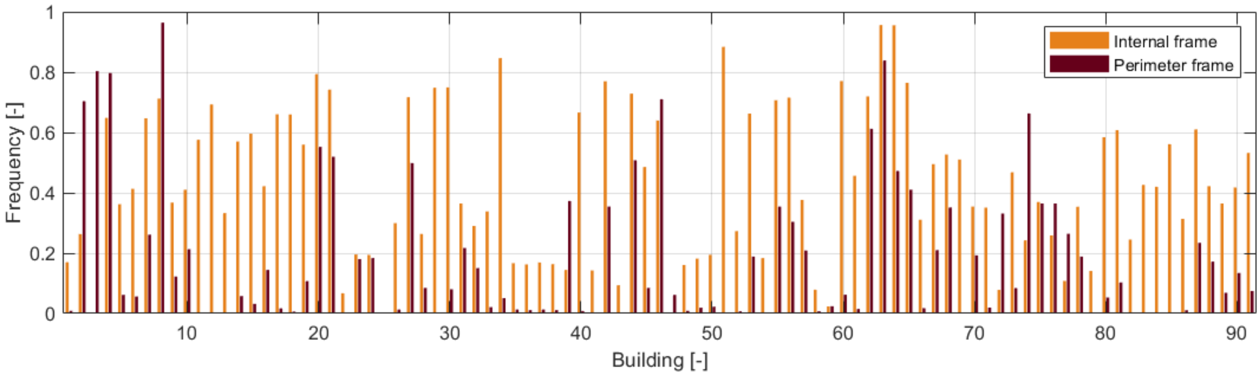

(a)

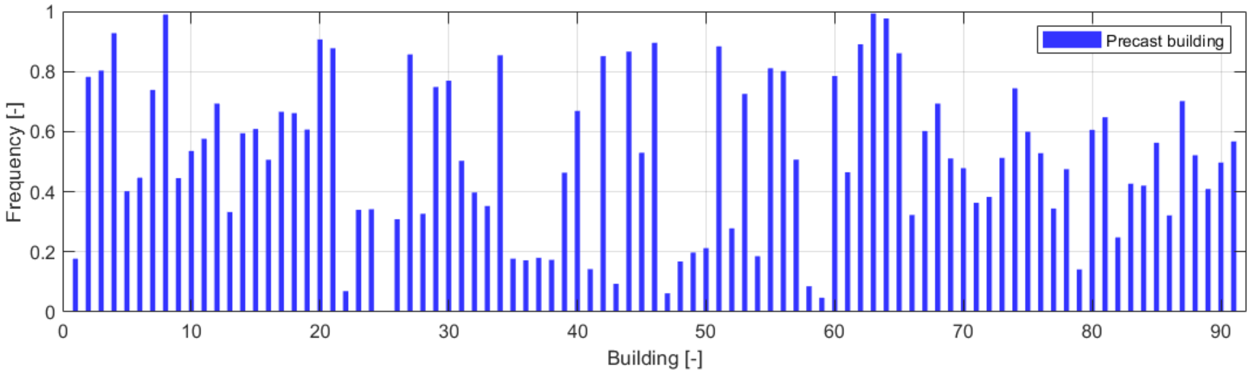

(b)

Figure 25. Disaggregation of the outcomes for the seismic input SIN3. The histograms represent the number of collapse cases out of the 100000 simulations for the 91 buildings, with reference to: (a) internal frames (in orange) and perimeter frames (in red), and (b) whole precast buildings (in blue).

comparison allows to evaluate the accuracy of the results not only at a “large-scale” point of view (total number of building collapsed in the area) but also at the point of view of the specific building (single precast building). The comparison shows that the outcomes of the MC simulation are, on average, in good agreement with the in-field data of real collapse for the majority of the investigated buildings. However, in some cases the simulation was not able to identify correctly the collapse occurred, in particular for buildings having a seismic capacity very close to the seismic demand.

Moreover, for buildings with irregularities highly affecting the seismic behavior, this method could lead to a wrong estimation of the seismic capacity, thus needing a more refined and time-consuming modelling strategy, which however requires the deep knowledge of the geometrical and material characteristics of the building (Belleri et al. 2015; Nastri et al. 2017; Dal Lago and Ferrara 2018; Magliulo et al. 2018; Bovo and Savoia 2018; Bovo and Savoia 2019; Dal Lago et al. 2019; Brunesi et al. 2020; Soydan et al. 2020).

Hence, the final result of the approach developed for a large-scale seismic damage assessment, is to be intended to provide an average value of the expected number of collapses in the building stock. This is considered acceptable within the purpose of a fast and simplified method and, indeed, the results may be not accurate for some particular buildings.

3.3.2.3. DIRECT SIMPLIFIED (DS) CALCULATION

A Direct Simplified (DS) and fast calculation method is proposed in this Section with the aim of conducting a preliminary estimation of the number of collapses at the territorial scale. The method is

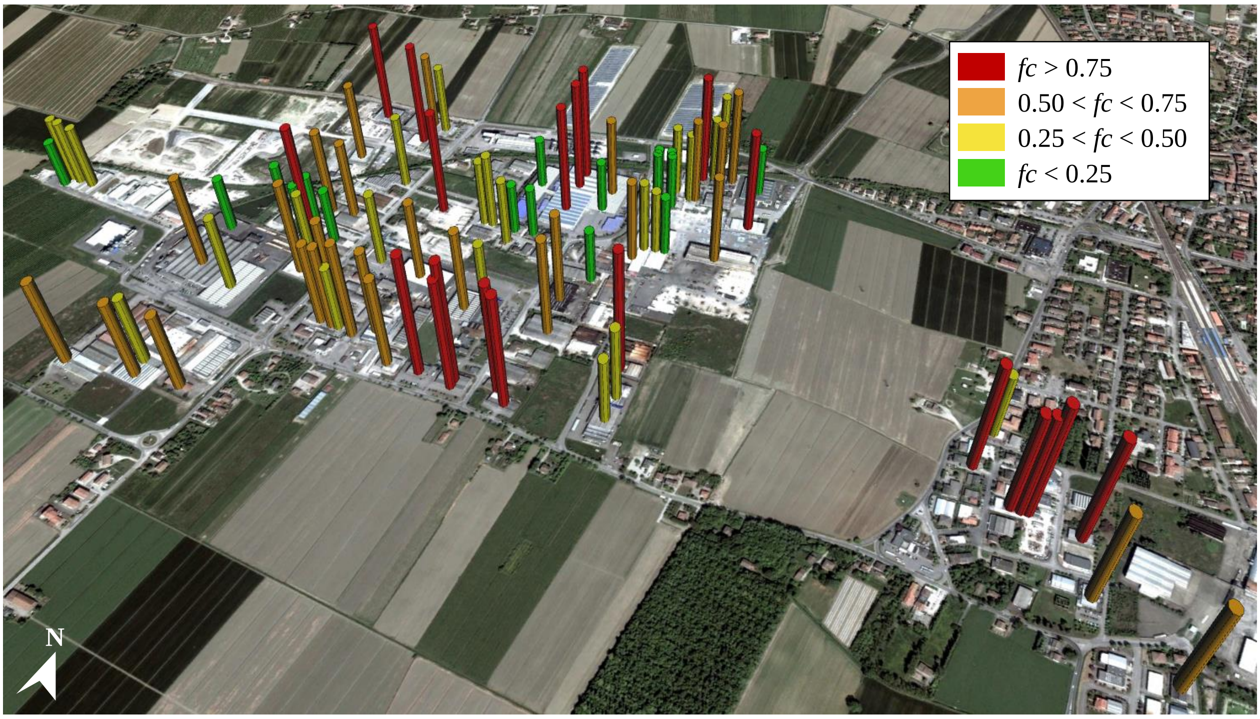

Figure 26. Google Earth (2020) aerial view of the case-study area with histograms representing the frequency of occurrence of the collapse condition (fc) of each of the 91 buildings; disaggregation of the Monte Carlo assessment with seismic input SIN3.

deemed to be alternative and simplified with respect to the Monte Carlo (MC) one, and does not requires a large number of simulations, therefore it is suitable for handling rapid results. Moreover, the epistemic uncertainties are not included in this process.

The DS calculation has been applied considering the same three seismic input models, i.e. SIN1, SIN2 and SIN3, adopted for the MC simulation. The mathematical procedure is based on the fundamental axioms of the probability theory and the algebra of datasets (Benjamin and Cornell 1970).

Considering the case-study building stock, the input data of the problem were the categories selected for the internal and the perimeter frames of each precast RC building, and the corresponding natural periods reported in Table 3. The parameters (i.e. median and standard deviation) of the lognormal fragility curves were calculated by means of the already discussed PRESSAFE-disp fragility surfaces, for the perimeter and internal frames of the 91 buildings in the stock. The collapse fragility curves are those shown in Figure 21. In this simplified procedure, both the fragility model and the seismic input have been assumed deterministic.

Considering a precast RC building, the frames identified within the same structural category (e.g. all the internal frames in a building, following the PRESSAFE-disp taxonomy) have been assumed to have an analogous seismic behaviour, therefore, in each building, the failures of the various frames of the same type are assumed to occur at the same time. Based on this assumption, it is possible to consider only one internal frame and one perimeter frame for each building.

Given the natural period of each frame, the corresponding pseudo-spectral acceleration S_a was obtained from the seismic input model and then, by making use of the fragility curves, the probability of collapse was computed for each frame. In the following, the collapse probability of the internal frame and of the perimeter frame of the *i*-th building is indicated as $\mathrm{P_i}(E_I)$ and $\mathrm{P_i}(E_P)$, respectively. With reference to a general building, these two probability values are considered associated to two random events, i.e. the collapse of the internal frames and the collapse of the perimeter frames, assumed statistically compatible (i.e. non-mutually exclusive) and statistically independent. Therefore, under the hypothesis of flexible roof (i.e. absence of diaphragm effect) and independent behaviour of internal and perimeter frames, the collapse of a building occurs if one of the internal or perimeter frames collapses, or both. Moreover, in a building, the collapse of the two frame types (internal and perimeter) can occur at the same time, meaning that the probability of the intersection of the events is not zero.

As a result of these hypotheses, the probability of the union of the two events, representing the collapse probability of the *i*-th building, can be calculated with the generalized additivity axiom:

$$\mathrm{P}_{B,i} = \mathrm{P}_i(E_I \cup E_P) = \mathrm{P}_i(E_I) + \mathrm{P}_i(E_P) - \mathrm{P}_i(E_I \cap E_P) \tag{3.8}$$

being E_I and E_P the internal and perimeter frame collapse events, respectively. Since the two events are considered independent, the following expression can be derived:

$$\mathrm{P}_{B,i} = \mathrm{P}_i(E_I \cup E_P) = \mathrm{P_i}(E_I) + \mathrm{P}_i(E_P) - \mathrm{P}_i(E_I) \cdot P(E_P) \tag{3.9}$$

Since the lognormal functions do not have the additive regenerative property, but they are characterized by a multiplicative regeneration ability (Benjamin and Cornell 1970), it is not possible to obtain an analytical expression for the fragility of the building as a function of the fragilities of the frames because the result would not be a lognormal function. Thus, the fragility curve of the entire *i*-th building can be obtained in a discrete form, by calculating the collapse probability $\mathrm{P}_{B,i}$ for a set of values of S_a.

Once the P_B of all the buildings in the cluster are estimated, the assessment of the number of collapsed buildings over the entire stock can be directly derived through a statistical combination. Considering that each precast building in the case-study stock has the same probability (equal to 1/91) to be randomly extracted from the population (the building stock), the combined average collapse probability of the mixed set of buildings considered (named P_{eq}) is computed with following the procedure outlined in Shinozuka et al. (2000):

$$\mathrm{P}_{eq} = \sum_{i=1}^{N} \mathrm{P}_{B,i} \cdot \frac{n_i}{N} = \sum_{i=1}^{N} \mathrm{P}_{B,i} \cdot \frac{1}{N} = \frac{1}{N} \sum_{i=1}^{N} \mathrm{P}_{B,i} \tag{3.10}$$

where: n_i is the cardinality of the *i*-th precast building equal to 1; N is the total number of buildings in the stock, equal to 91; $\mathrm{P}_{B,i}$ is the probability of collapse of the *i*-th building. Since P_{eq} can be also computed with the following ratio:

$$\mathrm{P}_{eq} = N_{c,est}/N \tag{3.11}$$

where $N_{c,est}$ is the number of collapsed buildings estimated, it follows that the average number of collapsed buildings can be estimated as:

$$N_{c,est} = \sum_{i=1}^{N} \mathrm{P}_{B,i} \tag{3.12}$$

Under these hypotheses, the DS calculation allows a direct assessment of the expected number of precast buildings exceeding a specific limit state (the collapse in the present case) in the building stock or in the productive area of interest. This straightforward calculation was carried out for the three seismic input models described in Section 3.3.2.1. The results are reported in Table 9. The prediction error referred to the actual number of collapsed buildings ($N_{c,act}$ = 42) was computed according to Equation (3.7).

Table 9. Outcomes of the direct simplified (DS) calculation for the three seismic input ($N_{c,est}$ is the estimated number of collapsed buildings in the stock; P_{eq} is the combined average collapse probability; E_R is the relative error in percentage).

	$N_{c,est}$ [-]	P_{eq} [%]	E_R [%]
SIN1	56.4	61.9%	+34.3%
SIN2	46.2	50.7%	+10.0%
SIN3	46.2	50.8%	+10.1%

The outcomes of the DS procedure are in very good agreement with the results of the MC simulations given in Table 6, for the three seismic inputs. The seismic inputs SIN2 and SIN3 are again deemed suitable for estimating the number of collapsed buildings in the case-study area, since the results differ about 10% with respect to the in-field real number of collapses observed after the 2012 earthquake. This confirms the soundness of this simplified but rapid procedure as a valid alternative to the MC simulation for this type of large scale applications.

3.3.3. CONCLUDING REMARKS

A large-scale seismic damage assessment was performed to estimate the number of a set of precast RC buildings, located in the productive area of San Felice sul Panaro (Modena), highly damaged during the 2012 seismic events. The damage assessment was outlined considering three different seismic input models for the scenario of the 29th May 2012. The fragility curves of the precast frames obtained with the PRESSAFE-disp method have been adopted to perform a large-scale Monte Carlo simulation and, as an alternative, a direct simplified calculation.

In terms of number of collapsed buildings, the agreement with the actual effects of the earthquake is very good, in particular for the seismic input which takes the ground-motion directionality into account, usually not considered in the calculations of damage scenarios. The results, for all the three seismic input models, show a small overestimation of the number of collapsed buildings. This discrepancy is, in part, due to the simplified modelling assumptions, related to the lack of precise structural knowledge of geometries and material properties of the buildings, a typical condition when the analyses are conducted at the territorial level.

In the literature, several studies focusing on the seismic response evaluation of individual precast buildings exist, but the level of details required is usually not compatible with that of a large scale structural assessment. Instead, the procedure proposed in this study requires few data, available from a visual building survey, and suitable for a large-scale assessment in which many uncertainties on the structural behaviour are present.

The outcomes presented in this s work offers promising results for the applicability of the collapse fragility curves of the PRESSAFE-disp method for the large scale seismic assessment of precast RC buildings. In fact, the PRESSAFE-disp method represents a first attempt to set a uniform approach in the development of fragility curves of precast RC buildings to be used in large scale evaluations, and already includes the in-plane seismic behaviour of a large variety of precast frames.

Hence, the availability of a general method allowing studying a diversified portfolio of precast RC buildings paves the way for the conduction of seismic assessments aimed at the evaluation of the seismic losses. In this context, the procedure developed may have different practical applications, such as to predict the impact of possible seismic scenarios and allow a suitable territorial planning, to guide the reconstruction phase and the allocation of funds after an exceptional event; or it could be used to forecast the most vulnerable industrial area under a specific seismic scenario and outline the prevention strategies.

3.4. A SIMPLIFIED METHODOLOGY FOR THE LOSS EVALUATION OF ALTERNATIVE RETROFIT OPTIONS OF RC FRAME BUILDINGS

The current rigorous procedures for the estimation of the seismic losses and the assessment of the performance of a building (e.g. the PEER methodology) appear to be too intricate and onerous for routine implementation in professional practice, as recognized by Cosenza et al. (2018). With both the time and budget constraints typical of the work of the engineer, the application of a fully probabilistic performance assessment for the comparison of different seismic retrofit alternatives would be not feasible. However, the assessment of the performance of various retrofit options, at the conceptual design stage, may provide valuable information for decision makers to select the optimal feasible solution. In this context, the application of a simplified displacement-based performance assessment methodology has been investigated, to be adopted in the framework of the seismic retrofit decision-making. This process is inherently complex due to the large number of intervention alternatives and the multitude of criteria to be evaluated.

Following the principles of the Direct Displacement Based seismic Assessment (DDBA) initially proposed in Welch et al. (2014), and modified after Ligabue (2015), a comprehensive methodology is outlined to calculate different loss terms and the benefit-cost ratio for the evaluation of the convenience of the intervention with respect to the initial cost of investment. All the terms evaluated can be adopted in a multi-criteria decision-making framework.

Since this method was born and calibrated for RC buildings (Priestley 2007, Sullivan et al. 2014, Welch et al. 2014, Landi et al. 2020), even if some recent applications to other typologies exist (Bosio et al. 2020, Ottonelli et al. 2020), a case study RC frame building has been considered in this work. To assess the effectiveness of different seismic retrofit interventions, the building has been evaluated in the As-Built condition, and after the application of different retrofit scenarios based on local interventions on columns. Indeed, the local interventions applied on the columns in RC ordinary buildings may have a significant effect in increasing the global ductility of the structure and thus, the resilience to seismic actions.

This framework may be applied to evaluate rapidly the seismic performance and the expected losses of various alternatives of interventions on an existing RC building, starting with the implementation of non-linear static analyses (Pushover analyses). Different quantitative performance and loss metrics are introduced, to be used in decision-making. Hence, the method is suitable for determining the relative seismic performance for a comparative analysis of the effectiveness of different feasible retrofit options.

3.4.1. OUTLINE OF THE METHOD

The methodology considered relies on several simplifying assumptions, thus it should not be intended as a rigorous assessment procedure. Loss estimates are obtained through a deterministic analytical procedure, hence, the results should be considered suitable only for comparison among retrofit alternatives at the preliminary design phase of a project.

The present method is adopted to evaluate the direct losses expected for a specific structure within a defined time frame (i.e., a time-based assessment, see Section 2.1), as a result of the hazard at the building site. These losses are defined as monetary costs meaning the amount an owner could expect to pay on average, in a given period, to repair the seismic damage or replace the building, considering all possible earthquakes at the site and their probabilities of occurrence. Indirect losses due to possible business disruption and downtime, or injuries and casualties, are neglected in this work.

The method is based on the principles of the Direct Displacement Based seismic Assessment (DDBA) to evaluate the performance of existing structures (Sullivan et al. 2014). The procedure, in its original version, started with the evaluation of the likely inelastic mechanism, which lead to the identification of the displaced shape corresponding to a considered limit state.

In this extended and modified version, the evaluation of the global performance of the existing building and the identification of the displaced shape, are carried out with a Pushover analysis. This is in line with the purpose of defining a simplified framework, since nowadays the non-linear static analysis is intuitive and easy to use for practitioners (Silva et al. 2019), being implemented in every software of structural calculation. Nevertheless, this method of analysis constitutes a step forward in the determination of the displaced shape and the level of damage in the single plastic hinges modelled,

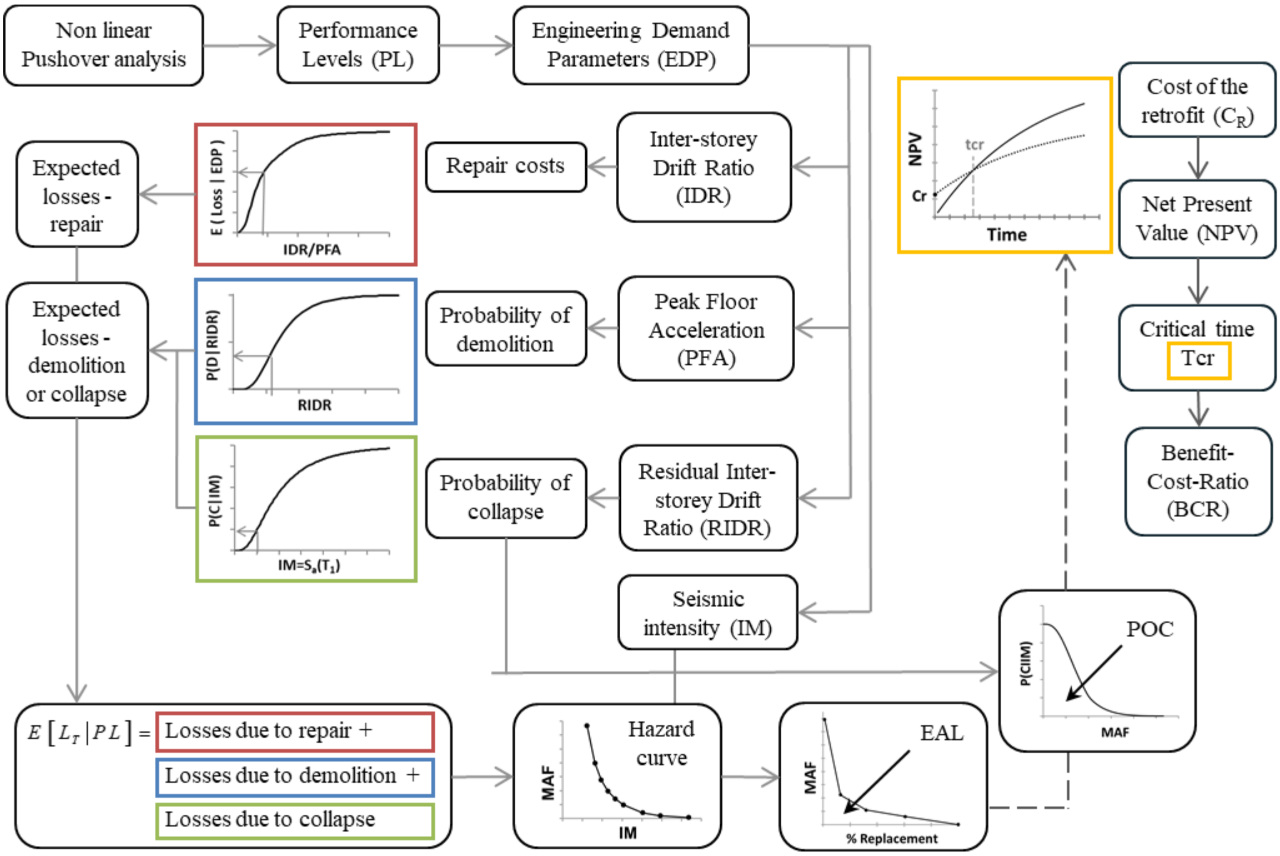

Figure 27. Framework of the time-based methodology applied.

compared to that previously adopted in the procedure. The software Midas GEN (CSPFEA) has been used for the non-linear finite element modelling (FEM) of the structure.

Furthermore, a simplified probabilistic framework to assess the annualized probability of collapse has been conducted to evaluate the collapse tendency of the structure As-Built and after the retrofit, following the concepts defined in Ligabue et al. (2018).

Finally, the cost-benefit analysis has been performed to derive suitable terms of comparison to support the decision-making phase, such as the critical time and the benefit-cost-ratio. A scheme of the entire framework is proposed in Figure 27.

3.4.1.1. EXPECTED ANNUAL LOSSES (EAL)

In the time-based assessment, different limit states are selected to perform a piecewise linear approximation of the continuous total loss curve. According to Welch et al. (2014), four performance levels should be considered, corresponding to: Zero Loss (ZL), Operational or Yielding (Y), Life safety (LS), and Near collapse (NC).

However, another level is introduced, being the Residual Inter-story Drift threshold of 1.5% (RIDR 1,5%). In the original methodology the definition of the latter limit state is not provided. The fifth performance level is defined selecting a residual inter-storey drift value of 1.5%, which corresponds to an unacceptable level of residual deformation according to FEMA P-58 (2018): once this level is reached, the building is more likely to be demolished than repaired. For what concern old existing RC buildings, in which the collapse is likely to be induced by a soft-storey mechanism, the damage is often concentrated at one story only. Thus, the expected losses due to repair are then lower than the losses expected in a code-conforming structure, were the damages are distributed over the height of the structure (Bovo et al. 2021). This fact justify the definition of a further performance level, which can be identified as a closure point of the Loss-Mean Annual frequency total loss curve. Moreover, if the residual deformation in the soft-storey reaches the threshold before the attainment of the ultimate rotation in one of the plastic hinges defined, the limit state RIDR 1.5% may be attained before the NC one.

Following the DBA approach for the estimation of the losses, the properties of an equivalent SDOF system corresponding to each performance level are estimated, as well as the intensity measure which is the spectral acceleration at the fundamental period of the structure, Sa(T_1), required to reach or exceed the same performance level. Based on the displaced shape (for each limit state) derived from the non-linear static analysis, it is possible to determine the characteristics of the SDOF systems. The following Equations allow finding, respectively: the displacement capacity of the equivalent structure, the effective mass, the effective height, the effective stiffness, the effective structural period, and the equivalent viscous damping term.

$$\Delta_c = \frac{\sum_{i=1}^{n}(m_i \cdot \Delta_i^2)}{\sum_{i=1}^{n}(m_i \cdot \Delta_i)} \tag{3.13}$$

$$m_e = \frac{\sum_{i=1}^{n}(m_i \cdot \Delta_i)}{\Delta_c} \tag{3.14}$$

$$H_e = \frac{\sum_{i=1}^{n}(m_i \cdot \Delta_i \cdot H_i)}{\sum_{i=1}^{n}(m_i \cdot \Delta_i)} \tag{3.15}$$

$$K_e = \frac{V_y}{\Delta_c} \tag{3.16}$$

$$T_e = 2\pi \sqrt{\frac{m_e}{K_e}} \tag{3.17}$$

$$\xi_{eq} = 0.05 + 0.565 \left(\frac{\mu - 1}{\mu\pi}\right) \tag{3.18}$$

Where: m_i and Δ_i are the seismic mass and displacement at level *i* respectively, Δ_c is the displacement capacity of the structure, m_e is the effective mass, H_e is the effective height, K_e is the effective stiffness and T_e is the effective structural period of the equivalent substitute structure. It is worth noticing that, within the DBA procedure, the effects of non-linear behaviour and energy dissipation are considered introducing an equivalent viscous damping term ξ_{eq}. This parameter accounts for the additional damping, beyond the 5% conventional elastic value, associated with the yielding of the system, following Priestley et al. (2007).

For each performance level, the structural response in terms of Inter-storey drift ratio (IDR), Peak floor acceleration (PFA) and Residual inter-storey drift ratio (RIDR) can be estimated. These quantities are generically referred to as Engineering Demand Parameters, EDPs. Damage in the structural components is usually assumed to be related to the IDR experienced by the building, while PFA together with the IDR are usually considered responsible for damage and losses of non-structural components and buildings contents (Ramirez and Miranda, 2009). The IDR are evaluated through the ratio between the relative displacement of two adjacent floors and the inter-storey height, from the results of the Pushover analysis, while simplified approaches are adopted to evaluate the other quantities, in particular:

- Peak floor accelerations are determined as follows (Welch et al. 2014):

$$\mathrm{PFA_i} = \Omega_\mathrm{i} \cdot \mathrm{PGA} \tag{3.19}$$

$$\Omega_i = 5 \left(\frac{H_i}{H_n}\right)\left(\frac{C_{pn}}{C_{h0}} - 1\right) + 1 \qquad if\ 0 < \frac{H_i}{H_n} \leq 0.2 \tag{3.20}$$

$$\Omega_i = \frac{C_{pn}}{C_{h0}} \qquad if\ 0.2 < \frac{H_i}{H_n} \leq 1 \tag{3.21}$$

$$\mathrm{C}_{pn} = \sqrt{\left[\frac{\eta_1}{R_1} C_h(T_1, 1)\right]^2 + 1.75\ln(n) C_{h0}^2} \tag{3.22}$$

$$\mathrm{R}_1 = \max\left[\frac{\mu}{2};1\right] \tag{3.23}$$

Where: C_{pn} is the basic horizontal coefficient for a part or diaphragm; η_1 is the first mode contribution coefficient and can be assumed equal to 1.5 for multi-storey buildings; R_1 is the first mode reduction factor; μ is the ductility demand; $C_h(T_1, 1)$ is the elastic spectral acceleration for 5% damping expressed at the fundamental period in units of g; n is number of the levels in the building; C_{h0} is the peak ground acceleration in units of g; Ω_i is the floor acceleration magnification factor at level i and gives the predicted mean peak floor acceleration at level i (PFA_i) when multiplied by the peak ground acceleration (PGA).

- Residual inter-storey drifts are estimated adopting empirical simplified relations given in Welch et al. (2014). The residual displacements are evaluated as functions of the peak transient drift experienced by the structure and the expected yield drift of the given storey.

$$\Delta_r = 0 \qquad \Delta \leq \Delta_y \tag{3.24}$$

$$\Delta_r = 0.3\left(\Delta - \Delta_y\right) \qquad \Delta_y < \Delta \leq 4\Delta_y \tag{3.25}$$

$$\Delta_r = \left(\Delta - 3\Delta_y\right) \qquad \Delta < 4\Delta_y \tag{3.26}$$

Where Δ_r is the residual inter-storey drift, Δ is the peak transient storey drift and Δ_y is the median story drift ratio calculated at yield.

A defined amount of expected annual losses of the structure can be evaluated at each performance level. Recalling that, on the basis of the DBA principles, a specific value of intensity measure required to reach each limit state is calculated, the discrete number of losses can be directly associated with the corresponding earthquake intensities.

The expected costs derive from three different contributions. One contribution is due to the costs associated with the building repair, given that the structure did not collapse under the specified earthquake intensity. Another contribution derives from the losses associated with the demolition of the building, given that the structure did not collapse but exhibits levels of residual drift such that is deemed irreparable. The third contribution depends on the expected losses associated with the collapse of the building.

These three contributions are highlighted in the following equation expressed in Ramirez and Miranda (2012) that allows computing the total loss associated to a performance level (PL):

$$L_T(PL) = L_{NC\cap R}(PL) + L_{NC\cap D}(PL) + L_C(PL) \tag{3.27}$$

Where: L_T is the total loss at the considered performance level (PL); $L_{NC\cap R}$ is the loss given that the structure did not collapse (NC) and the building is repaired (R); $L_{NC\cap D}$ is the loss given that there is no collapse (NC) but the building is demolished (D) and L_C is the loss due to collapse (C). Thus, both collapse and demolition are considered as possible outcomes of a seismic event.

Once the three mutually exclusive terms are defined, the total probability theorem gives:

$$
\begin{aligned}
E[L_T|PL] = {} & E[L_T|NC \cap R, PL] \cdot \{1 - \mathrm{P}(D|NC, PL)\} \cdot \{1 - \mathrm{P}(C|PL)\} \\
& + E[L_T|NC \cap D, PL] \cdot \{\mathrm{P}(D|NC, PL)\} \cdot \{1 - \mathrm{P}(C|PL)\} \\
& + E[L_T|C, PL] \cdot \{\mathrm{P}(C|PL)\}
\end{aligned} \tag{3.28}
$$

Where: $\mathrm{P}(D|NC, PL)$ is the probability of demolition, given that the structure survived the earthquake, for a define PL; $\{1 - \mathrm{P}(D|NC, PL)\}$ is the probability that the structure is not demolished given that it survived the earthquake, for a define PL; $\mathrm{P}(C|PL)$ is the probability of collapse given a defined PL, $\{1 - \mathrm{P}(C|PL)\}$ is the probability that the structure is not collapsed given a define PL. Thus: $E[L_T|NC \cap R, PL]$ is the repair cost; $E[L_T|NC \cap D, PL]$ is the loss in case of demolition; $E[L_T|C, PL]$ is the loss in case of collapse.

Repair costs are evaluated adopting storey-based fragility functions, introduced by Ramirez and Miranda (2009). These functions correlate directly the structural parameters (EDP) with the decision variable (DV), which corresponds to the monetary cost needed to restore the building to its original state after an earthquake. This step allows simplifying the loss assessment methodology of PEER (see Figure 1) by performing the third step in advance, i.e., the damage estimation, and thus reducing the amount of data and computational effort required. The different components of the building are not equally sensitive to each demand parameter, therefore each damaged component should be evaluated according to the more relevant EDP. The EDP chosen in this study for the different components are the same selected by Ramirez and Miranda (2009): the inter-storey drift ratios (IDR) and the peak floor accelerations (PFA). Indeed, the authors differentiated the components as either drift-sensitive or acceleration sensitive, but also as structural and non-structural. Assuming that the structural damage may be attributed to high inter-storey drifts, they considered drift-sensitive structural components, drift-sensitive non-structural components and acceleration sensitive non-structural components.

Thus, to evaluate the expected losses due to non-collapse, the EDP-DV functions provided for mid-rise (5-10 floors) buildings, with non-ductile reinforced concrete moment resisting frames, have been

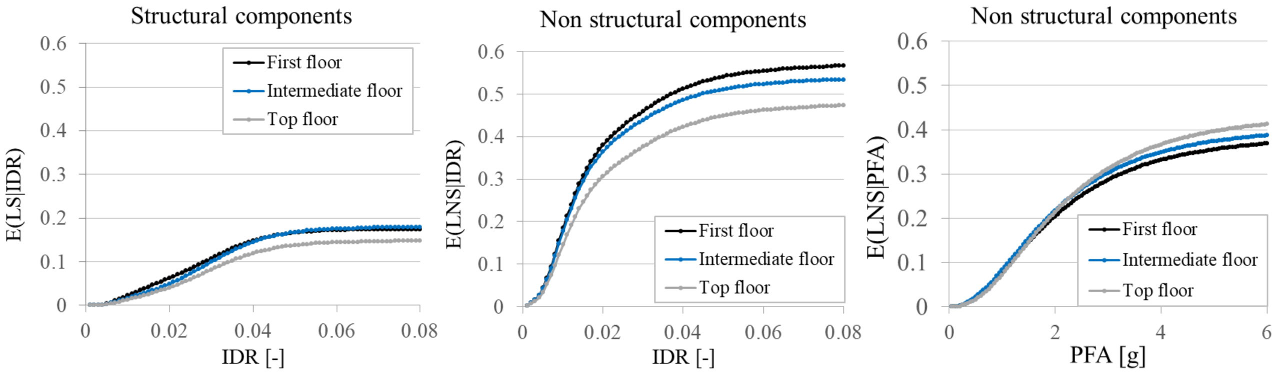

(a) *(b)* *(c)*

Figure 28. EDP-DV functions for different floors of a mid-rise building, adapted from Ramirez and Miranda (2009): (a) drift-sensitive structural components; (b) drift-sensitive non-structural components; (c) acceleration sensitive non-structural components.

adopted in this study. The functions are defined for space moment-frame and occupancy type ‘office’, and are reported in Figure 28, in which the loss is normalized by the replacement value of the storey. The findings of Ramirez and Miranda (2012), concerning the probability of demolition for a building that survived an earthquake, are adopted in this simplified displacement-based performance assessment methodology. Indeed, the authors proposed a fragility function correlating the probability of demolishing a building that did not collapsed and the peak residual IDR (RIDR), named Residual Inter-storey Drift Ratio-Demolition Fragility. This fragility function follows a lognormal distribution with median 0.015 and dispersion 0.3. According to the authors, this distribution may be interpreted as the number of professionals that would suggest the demolition of a building that did not collapse after a seismic event, but exhibits a high level of peak residual inter-storey drift that overcomes the threshold of 1.5%. Moreover, following the FEMA P-58 approach, the site clearance from debris is assumed to have an impact on the building replacement cost of the 20%, and, of the 30% if the demolition of the residuals is considered.

In addition, the probability of collapse is estimated by means of a fragility function which expresses the probability of the building collapse as a function of the earthquake intensity (IM). Typically, these fragilities are assumed to follow a lognormal distribution that can be fully described by a median IM and a dispersion term. In this framework, a judgment-based fragility method is adopted following the method of Ligabue (2015): the median value is chosen as the spectral acceleration associated with the development of the near-collapse limit state introduced before, and the dispersion of 0.6 has been assumed given the regular layout of the structure.

Finally, for the determination of the Expected Annual Losses (EAL), which is the main result of the time-based seismic loss assessment, the area enclosed by the total loss curve has to be determined. In order to assign a Mean Annual Frequency (MAF or λ) for each performance level, the hazard curve is determined considering the hazard data given in D.M. (2018) for a specific Italian site location of the building. Thus, the hazard curve is defined with discrete points, and, to achieve a higher level of accuracy in the calculations, it is approximated with the exponential fit law reported in Equation 3.29 (Ligabue 2015). The hazard data adopted in this work are reported in Figure 29.

T_R [year]	a_g [g]	F_0	T_c^* [s]
30	0.063	2.416	0.248
50	0.082	2.439	0.253
72	0.097	2.417	0.259
101	0.113	2.391	0.265
140	0.131	2.377	0.269
201	0.149	2.398	0.275
475	0.205	2.398	0.282
975	0.262	2.399	0.286
2475	0.348	2.398	0.319

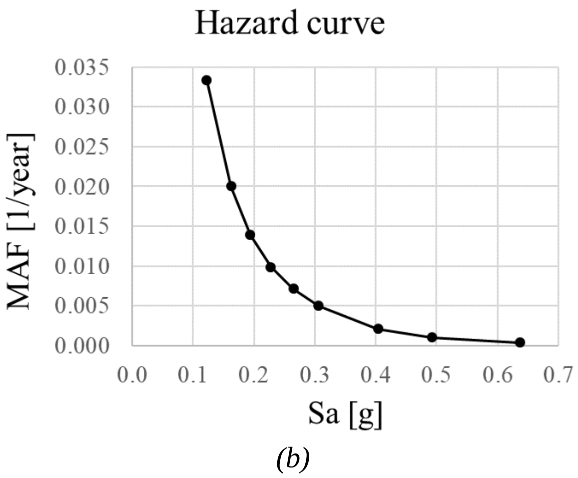

(a) *(b)*

Figure 29. Hazard data considered in this work taken from the Italian D.M. (2018): (a) spectral parameters for different return periods; (b) hazard curve.

Since the procedure does not account for any source of uncertainty, the following empirical formulas from Welch et al. (2014) may be adopted to incorporate the uncertainties. Hence, by scaling the mean annual frequencies by a coefficient C, an increase in the expected annual losses (EAL) is produced.

$$\lambda(IM) = k_0(IM)^{-k} \tag{3.29}$$

$$\lambda_{PL}^{x} = \lambda(S_a^C)\, C_H\, C_f\, C_x \tag{3.30}$$

$$C_H = \exp\left[\frac{1}{2}\beta_H^2\right] \tag{3.31}$$

$$C_f = \exp\left[\frac{k^2}{2b^2}\left(\beta^2{}_{DR} + \beta^2{}_{CR}\right)\right] \tag{3.32}$$

$$C_x = \exp\left[K_x\sqrt{\frac{k^2}{\beta^2}\left(\beta^2{}_{DU} + \beta^2{}_{CU}\right)}\right] \tag{3.33}$$

Where: k and k_0 are exponential fitting coefficients; $\lambda(S_a^C)$ is the median estimate of the mean annual frequency of the spectral acceleration at a given limit state, C_H considers the distance between mean and median hazard values; C_f accounts for the dispersion in structural demand and capacity and C_x is a function of the selected confidence level through the parameter K_x, the standardized Gaussian variation associated with probability x of not being exceeded. The coefficients β account for the record-to-record randomness, the epistemic uncertainty and the aleatory randomness.

3.4.1.2. ANNUALIZED PROBABILITY OF COLLAPSE (POC)

In this Section, the procedure for the assessment of the expected average annualized probability of collapse (POC) is determined, following the time-based framework described in Ligabue et al. (2018). By combing the collapse fragility function with the hazard curve, it is possible to evaluate the annualized probability of collapse as the area enclosed by the resulting curve, reporting the probability of collapse versus the mean annual frequency. The evaluation of the annualized POC of the structure with different retrofit techniques allows performing comparative considerations of the effectiveness of the interventions, and easing the decision-making phase. In particular, it is possible to determine the seismic retrofit that mostly reduce the collapse risk of the existing building.

To this aim, a simplified “static-incremental dynamic analysis” has been implemented to define the collapse fragility of the structure, by adopting the Capacity Spectrum method, following the simplified procedure outlined in Ligabue et al. (2017). The fragility curves is evaluated based on the selection of 20 ground-motion records performed with an *ad-hoc* algorithm in Matlab, which are compatible with the elastic demand spectrum defined according to the hazard of the site of the structure. It is worth saying that this step can be easily conducted with REXEL, a software specifically developed for the selection of seismic records developed by ReLUIS.

Thus, the seismic action, represented by the 20 corresponding response spectra, is gradually scaled in the ADRS format, in order to match the ultimate point of the capacity curve of the structure. The cumulative fraction of points reaching collapse at different values of the intensity measure is counted, and the collapse fragility is defined by fitting the data. The fragility is expressed in terms of spectral acceleration at the fundamental period T_1 of the building under consideration.

The hazard curve allows assigning a Mean Annual Frequency (MAF or λ) to each value of Sa computed. Thus, the average annual probability of collapse of the structure is evaluated as the area enclosed by the curve defined by the probability of collapse against the corresponding mean annual frequency (Ligabue et al. 2018).

3.4.1.3. COST-BENEFIT ANALYSIS (BCR)

At the end of the procedure, once the losses are computed for the As-Built structure and the structures with different retrofit solutions, the cost-benefit analysis is performed. The adimensional parameter named Benefit-Cost-Ratio (BCR) is adopted to find the retrofit solution that maximises the Net Present Value (NPV). The NPV is the value of expected loss after a specific period of time: it is common to refer to the life-time of the structure, which is 50 years for ordinary buildings according to Codes. Once the initial cost of investment is computed for a specific retrofit scenario, i.e., the cost for the installation of the retrofit (C_r), the BCR can be estimated. Thus, the direct cost of the retrofit and the expected annual loss (EAL) associated with each retrofit option need to be estimated in order to find the expected loss, calculated with the following Equation (Bradley et al. 2008):

$$NPV = \frac{\left(1 - e^{-\lambda t}\right)}{\lambda} EAL + C_r \tag{3.34}$$

Where: EAL is the expected annual loss in €; λ is the discount rate (to convert the losses to the net present value) assumed equal to 3% (Welch et al. 2014); t is the life of the building assumed equal to 50 years for the case-study building; and C_r is the cost of retrofitting.

Therefore, the benefit cost ratio (BCR) can be calculated with the following formula (Beetham 2013):

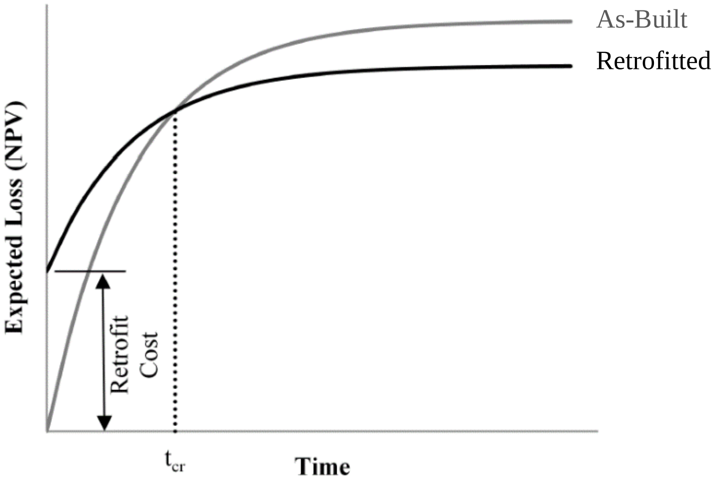

Figure 30. Graphical evaluation of the critical service life, adapted from Beetham (2013).

$$BCR = \frac{(NPV_{As-built} - NPV_r)}{C_r} \cdot \frac{1 - e^{-\lambda t}}{\lambda} \tag{3.35}$$

Where: $EAL_{As-built}$ is the expected annual loss of the original building; EAL_r is the expected annual loss of the retrofitted building. Moreover, Bradley et al. (2008) presented the following equation to calculate the critical service life (t_{cr}) of a structure, which is the time after which a retrofit alternative becomes economically convenient. This concept is also presented graphically in Figure 30.

$$t_{cr} = \frac{-1}{\lambda} \ln\left(1 - \frac{\lambda}{(1-\alpha)} \frac{C_r}{EAL_{As-built}}\right) \tag{3.36}$$

Where: $\alpha = EAL_R / EAL_{As-built}$ is the ratio between the expected annual losses of the retrofitted structure and the As-Built one. The comparative evaluation of C_r, BCR and t_{cr} for different possible interventions gives additional significant information for the decision-making.

3.4.2. APPLICATION TO A CASE-STUDY BUILDING

The whole simplified procedure is applied to an existing concrete frame building not conform to the actual seismic regulations. The results are presented for the As-built structure and for the structure after the application of different local intervention techniques on the columns: the fiber reinforced polymers (FRP), the Italian ‘cerchiatura attiva dei manufatti’ (CAM) and the concrete jacketing (CJ). The second system has been developed in Italy for the structural rehabilitation of existing masonry buildings, and lately successfully adapted to the RC ones (Dolce et al. 2003).

The non-linear FEM models of the main frame of the building are analysed with the software Midas GEN (CSPFEA), considering bilinear flexural plastic hinges concentrated at the extremities of beams and columns. The shear resistance is verified with the formula prescribed in Eurocode 8 accounting for the cyclic shear resistance (CEN 2005), avoiding the modelling of non-linear shear hinges.

Since the objective of the work is to outline a comprehensive method to investigate the seismic losses of alternative retrofit options, a simplified FEM model not considering the non-linear behaviour of beam-column nodes has been adopted. This simplified assumption is acceptable within the scope of this comparative method, although the modelling of hinges located at the joints would likely anticipate the damage mechanisms in all the structures modelled (Ligabue et al. 2018, Gentile et al. 2018).

3.4.2.1. AS-BUILT STRUCTURE

The As-Built structure is a regular RC frame building of four floors built without seismic details in the 70’s, and made of concrete C20/25 and steel FeB44K.

The height of the first floor is 3.1 m, while the height of the upper floors is 3.5 m. The five beam spans are symmetric, with dimensions (from left) of 6.75 m, 6.10 m, and 7.50 m in the middle. In Tables 10 and 11 the sections and the reinforcement of the structural elements are reported. It is worth noting that there is a decrease of the section dimensions of columns at the third floor, which is likely to entail a soft-storey damage mechanism, as discussed in the following. The representation of the model is reported in Figure 31.

The plastic hinges are modelled considering bilinear moment-rotation laws, adopting the formulations given in Eurocode 8 for the calculation of the yielding and the ultimate rotations (see Equations in Appendix A). The hinges in columns take into account of the evolution of the axial load at the different steps of analysis. The Pushover analysis is performed applying increasing displacements proportional to the first mode of vibration of the frame, considering the top left master node, and 500 increment steps.

Table 10. Sections of the structural elements in the As-built structure.

Type	b [cm]	h [cm]	Nominal cover c [cm]
Columns of 1st and 2nd floors	50	40	4
Internal columns of 3rd and 4th floors	50	40	4
External columns of 3rd and 4th floors	40	30	4
Beams of the 1st floor	50	70	4
Beams of the 2nd and 3rd floors	85	45	4
Beams of the roof	85	45	4

Table 11. Reinforcement of the structural elements in the As-built structure.

Type	Longitudinal	Transversal
Columns of 1st and 2nd floors	8Φ16	Φ8/20
Internal columns of 3rd and 4th floors	8Φ14	Φ8/20
External columns of 3rd and 4th floors	8Φ14	Φ8/20
Beams of the 1st floor	Top: 6Φ18+3Φ12 Bottom: 8Φ16	Φ8/10
Beams of the 2nd and 3rd floors	Top: 10Φ18+4Φ12 Bottom: 12Φ16	Φ8/10
Beams of the roof	Top: 7Φ20+3Φ12 Bottom: 8Φ16	Φ8/10

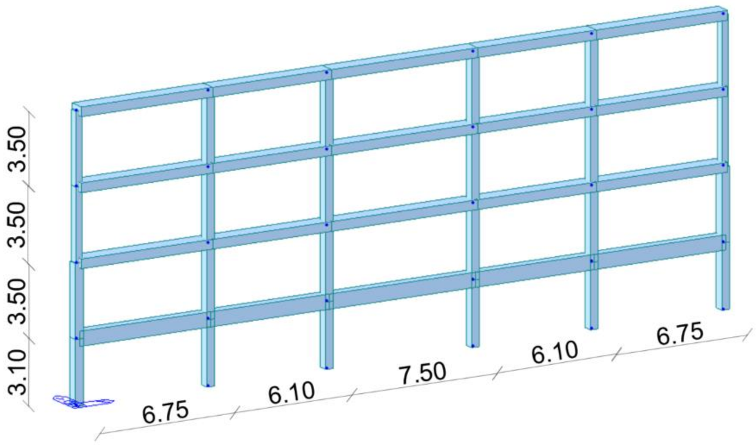

Figure 31. Scheme of the finite element model considered, with indication of the span dimensions.

The masses are modelled in the seismic combination of loads, as prescribed by Codes. P-Δ effects are also taken into account in the analyses, even if they are not particularly relevant for this structure. The different global performance levels are identified considering the following rule calibrated observing the development of damage and the decrease of the stiffness in the case study structure: the attainment of the yielding rotation in the first plastic hinge (ZL), the formation of plastic hinges at the bottom and top sides of three aligned columns (Y), the formation of plastic hinges at the bottom and top sides of five aligned columns (Y), the last step before collapse (NC), the attainment of a residual drift of 1.5% (RIDR 1.5%). In the As-Built structure, the first plastic hinges forms in a top column of the fourth storey, while all the subsequent damage mechanisms are registered in the third storey, producing a column-sway mechanism in the frame (visible in Figure 33).

The result is the capacity curve depicted in Figure 32. The ultimate point corresponds to a displacement of 0.046 m and a total base shear of 795.7 kN, and the structural ductility (ratio between ultimate and yielding displacements) is nearly 1.6. The RIDR 1.5% is not reached before the

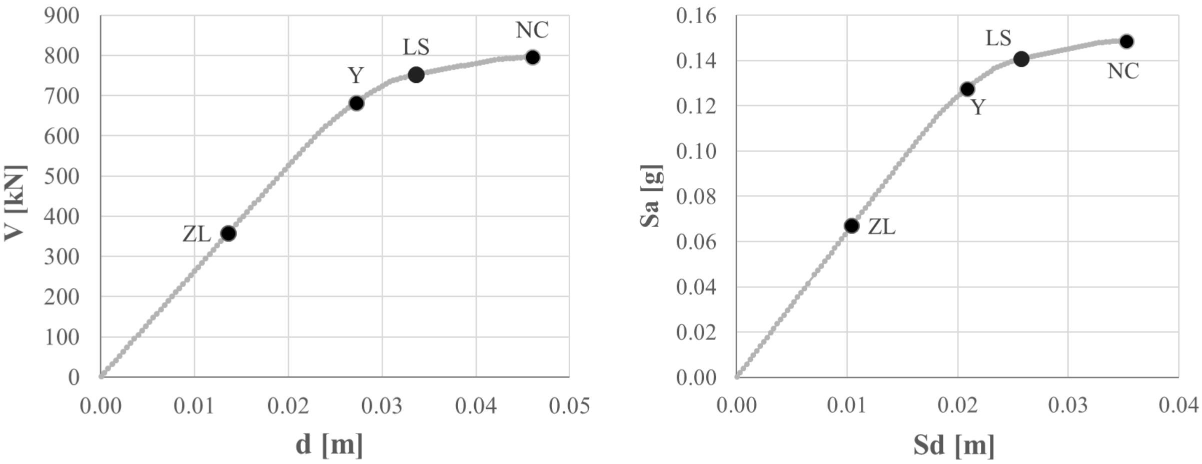

(a) *(b)*

Figure 32. Capacity curve of the As-Built structure: (a) Shear-displacement; (b) ADRS format.

Table 12. Properties of equivalent SDOF systems corresponding to the limit states in the As-Built structure.

		ZL	**O/Y**	**LS**	**NC**	**RIDR 1.5%**
Displacement of the effective mass	Δ_c [mm]	10	21	26	36	130
Effective mass	m_e [kN]	6204	6146	6040	5760	5760
Effective height	H_e [mm]	3469	3469	3472	3477	3477
Base shear	V_b [kN]	359	682	753	796	796
Effective stiffness	K_e [kN/m]	34514	32862	29213	22068	6130
Ductility	μ	0.501	1.00	1.242	1.736	6.251
Spectral acceleration	S_a (T_1) [g]	0.365	0.358	0.340	0.303	0.159
Effective period	T_e [s]	0.85	0.87	0.91	1.02	1.94
MAF	λ [1/year]	0.1132	0.0324	0.0145	0.0047	2.36E-05

attainment of the collapse, however, the loss assessment is performed taking into account the probable occurrence of this damage state causing a loss equal to the entire replacement cost of the building. Thus, the frame is transformed into an equivalent SDOF system at each limit state to perform the simplified loss-assessment procedure, deriving the dynamic properties reported in Table 12, and the EDPs in Figure 33, implementing the formulas described in Section 3.4.1. The spectral acceleration is computed through the demand spectrum at the effective period of vibration of each SDOF.

Once the building response at different limit states is evaluated, the economic losses due to repair, collapse and demolition are computed. The economic loss is expressed as a fraction of the total replacement cost of the building, which is computed considering a value of 1300 €/mq of surface in plan. The storey cost distribution of the different components (structural, non-structural drift sensitive and non-structural acceleration sensitive) is assumed equal to the one described in Ramirez and Miranda (2009), and reported in Table 13. The non-structural drift sensitive components are basically the interior elements, such as the partitioning, the doors, the finishing, and the ceiling. The non-structural acceleration sensitive elements are the services, like the plumbing, the conveying and the electrical lines.

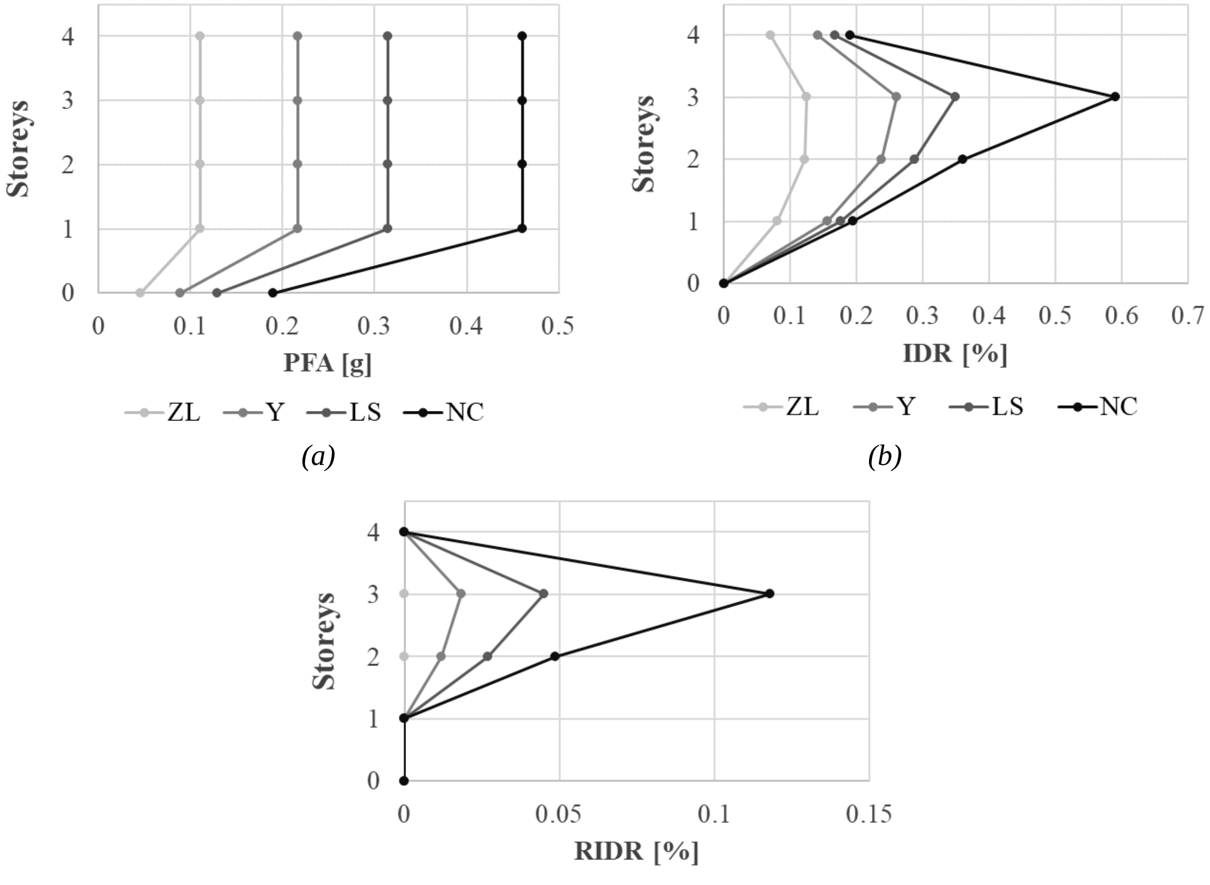

(a) *(b)*

(c)

Figure 33. Engineering demand parameters for the As-Built structure: (a) peak-floor accelerations; (b) inter-storey drift ratios; (c) residual inter-storey drift ratios.

The expected losses at each performance level are summarized in Table 14 and illustrated in Figure 34a. It is worth noting that the entire expected loss of the last limit state has been set to the threshold 100% of the reconstruction costs, but it would be higher from the computation since the costs due to demolition are accounted (see Section 3.4.1.1).

In general, the expected losses due to collapse are significantly higher compared with the other amounts, at each limit state. This is because the spectral accelerations of the SDOF at the low limit states are similar to that at near collapse (mean value of the collapse fragility, following Ligabue 2015), leading to a high collapse probability; moreover, the IDR and RIDR at the different performance levels are rather similar to each other, leading to low and comparable repair costs.

It is worth noting that the expected losses due to the first two limit states are not negligible, since they constitute nearly the 14% of the total replacement cost of the structure. This fact is due to the frequent probability of occurrence of these performance levels.

The total loss curve is reported in Figure 34b; the area under the curve is the expected annual loss, which is equal to 1.73% of the total reconstruction cost of the building. In addition, the value of EAL computed with the empirical method allowing considering the uncertainties, is equal to 2.64%.

Based on the values of equivalent elastic spectral displacement and the effective period at each limit state, the spectral acceleration of capacity is computed. Thus, the ratio between the capacity and the demand, in terms of spectral acceleration, provides a factor named new building standard (NBS). This parameter is used in the New Zealand structural regulations (Ligabue et al. 2018) to indicate the percentage of the design earthquake, relative to a newly designed structure, that the existing building can sustain without exceeding a selected limit state (for instance, the life safety). Existing buildings can be graded as either potentially earthquake prone (NBS < 33%), potentially earthquake risk (33% < NBS < 67%) or unlikely to be an earthquake risk building (NBS > 67%). The NBS has been assessed at each performance level, and the corresponding design spectrum at life-safety, scaled to match the capacity levels, is represented in Figure 35. At the life safety limit state the building has nearly 45% NBS, thus it is potentially in earthquake risk.

Table 13. Cost distributions assumed for the case-study building.

	1st floor	2nd-3rd floors	Roof
Structural	36.70 %	34.7 %	36.8 %
Non-structural, drift sensitive	20.7 %	21.4 %	11.1 %
Non-structural, acceleration sensitive	42.6 %	43.9 %	52.1 %
Total	100 %	100 %	100 %

Table 14. Expected losses of the As-Built structure at each performance level.

	P(D|IM)	P(C|IM)	L(NC∩R) %	L(NC∩D) %	L(C) %	L(NC) %	E[LT|IM] %	MAF [1/year]
ZERO LOSS	0.000	0.009	0.04	0.00	1.06	0.04	1.1	0.1132
YIELDING	0.000	0.104	0.25	0.00	12.53	0.25	12.8	0.0324
LIFE SAFETY	0.000	0.261	0.42	0.00	31.34	0.42	31.8	0.0145
NEAR COLLAPSE	0.000	0.500	0.68	0.00	60.00	0.68	60.7	0.0047
RIDR 1.5%	0.529	0.921	0.26	5.41	110.56	5.67	100.0	2.36E-05

Based on the values of equivalent elastic spectral displacement and the effective period at each limit state, the spectral acceleration of capacity is computed. Thus, the ratio between the capacity and the demand, in terms of spectral acceleration, provides a factor named new building standard (NBS).

This parameter is used in the New Zealand structural regulations (Ligabue et al. 2018) to indicate the percentage of the design earthquake, relative to a newly designed structure, that the existing building can sustain without exceeding a selected limit state (for instance, the life safety). Existing buildings can be graded as either potentially earthquake prone (NBS < 33%), potentially earthquake risk (33% < NBS < 67%) or unlikely to be an earthquake risk building (NBS > 67%). The NBS has been assessed at each performance level, and the corresponding design spectrum at life-safety, scaled to match the capacity levels, is represented in Figure 35. At the life safety limit state the building has nearly 45% NBS, thus it is potentially in earthquake risk.

The average annual probability of collapse of the As-Built building is estimated following the procedure explained in Section 3.4.1.2.

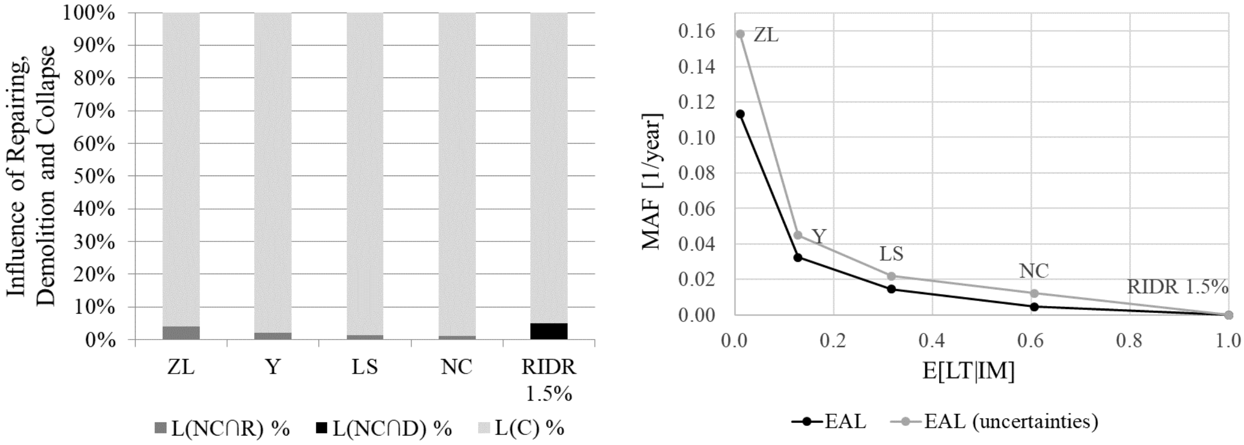

(a) *(b)*

Figure 34. (a) Percentage of influence on the total loss of repairing, demolition and collapse; (b) approximated total loss curve for the As-Built structure.

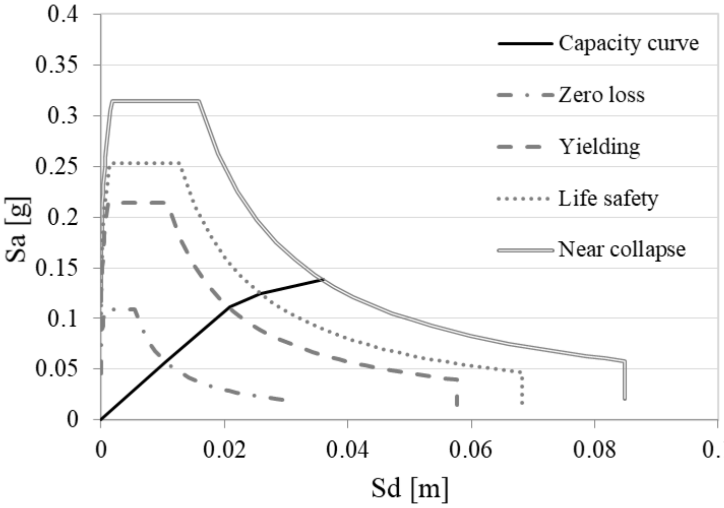

PL	%NBS
ZL	15.8
Y	31.0
LS	44.9
NC	65.9

Figure 35. Percentage of NBS for the existing building at different performance levels.

A selection of 20 ground-motions has been performed with an *ad-hoc* algorithm fully described in Appendix A. In order to be consistent with the characteristics of the site of the structure, the selection of the records takes into consideration the seismic hazard parameters and the source mechanisms. The following input parameters have been set: the fundamental period of vibration T_1 of the existing frame equal to 0.767 s, the reference moment magnitude (5.11) and the source-to-site distance (6.57 km), the limits of the scaling factor equal to 0.33 to 3, the hazard data of the reference site spectrum.

The spectra selected are shown in Figure 36a, while Figure 36b shows the collapse fragility curve estimated for the As-Built structure. Once the spectra are scaled in the ADRS format, following the capacity spectrum method, the cumulative fraction of data overcoming each spectral acceleration is computed. Hence, the resulting point are fitted with a lognormal cumulative distribution through a linear regression procedure. The main descriptors of the fragility function are: μ equal to -1.491 and σ equal to 0.25.

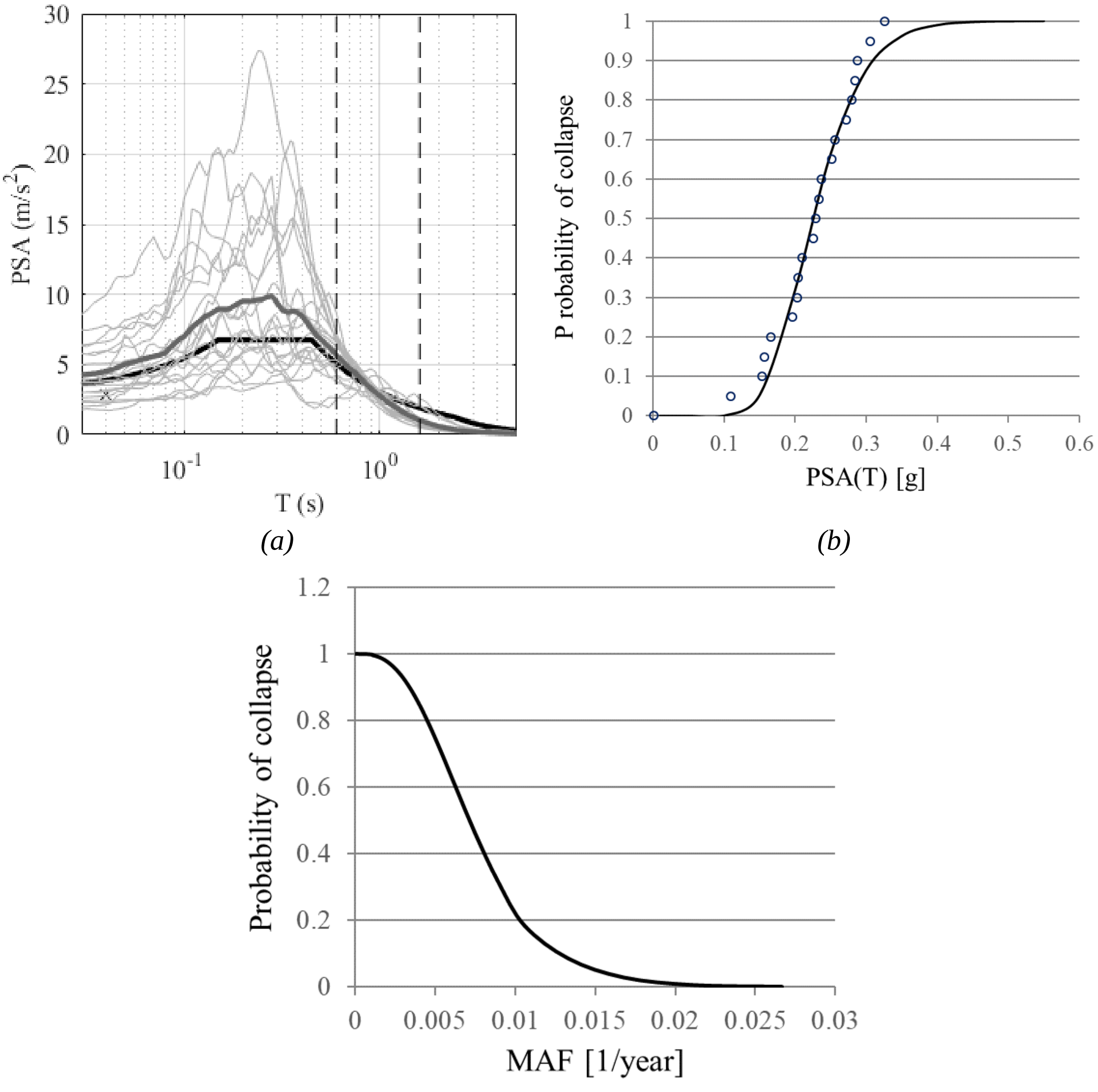

(a) *(b)*

(c)

Figure 36. (a) Spectra of the ground-motion selected; (b) approximated collapse fragility curve for the As-Built building; (c) annual probability of collapse curve.

Finally, the final curve defining the probability of collapse depending on the mean annual frequency is assessed, by combining the fragility curve and the hazard curve of the site (PSA-based). Figure 36c illustrates the final curve obtained for the As-Built structure: the area enclosed is the annual probability of collapse, equal to 1.15%. This high value reflects the outcomes obtained previously, indicating a low seismic performance of the structure and a high average collapse tendency.

In order to increase the capacity of the building, to lower the EAL and the POC, different local interventions are proposed in the following Sections.

3.4.2.2. STRUCTURE WITH FRP

The first intervention consists in confining the columns by wrapping the elements with FRP sheets made of fibers, orthogonal to the direction of the member axis. This technique is useful to increase the shear and axial load carrying capacity of the columns, and raise the ductility of the entire structure. Moreover, the ease of installation and the durability make this solution efficient and cost-effective (Del Vecchio et al. 2021).

Different possible layout of applications to the case-study frame have been tested, but only one of the most efficient is reported to be evaluated as a design retrofit. In particular, in the model, the fibers are applied at the critical regions of the columns of the third and fourth floors. Following the formulas provided in the official guidelines (see ReLUIS), the effect of the intervention made with two layers of fibers with a wet lay-up system is modelled computing a equivalent amount of transversal reinforcement in the columns. This allows facilitating the modelling of the intervention.

The result of this first application is the capacity curve depicted in Figure 37, with the identification of the performance levels. The formation of the plastic hinges follows the same order described in the As-Built condition, but at higher steps of the Pushover analysis, resulting in an increase of the displacement capacity. Indeed, the capacity in terms of base shear is the same of that in the As-Built condition, while the ultimate displacement is significantly higher, resulting in a global ductility of 3.24, which is almost twice the previous one.

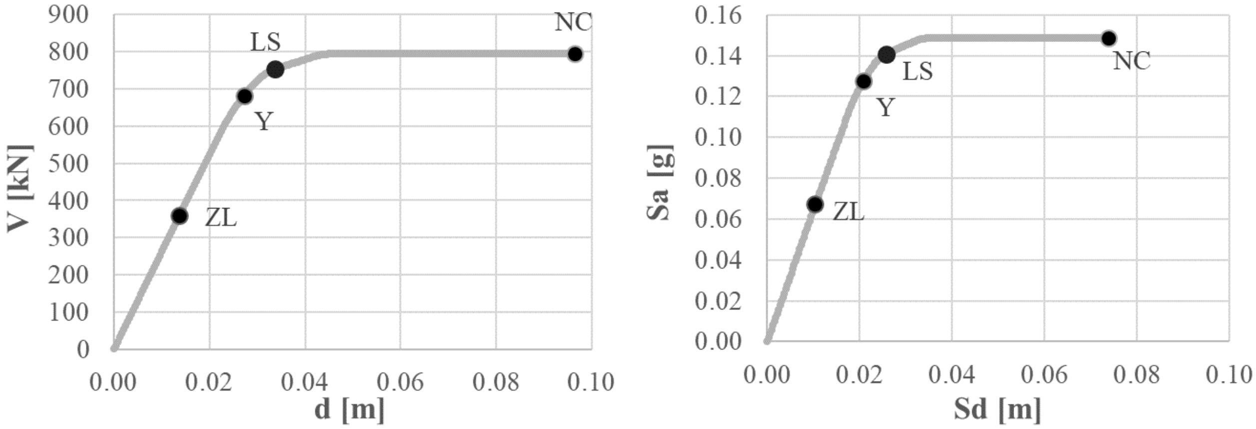

(a) *(b)*

Figure 37. Capacity curve of the structure with FRP: (a) Shear-displacement; (b) ADRS format.

Table 15. Properties of equivalent SDOF systems corresponding to the limit states in the structure with FRP.

		ZL	O/Y	LS	NC	RIDR 1.5%
Displacement of the effective mass	Δ_c [mm]	10	21	26	83	86
Effective mass	m_e [kN]	6204	6146	6040	4764	4764
Effective height	H_e [mm]	3469	3469	3472	3488	3488
Base shear	V_b [kN]	359	682	753	796	796
Effective stiffness	K_e [kN/m]	34514	32862	29213	9591	9266
Ductility	μ	0.501	1.00	1.242	3.996	4.135
Spectral acceleration	S_a (T_1) [g]	0.365	0.358	0.340	0.219	0.215
Effective period	T_e [s]	0.85	0.87	0.91	1.41	1.44
MAF	λ [1/year]	0.1132	0.0324	0.0145	0.00014	0.00012

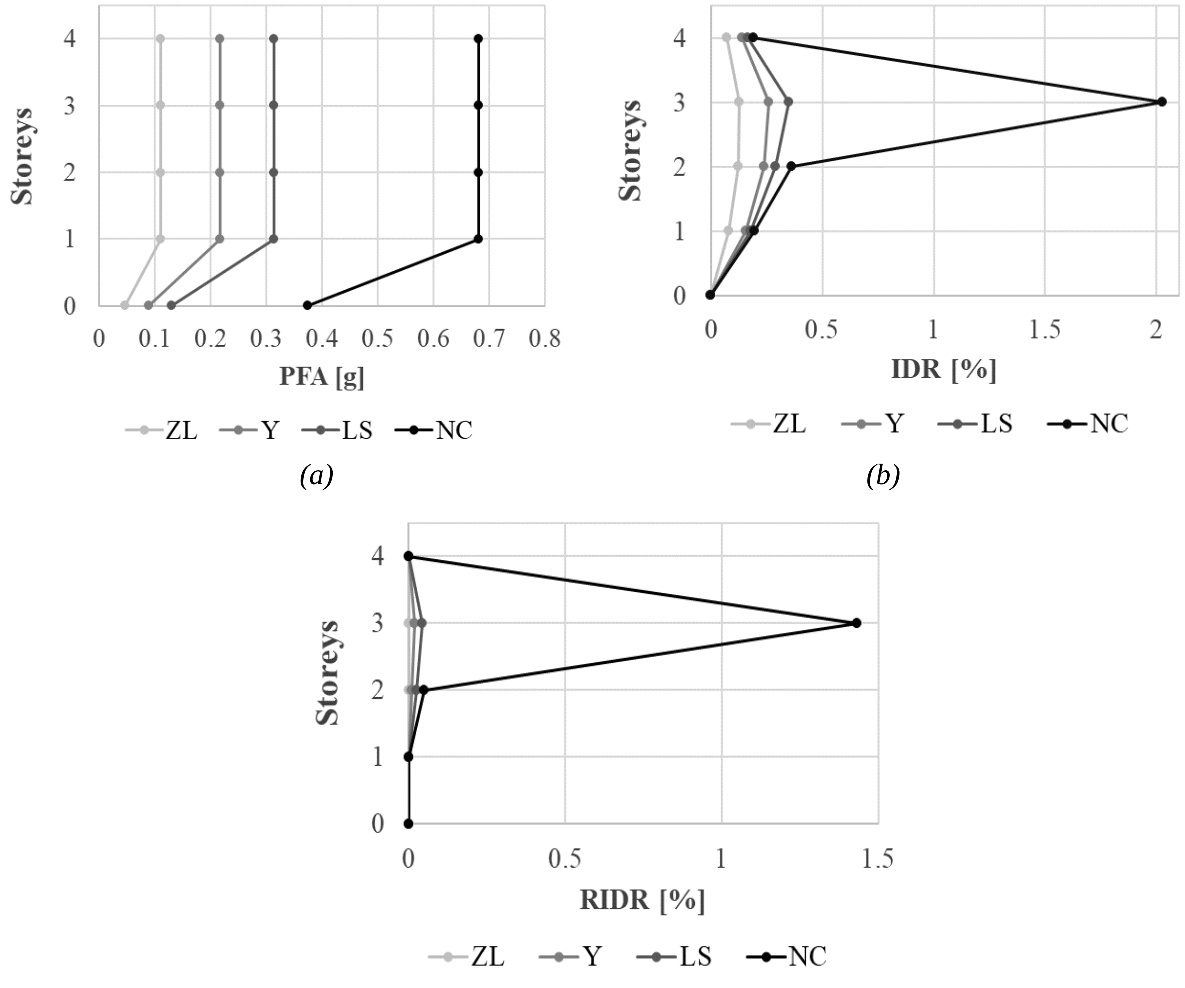

(a) *(b)*

(c)

Figure 38. Engineering demand parameters for the structure with FRP: (a) peak-floor accelerations; (b) inter-storey drift ratios; (c) residual inter-storey drift ratios.

Thus, the transformation into equivalent SDOF systems is computed to carry out the simplified loss assessment, and the dynamic properties are reported in Table 15. The engineering demand parameters of this structure are shown Figure 38. It is worth noting that all the EDP reach higher values compared to those in the As-Built condition, which is a sign of the overall improvement in the structural behavior. Moreover, the RIDR at the near collapse limit state nearly reaches the limit value of demolition, i.e, 1.5%.

The loss assessment procedure is conducted computing the expected losses at each performance level. The results are reported in Table 16 and Figure 39. In this case, the expected losses due to demolition are significant at the ultimate limit states due to the high residual inter-storey drift ratio. Whereas, the losses due to repair are high at the first three limit state, differently than the As-Built condition. This is because the spectral accelerations at the near collapse limit state is quite different than those at the other limit states, leading to a lower collapse probability compared to the previous case. It is worth noting that the expected losses due to the first two limit states are nearly one third of those found for the As-Built condition. The area under the total loss curve, shown in Figure 39b, corresponds to an EAL of 0.802%. The one computed considering the uncertainties is higher, equal to 1.22%.

Since the capacity of the structure with FRP is equal to the As-Built one in terms of total base shear, but higher in terms of the ultimate displacement capacity, the differences in the NBS can be detected only at the near collapse limit state. The percentage of NBS at the different performance levels is

	P(D|IM)	P(C|IM)	L(NC∩R) %	L(NC∩D) %	L(C) %	L(NC) %	E[LT|IM] %	MAF [1/year]
ZERO LOSS	0.000	0.000	0.04	0.00	0.03	0.044	0.071	0.1132
YIELDING	0.000	0.008	0.28	0.00	1.01	0.28	1.29	0.0324
LIFE SAFETY	0.000	0.038	0.55	0.00	4.55	0.55	5.09	0.0145
NEAR COLLAPSE	0.439	0.500	1.23	28.55	60.00	29.78	89.78	0.00014
RIDR 1.5%	0.503	0.514	1.09	31.78	61.71	32.87	100.00	0.00012

Table 16. Expected losses of the structure with FRP at each performance level.

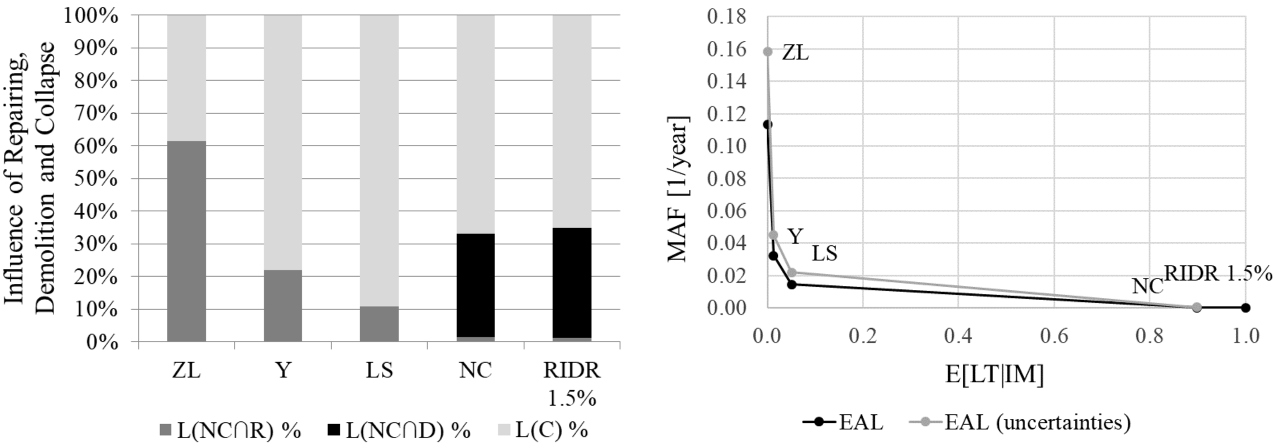

(a) *(b)*

Figure 39. (a) Percentage of influence on the total loss of repairing, demolition and collapse; (b) approximated total loss curve for the structure with FRP.

shown in Figure 40. The value at the ultimate limit state has significantly increased compared with that of the As-Built structure.

Furthermore, the annualized probability of collapse is assessed. Since the first period of vibration of the building and the hazard are not changed, the ground-motion selected are those reported in Figure 36a. However, since the capacity of the building with FRP is different, the collapse fragility curve and the POC differ from those in the As-Built condition.

The two results are reported in Figure 41: the main descriptors of the fragility curve are μ equal to -0.655 and σ equal to 0.37, while the POC is 0.17%. This high reduction with respect to the As-Built condition is due to the increased seismic capacity (i.e., ductility) of the structure, and the higher mean value of the collapse fragility function.

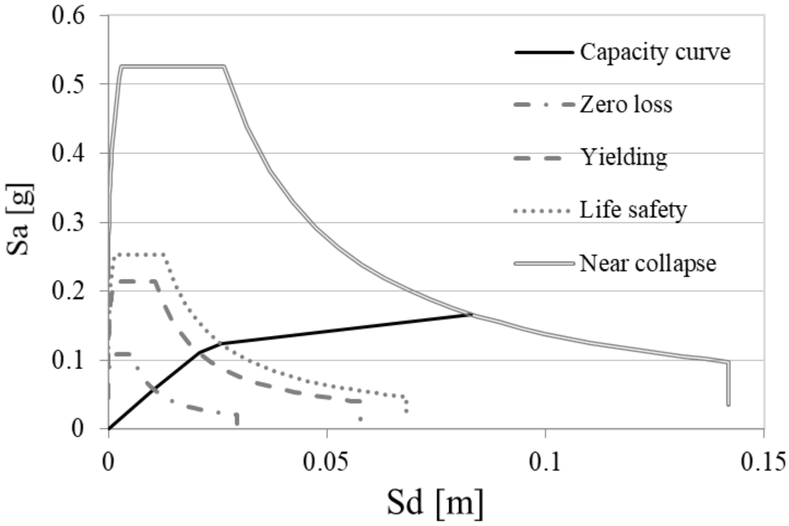

PL	%NBS
ZL	15.8
Y	31.0
LS	44.9
NC	130.3

Figure 40. Percentage of NBS for the structure with FRP at different performance levels.

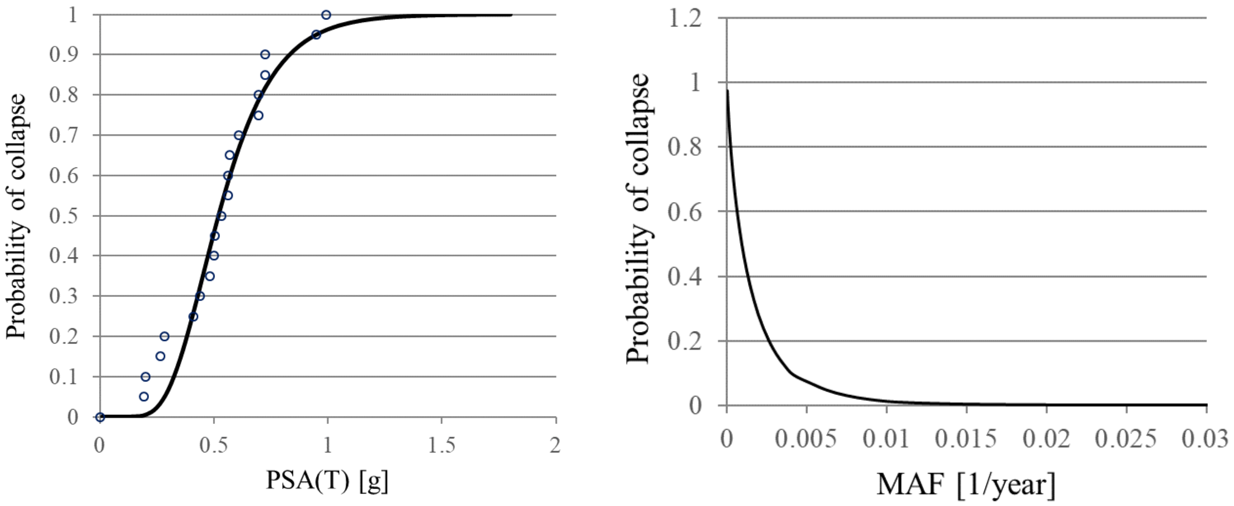

(a) *(b)*

Figure 41. (a) Approximated collapse fragility curve for the structure with FRP; (b) annual probability of collapse curve.

3.4.2.3. STRUCTURE WITH CAM

The second intervention consists in confining the columns with the CAM® system, which is a steel jacketing technique with thin transverse elements, developed in Italy. Several thin stainless steel strips (thickness ≤ 1mm) are applied and pre-stressed during the installation. In the corners, post-tensioned stainless-steel ribbons are applied to connect the strips and provide a suitable immediate confinement. The effectiveness of this strategy mainly relies in the increase of the ductility of the elements thanks to the active lateral confinement applied (Sorace et al. 2021).
Several possible applications to the case-study structure have been tested, but one of the most effective to be proposed as a design retrofit is the one considering the application to the internal columns of the third floor. Following the formulas provided in the CAM guidelines, the effect of the intervention is modelled computing an equivalent amount of transversal reinforcement in the columns, and four equivalent longitudinal bars in the corners of the column sections (with higher diameters compared to the As-Built sections).

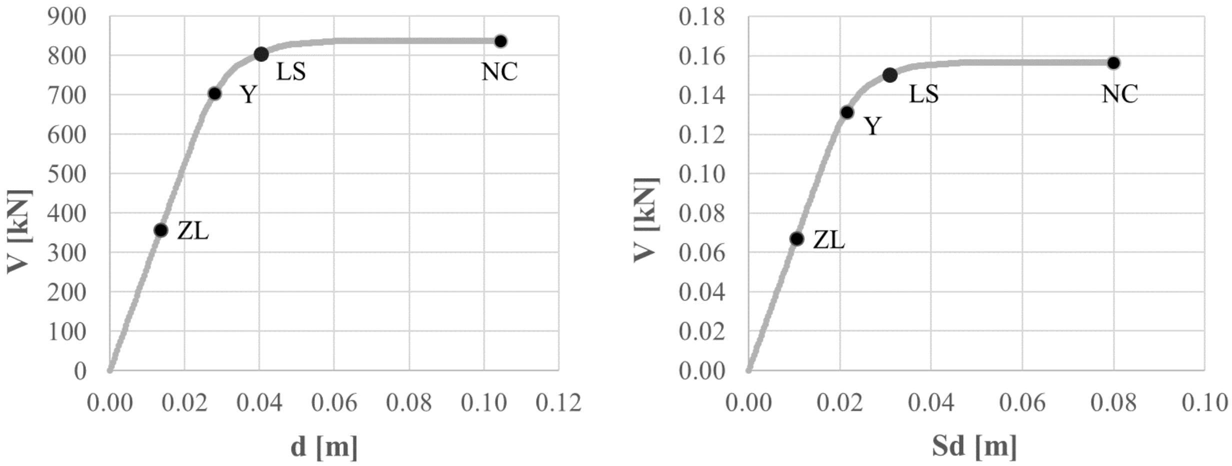

(a) *(b)*

Figure 42. Capacity curve of the structure with CAM: (a) Shear-displacement; (b) ADRS format.

Table 17. Properties of equivalent SDOF systems corresponding to the limit states in the structure with CAM.

		ZL	**O/Y**	**LS**	**NC**	**RIDR 1.5%**
Displacement of the effective mass	Δ_c [mm]	10	21	31	88	92
Effective mass	m_e [kN]	6204	6159	6022	4983	4983
Effective height	H_e [mm]	3469	3469	3473	3488	3488
Base shear	V_b [kN]	359	704	805	837	837
Effective stiffness	K_e [kN/m]	34514	32970	25774	9462	9054
Ductility	μ	0.487	1.00	1.464	4.144	4.331
Spectral acceleration	S_a (T_1) [g]	0.365	0.358	0.320	0.213	0.208
Effective period	T_e [s]	0.85	0.87	0.97	1.46	1.49
MAF	λ [1/year]	0.1131	0.0312	0.0079	0.00011	8.95E-05

The result of the Pushover analysis is the capacity curve depicted in Figure 42, with the identification of the performance levels. The formation of the plastic hinges follows the same order described in the As-Built condition, but all at higher steps of the Pushover analysis. The capacity in terms of base shear is slightly higher of that in the As-Built condition, while the ultimate displacement is significantly higher resulting in a global ductility of 3.35.

Thus, the simplified loss assessment is performed, and the dynamic features of the equivalent SDOF systems are reported in Table 17. The overall increase in the capacity of the building is reflected in the different properties of the structure with CAM compared with those of the As-Built, for the SDOF systems at the LS and NC limit states. Moreover, all the EDP, shown in Figure 43, have higher values compared to those illustrated in Figure 33, as a result of the improved seismic performance of the retrofitted structure.

Furthermore, the estimated losses due to repair, collapse and demolition are computed at each performance level, in order to derive the total loss curve, reported in Figure 44b. A graphical representation of the influence of each loss term is provided in Figure 44a, in which the percentage impact of repairing, demolition and collapse costs are disaggregated over the total value of loss at each limit state. The structure is subjected to a lower probability of collapse due to the improved

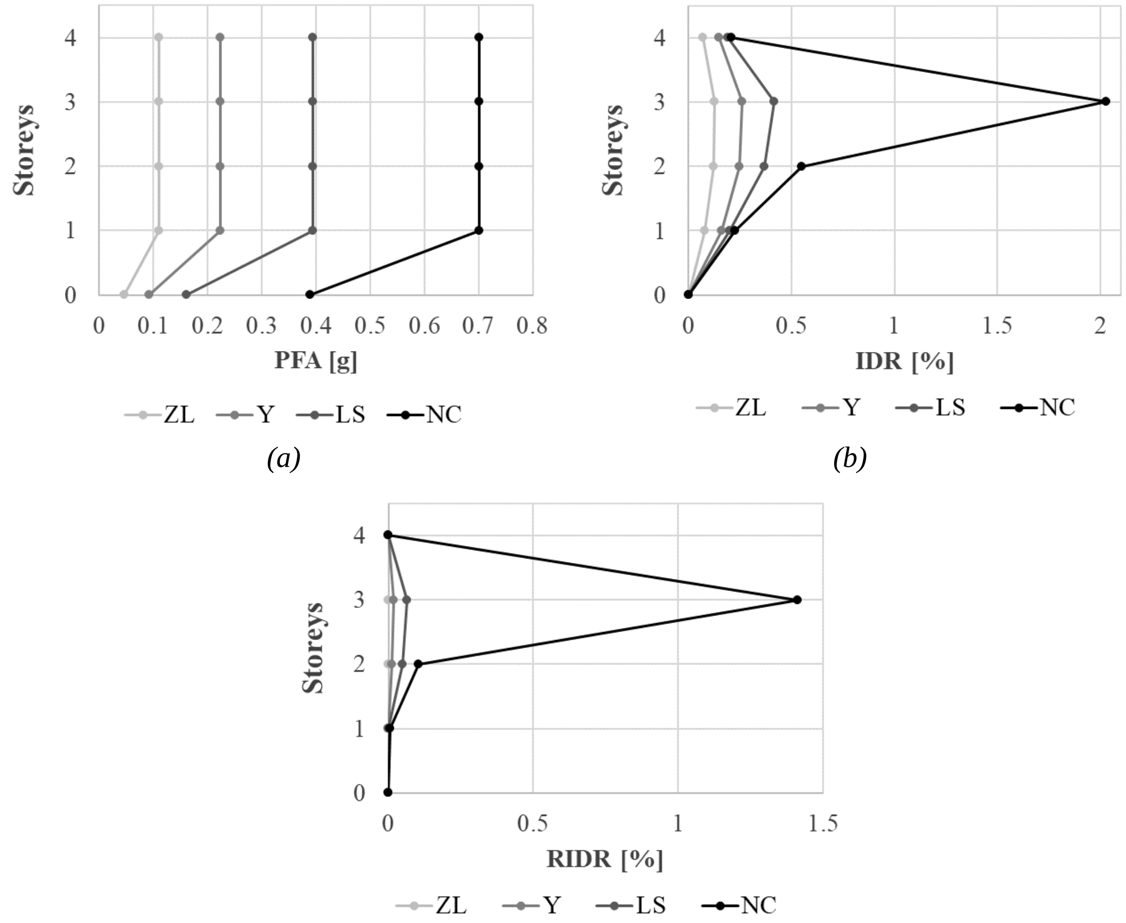

(a) *(b)*

(c)

Figure 43. Engineering demand parameters for the structure with CAM: (a) peak-floor accelerations; (b) inter-storey drift ratios; (c) residual inter-storey drift ratios.

seismic behaviour, thus the losses at the first limit states are significantly lower (see Table 18), and the average expected annual loss is reduced compared with that of the As-Built structure.

Thea area enclosed under the total loss curve corresponds to an amount of EAL equal to 0.57%, while the value including the uncertainties raises up to 0.85%. Since the expected losses at the first three damage states are consistently lower compared to those in the As-Built condition, the total loss curve of the structure with CAM is more prone to the vertical axis. Consequently, the area under the curve is lower: this effect reflects the important role of the seismic losses also at the serviceability limit states.

Finally, the collapse fragility curve and the annualized probability of collapse are derived. As for the structure with FRP, the same spectra selected for the As-Built structure are adopted. The two results are reported in Figure 46. The main descriptors of the fragility curve are μ equal to –0.572 and σ equal to 0.38. The average annual POC for the structure with CAM is 0.13%, which is significantly lower compared with that in the As-Built condition, but also lower than that of the structure with FRP. This is due to the lower mean value of the fragility curve at collapse estimated for the structure with CAM, while the hazard is the same adopted in the previous cases.

Table 18. Expected losses of the structure with CAM at each performance level.

	P(D|IM)	P(C|IM)	L(NC∩R) %	L(NC∩D) %	L(C) %	L(NC) %	E[LT|IM] %	MAF [1/year]
ZERO LOSS	0.000	0.000	0.04	0.00	0.02	0.044	0.065	0.1131
YIELDING	0.000	0.008	0.30	0.00	0.96	0.30	1.26	0.0312
LIFE SAFETY	0.000	0.072	0.86	0.00	8.60	0.86	9.46	0.0079
NEAR COLLAPSE	0.420	0.500	1.37	27.29	60.00	28.65	88.65	0.00011
RIDR 1.5%	0.502	0.517	1.17	31.52	62.10	32.69	100.00	0.00009

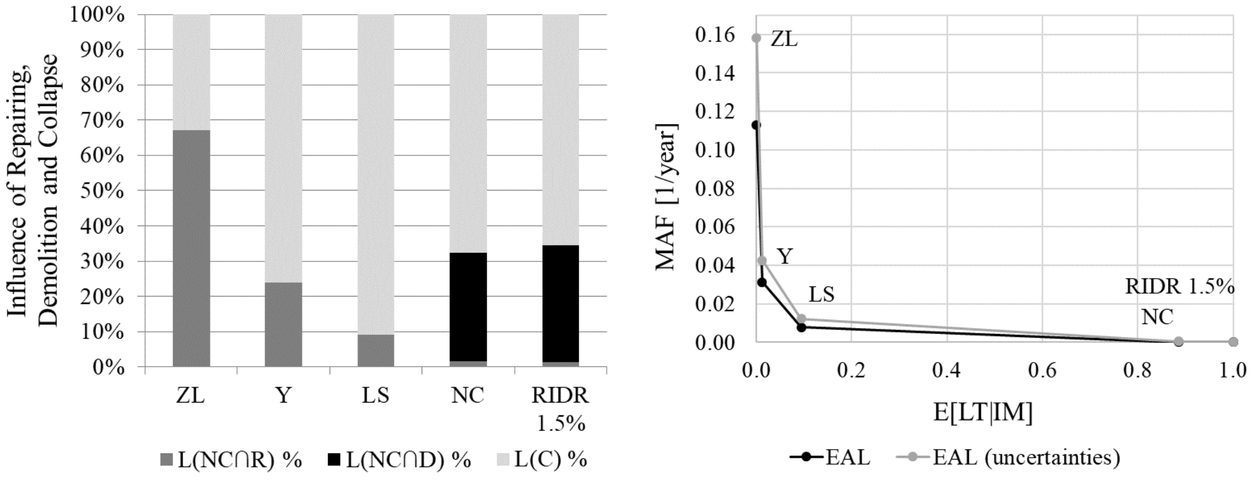

(a) (b)

Figure 44. (a) Percentage of influence on the total loss of repairing, demolition and collapse; (b) approximated total loss curve for the structure with CAM.

3.4.2.4. STRUCTURE WITH CJ

The last approach of seismic intervention consists in the concrete jacketing of the columns. This is a quite common technique improving the durability of the existing elements and leading to a uniformly distributed increase in strength and stiffness of the members (Ligabue et al. 2018).

In this case, the columns are confined with an external layer of concrete, in which additional longitudinal and transversal reinforcement is placed, and appropriately anchored. The original internal columns of the first three floors are strengthened with an external layer of 6 cm on each side, with additional bars 8Φ12. To simplify the modelling, an equivalent section has been computed in so that to achieve the same bending and axial capacity of the actual retrofitted one.

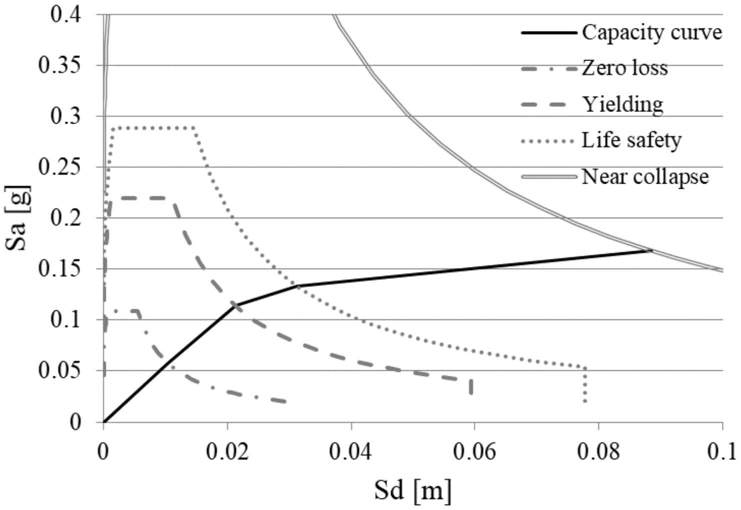

PL	%NBS
ZL	15.8
Y	31.0
LS	56.3
NC	135.5

Figure 45. Percentage of NBS for the structure with CAM at different performance levels.

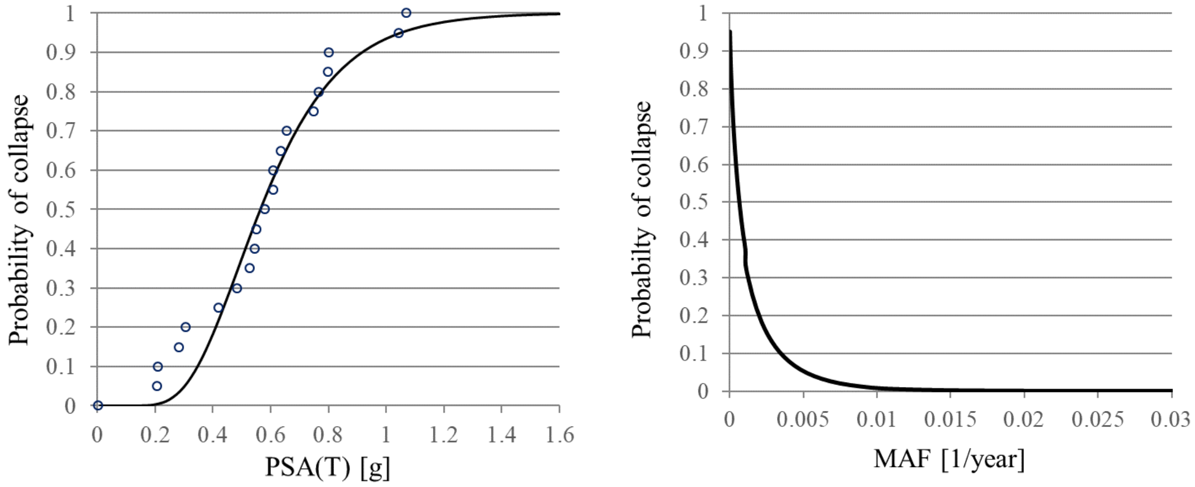

(a) *(b)*

Figure 46. (a) Approximated collapse fragility curve for the structure with FRP; (b) annual probability of collapse curve.

Thus, the Pushover analysis is performed to assess the capacity curves reported in Figure 47. In this case, the formation of the plastic hinges occurs at the fourth floor for each performance level. Indeed, a soft storey mechanism occurs at the last storey, but at higher steps of the Pushover analysis compared with the As-Built case. The shear capacity at the base is increased up to more than 1000 kN, and the ductility is equal to 4.01. The better seismic performance of the building is due to the increased sections of columns, which also raise the effective stiffness at each limit state. Indeed, the values of the effective stiffness K_e reported in Table 19 are higher compared to those of all the other structures previously reported, at each limit state.

All the dynamic properties of the SDOF systems are derived, and the EDP parameters are calculated. From Figure 48 it is possible to infer that the fourth storey is the most vulnerable to seismic actions, due to the concentration of damage. It is worth noting that the fourth storey reaches the limit of 1.5% of RIDR before the attainment of the collapse limit state.

The simplified loss assessment procedure is developed to estimate the seismic losses due to three aforementioned components. The amount of estimated losses at each performance level are shown in

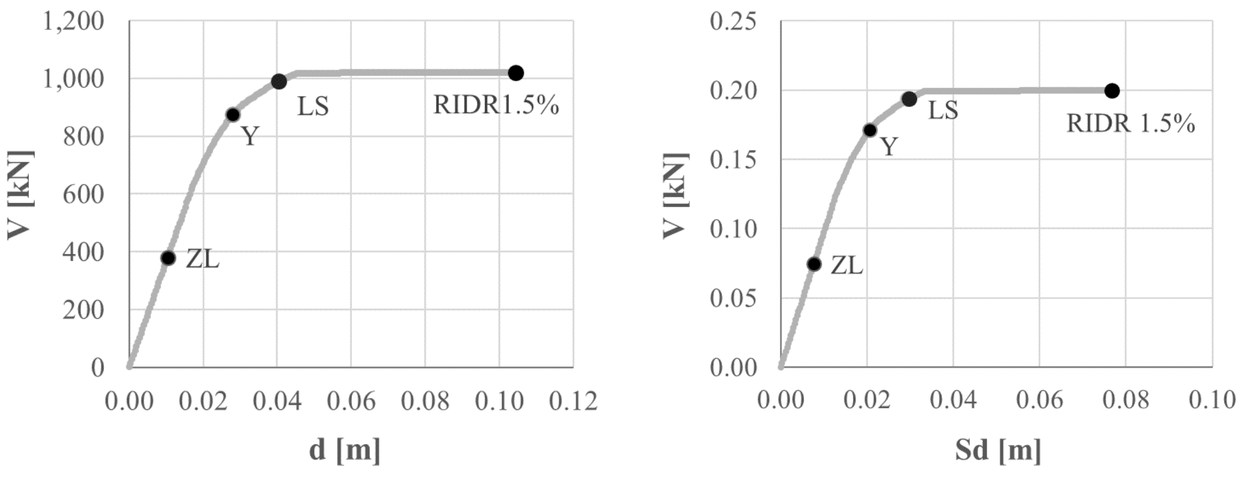

(a) *(b)*

Figure 47. Capacity curve of the structure with CJ: (a) Shear-displacement; (b) ADRS format.

Table 19. Properties of equivalent SDOF systems corresponding to the limit states in the structure with CJ.

		ZL	**O/Y**	**LS**	**RIDR 1.5%**	**NC**
Displacement of the effective mass	Δ_c [mm]	8	20	29	73	77
Effective mass	m_e [kN]	5982	5935	5779	3890	3800
Effective height	H_e [mm]	3473	3473	3475	3484	3485
Base shear	V_b [kN]	381	874	990	1019	1019
Effective stiffness	K_e [kN/m]	49948	42966	34146	13905	13209
Ductility	μ	0.374	1.00	1.425	3.602	3.792
Spectral acceleration	S_a (T_1) [g]	0.448	0.417	0.376	0.292	0.286
Effective period	T_e [s]	0.69	0.75	0.83	1.06	1.08
MAF	λ [1/year]	0.1514	0.0265	0.0068	0.00013	0.00011

Table 20, and the percentage distribution is illustrated in Figure 49a. In this case, the contribution due to demolition is higher compared to the previous ones, since the limit of the residual inter-storey drift ratio is reached at the ultimate performance point.

The cumulative loss of the two first performance levels is nearly one tenth of that computed in the As-Built condition, showing the effectiveness of this intervention. This aspect has an effect on the expected annual losses assessed for the structure with CJ. Indeed, the total loss curve reported in Figure 49b, has a total subjected area of 0.503%. This EAL is the lowest among the ones calculated in this work. The one computed considering the uncertainties is equal to 0.857%, which is slightly higher compared to that of the structure with CAM, but still significantly lower than the As-Built one. The NBS reached for this structure at the life safety limit state is equal to 60.6. For the Italian regulations (D.M. 2018) this is the limit to achieve to improve the seismic safety of an existing building entirely retrofitted. The increase of the NBS index is a proof of the significantly improved seismic behaviour of the building, but cannot describe alone the effectiveness of this retrofit solution. Therefore, the annual probability of collapse is determined. Since the structure with CJ has a modified stiffness and strength, the first period of vibration decreases to 0.622 s.

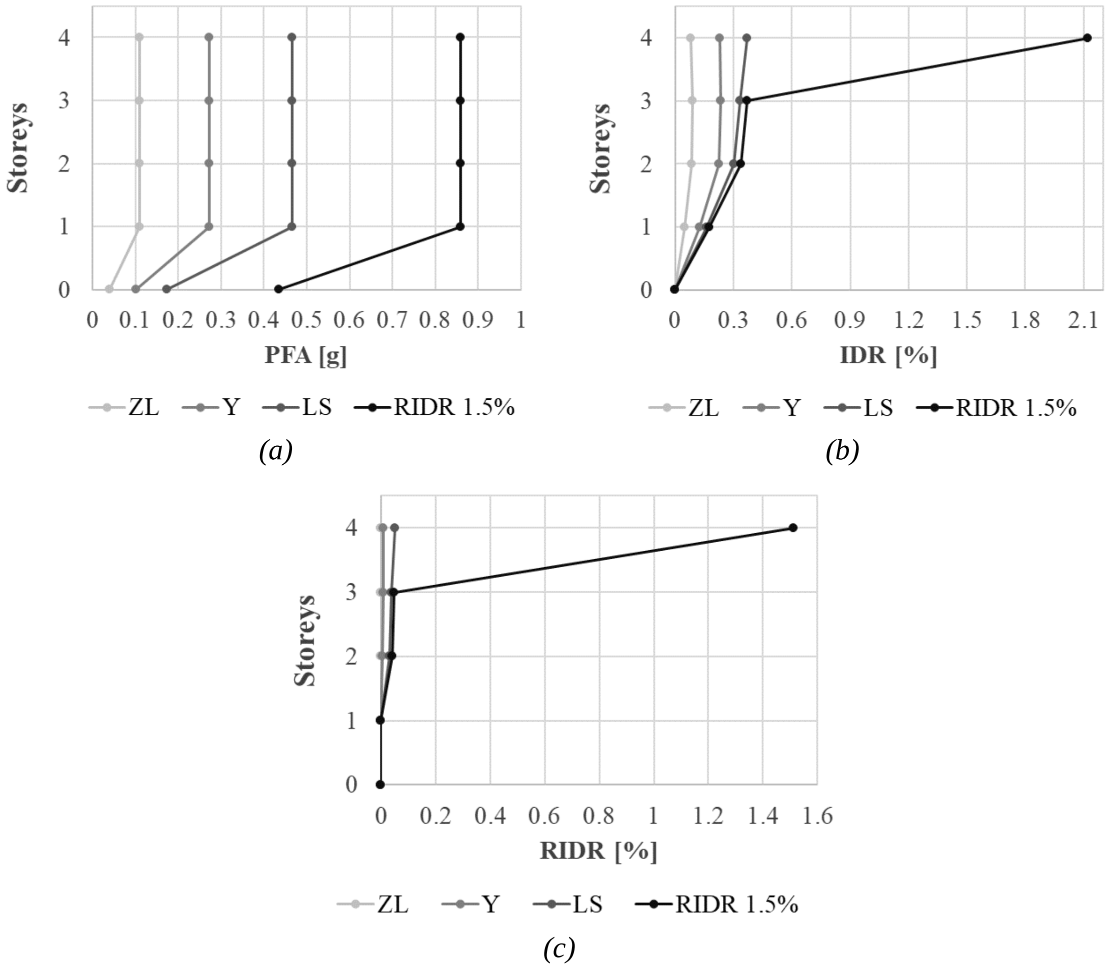

(a) (b)

(c)

Figure 48. Engineering demand parameters for the structure with CJ: (a) peak-floor accelerations; (b) inter-storey drift ratios; (c) residual inter-storey drift ratios.

Thus, another selection of the spectra has been performed considering this new reference value of the period. The selected spectra are shown in Figure 51a, while Figure 51b shows the collapse fragility curve estimated. Once the spectra are scaled in the ADRS format to apply the capacity spectrum method, the cumulative fraction of data overcoming each spectral acceleration is computed.

Table 20. Expected losses of the structure with CJ at each performance level.

	P(D|IM)	P(C|IM)	L(NC∩R) %	L(NC∩D) %	L(C) %	L(NC) %	E[LT|IM] %	MAF [1/year]
ZERO LOSS	0.000	0.000	0.00	0.00	0.00	0.004	0.008	0.1514
YIELDING	0.000	0.006	0.38	0.00	0.75	0.38	1.13	0.0265
LIFE SAFETY	0.000	0.055	1.02	0.00	6.54	1.02	7.56	0.0068
RIDR 1.5%	0.509	0.470	1.11	35.07	56.44	36.18	92.62	0.00013
NEAR COLLAPSE	0.623	0.500	0.85	40.48	60.00	41.33	100.00	0.00011

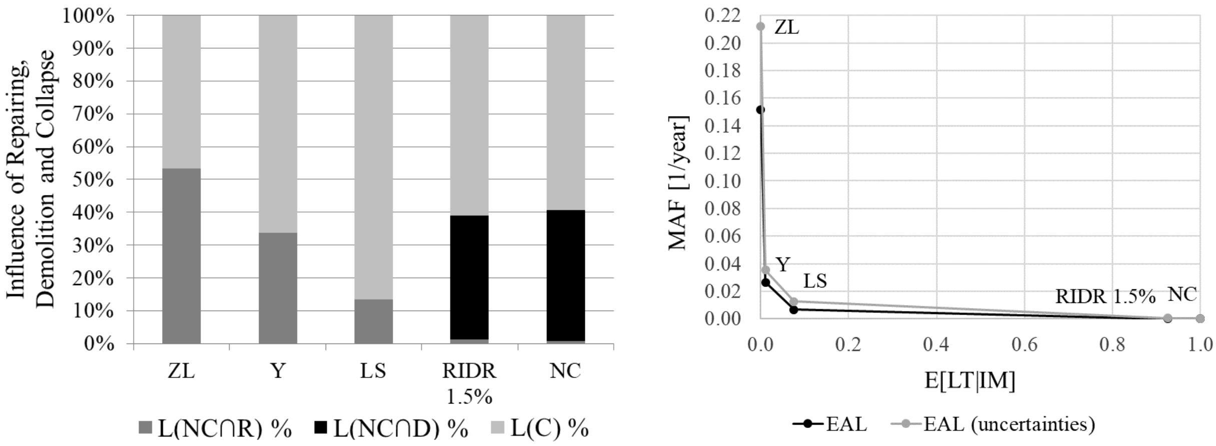

(a) *(b)*

Figure 49. (a) Percentage of influence on the total loss of repairing, demolition and collapse; (b) approximated total loss curve for the structure with CJ.

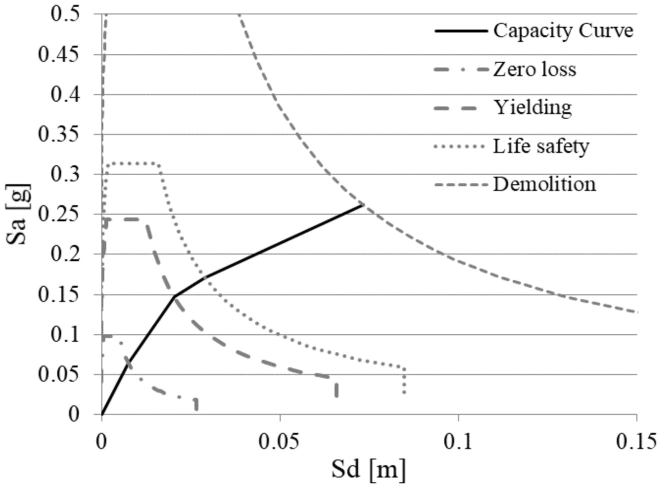

PL	%NBS
ZL	14.2
Y	35.4
LS	60.6
NC	151.5

Figure 50. Percentage of NBS for the structure with CJ at different performance levels.

Thus, the resulting points are fitted with a lognormal cumulative distribution obtained through a linear regression procedure. The main descriptors of the fragility curve are: μ equal to -0.408 and σ equal to 0.45. In this case, also the PSA-based hazard curve is different compared to the one adopted in the As-Built condition, since the first period of vibration is lower. Figure 51c illustrates the final probable collapse curve: the area enclosed is the annual probability of collapse, equal to 0.19%.

The value is lower compared to that obtained in the As-Built condition, but higher compared with those resulting with the other intervention strategies, meaning that the structure with CJ, on average, is more prone to collapse.

3.4.2.5. COST-EFFECTIVENESS ANALYSIS

In this Section, the analysis of the costs of investment and the cost-benefit evaluation of the different retrofit options are performed. The unitary costs of the different techniques are computed considering the prices of the materials applied to columns and the cost of all the works needed to prepare the

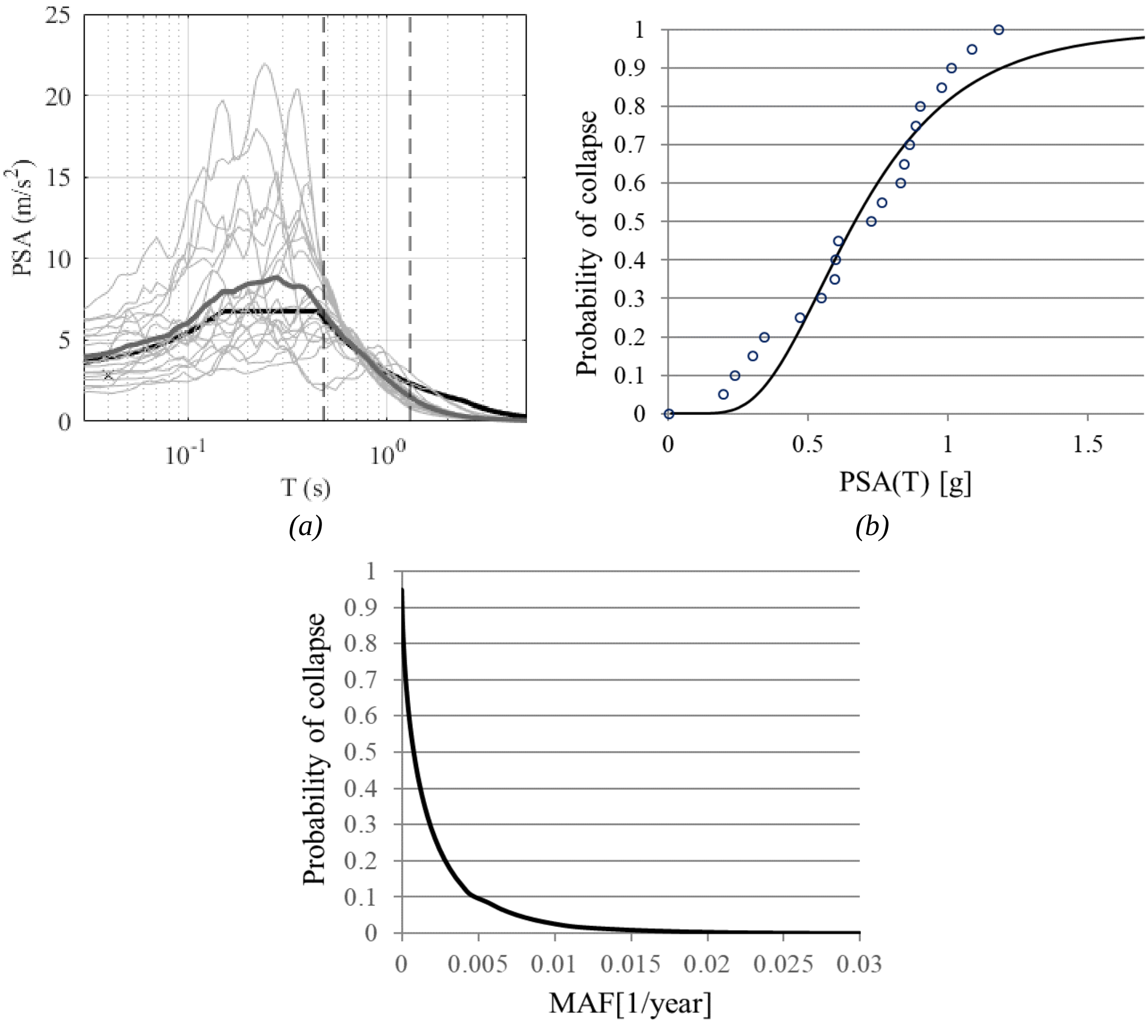

(a) *(b)*

(c)

Figure 51. (a) Spectra of the ground-motion selected; (b) approximated collapse fragility curve for the buildi with CJ; (c) annual probability of collapse curve.

surfaces. Following the regional pricelists of the structural works, the initial cost C_r of each retrofit intervention applied on the entire As-Built structure is estimated. However, some components of the works are not considered, such as the additional costs for the preparation of the construction site, the technical costs, the transports and the professionals' fees. Thus, to achieve a more realistic result, the values are increased of three times, resulting in a total amount of C_r between the 2% and the 4% of the total replacement cost of the building. Yet, these outcomes may be underestimated according to the findings of Beetham (2013), which rated the average cost of intervention of more than the 10% of the total replacement cost of the RC building.

By applying the formulas reported in Section 3.4.1.3, the net present value (NPV) is assed in a time frame of 50 years, and the critical return time of the initial investment is evaluated for each retrofit option. The t_{cr} obtained allows comparing the convenience of the different retrofit solutions, taking into account that the lowest value of critical time indicates the most convenient option. Another measure of the effectiveness is the benefit-cost-ratio BCR, which is inversely proportional to the critical time. Indeed, the highest index obtained indicates the most economically advantageous solution.

The evaluation of the critical time is reported in Figure 52: t_{cr} is similar for the three retrofit, being equal to 2.3 years for CAM, 3.3 years for CJ and 4.2 years for FRP.

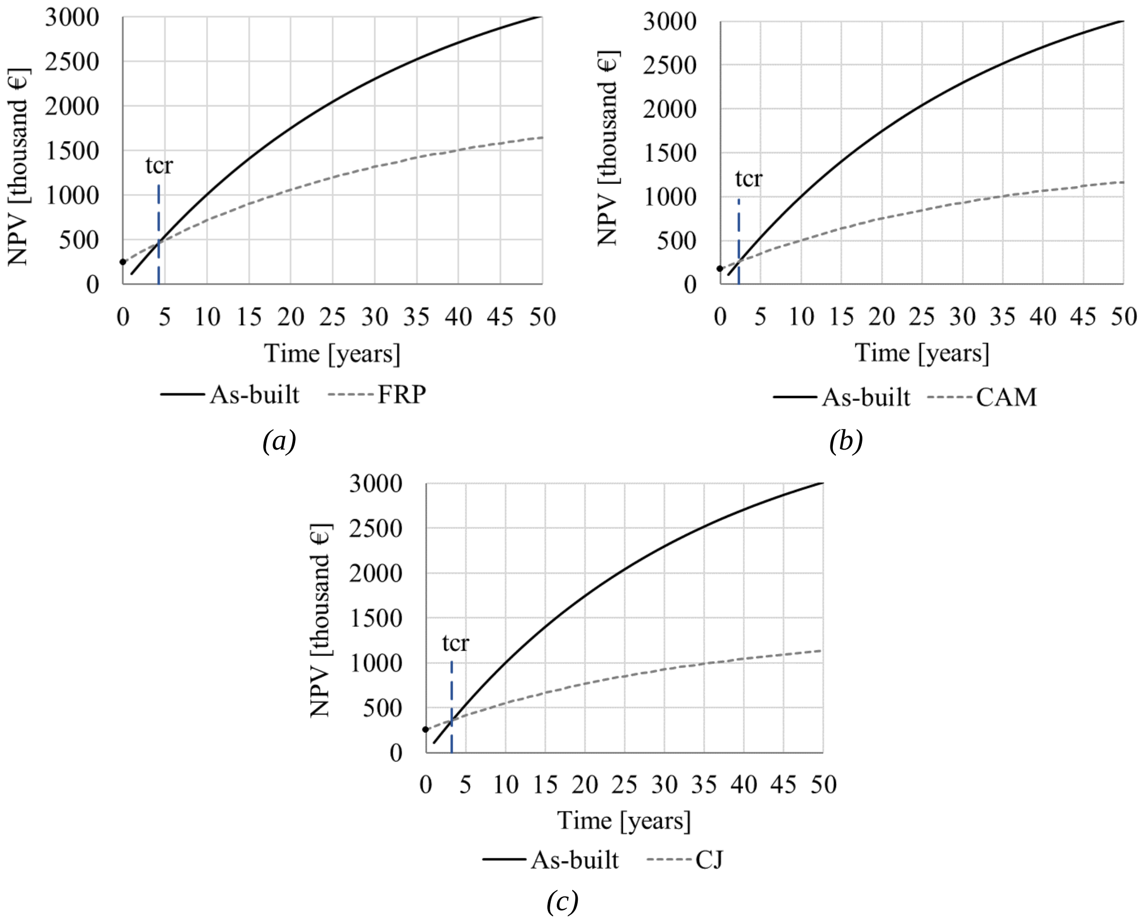

(a) *(b)*

(c)

Figure 52. Graphical representation of the net present value and the critical time for: (a) structure with FRP; (b) structure with CAM; (c) structure with CJ.

These quite low values are due to the costs C_r considered. In the Figures, the initial cost of investment is marked by a dark dot at the intersection of the retrofit curve with the vertical axis. The NPV after fifty years of life is in general smaller for the retrofitted structures compared to the As-Built one, and the lowest comparable losses can be detected for the CAM and the CJ solutions.

Figure 53a reports a comparative evaluation of the values of BCR computed for the three options, according to which the CAM is apparently the most convenient. Moreover, Figure 53b shows the values of the initial cost of the retrofit for each techniques applied and Figure 53c illustrate a summary of the main results obtained for the different scenarios. In the latter, the most significant results are underlined. It is worth noting that the EAL reported in the Figure are those computed for each different structure without the uncertainties.

Following the Codes, by only computing the NBS index (i.e., the safety index of each structure) one would likely chose the CJ retrofit option for the seismic retrofit of the existing building considered. However, the high initial cost of investment of the CJ option may discourage the selection of this solution, as well as the FRP one. The evaluation of the annualized terms, the EAL and the POC may lead to assess that CJ and CAM are the best solutions, even if the structure with CJ has a slightly higher POC compared with those of the other structures. The cost-benefit analysis, leading to the

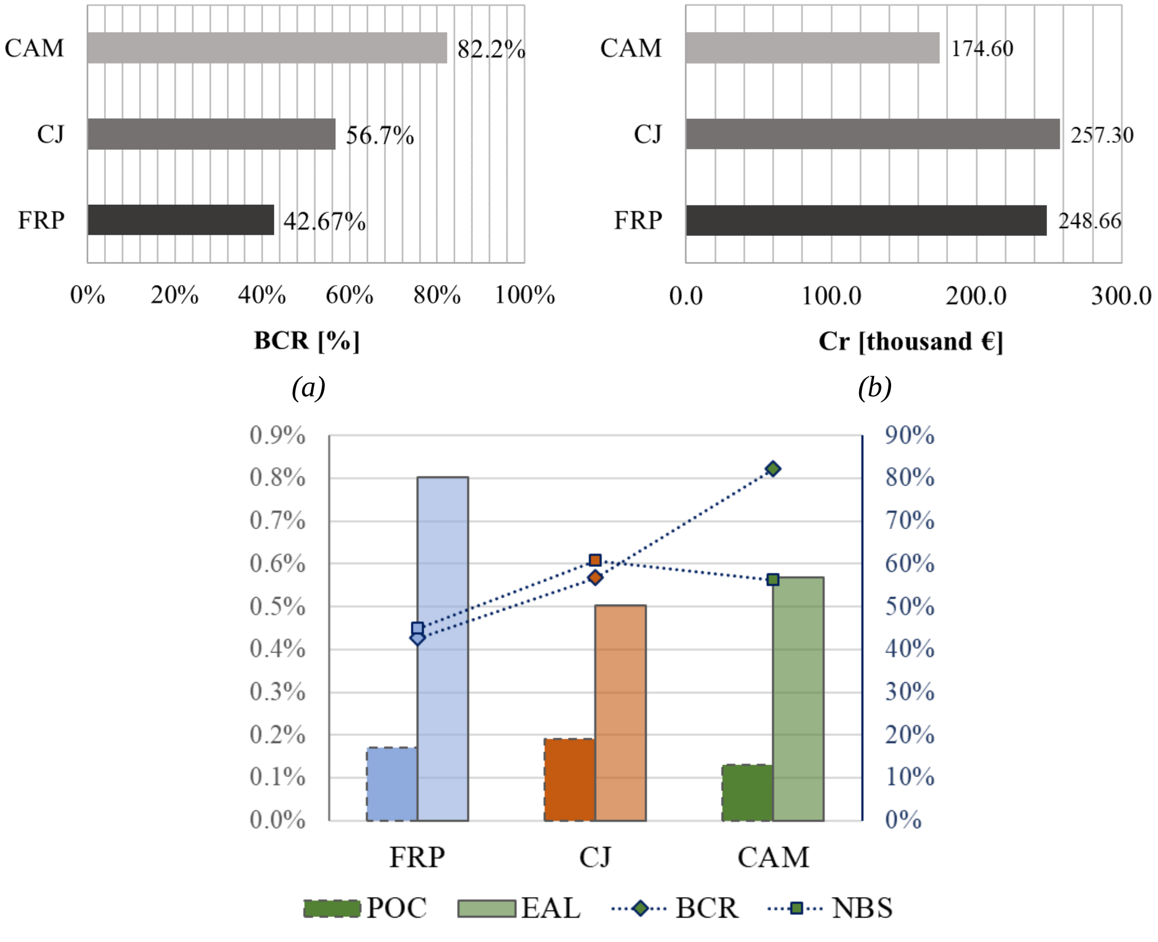

Figure 53. Graphical representation of the following quantities for the different structures: (a) BCR; (b) C_r; (c) all the different loss terms.

computation of t_{cr} and BCR, allows identifying the most cost- and time-effective solution, which is likely to be the CAM technique in this case. Indeed, the CAM solution corresponds to quite low expected annual losses, the lowest value of POC, a moderate increase in NBS with respect to the As-Built solution, but mainly the lowest values of initial cost of investment and critical time. All this suggests that a comprehensive loss assessment procedure should account for all these terms in order to be able to give indications for the evaluation of the most effective design solution for the seismic retrofit of an existing building.

3.4.3. CONCLUDING REMARKS

The vulnerability assessment of an existing RC building is commonly achieved, following the Codes, by computing a performance index representing the capability to sustain a seismic action comparable to that adopted in the design of a new building in the same location. This procedure follows a deterministic approach, which is not able to describe the seismic performance of the building at different damage states, nor to consider the contribution of different components.

In this context, the simplified method proposed herein constitutes a comprehensive framework that allows evaluating not only the seismic vulnerability of a structure, but also the probable expected seismic losses. The method should not be intended as a robust tool for assessing the EAL of a building, even if a good matching with the results obtained with the software PACT (FEMA, 2018) has been observed in the DBA work of Ligabue (2015).

Indeed, this method is devoted to the relative comparison between different retrofit options, and as such, it should be used to get valuable indications on the effectiveness the economic convenience of each solution. The modified displacement-based assessment method fully expresses its potentialities in the quantification of the relative seismic performance of different design options.

However, the definition of some input parameters, such as the collapse and the demolition fragility of the SDOF systems, may require further refinement. Moreover, at the initial stage, a simplified FEM modelling of the building has been considered in this work, neglecting the non-linear modelling of beam-column joints, which should be included for a reliable evaluation of the structural capacity.

Nevertheless, the application showed that the EAL are typically affected most by the losses at the low-intensity ranges, suggesting that the so-called serviceability limit states should be taken into account for an extensive seismic performance evaluation. The comparative consideration of the annualized probability of collapse, the expected annual losses, the new building standard, and the benefit-cost ratio allows performing a multifaceted evaluation of different structural to economical parameters in the decision-making phase. Among these, the EAL could be considered to provide an indication of the resilience of the building (Sullivan et al. 2014), while, the annualized POC, to provide an indication of the collapse tendency.

It is worth noting that a more detailed analysis of the initial costs of the retrofit should be performed to obtain realistic and comparable results in the last phase of cost-benefit evaluation, since those considered in this work are approximated. However, in the everyday work of practitioners this can be achieved through a simple preliminary estimate of the costs. Thus, this method could be adopted to give a uniform approach in the decision-making at the conceptual design phase.

4. OBSERVATIONAL DATA COLLECTION: LOSSES OF PRECAST RC BUILDINGS AFTER THE 2012 EMILIA EARTHQUAKE

4.1. THE SFINGE DATABASE AND THE CREATION OF A SPECIFIC SEISMIC REPOSITORY OF ONE-STOREY PRECAST RC BUILDINGS

The Emilia Earthquake of 2012 occurred in a highly industrialized area, characterized by an estimated presence of one firm every 9 inhabitants (Caselli 2020). The area affected by the seismic sequence embraced 59 districts, producing around the 2.5% of the National GDP (Gross Domestic Product) according to Agenzia Regionale per la Ricostruzione (2018), but the industrial heart of the area was smaller (see the red area in Figure 54).

Before the Earthquake, the industrial core hosted many important industrial clusters: Motor Valley, Food Valley, Packaging, Tiles, Wellbeing, Health and Fashion; these involved the work of 20’000 companies and 53’000 employees. In 2012, the GDP of the area affected by the Earthquake was -3%, and the whole Region registered -2.3%. However, after this major decline due to the Earthquake, the area grew stronger, with +1.6% GDP compared with 0.4% of the entire Region (data from Caselli 2020). This positive estimate was possible thanks to a huge amount of regional contributions spent for the reconstruction and the economic aid to companies, allowing to trigger new investments and to increase the employment rate.

The SFINGE-SISMA platform (Agenzia Regionale per la Ricostruzione 2018), implemented by the Emilia Romagna Region after the Earthquake to manage the reconstruction process, is a valuable repository of seismic damage and loss data of industrial buildings. In particular, regarding the production companies, the ‘Ordinanza Commissariale 57/2012’ defined the criteria for the request of funds for the reconstruction of buildings, the restoration of products and stocks, the reparation of machineries and equipment, and the temporary relocation of the activities. In addition, the ‘Bando INAIL’ defined the process for the location of funds for the seismic retrofit of the non-damaged buildings, which are not treated in this dissertation.

According to the data collected by the Region, the total amount of requests accepted in SFINGE were 3450: among these, 2850 included the reconstruction of buildings, and 590 were dedicated to the other voices mentioned. The 2850 requests are equivalent to 6210 different building units admitted for funding, whose 2780 were classified as long-span buildings made with precast technologies. Another step of selection based on the surface and the amount requested allowed to identify the number of precast buildings usable in the analyses to 2105, corresponding to a total amount of regional funds of 942’965’840,23€.

The study of this data allowed the Region to analyse the allocation of funds focusing on: the use of the buildings, the damage scale adopted, the insurance and the contribution given, and the surface in plan of the buildings. However, the analyses provided do not account for the different typologies of precast buildings, and do not disaggregate losses in different component (structural and non-structural). For these reasons, to investigate deeply the structural-related aspects of these losses, a smaller repository of selected seismic data has been formed, starting from the in-depth analysis of a sub-set of documents for the request of funds. This is a database of 600 precast RC buildings corresponding to a total amount of regional funds of 309’839’479,80€, which constitutes the 29% of the total amount of buildings and the 33% of the total amount of funds given with respect to the dataset considered in the analyses of the Region (Agenzia Regionale per la Ricostruzione 2018).

The database was created through a process of progressive selection and refinement:

i) Study of each document provided for the request of funds for the reconstruction;
ii) Selection of the requests corresponding to one-storey precast RC buildings;
iii) Selection of the damaged buildings, classified according to scale indicated by the Region;
iv) Depuration of all the VAT (value added tax), which is not a constant percentage in the different voices of the costs;
v) Differentiation of the economic data presented for entire estates into single amount for each structural unit;
vi) Identification of the coordinates of the single building units;
vii) Evaluation of the surface in plan of the single building units;

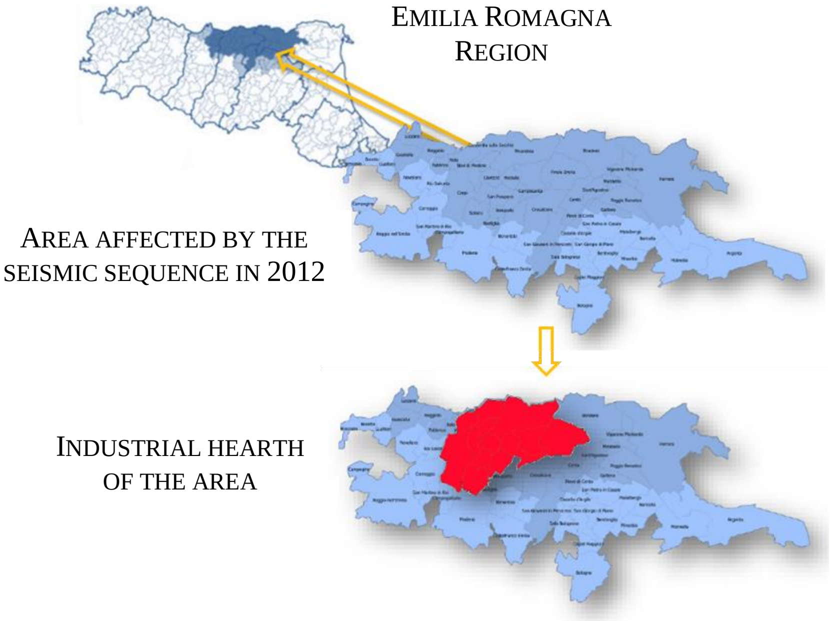

Figure 54. Schematic representation of the area affected by the 2012 Earthquake and of the industrial hearth of the area (adapted from Caselli 2020).

viii) Classification of the structural typology;
ix) Disaggregation of the seismic losses into different components;
x) Estimation of the maximum peak-ground-acceleration (PGA) occurred at each building unit through *ad hoc* shake-maps calibrated for the seismic events of 2012.

In particular, the diversification of the economic data (see point ix) allowed distinguishing between the following quantities:

- the Conventional costs, which are those determined by the technicians delegated by the business owners in the phase of funding application, determined by multiplying the surface in plan by a parametric unitary loss based on the damage level, and eventually taking into account additional modifiers depending on the geometry of each building (see Table A, Ordinanza 57, 2012);
- the Estimated costs, which are the money actually spent for the reconstruction process, determined considering reference unitary price lists and material and work quantities. These costs are computed through the forms called 'Computo metrico Estimativo' (CME), which reports all the quantities. The total costs can be divided into four additional sub-classes (Ordinanza 57, 2012):
  - A: the structural costs for the reparation of buildings, of the structural components and the necessary structural and geotechnical tests;
  - B1: the technical fees not depending on the typology of intervention, such as the registration in the land-office, the environmental reports and the evaluation of conformity;
  - C: the non-structural costs due to the repair of the finishing and the ordinary systems and plants (for the reparation of the industrial machineries *ad hoc* requests for funds were presented);
  - D: the professionals' fees linked to the architectural and structural project and the direction of the construction site;
- the Insurance which is the amount of money given by private Insurance companies, if the building was covered by one;
- the Final fund given, corresponding to the lowest amount between the Conventional cost and the Estimated cost subtracted by the Insurance, if present.

To ease the comparison with other parallel works, it is worth saying that the Conventional costs in € are called DREL in Rossi et al. (2020), and 'Importo da danno, costo convenzionale' in Agenzia Regionale per la Ricostruzione (2018). Moreover, the Estimated costs in € are named DREC in Rossi et al. (2020), and 'Importo lavori da CME ammessi' in Agenzia Regionale per la Ricostruzione (2018). It is important to note that the costs for the repair of particular industrial machineries and for the restoration of products are not included in the aforementioned category C. Indeed, the losses due to these quantities were collected in specific requests, which were issued for some buildings only and are not available for all the units. These spare costs, even if highly significant, are not included in this work, and will be part of future research since they need to be analysed with different criteria.

The damage scale adopted in the database is that defined by the Ordinanza 57 (2012), identifying five damage degrees, each of which entails a specific approach of structural intervention. The Regional damage scale, originally composed by letters, is listed with numbers for simplicity, in line with the works of Buratti et al. (2017) and Ongaretto et al. (2019). The damage scale is reported in Table 21. The damage levels considered are practically coincident with those defined in the European Macroseismic Scale (EMS-98, 1998), as enhanced by Buratti et al. (2017). For a direct comparison, Table 22 schematize the conceptualized seismic damage to ordinary masonry and RC buildings in EMS-98 (1998), together the pictures documenting the damaged precast RC buildings after the 2012 Earthquake. The pictures in the Table are taken from the documentations presented for the request of funds for the reconstruction, thus different technicians made them.

Table 21. Damage scale considered, adapted from Agenzia Regionale per la Ricostruzione (2018).

Damage level		**Intervention**
D1 (c):	Local or widespread light damage on vertical and/or horizontal structural elements, on less than 20% of the surfaces, with no collapses.	Local strengthening intervention or seismic retrofit
D2 (b):	Widespread light damage to vertical and/or horizontal structural elements on at least 20% of the surfaces, with no collapses.	Local strengthening intervention or seismic retrofit
D3 (d):	Moderate structural damage, with: · local collapses on up to 15% of the surfaces; · and/or damage to one or more joints, with relative permanent displacement greater than 2% of the column’s height; · and/or relevant absolute settlement of the footings (i.e., greater than 10 cm and lower than 20 cm); · and/or relevant relative settlement of the footings (i.e., greater than 0.003L and lower than 0.005L, with L=distance between the columns).	Repair and seismic retrofit
D4 (e):	Heavy structural damage, with: · partial collapse, on up to 30% of the surfaces; · and/or damage to up to 20% of joints, with relative permanent displacement of more than 2% of the column’s height; · and/or formation of plastic hinges at the base of the column, in up to the 20% of the columns; · and/or relevant absolute settlement of the footings (i.e., greater than 20 cm); · and/or relevant relative settlement of the footings (i.e., greater than 0.005 L, with L=distance between the columns).	Repair and seismic retrofit
D5 (a):	Total or partial collapse, of more than the 30% of the surfaces, and/or damage to more than the 20% of columns.	Demolition and reconstruction

The structural typologies of precast RC buildings analysed in the database are those defined in Ongaretto et al. (2019), and previously described in Savoia et al. (2012). As already mentioned, the precast elements are strongly standardized following different technologies adopted in the years. Even if the sections and shapes of the elements may recur, the spans and the dimensions differ. Thus, it is possible to distinguish between several typologies based on the year of construction and the building dimensions. In the following list, the six most relevant typologies of precast RC buildings considered in this study are reported, among which the most common ones (and interesting from the structural point of view) are T1, T2 and T3:

- T1 buildings feature double-slope precast main beams simply-supported at the top of the columns. On the perimeter, masonry infills or horizontal precast cladding panels are placed between the columns. This is a typical technology adopted in the 70's and 80's, and more recently for small constructions. The roof can be made either of precast elements with hollow-clay-blocks or, of TT or of hollow-core concrete elements. Columns are usually quite slender, with square or rectangular cross-sections of about 30-50 cm per side. No beam-column connection devices are present in the as-built condition. The main beams can be up to 2 m deep in the middle of their length, and typically have no or little restraints against the out-of-plane movements with the exception of upper pocket supports at the top of columns. Often, there is an intermediate floor on one side of the building, which causes an irregularity in the structural behaviour with negative effects during ground-motions. It is worth noting that often there are no secondary beams to connect the main frames in transverse direction.
- T2 buildings feature double-slope precast main beams simply supported at the top of the columns. On the perimeter, precast heavy cladding panels are fixed externally to columns. The cladding panels can be either horizontal or vertical: this is a typical technology adopted after the 80's. Like typology T1, T2 can be characterized by different kinds of precast roof or slab elements, based on the span lengths, as well as the insulation and lightening requirements. Rarely, T2 buildings may have a planar roof with straight I- or T-shaped main beams.
- T3 buildings have a flat roof, made of long-span pre-stressed roof or floor elements simply supported on precast girder beams. This technology was widely used after the 80's, typically for large industrial facilities with few columns inside and large empty spaces. On average, the surface in plan of these buildings is almost twice that of buildings T1 and T2. Planar precast RC girders are supported on columns. In order to reach significant spans in the slab direction, different kinds of pre-stressed elements are adopted, such as TT or Y-shaped. More recently, the use of precast vaulted thin-web elements (called "wing shaped beams") allowed covering roof spans over 30 m long (Savoia et al. 2012; Savoia et al. 2017). In this case, curved panels made of glass or transparent polycarbonate are placed between the structural thin-web elements with lighting purpose. RC columns feature large cross-sections (with sides up to 60-100 cm); cladding panels are made of reinforced concrete, externally fixed to columns and upper beams, and can be either horizontal, vertical or in some cases with a mixed layout.
- T4 buildings have a shed roof, which is a not so common technology adopted from the 70's to the 90's. The shed roof can be realized either with "knee" shaped beams, or oblique beams

or, less commonly, through reticular beams. This type of building is characterized by a very poor seismic behaviour.

- T5 buildings are all those with a sort of irregularity. The most common cases are the following: irregularity in plan (L shape, T shape, etc.); irregularity in height due to the interaction with adjacent precast buildings built without seismic joints and often characterized by a different structural typology; the presence of a portion with offices or residential destination, usually in masonry walls and often located in one extremity of the precast structure; the presence of a portion cast in place.
- T6 buildings are all the precast structures not belonging to one of the previous typologies since they are characterized by very uncommon characteristics.

Table 22. Visual comparison between the damage scale defined in the EMS-98 and the one adopted in the database of precast RC buildings (pictures selected from the documents of funding request).

Damage level	**Masonry buildings**	**RC frame buildings**	**Precast RC buildings**
Grade 1		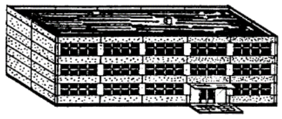	
Grade 2		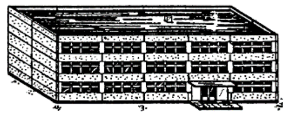	
Grade 3		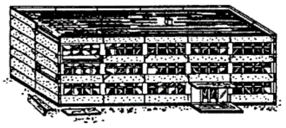	
Grade 4		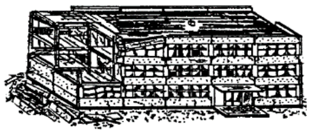	
Grade 5		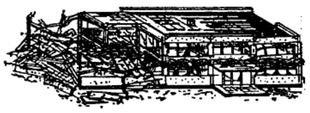	

It is evident that T5 and T6 feature two very mixed population of buildings without a homogeneous seismic behaviour. In addition, T4 buildings are not common, as demonstrated by the analysis of Ongaretto et al. (2019), whose extensive database has only the 4% of shed buildings.

Finally, an additional sub-set of 150 buildings of typologies T1, T2 and T3 has been analysed in order to create a structural-loss database. This is a database of 150 one-storey precast RC buildings corresponding to a total amount of regional funds of 93’066’515,31€, which constitutes the 8% of the total amount of buildings and the 10% of the total amount of funds given with respect to the dataset considered in the analyses of the Region (Agenzia Regionale per la Ricostruzione 2018).

For this insight, the documents of the buildings have been studied in order to classify also the following information (in addition to those described before), whenever it was possible to complete them all:

i) Classification of general data: construction year, district, cadastral category, number of workers at the time of the earthquake, geographical orientation of the main beam (identified with the use of Google Earth (2021));
ii) Geometrical classification: number of main beams, number of secondary beams, type of roof, height of columns (up to the main beam), length of the main beams, length of the secondary beams, typology of perimeter cladding;
iii) Classification of columns: number of columns on each side of the perimeter, on the corners and inside the buildings (if present), area of influence of each column, sectional dimensions of each column;
iv) Estimation of loads: linear load of the main beam, surface load of the roof, weight of the precast cladding elements, axial force on each column;
v) Other relevant features: presence of intermediate floors, height and surface of the intermediate floor, presence of local shed elements, presence of local top openings for lightning purpose, presence of strip windows, presence of upper pocket supports at the top of columns, presence of steel connectors between structural elements.
vi) Estimation of the maximum spectral acceleration (PSA) occurred at each building unit through *ad hoc* shake-maps calibrated for the seismic events of 2012.

It is worth noting that the procedure for the derivation of the aforementioned shake-maps, adopted to estimate the PGA and the PSA, is fully described in Buratti et al. (2022). Over the largest part of the territory hit by the seismic sequence, the maximum ground-motion intensity was recorded during the two main-shocks occurred on the 20th May and 29th May 2012 (Dolce et al. 2012).

In this work, the outcomes of the shake-maps have been adopted to estimate the maximum horizontal intensity measures (IM) between those registered in the two main events occurred, at the geographical location of each building. In line with the works of Buratti et al. (2017) and Ongaretto et al. (2019), the assumption of adopting the maximum value of IM means considering that the damage produced by the seismic events was not correlated. According to Savoia et al (2012), the precast RC buildings in Emilia were characterized by fragile failure modes mainly, due to the lack of structural redundancy and the widespread adoption of friction based connections. In this light, the accumulation of damage, for the majority of precast building, was not relevant. Moreover, due to the position of the industrial districts with respect to the epicentres of the two main shocks, many buildings have been damaged by only one of the two events, in particular at the highest damage levels.

4.2. THE TYPOLOGICAL-LOSS DATABASE: A SET OF 600 PRECAST RC BUILDINGS

4.2.1. THE DAMAGED BUILDING STOCK

The scheme in Figure 55 illustrates the geographical distribution of the precast buildings in the typological-loss database, where each unit is identified with a coloured dot depending on the damage level. The coordinates in decimal degrees define the location of each building, and the position of the main cities near the seismic area (Reggio Emilia, Modena and Ferrara). The towns with the main industrial clusters are identified with light-blue squares, and the position of the epicentres of the two seismic events is marked in red, together with the geographical extension of the two faults defined with a dot and a dashed line. Clearly, the majority of the highly damaged structures (D4 and D5) are located close to the epicentres, whereas the others are spread all around identified with the green colour.

The geographical map of the different structural typologies is not reported since they are randomly positioned in the territory regardless the two epicentres. Nevertheless, the percentage distribution of typologies T1-T6 in the database can be observed in Figure 56a: the most significant ones are T1, T2 and T3, constituting the 74% of the database, whereas T4 is almost negligible. Figure 56b reports the number of buildings belonging to the different typologies, at different damage states. There is a higher number of buildings belonging to damage levels D1 and D2, like in the distributions observed in Agenzia Regionale per la Ricostruzione (2018) and Buratti et al. (2017). Table 23 reports the total number of buildings in the database, both divided according to typology and damage level.

As already mentioned, the shake-maps (Buratti et al. 2022) allowed calculating the maximum PGA between those computed in the events of the 20th and the 29th May 2012. The values obtained have been divided into intervals considering the same adopted in Buratti et al. (2017) for the sake of comparison. The values are reported considering the different damage levels, and can be observed in Figure 57 and in Table 24. The PGA reported in this work tend to be higher than those presented by the authors, and higher than the maximum values registered by the recording stations during the Earthquake (around 0.35 g according to Dolce et al. 2012). Indeed, the shake-maps allow predicting all the values of PGA occurred at each location through the attenuation relationships, even in the fault area and close to the epicentre, while the data from the punctual recording stations are typically lower. As expected, in Figure 57 the buildings at damage level D5 are concentrated in the higher PGA intervals.

Furthermore, Table 25 presents a statistical analysis of the PGA at different damage levels, showing: the mean value of the data, the standard deviation, the maximum and the minimum values, the coefficient of variation (CoV), the median (50° Percentile), and the 16° and 84° Percentiles. The CoV is defined as the percentage ratio between the standard deviation and the median of the samples. It can be observed that the mean values of the PGA are ordered following the scale of damage levels, while the median values are not.

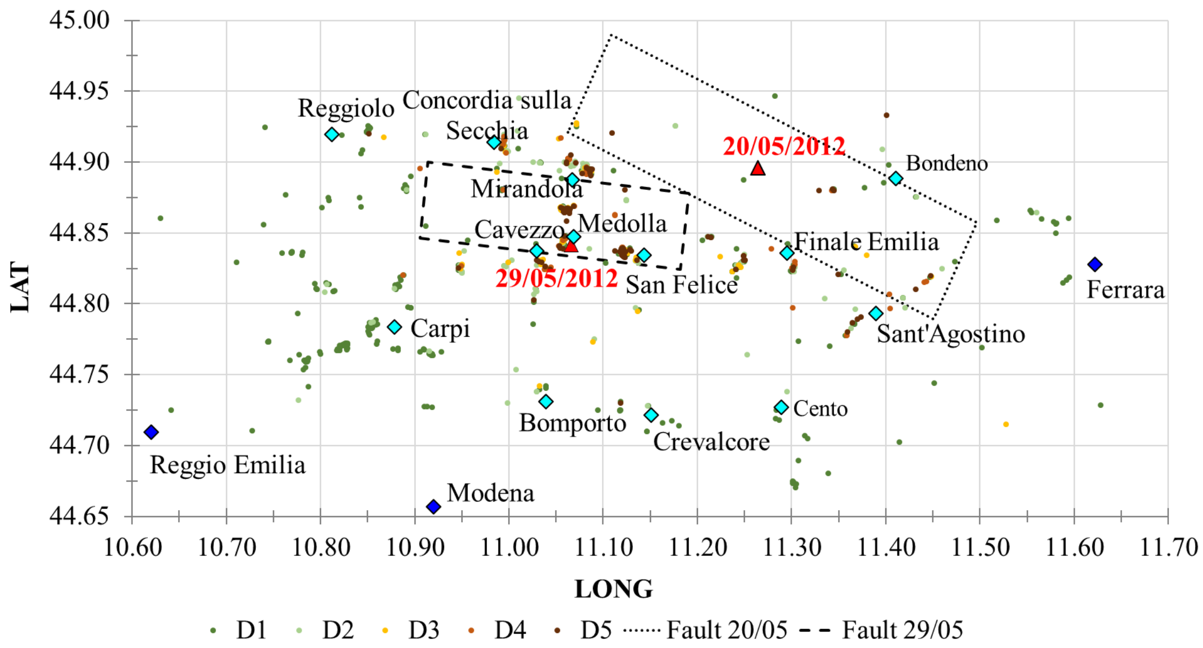

Figure 55. Geographical distribution of the buildings in the typological-loss database at different damage levels. Position of the main cities in blue, the main industrial districts in light blue, the epicenters of the main-shocks of 2012 in red, and identification of the faults. Coordinates are in decimal degrees.

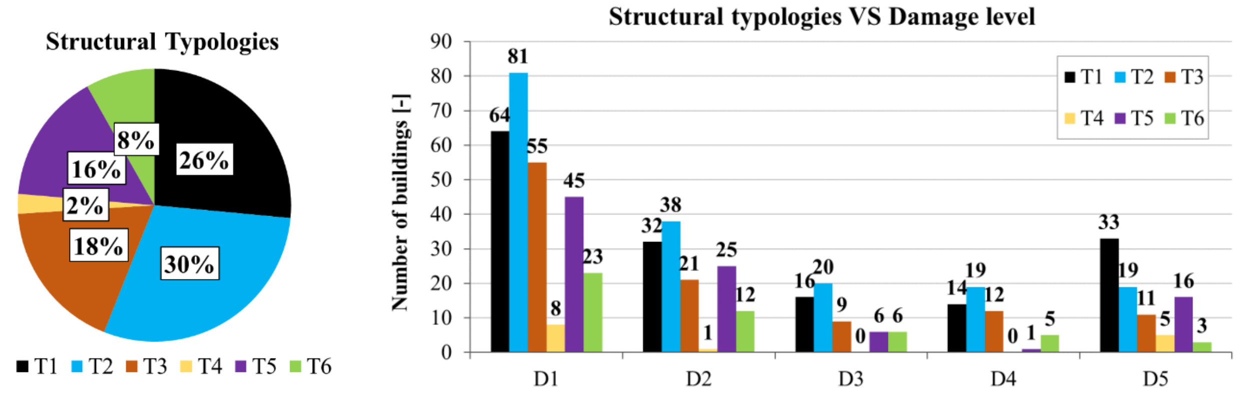

(a) *(b)*

Figure 56. Layout of the buildings in the database: (a) percentages of the typologies; (b) disaggregation of the buildings in typologies at different damage levels.

Table 23. Total number of buildings in the database per damage level and structural typology.

Damage Level	**D1**	**D2**	**D3**	**D4**	**D5**	
N° of buildings in the database	276	129	57	51	87	
Structural Typology	**T1**	**T2**	**T3**	**T4**	**T5**	**T6**
N° of buildings in the database	159	177	108	14	93	49

Indeed, the median at damage D4 is lower than the one at D3, but this can be due to the lower number of data belonging to D4, reported in Table 24. Moreover, in the map in Figure 55, some buildings at damage level D4 are located outside the two faults and may be subjected to lower PGA values.
The median and the two percentiles are reported in Figure 58 to show the distributions of the PGA at each damage state. The PGA at high damage levels are less scattered compared to those at low damage levels, which have a higher standard deviation and coefficient of variation. This is because the highly damaged buildings are mainly concentrated close to faults, whereas the buildings tagged with slight damage are spread in the area considered, but some are also close to faults. Indeed, in the database there are some few cases of less vulnerable buildings which experienced low damage, even if they are located close to epicentres (high PGA values estimated).

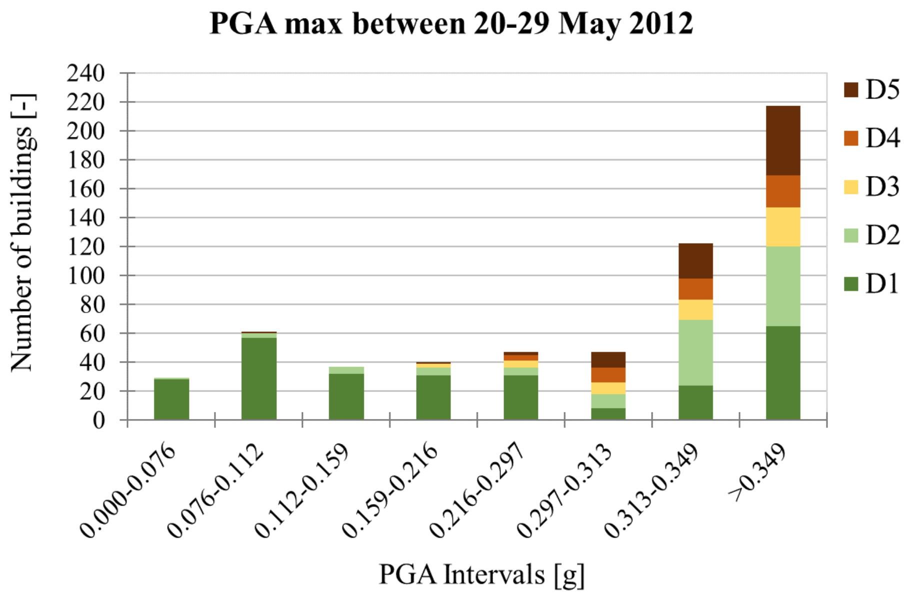

Figure 57. Values of PGA estimated at each building's location, divided into intervals and damage levels following a colored scale.

Table 24. Total number of PGA in each interval and per damage level.

PGA Intervals	D1	D2	D3	D4	D5
0.000g - 0.076g	28	1	0	0	0
0.076g - 0.112g	57	3	0	0	1
0.112g - 0.159g	32	5	0	0	0
0.159g - 0.216g	31	5	3	0	1
0.216g - 0.297g	31	5	5	4	2
0.297g - 0.313g	8	10	8	10	11
0.313g - 0.349g	24	45	14	15	24
> 0.349g	65	55	27	22	48
Total	*276*	*129*	*57*	*51*	*87*

4.2.2. CONVENTIONAL COSTS VERSUS ESTIMATED COSTS

In this Section, the conventional costs established with the parametric criteria of the Region are compared with the actual costs estimated by the technicians.

The conventional costs are determined *ex-ante*, while the estimated costs are the losses actually spent *ex-post* for the reconstruction of the damaged buildings. In order to perform a comprehensive analysis of the typological-loss database, the data was appropriately filtered. Indeed, considering the monetary losses in € over square meter of surface in plan of each building, the outliers have been removed at each damage state considering the following statistical rule: the outliers have been defined as elements equal to more than 1.5 interquartile ranges above the upper quartile (75° percentile) or below the lower quartile (25° percentile). This method has been applied in order to neglect the isolated values of loss that may be due to the presence of buildings with a very small or large surface in plan, or too small or large values of costs. The method has been implemented both to conventional and estimated costs to avoid a biased estimation of the statistical parameters of the losses.

Thus, the two group of losses have been statistically analysed considering the disaggregation into different damage levels, and into different structural typologies.

Table 25. Statistical analysis of the PGA values at different damage levels.

Damage Level	Mean [g]	Standard Dev. [g]	Max [g]	Min [g]	CoV [%]	Median [g]	16° Percentile [g]	84° Percentile [g]
1	0.218	0.125	0.489	0.029	64.4	0.194	0.092	0.364
2	0.338	0.086	0.489	0.058	26.3	0.327	0.298	0.429
3	0.347	0.065	0.473	0.160	18.9	0.343	0.299	0.430
4	0.349	0.055	0.472	0.234	16.8	0.326	0.303	0.400
5	0.353	0.057	0.480	0.103	16.2	0.355	0.312	0.389

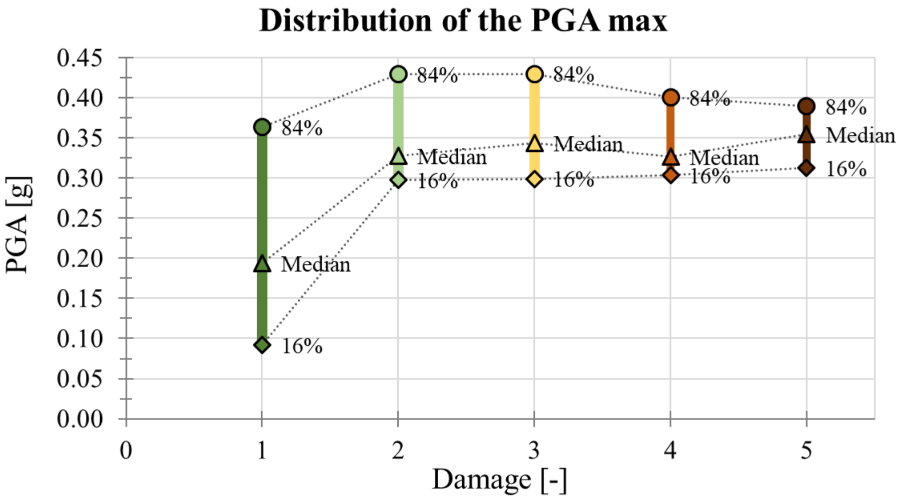

Figure 58. Distribution of the PGA at different damage levels with indication of: median values (50° Percentile), 16° Percentile and 84° Percentile.

The main descriptors of the curves have been computed with an iterative last-squares estimation, implemented in a Matlab routine (MathWorks 2020). In this way, it is possible to derive the empirical continuous distributions of the monetary losses of precast RC buildings based on the observational data. The sanity check of the fitted models (da Porto et al. 2021) has been confirmed by the values of root mean square error (RMSE) observed, a scalar value giving an estimate of the variance of the error term, which have been always comparable and lower than 0.5.

It is worth noting that the values of losses at damage states D1 and D2 have been further divided into two sub-groups. Indeed, the buildings subjected to these damage states could have been retrofitted if the vulnerability (i.e., the ratio between seismic capacity and demand calculated by the technicians) in the as-built condition was estimated to be lower than 60, or, only repaired with local interventions techniques if it was higher or equal to 60 (see Table 21). Thus, the two sub-groups include buildings subjected to damage D1 (or D2) being entirely retrofitted, or buildings subjected to damage D1 (or D2) which have been repaired with local interventions only. This separation led to quite different results between the two sub-groups in terms of distribution of losses and fitting curves. Some examples of common retrofit solutions for precast RC buildings can be found in Minghini and Tullini (2021) aimed at the strengthening of columns, the interventions or substitution of cladding panels, or the use of steel bracing systems. Moreover, it is worth mentioning the use of seismic dissipative devices, such as that adopted in the insight analysis described in the Appendix A.

The Tables in the following Sections report the statistical analysis of the losses, considering the data without outliers at different damage levels. The following quantities have been estimated: the mean, the median, the maximum, the minimum and the standard deviation of the values, the total number of data, the 16° and 84° percentiles, the Kurtosis index, the skewness, the coefficient of variation, and the lower and upper limit of the 90% confidence interval of the mean. The Kurtosis is a measure of how outlier-prone is the data-set considered: data with low Kurtosis tend to have low tails, or lack of outliers; the normal distribution has an index equal to +3. The skewness is a measure of the data around the mean: if the index is negative, the data spreads out more to the left of the mean; if it is positive, the data spreads out more to the right; the skewness of the normal distribution (or any perfectly symmetric distribution) is zero (Fisz 1963).

In the following Sections, the comparison between conventional and estimated losses is analysed under different aspects: firstly, the costs at different damage levels and for the six structural typologies are computed; thus, a linear interpolation of the conventional losses against the estimated ones is calculated; finally, a linear interpolation of the losses against the surface in plan, and the PGA, is defined.

4.2.2.1. LOSSES AT DIFFERENT DAMAGE LEVELS

In the Figures presented in this Section, the normalized probability distributions and the cumulative distributions of the data are plotted together with the continuous lognormal fitting functions. A specific algorithm allows normalizing the probability distribution according to the following rule: once the bin-width is set, the number of elements in a bar is divided by the total number of samples multiplied times the bin-width. In this way, the area of each bar is the relative number of observations, and the sum of the areas of all bars is less than or equal to one, producing an estimate of the probability density distribution.

The losses are reported as total conventional costs in €/mq and total estimated costs in €/mq. The latter are further analysed considering the structural costs in €/mq (Section 4.2.1.1.3), and the non-structural costs in €/mq (Section 4.2.1.1.4). These correspond to losses of category A and C, whereas the technical and professionals' fees B1 and D are mentioned in Section 4.2.4, since they represent a smaller amount of losses determined as a fixed percentage on the total amount.

The losses are analysed individually at each damage state, thus a final image with the cumulative distributions of the data and the fitting functions is proposed in Figures 63, 68, 73, 78 for comparison. The main descriptors of each function are shown in the cumulative distributions with letters μ and σ, together with the analogous values of mean and the standard deviation of the samples. The bin-width considered in the histograms of the conventional costs, the estimated costs and the estimated structural costs is 25 €/mq for losses at damage levels D1 and D2, and 50 €/mq for losses at damage levels D3 to D5. For the non-structural costs, a bin-width of 5 €/mq is adopted at D1 and D2, 10 €/mq at D3 and D4, and 50 €/mq at D5.

The outcomes of this Section may be interpreted to evaluate the accuracy of the conventional losses with respect to the actual losses experienced after the earthquake. Moreover, the continuous curves of the estimated losses are a valuable tool for the seismic loss assessments of precast RC buildings, giving the opportunity to evaluate the amount related to both structural and non-structural components. Nevertheless, the results of this Section do not account for the presence of different structural typologies, since the data are partitioned per damage level, while the full disaggregation of the costs of typologies T1, T2 and T3 at different damage levels is proposed in Section 4.2.3.

In general, the losses at D1 with local interventions are lower than those at D1 with retrofit (Figures 59, 64, 69, 74), and the same occurs at damage level D2. The local strengthening interventions aim at increasing the stiffness and/or the ductility of some structural elements only (typically the columns and the connections), while a complete retrofit increases the seismic capacity of the entire buildings. The latter approach results in a more complex procedure affecting the overall seismic behaviour of the structure, often involving the application of different strengthening techniques; therefore, it is expected to be more expensive. In this light, the evidences found in this work are in line with those found in Di Ludovico et al. (2017a) after L'Aquila earthquake.

It is worth saying that the losses in €/mq are calculated dividing the amount in € by the surface in plan of the buildings in the pre-earthquake condition, following the principles adopted in the funding requests. In addition, it is worth noting that the reconstruction process has been applied, in almost all cases, maintaining the same plan configuration and soil occupancy of the structures before the seismic events. The only difference may be detected at damage state D5, in which a process of demolition and reconstruction has been engaged. In this case, whether possible, the reconstruction of the buildings aimed at exploiting the whole potential of soil use leading to a higher surface in plan in the post-earthquake condition. Thus, the monetary costs at damage state D5 are calculated both considering the surface PRE as for the other damage states, both considering the surface POST. The actual expected losses due to demolition and reconstruction are those in damage level D5-POST, since the technicians computed the costs with respect to the newly built structures. However, for the sake of comparison, both D5 and D5-POST analyses are reported in this Section: all the curves at D5-POST have a slightly lower μ compared to D5, and a very similar σ (Figures 62, 67, 72, 77). The difference is not remarkable, but it confirms the outcomes expected since the same costs in € are divided by larger surfaces in D5-POST.

The fitting curves of both conventional and estimated costs at damage levels D3, D4 and D5 (or D5-POST) follow different distributions, with increasing values of mean and rather comparable deviations. This occurs for conventional losses, estimated losses and structural estimated losses, while the non-structural losses show a different behaviour. In particular, the mean values of the non-structural losses at damage levels D5 and D5-POST are almost four times higher than that of losses at damage level D4. This fact may be again due to the approach of intervention considered. Indeed, at the first four damage levels, the interventions are mainly applied to the structural members only. Considering the destination of the industrial buildings, the finishing is often present only in the portions adopted as offices, and, to a minimal extent in the larger production areas. Thus, the retrofit of the buildings may involve partially the finishing and the plants, leading to rather negligible non-structural costs up to damage level D4 (see Table 29). Whereas, at damage level D5 (and D5-POST), the buildings were entirely reconstructed, so the non-structural costs correspond to a complete renovation of the finishing and systems, leading to a huge increase of the monetary non-structural costs compared with the previous damage states.

In general, the mean and median values of the total conventional losses appear to be higher in comparison to those of the total estimated losses, apart from those at the highest damage level (see Table 26 and 27). However, both the deviations of the values and the fitting curves of conventional costs are lower compared to those of the estimated costs, since the latter are more dispersed (higher CoV of the data observed). This phenomenon is further analysed in Section 4.2.2.3.

4.2.2.1.1. CONVENTIONAL

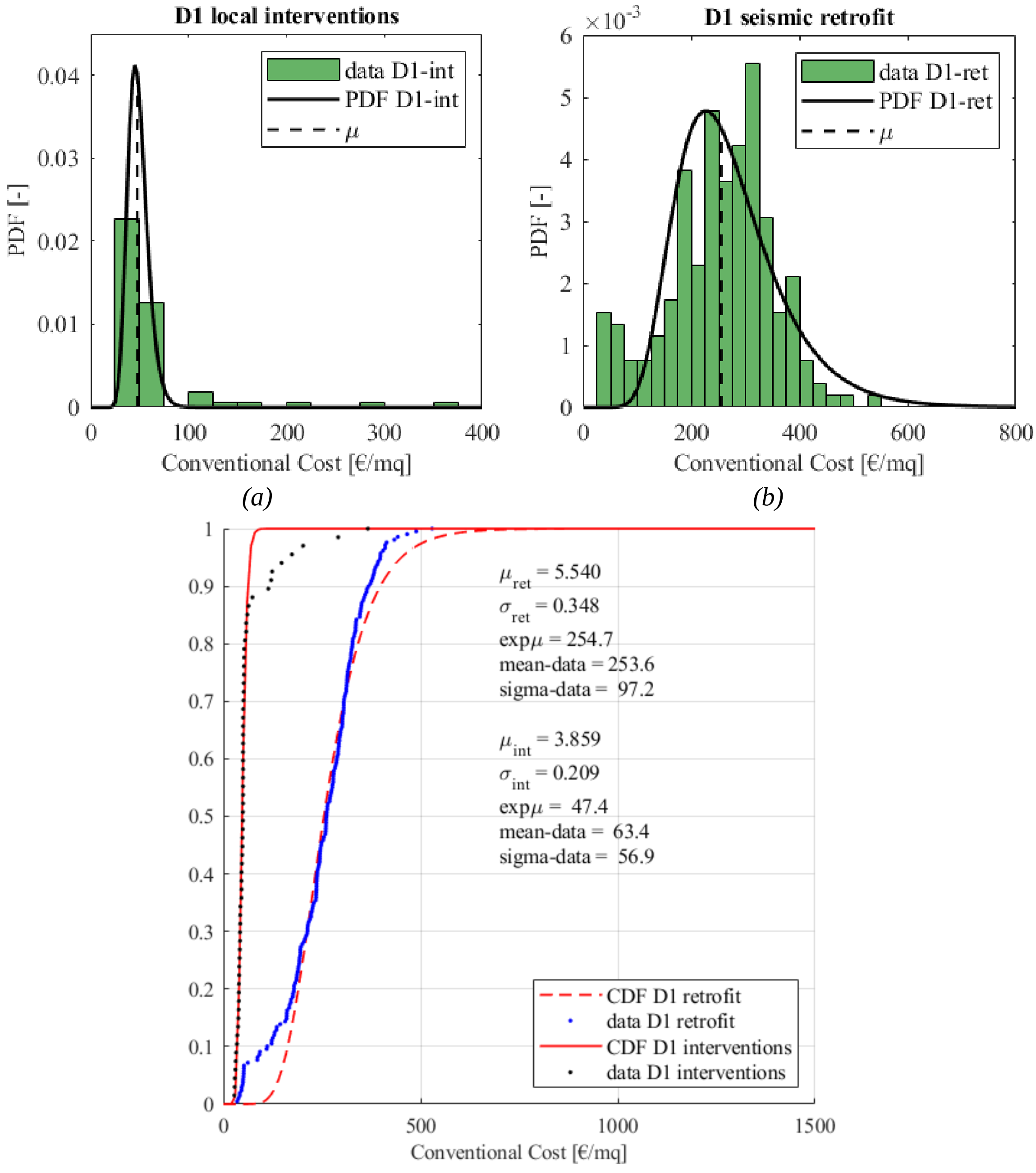

(a) *(b)*

(c)

Figure 59. Conventional costs at damage level D1 and lognormal fitting curves: (a) probability distribution for D1 with local interventions; (b) probability distribution for D1 with retrofit; (c) cumulative distribution. Indication of the main descriptors of the function, and the mean and the standard deviation of the data.

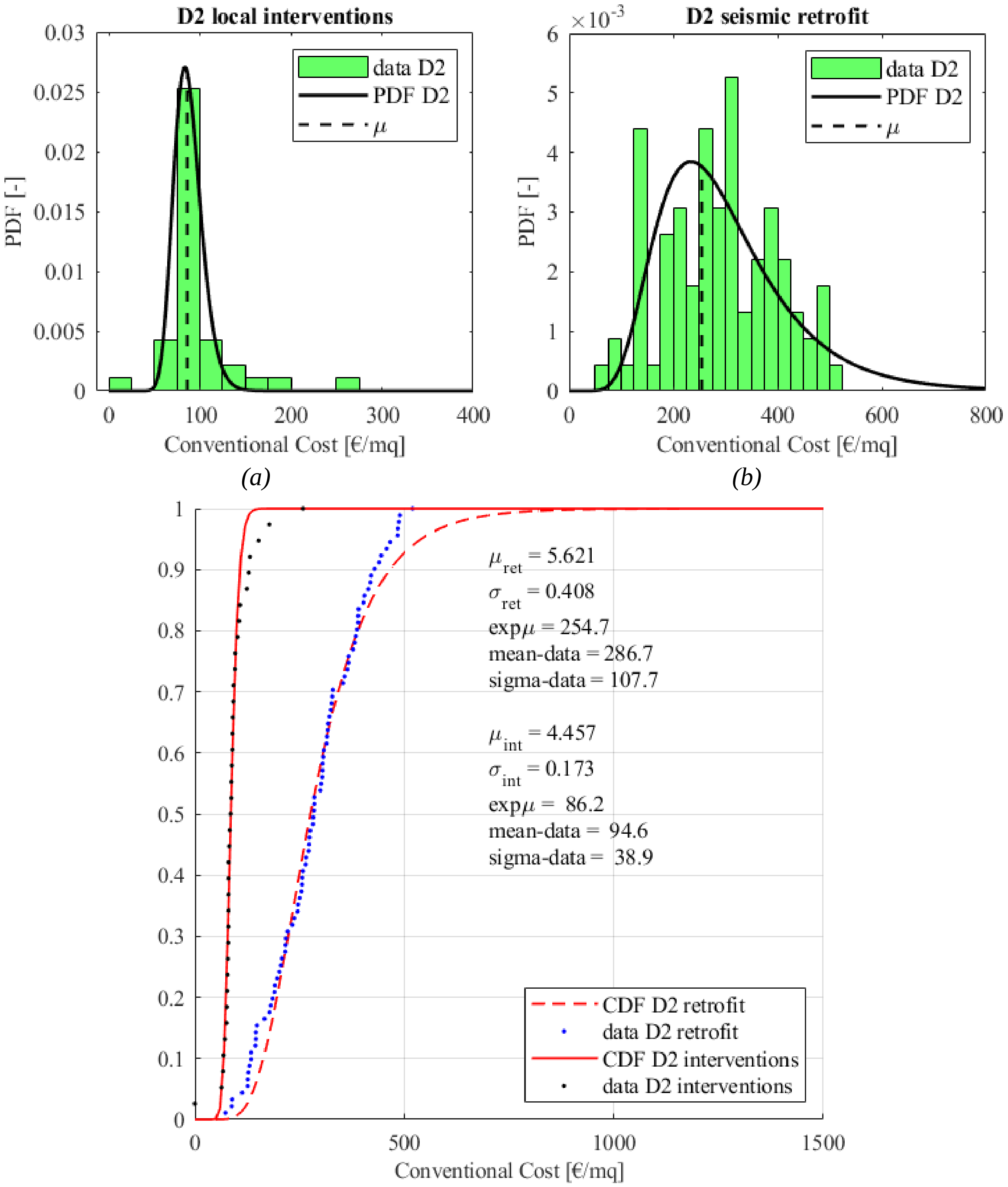

(a) *(b)*

(c)

Figure 60. Conventional costs at damage level D2 and lognormal fitting curves: (a) probability distribution for D2 with local interventions; (b) probability distribution for D2 with retrofit; (c) cumulative distribution. Indication of the main descriptors of the function, and the mean and the standard deviation of the data.

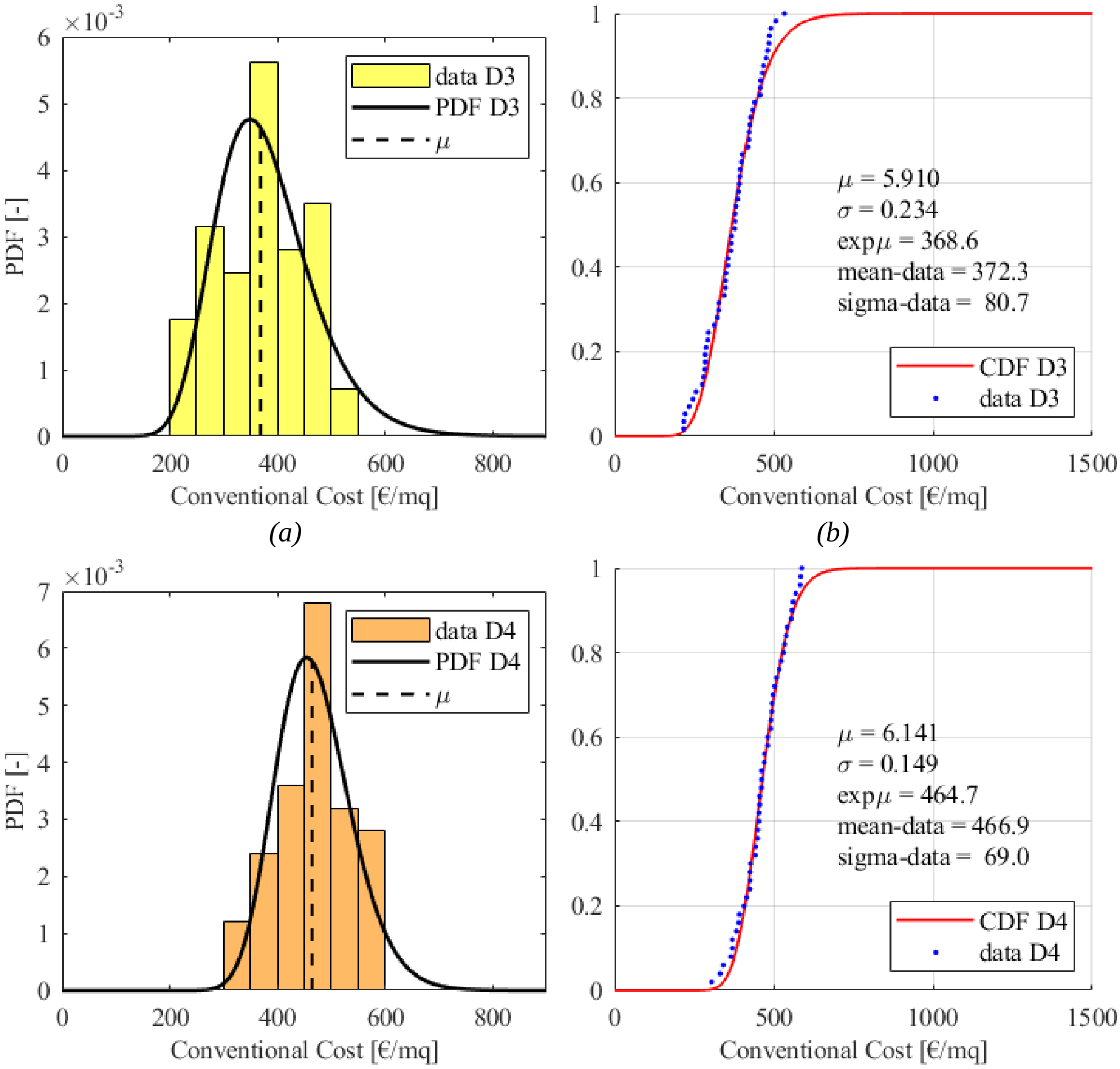

(a) *(b)*

(c) *(d)*

Figure 61. Conventional costs at damage levels D3, and D4 and lognormal fitting curves: (a) (c) probability distribution; (b) (d) cumulative distribution. Indication of the main descriptors of the function, and the mean and the standard deviation of the data.

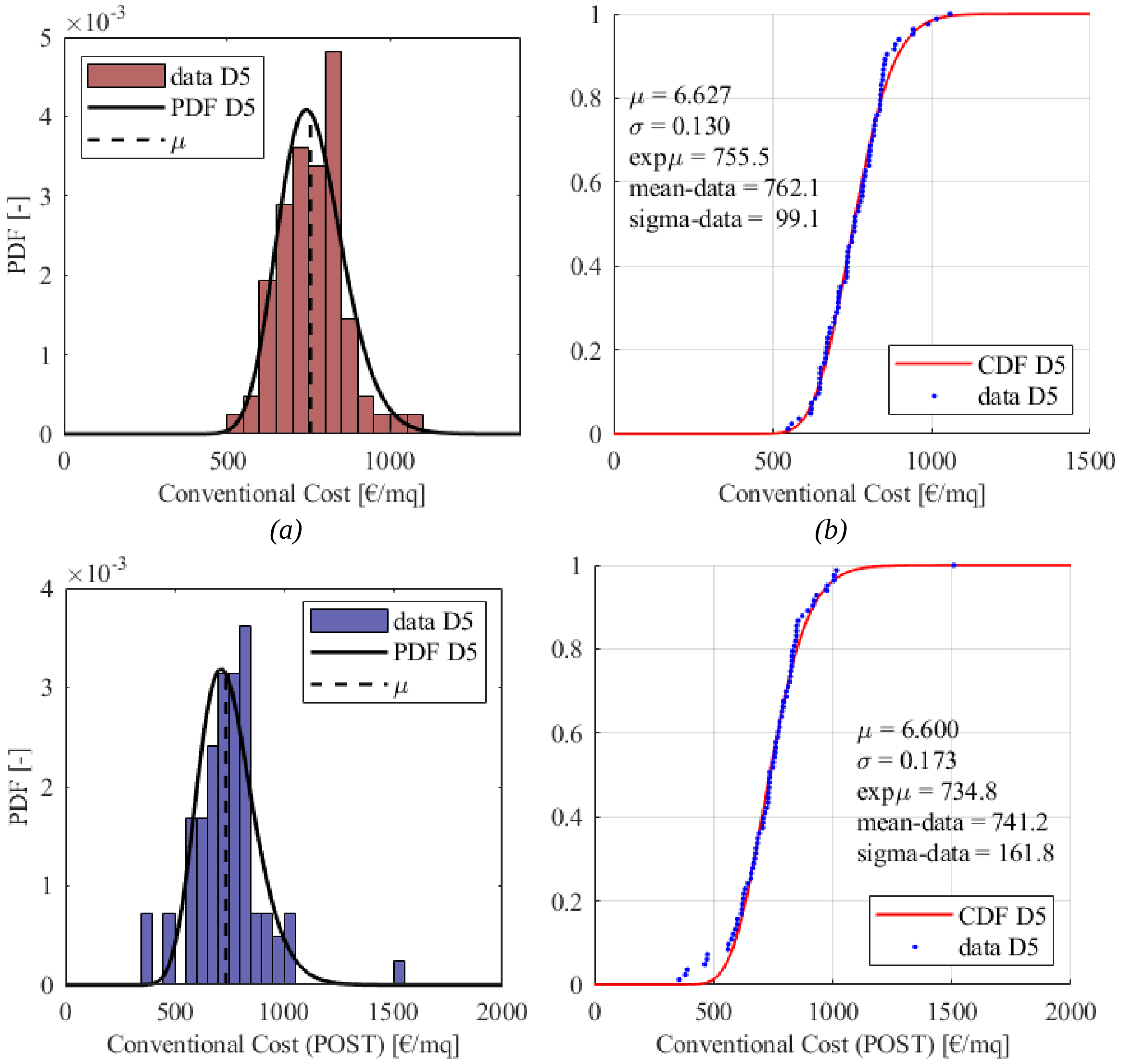

(a) *(b)*

(c) *(d)*

Figure 62. Conventional costs at damage levels D5, and D5-POST and lognormal fitting curves: (a) (c) probability distribution; (b) (d) cumulative distribution. Indication of the main descriptors of the function, and the mean and the standard deviation of the data.

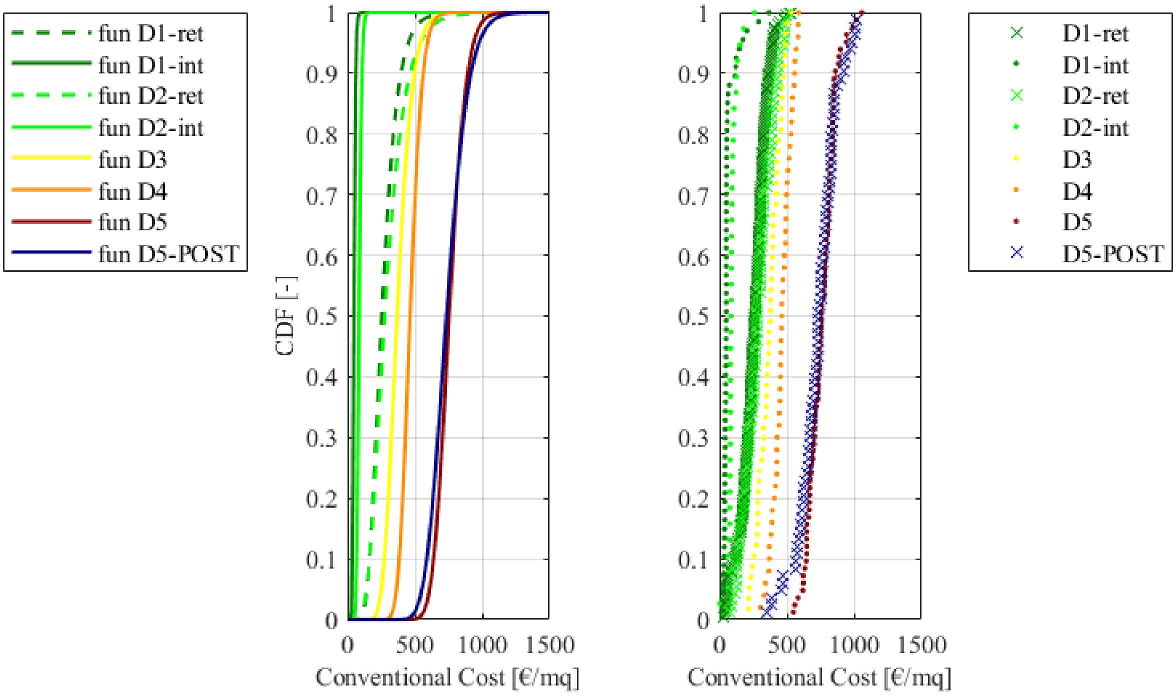

(a) *(b)*

Figure 63. Cumulative distribution of the conventional costs and lognormal fitting curves at different damage levels: (a) lognormal fitting curves; (b) cumulative representation of the data.

Table 26. Statistical analysis of the conventional costs at different damage levels.

	D1-ret	**D1-int**	**D2-ret**	**D2-int**	**D3**	**D4**	**D5**	**D5-post**
Mean [€/mq]	253.59	63.40	286.73	94.62	372.28	466.90	762.12	741.16
Median [€/mq]	261.67	49.40	284.40	86.64	379.35	462.50	759.12	736.61
Max [€/mq]	529.40	365.95	519.33	258.62	534.02	588.79	1058.33	1508.32
Min [€/mq]	34.88	27.49	73.20	0.06	217.48	305.56	548.65	355.50
Standard deviation [€/mq]	97.15	56.93	107.65	38.92	80.66	68.96	99.08	161.80
Total number [-]	209	67	91	38	57	50	83	83
16° percentile [€/mq]	161.42	38.84	167.24	76.36	284.36	391.61	659.66	612.00
84° percentile [€/mq]	337.69	59.87	401.64	114.51	461.52	540.64	846.47	848.29
Kurtosis [-]	0.0	15.3	-0.7	8.8	-0.8	-0.4	0.4	5.5
Skewness [-]	-0.3	3.6	0.1	2.0	-0.1	-0.2	0.4	0.9
CoV [%]	38.3	89.8	37.5	41.1	21.7	14.8	13.0	21.8
90% C.I. mean (-) [€/mq]	242.57	51.99	268.22	84.27	354.76	450.90	744.29	712.04
90% C.I. mean (+) [€/mq]	264.61	74.80	305.24	104.98	389.80	482.89	779.96	770.29

4.2.2.1.2. ESTIMATED

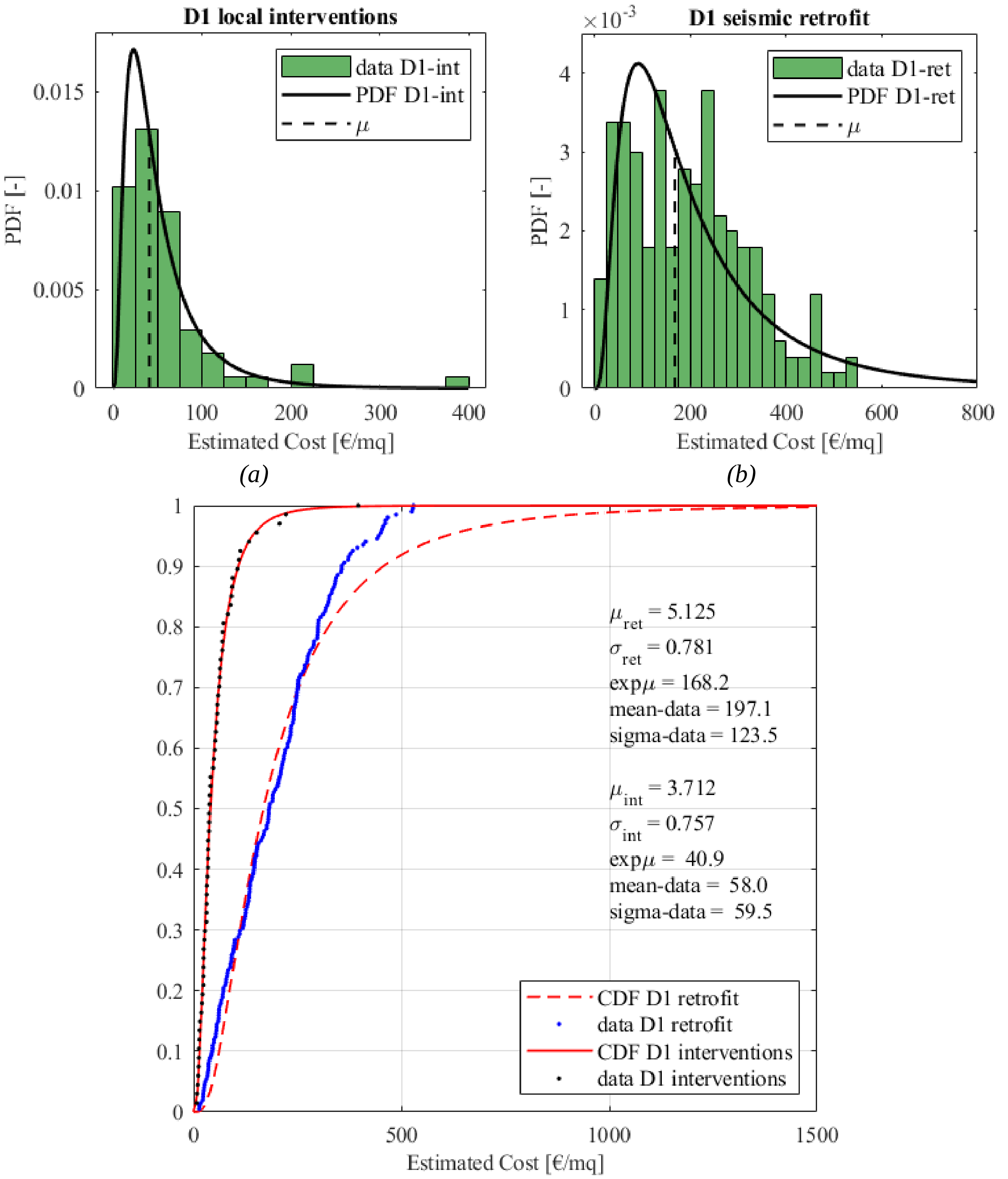

(a) *(b)*

(c)

Figure 64. Estimated costs at damage level D1 and lognormal fitting curves: (a) probability distribution for D1 with local interventions; (b) probability distribution for D1 with retrofit; (c) cumulative distribution. Indication of the main descriptors of the function, and the mean and the standard deviation of the data.

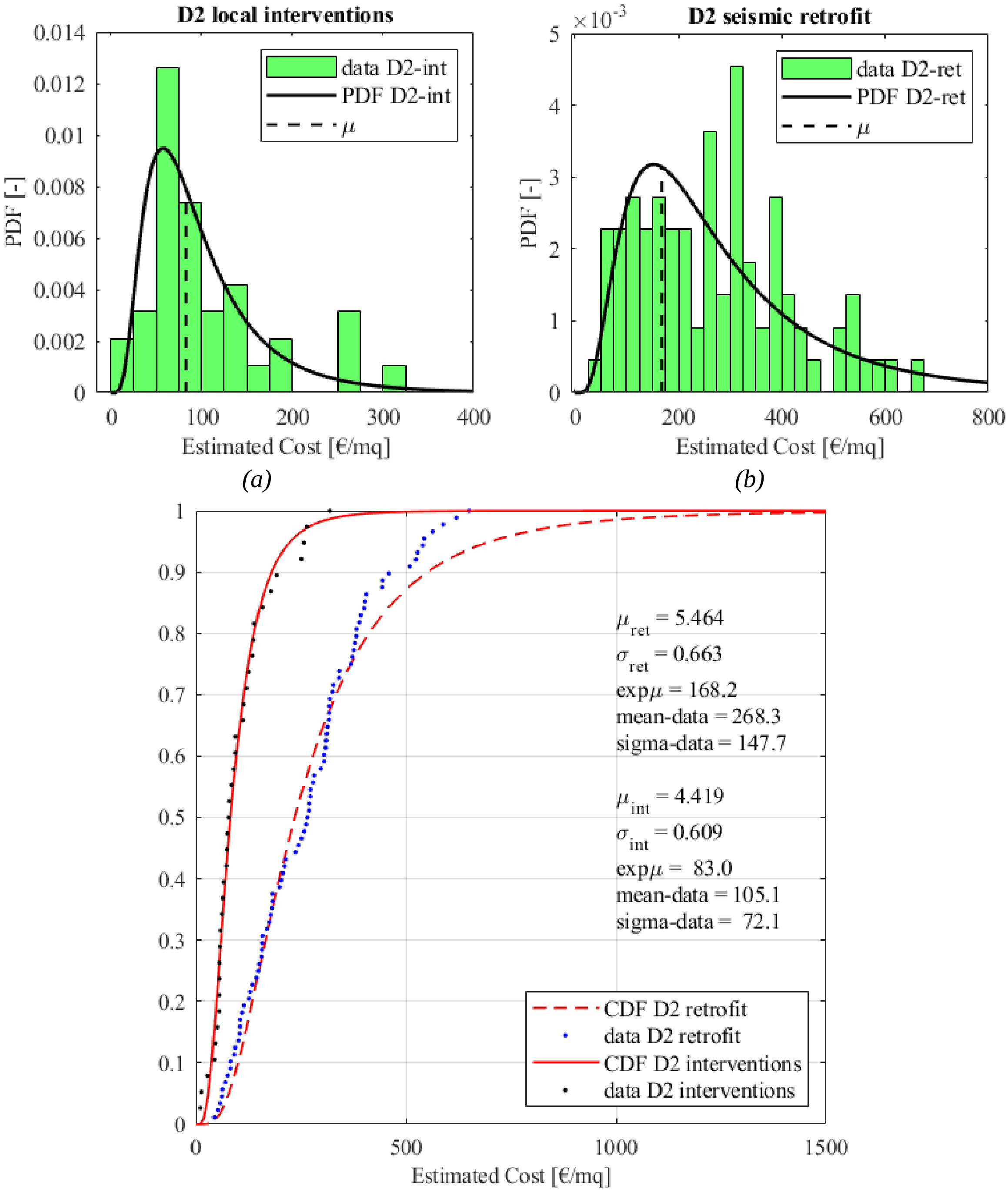

(a) *(b)*

(c)

Figure 65. Estimated costs at damage level D2 and lognormal fitting curves: (a) probability distribution for D2 with local interventions; (b) probability distribution for D2 with retrofit; (c) cumulative distribution. Indication of the main descriptors of the function, and the mean and the standard deviation of the data.

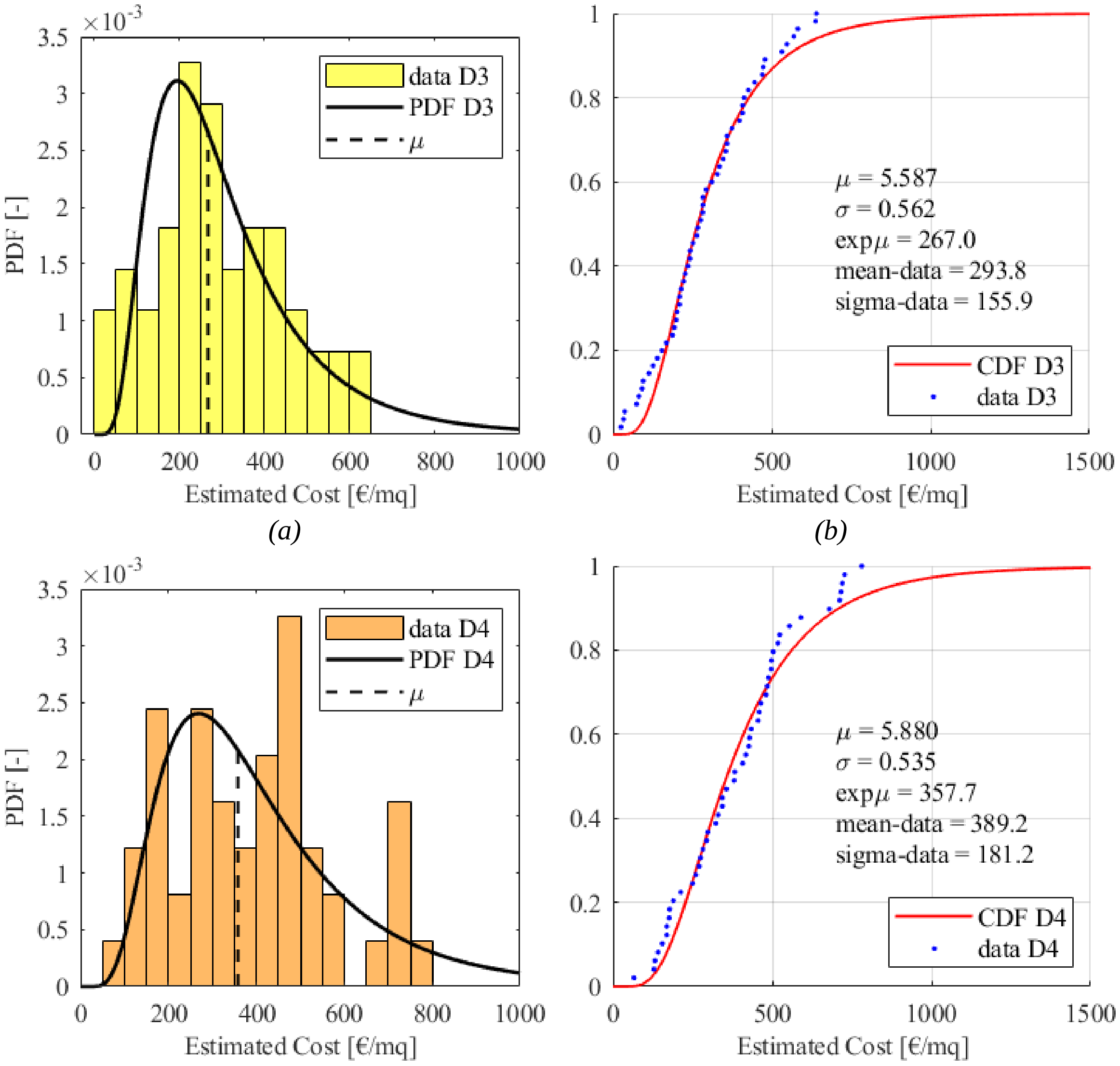

(a) *(b)*

(c) *(d)*

Figure 66. Estimated costs at damage levels D3, and D4 and lognormal fitting curves: (a) (c) probability distribution; (b) (d) cumulative distribution. Indication of the main descriptors of the function, and the mean and the standard deviation of the data.

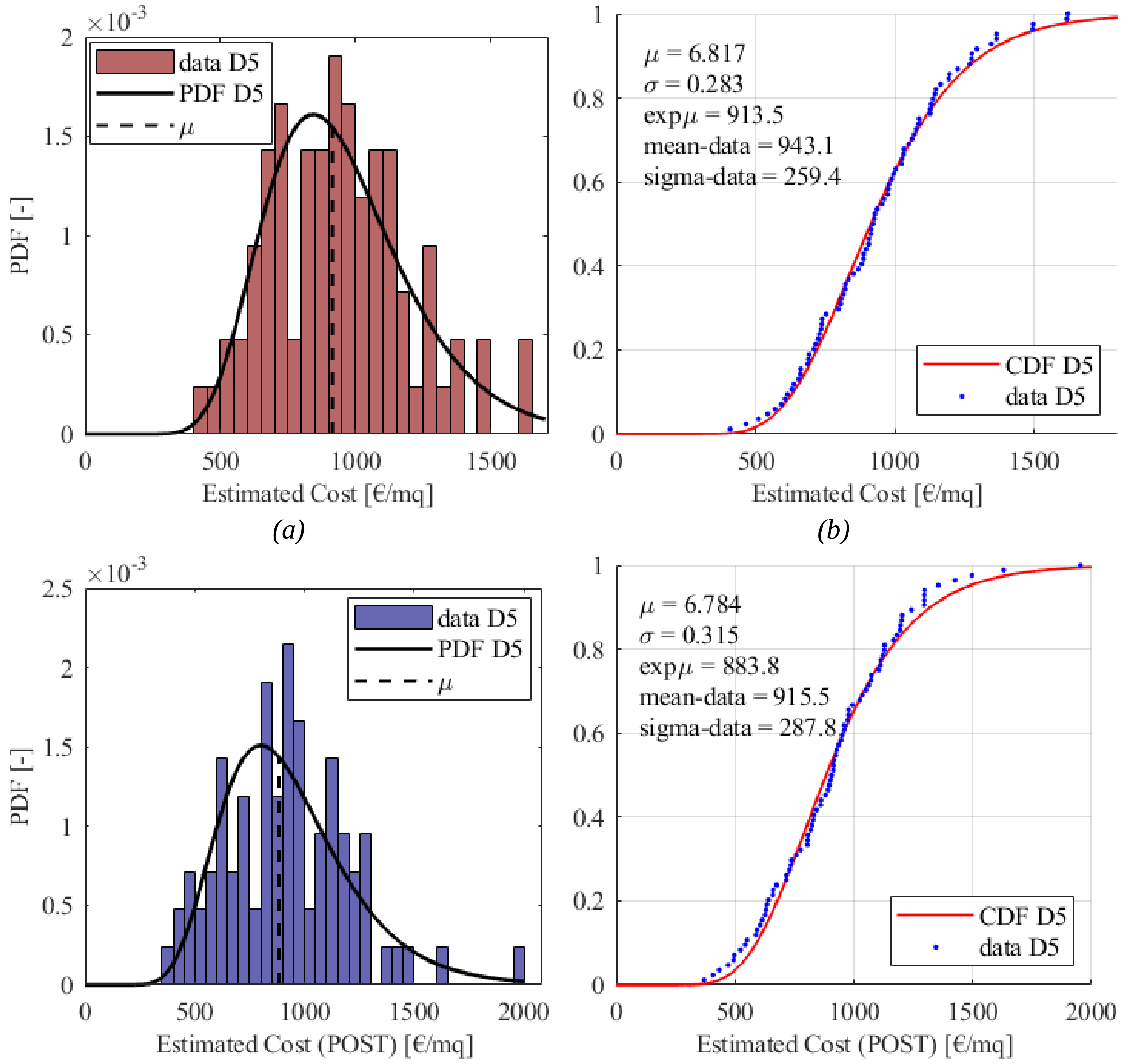

(a) *(b)*

(c) *(d)*

Figure 67. Estimated costs at damage levels D5, and D5-POST and lognormal fitting curves: (a) (c) probability distribution; (b) (d) cumulative distribution. Indication of the main descriptors of the function, and the mean and the standard deviation of the data.

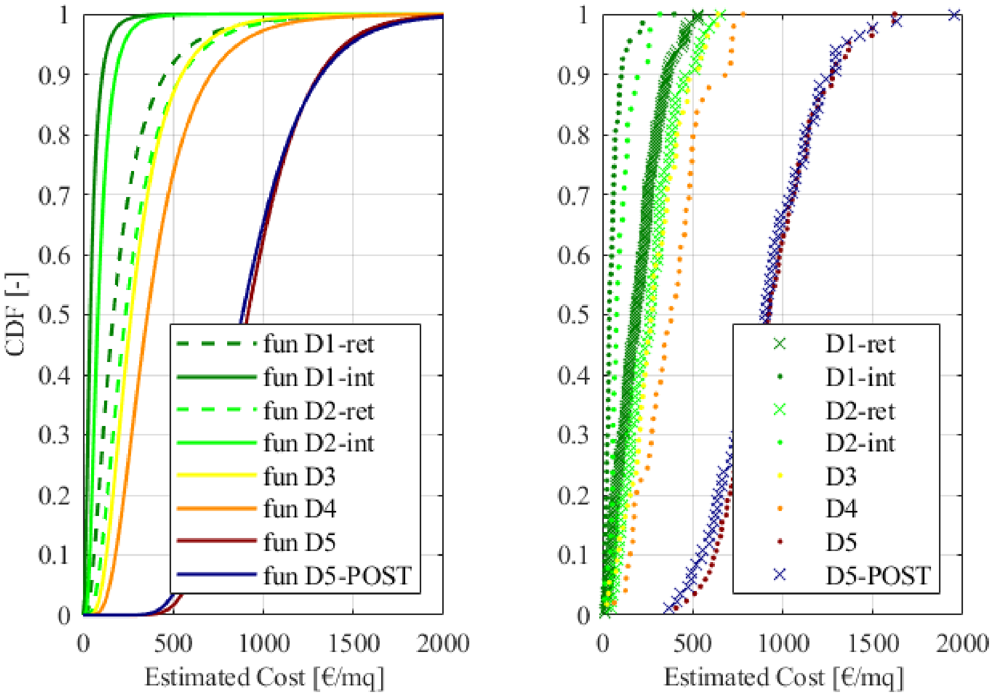

(a) *(b)*

Figure 68. Cumulative distribution of the estimated costs and lognormal fitting curves at different damage levels: (a) lognormal fitting curves; (b) cumulative representation of the data.

Table 27. Statistical analysis of the estimated losses at different damage levels.

	D1-ret	**D1-int**	**D2-ret**	**D2-int**	**D3**	**D4**	**D5**	**D5-post**
Mean [€/mq]	197.13	58.05	268.35	105.14	293.76	389.22	943.15	915.51
Median [€/mq]	183.05	38.94	267.48	79.58	277.21	382.17	925.05	909.73
Max [€/mq]	529.31	396.63	650.87	318.92	641.06	781.01	1621.01	1952.53
Min [€/mq]	13.99	8.06	44.65	11.67	25.97	66.23	409.06	369.94
Standard deviation [€/mq]	123.54	59.54	147.75	72.13	155.91	181.19	259.39	287.81
Total number [-]	201	67	88	38	55	49	84	84
16° percentile [€/mq]	61.02	19.69	105.79	54.05	130.84	177.15	686.05	626.59
84° percentile [€/mq]	325.18	91.57	402.10	167.42	463.07	544.11	1194.06	1194.97
Kurtosis [-]	-0.3	16.1	-0.3	1.5	-0.4	-0.5	0.0	1.1
Skewness [-]	0.6	3.4	0.5	1.3	0.4	0.3	0.4	0.6
CoV [%]	62.7	102.6	55.1	68.6	53.1	46.6	27.5	31.4
90% C.I. mean (-) [€/mq]	182.84	46.12	242.52	85.95	259.28	346.77	896.74	864.01
90% C.I. mean (+) [€/mq]	211.42	69.98	294.18	124.33	328.24	431.67	989.56	967.01

4.2.2.1.3. ESTIMATED – STRUCTURAL (A)

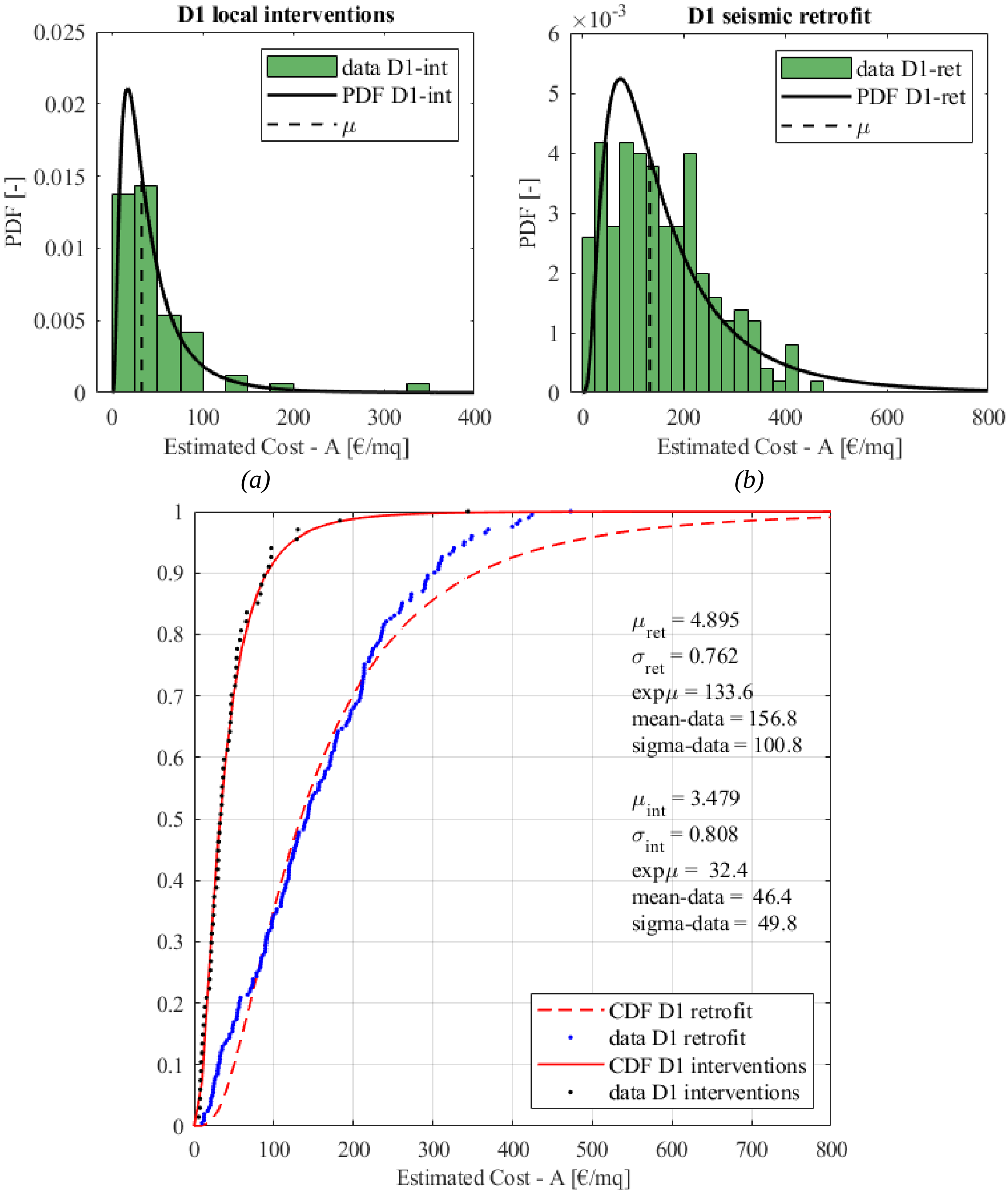

(a) *(b)*

(c)

Figure 69. Estimated structural costs at damage level D1 and lognormal fitting curves: (a) probability distribution for D1 with local interventions; (b) probability distribution for D1 with retrofit; (c) cumulative distribution. Indication of the main descriptors of the function, and the mean and the standard deviation of the data.

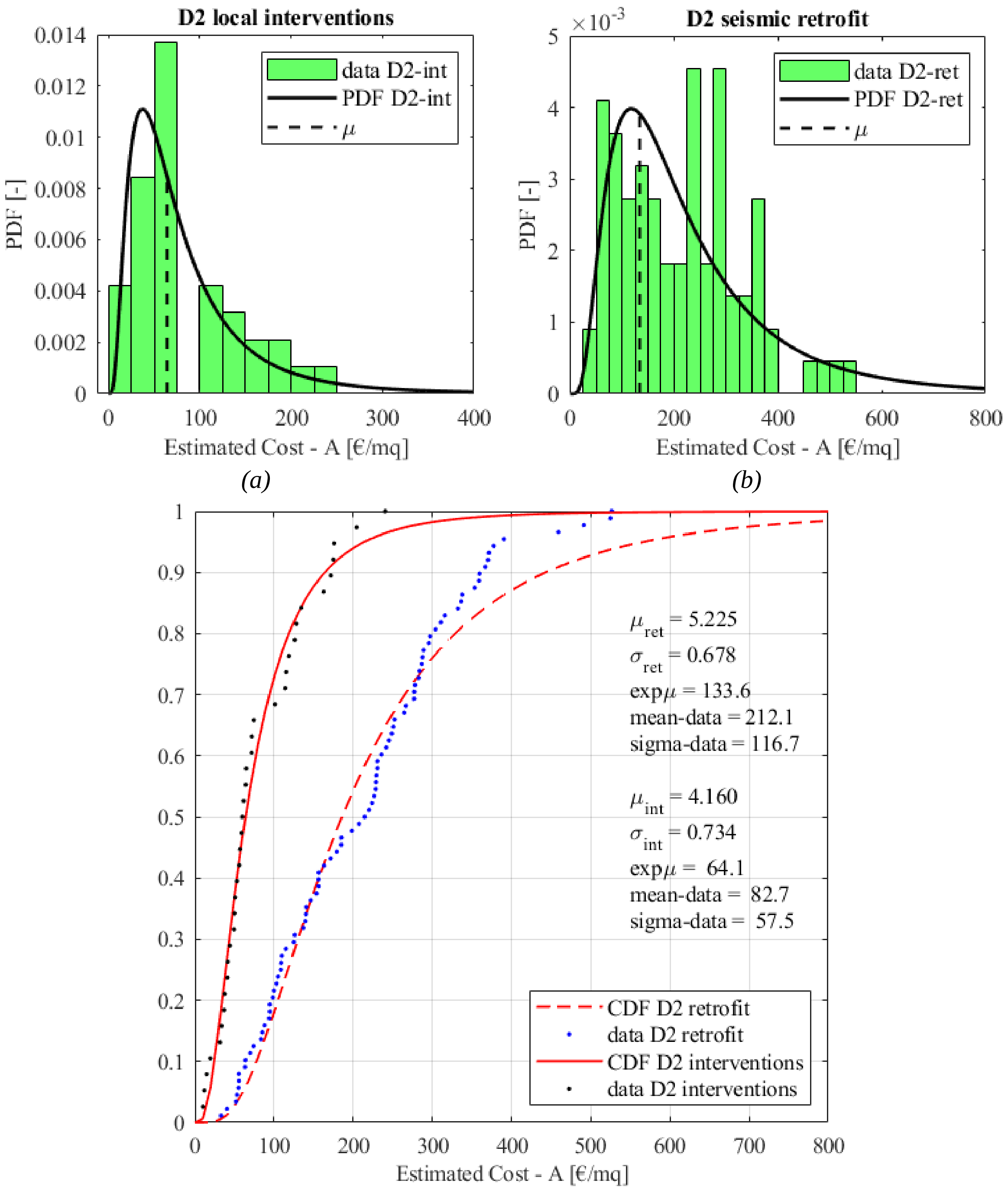

(a) *(b)*

(c)

Figure 70. Estimated structural costs at damage level D2 and lognormal fitting curves: (a) probability distribution for D2 with local interventions; (b) probability distribution for D2 with retrofit; (c) cumulative distribution. Indication of the main descriptors of the function, and the mean and the standard deviation of the data.

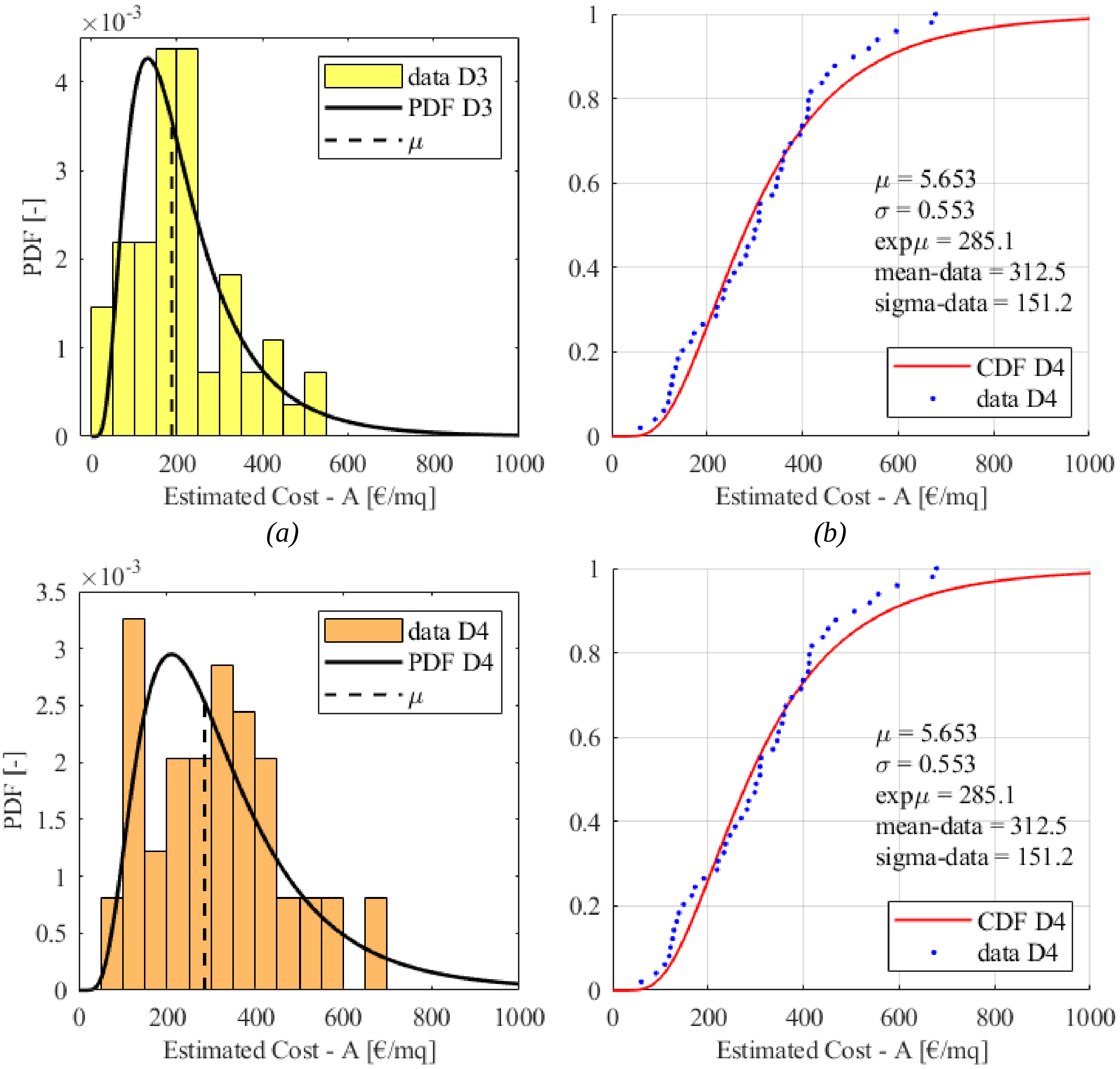

(a) *(b)*

(c) *(d)*

Figure 71. Estimated structural costs at damage levels D3, and D4 and lognormal fitting curves: (a) (c) probability distribution; (b) (d) cumulative distribution. Indication of the main descriptors of the function, and the mean and the standard deviation of the data.

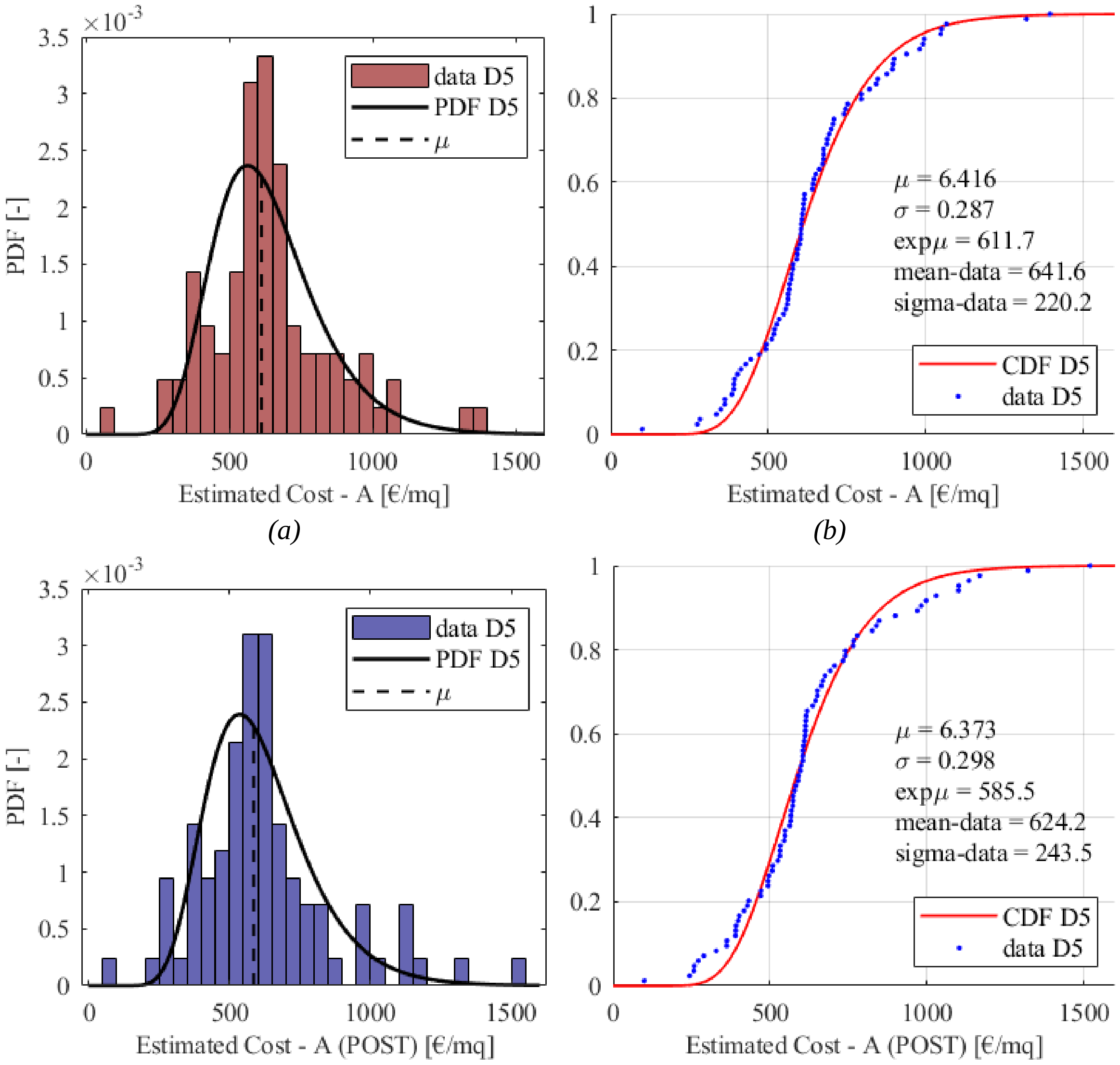

(a) *(b)*

(c) *(d)*

Figure 72. Estimated structural costs at damage levels D5, and D5-POST and lognormal fitting curves: (a) (c) probability distribution; (b) (d) cumulative distribution. Indication of the main descriptors of the function, and the mean and the standard deviation of the data.

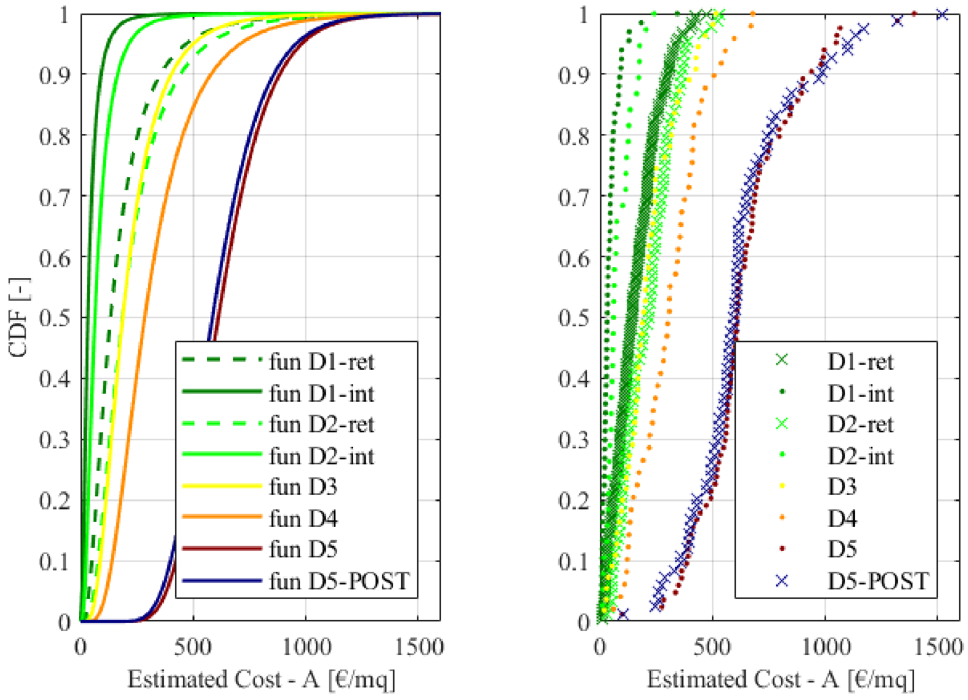

(a) *(b)*

Figure 73. Cumulative distribution of the estimated structural costs and lognormal fitting curves at different damage levels: (a) lognormal fitting curves; (b) cumulative representation of the data.

Table 28. Statistical analysis of the estimated structural losses at different damage levels.

	D1-ret	**D1-int**	**D2-ret**	**D2-int**	**D3**	**D4**	**D5**	**D5-post**
Mean [€/mq]	156.84	46.45	212.06	82.69	213.50	312.50	641.58	624.18
Median [€/mq]	142.81	33.55	217.29	61.01	194.21	309.06	606.13	594.35
Max [€/mq]	473.06	343.65	526.61	240.64	515.44	678.17	1394.42	1519.57
Min [€/mq]	9.73	5.80	33.15	10.26	19.39	59.85	99.65	99.65
Standard deviation [€/mq]	100.83	49.75	116.67	57.49	123.89	151.24	220.24	243.49
Total number [-]	201	67	88	38	55	49	84	84
16° percentile [€/mq]	49.00	12.08	91.60	35.59	89.74	135.94	427.55	402.07
84° percentile [€/mq]	259.62	76.94	334.26	146.25	340.58	447.66	849.35	826.41
Kurtosis [-]	0.0	19.4	-0.1	0.3	0.0	-0.2	1.7	2.2
Skewness [-]	0.7	3.7	0.6	1.0	0.7	0.5	0.8	1.1
CoV [%]	64.3	107.1	55.0	69.5	58.0	48.4	34.3	39.0
90% C.I. mean (-) [€/mq]	145.18	36.48	191.67	67.39	186.10	277.07	602.17	580.61
90% C.I. mean (+) [€/mq]	168.51	56.42	232.46	97.98	240.90	347.93	680.99	667.75

4.2.2.1.4. ESTIMATED – NON-STRUCTURAL (C)

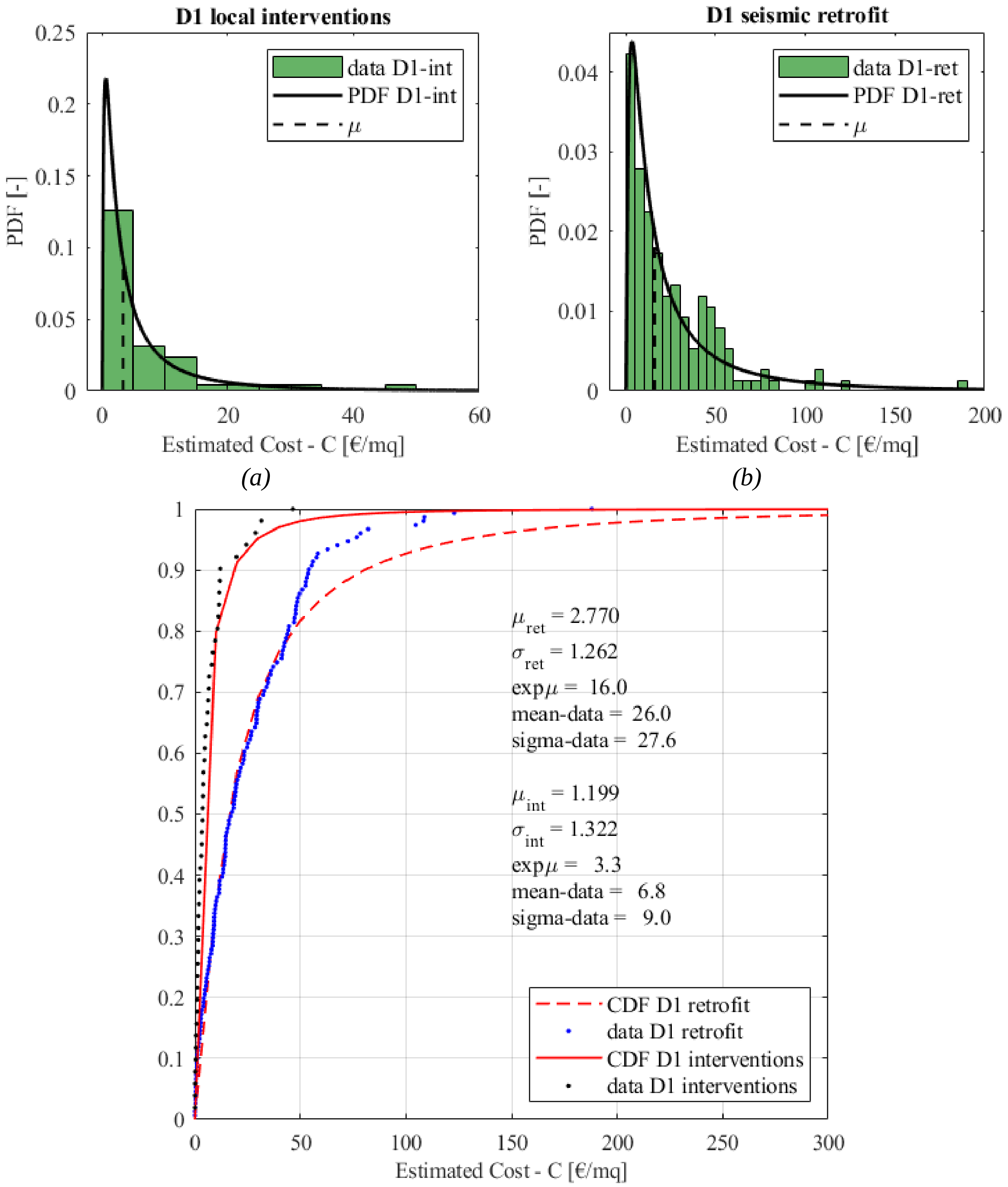

(a) *(b)*

(c)

Figure 74. Estimated non-structural costs at damage level D1 and lognormal fitting curves: (a) probability distribution for D1 with local interventions; (b) probability distribution for D1 with retrofit; (c) cumulative distribution. Indication of the main descriptors of the function, and the mean and the standard deviation of the data.

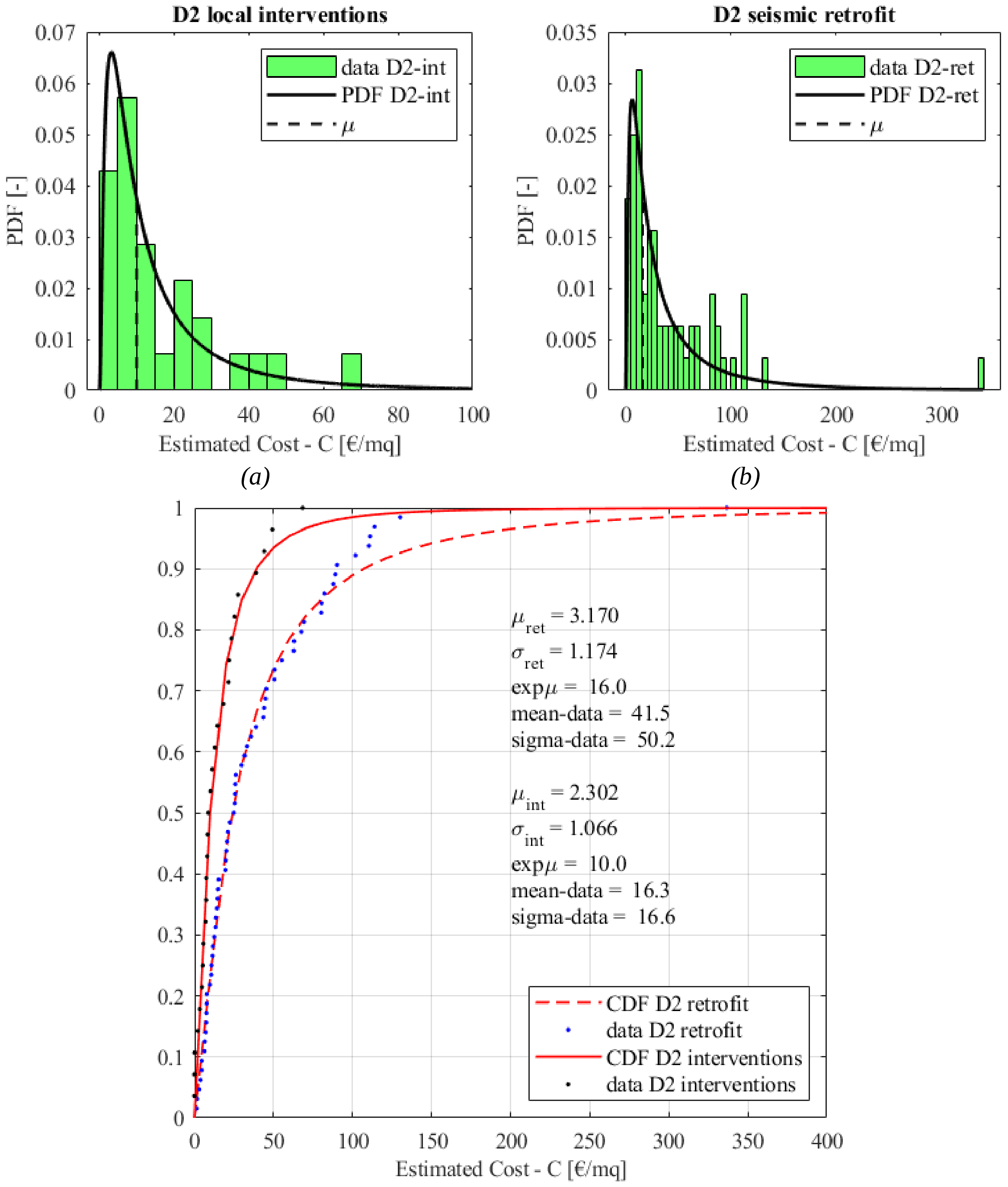

(a) *(b)*

(c)

Figure 75. Estimated non-structural costs at damage level D2 and lognormal fitting curves: (a) probability distribution for D2 with local interventions; (b) probability distribution for D2 with retrofit; (c) cumulative distribution. Indication of the main descriptors of the function, and the mean and the standard deviation of the data.

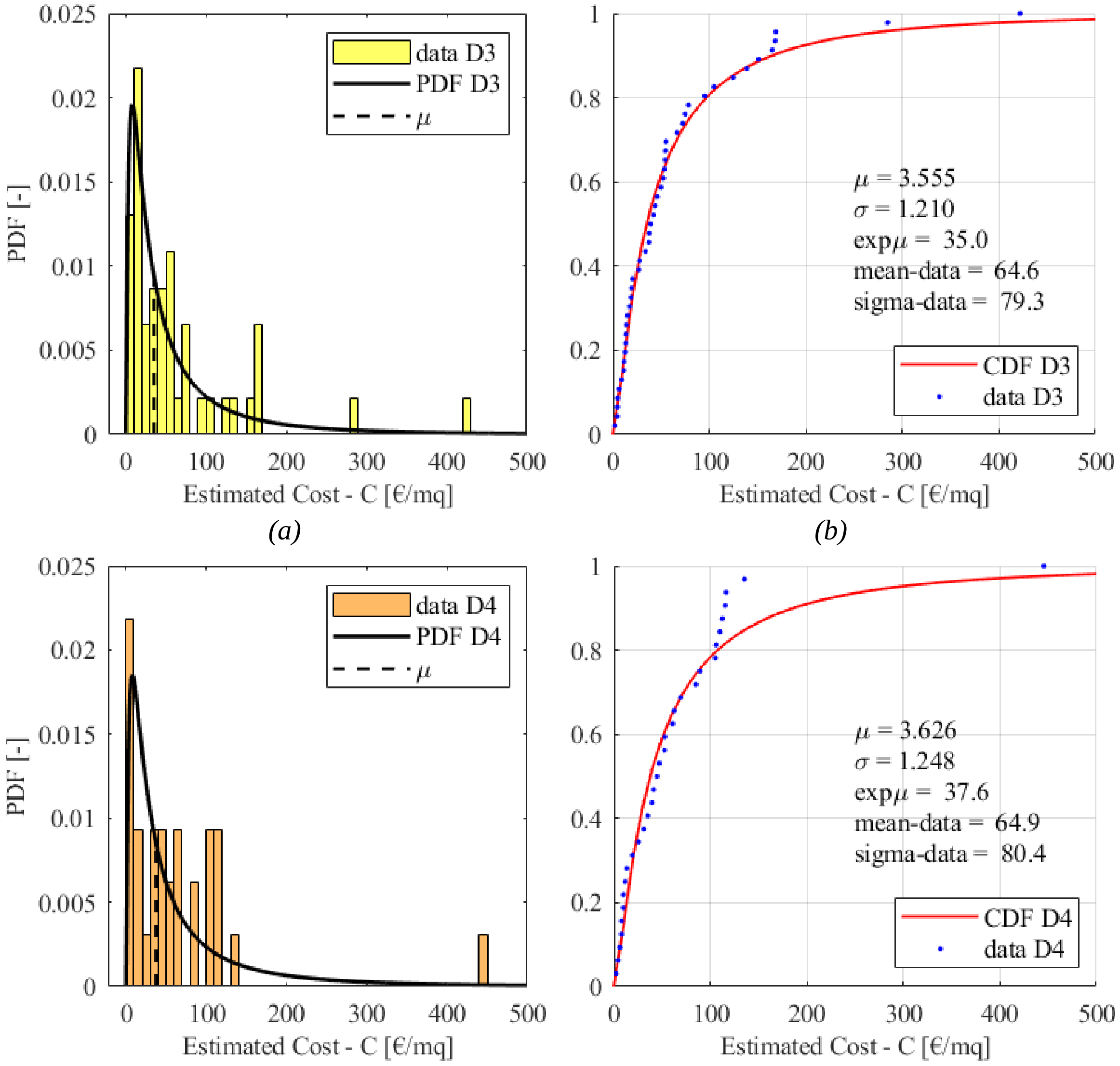

(a) *(b)*

(c) *(d)*

Figure 76. Estimated non-structural costs at damage levels D3, and D4 and lognormal fitting curves: (a) (c) probability distribution; (b) (d) cumulative distribution. Indication of the main descriptors of the function, and the mean and the standard deviation of the data.

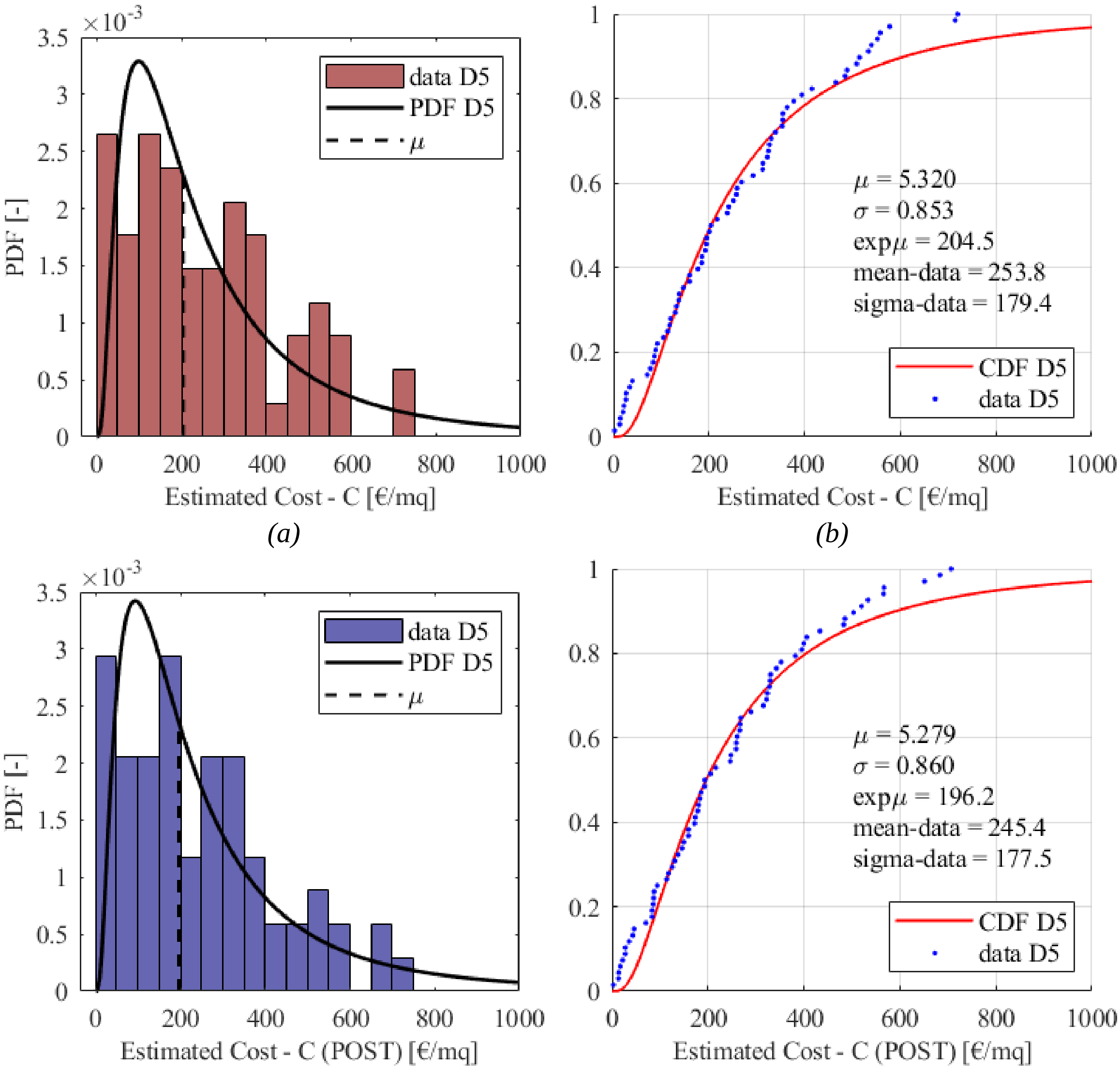

(a) *(b)*

(c) *(d)*

Figure 77. Estimated non-structural costs at damage levels D5, and D5-POST and lognormal fitting curves: (a) (c) probability distribution; (b) (d) cumulative distribution. Indication of the main descriptors of the function, and the mean and the standard deviation of the data.

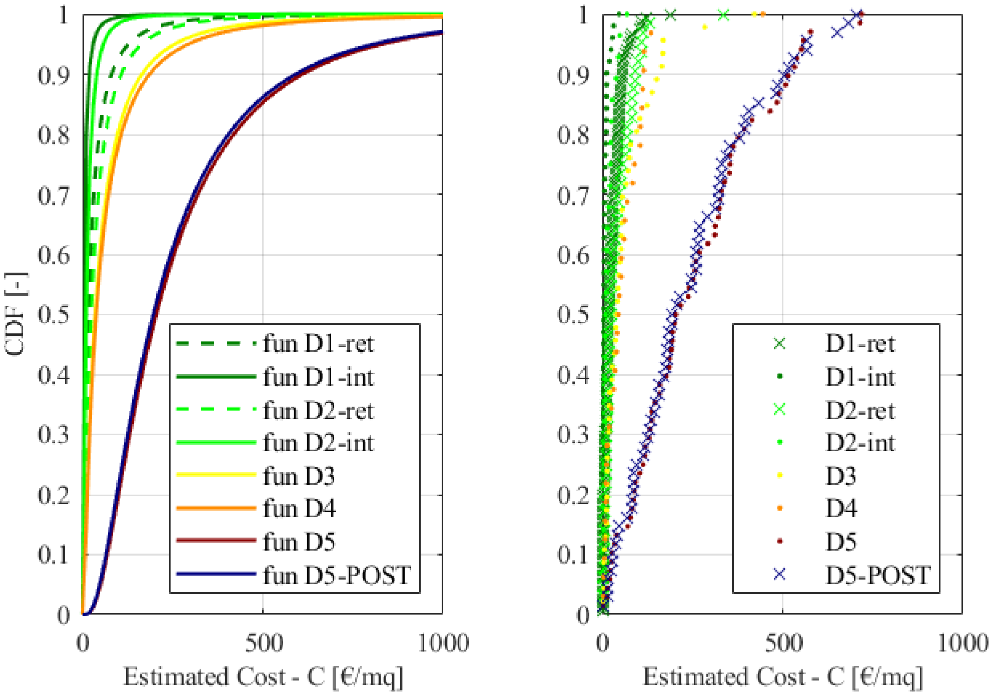

(a) *(b)*

Figure 78. Cumulative distribution of the estimated structural costs and lognormal fitting curves at different damage levels: (a) lognormal fitting curves; (b) cumulative representation of the data.

Table 29. Statistical analysis of the estimated non-structural losses at different damage levels.

	D1-ret	**D1-int**	**D2-ret**	**D2-int**	**D3**	**D4**	**D5**	**D5-post**
Mean [€/mq]	25.96	6.76	41.53	16.34	64.57	64.90	253.76	245.41
Median [€/mq]	17.70	3.74	25.27	9.50	40.70	46.04	211.01	199.42
Max [€/mq]	187.95	46.47	336.79	68.43	421.84	445.27	719.64	706.49
Min [€/mq]	0.00	0.02	1.40	0.06	2.14	2.65	3.01	3.01
Standard deviation [€/mq]	27.61	9.03	50.22	16.62	79.31	80.38	179.41	177.48
Total number [-]	151	51	64	28	46	32	68	68
16° percentile [€/mq]	2.89	0.94	7.61	3.35	11.64	9.08	79.85	75.52
84° percentile [€/mq]	48.25	11.47	80.82	27.98	126.74	110.83	477.29	422.49
Kurtosis [-]	8.5	7.9	18.3	2.6	9.1	16.5	-0.2	-0.1
Skewness [-]	2.3	2.5	3.4	1.5	2.6	3.4	0.7	0.7
CoV [%]	106.3	133.6	120.9	101.7	122.8	123.9	70.7	72.3
90% C.I. mean (-) [€/mq]	22.28	4.69	31.24	11.19	45.40	41.59	218.08	210.11
90% C.I. mean (+) [€/mq]	29.65	8.83	51.83	21.49	83.75	88.20	289.44	280.70

4.2.2.2. LOSSES OF DIFFERENT STRUCTURAL TYPOLOGIES

In this Section, the trends of the conventional and the estimated costs are analysed for the six different building typologies T1 to T6, considering all the five damage levels together. The typologies are those described in Section 4.1. The hypothesis of including all damage states in a single distribution is clearly visible in the probability distributions shown in the following, since there are several peaks in the bins due to the presence of costs at different damage degrees (Figures 79, 80, 82, 83). The bin-width adopted in the histograms is 50 €/mq for both conventional and estimated losses of all the structural typologies.

The statistical analysis of the conventional costs is reported in Table 30, while that for the estimated costs in Table 31. The loss data of each typology are analysed individually, thus a final image with the cumulative distributions of the data and the fitting functions is proposed in Figures 81 and 84 for comparison.

The analyses of the losses are proposed for all the typologies even if there are not enough data for a suitable interpretation of those of T4 (the shed buildings) compared to the others. Moreover, typologies T5 and T6 are less relevant since they represent a mixed population of buildings (buildings with irregularities and buildings with uncommon features, respectively).

The data and the functions presented are not directly useful for a comprehensive loss assessment since there is not a direct interpretation of the degree of the seismic damage. Nevertheless, it is interesting to evaluate the discrepancies between the average terms and the different trends of the conventional and the estimated costs.

Indeed, the mean and median values of the conventional costs are again higher than those of the estimated costs for all the typologies, except T4, and the standard deviations are lower.

In addition, from the outcomes it is possible to infer which is the most expensive typology in terms of average repair costs. In particular, concerning the estimated losses, the functions illustrated in Figure 84 indicate that the estimated costs of T3 seem to be lower than T2, while T1 seems to be the most expensive typology (on average). This aspect may be due to the structural and geometrical features of the buildings. Indeed, T1 represents a class of older buildings with lower span dimensions, thus, a higher number of columns per square meter, while T3 represents industrial buildings with larger span dimensions and broad empty internal spaces with few columns. Therefore, with reference to the monetary losses over meter square of surface in plan, the repair costs of typology T3 are lower than T1 (and T2, which have geometrical features in plan similar to T1) considering, for instance, a local strengthening intervention of all the columns. This means that the higher density of columns in T1 buildings may lead to an increase of the costs for all the structural retrofit that involve operations on the columns. Those kind of retrofit techniques were highly adopted in the reconstruction and retrofit phase after 2012 (Minghini and Tullini 2021).

This aspect is furtherly deepened in Section 4.2.3, while the structural features of the different typologies are studied in the analyses of the structural-loss database, presented in Section 4.3.

4.2.2.2.1. CONVENTIONAL

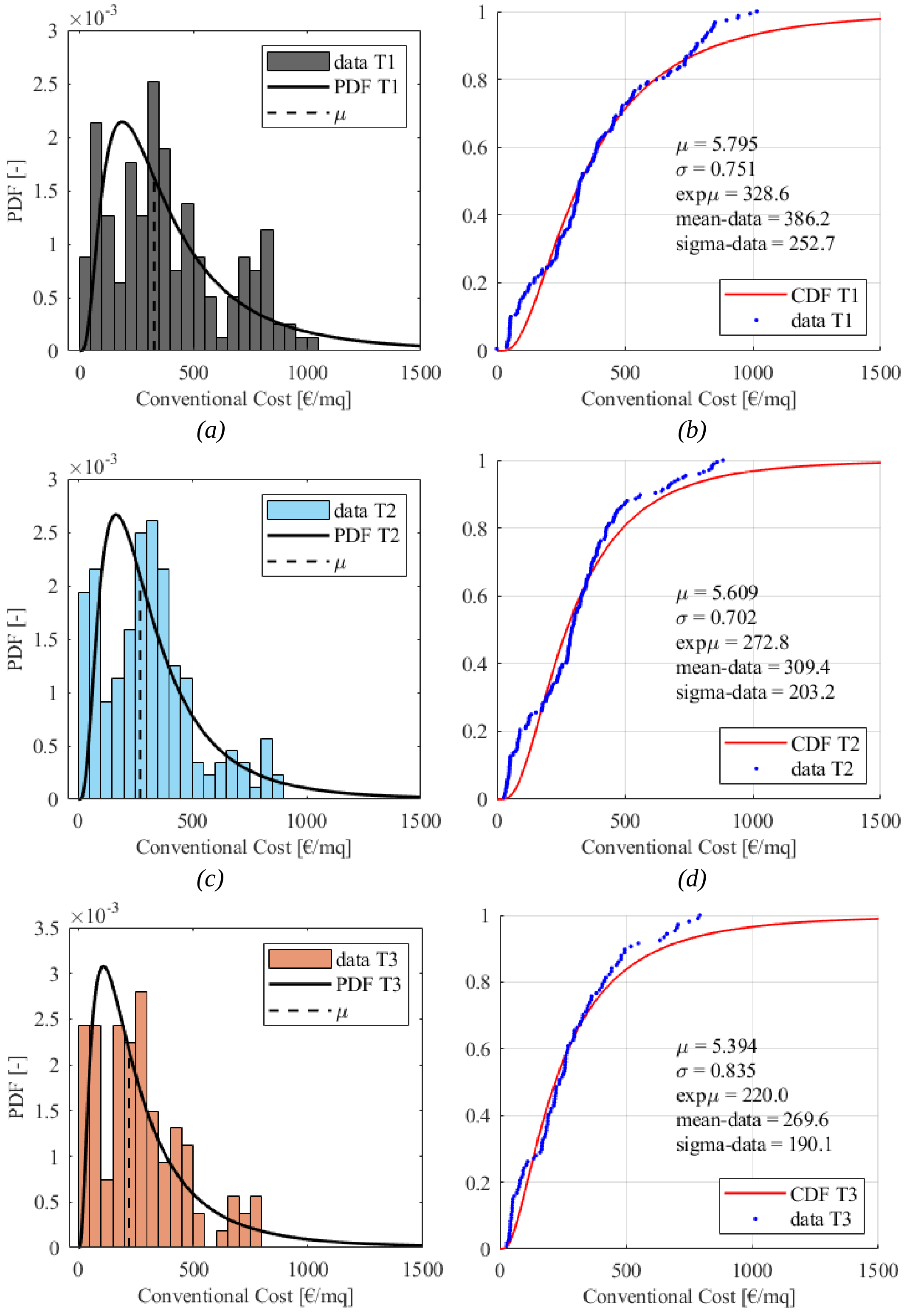

(a) *(b)*

(c) *(d)*

(e) *(f)*

Figure 79. Conventional costs of typologies T1, T2 and T3 and lognormal fitting curves: (a) (c) (e) probability distribution; (b) (d) (f) cumulative distribution.

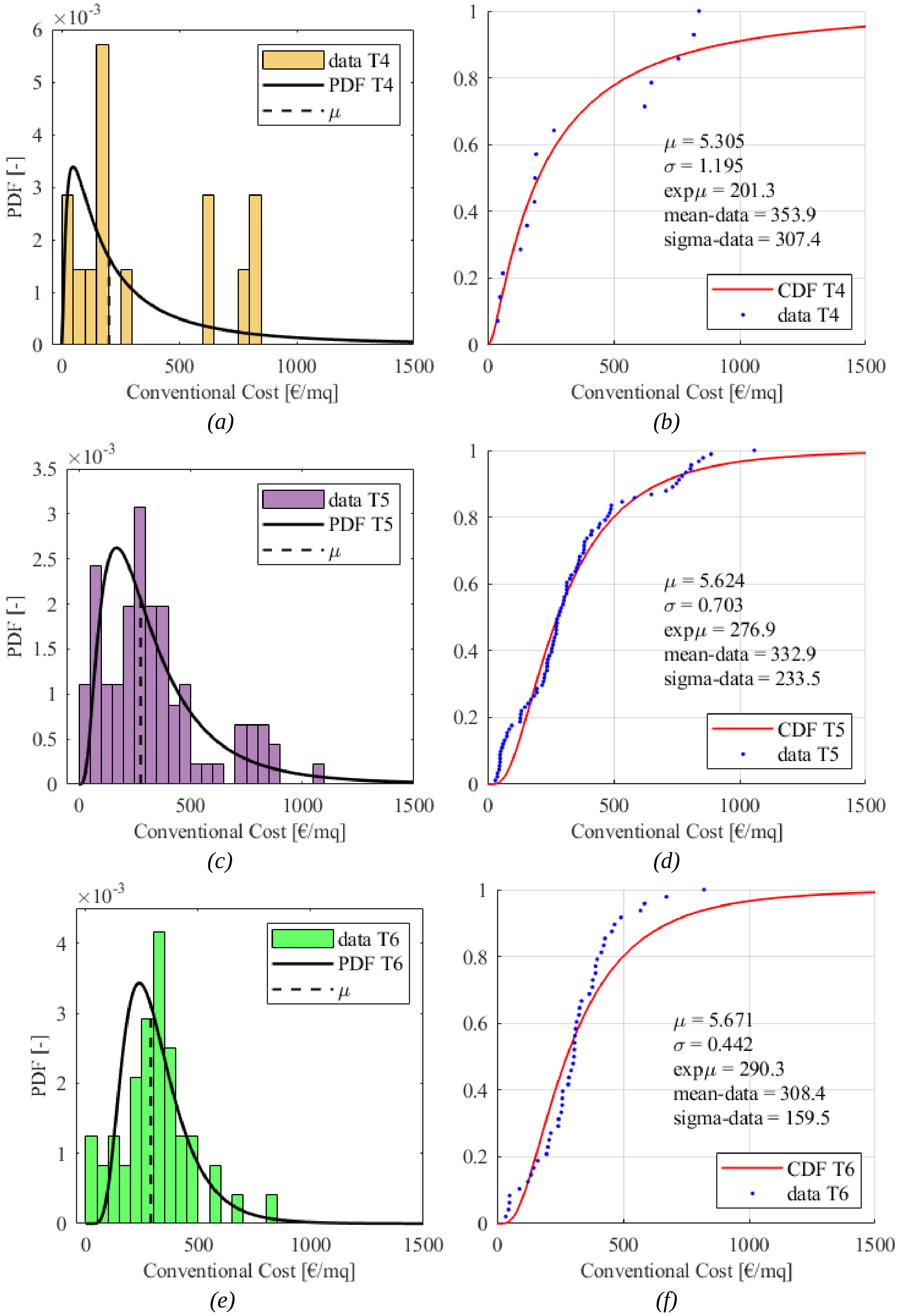

(a) (b) (c) (d) (e) (f)

Figure 80. Conventional costs of typologies T4, T5 and T6 and lognormal fitting curves: (a) (c) (e) probability distribution; (b) (d) (f) cumulative distribution.

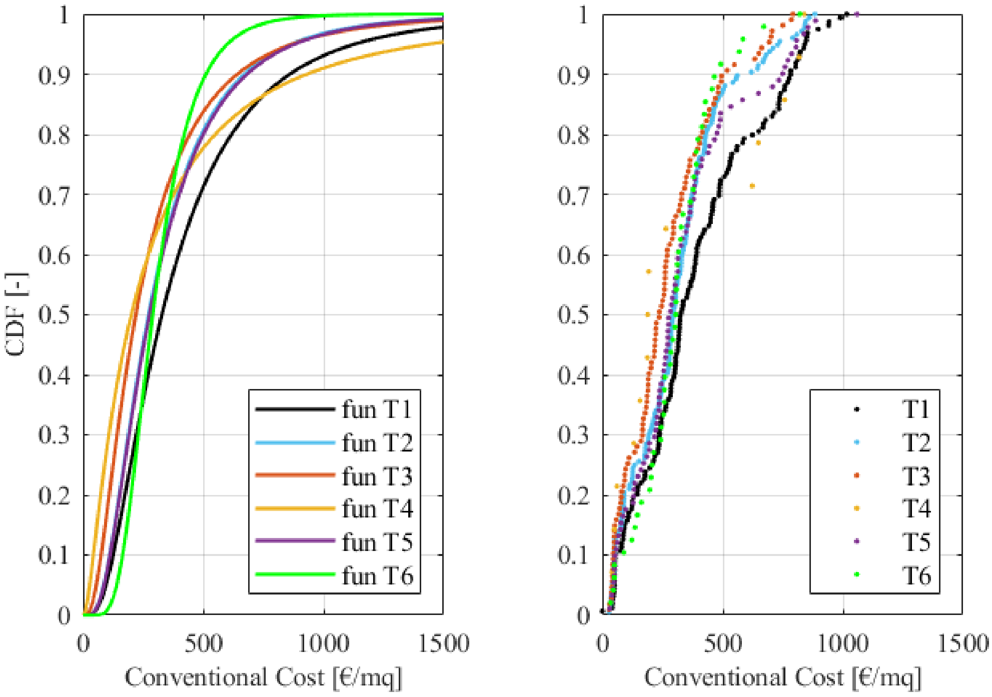

(a) *(b)*

Figure 81. Cumulative distribution of the conventional costs and lognormal fitting curves of different typologies: (a) lognormal fitting curves; (b) cumulative representation of the data.

Table 30. Statistical analysis of the conventional costs of different structural typologies.

	T1	**T2**	**T3**	**T4**	**T5**	**T6**
Mean [€/mq]	386.22	309.36	269.58	353.90	332.92	308.41
Median [€/mq]	327.38	293.41	236.94	190.33	282.72	305.92
Max [€/mq]	1015.86	883.44	792.17	838.68	1058.33	820.71
Min [€/mq]	0.06	27.49	28.43	40.00	30.45	34.40
Standard deviation [€/mq]	252.72	203.15	190.13	307.43	233.48	159.46
Total number [-]	159	176	107	14	91	48
16° percentile [€/mq]	107.32	80.50	64.29	57.62	86.62	148.78
84° percentile [€/mq]	733.33	464.36	451.02	773.08	531.45	426.82
Kurtosis [-]	-0.6	0.5	0.4	-1.5	0.6	1.5
Skewness [-]	0.6	0.8	0.9	0.6	1.0	0.7
CoV [%]	65.4	65.7	70.5	86.9	70.1	51.7
90% C.I. mean (-) [€/mq]	353.35	284.25	239.43	219.15	292.78	270.67
90% C.I. mean (+) [€/mq]	419.09	334.48	299.72	488.65	373.06	346.16

4.2.2.2.2. ESTIMATED

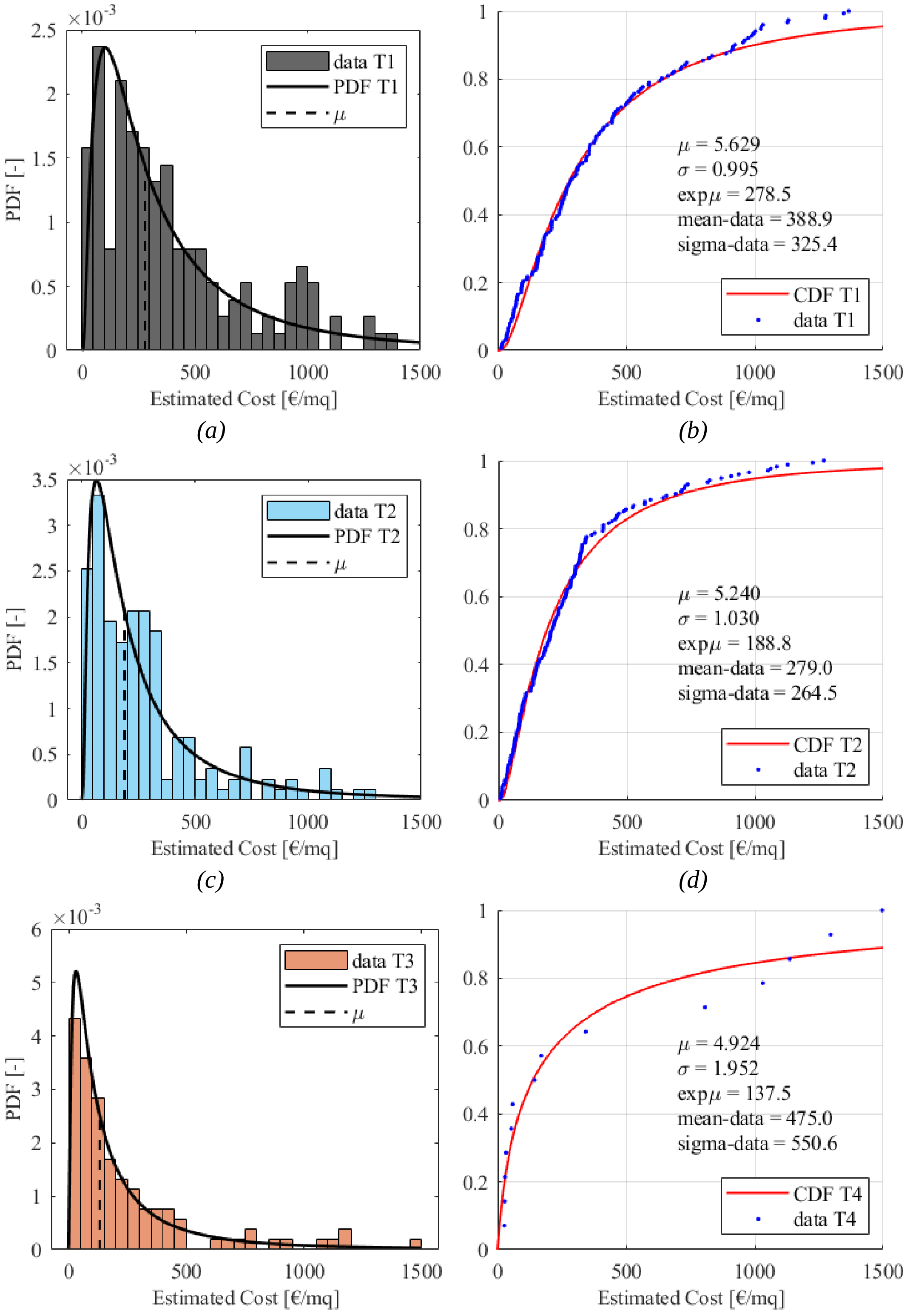

(a) *(b)*

(c) *(d)*

(e) *(f)*

Figure 82. Estimated costs of typologies T1, T2 and T3 and lognormal fitting curves: (a) (c) (e) probability distribution; (b) (d) (f) cumulative distribution.

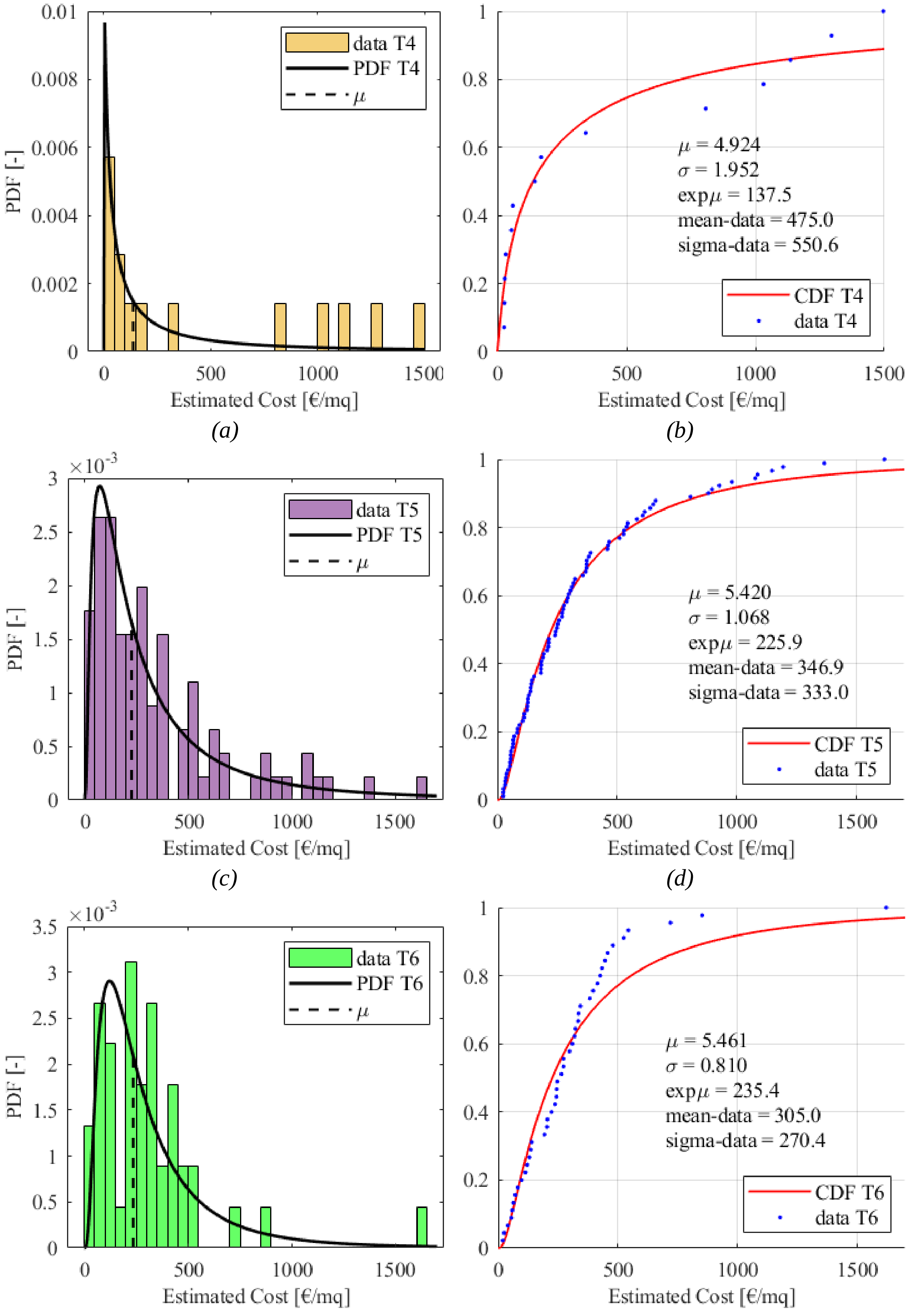

(a) *(b)*

(c) *(d)*

(e) *(f)*

Figure 83. Estimated costs of typologies T4, T5 and T6 and lognormal fitting curves: (a) (c) (e) probability distribution; (b) (d) (f) cumulative distribution.

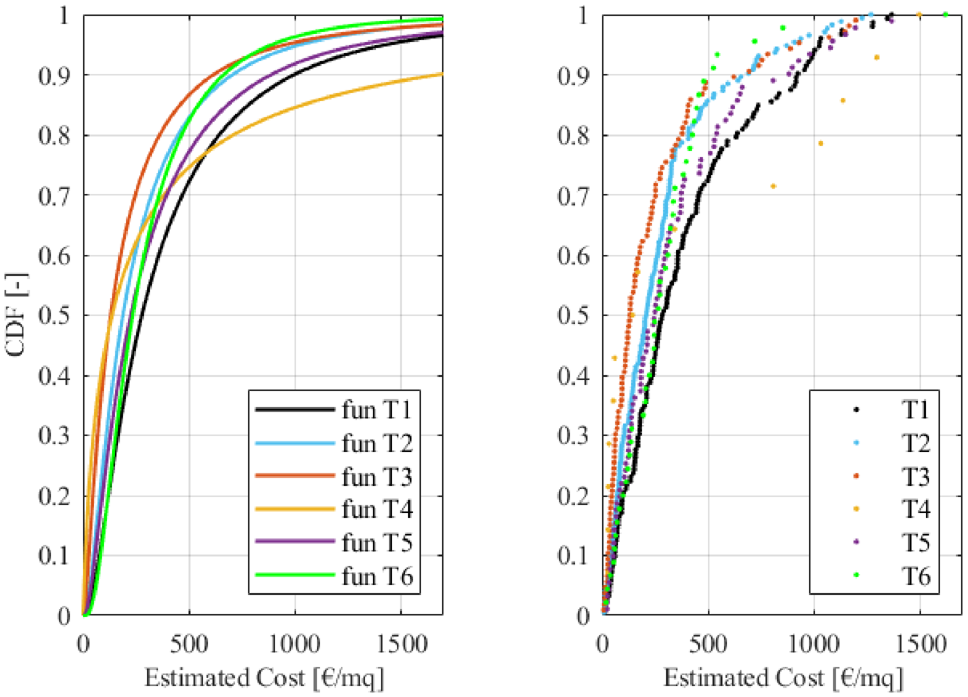

(a) (b)

Figure 84. Cumulative distribution of the estimated costs and lognormal fitting curves of different typologies: (a) lognormal fitting curves; (b) cumulative representation of the data.

Table 31. Statistical analysis of the estimated costs of different structural typologies.

	T1	**T2**	**T3**	**T4**	**T5**	**T6**
Mean [€/mq]	388.90	278.98	245.06	474.97	346.94	304.96
Median [€/mq]	287.04	208.89	132.49	156.94	249.34	264.28
Max [€/mq]	1365.65	1268.34	1494.78	1496.18	1617.17	1621.01
Min [€/mq]	13.12	8.66	8.06	25.86	24.06	19.35
Standard deviation [€/mq]	325.39	264.52	294.57	550.64	332.95	270.43
Total number [-]	152	174	106	14	91	45
16° percentile [€/mq]	78.47	62.14	37.95	28.00	65.98	78.27
84° percentile [€/mq]	730.91	468.11	405.34	1177.48	614.91	449.40
Kurtosis [-]	0.5	2.8	4.7	-1.1	2.6	12.2
Skewness [-]	1.1	1.7	2.1	0.7	1.6	2.8
CoV [%]	83.7	94.8	120.2	115.9	96.0	88.7
90% C.I. mean (-) [€/mq]	345.61	246.09	198.13	233.62	289.70	238.85
90% C.I. mean (+) [€/mq]	432.18	311.86	291.98	716.32	404.18	371.07

4.2.2.3. COMPARISON OF CONVENTIONAL AND ESTIMATED LOSSES

From the previous results, from the evaluation of the mean values of the losses both at different damage levels and of various structural typologies, it appears that the conventional costs (evaluated with the parametric tables given by the Region) are higher than the actual estimated losses. Actually, the conventional costs are characterized by a lower dispersion corresponding, in general, to a lower standard deviation of the fitting curves and the data, and a lower Kurtosis of the data, whereas the estimated costs are more scattered and outlier-prone. All this is due to the parametric nature of the conventional costs, calculated by means of pre-set unitary values, while the actual estimated costs are more dispersed.

This outcome is confirmed in Figure 85, where the schematic distributions of the data are reported at the five damage levels. In particular, the 16° and 84° percentiles mark the limits of the lines, and the mean and median of the data are indicated with different markers (see Tables 26 and 27 for the values). From the Figure, it is possible to observe that the dark lines cover a wider range of values compared to blue lines, and often attain higher upper limits. This last aspect is relevant for losses at D1 and D2 with local interventions, and in particular at D5. At damage level D3 and D4, the estimated losses cover a range that is almost twice that of the conventional losses, resulting in lower mean values. It is interesting to note that a very similar trend of the mean values of the losses at the five damage levels has been reported in Rossi et al. (2019b) considering a larger dataset of buildings, but without a distinction among different typologies.

In order to explore further this aspect, the linear interpolations of the conventional losses against the estimated ones are derived at each damage level. These allow proposing a tool to evaluate directly the conventional costs from the estimated costs, and visually appreciate the relationship between the two. The differentiation in structural typologies has not been considered in this analysis.

In this case, a linear interpolation has been conducted considering both group of costs without outliers. The lognormal distributions of the data have been reported in a grey dashed line on each axis, and the mean values of the curves are marked with a dashed-dot grey line. It is worth noting that the values of the ordinates of the lognormal curves in grey cannot be appreciated in the Figures. The diagonal of the graphs (line y=x) is indicated with a grey dotted line for a direct comparison with the inclination of the interpolating line. All the interpolating functions reported in Figure 86 (in the form y=ax+b) are characterized by an increasing trend of the lines, all with a slope coefficient lower than one. This means that, after the intersection point between the interpolating line and the diagonal line, at each value of estimated loss corresponds a lower value of conventional cost. Whereas, before the intersection point, at each estimated loss correspond a higher conventional cost. Therefore, the conventional costs in €/mq are only apparently higher than the actual estimated costs, and this can be considered valid before a certain value of estimated loss (intersection point) depending on the damage degree.

In general, these tools allow appreciating the discrepancy between conventional costs established *ex-ante*, and the estimated costs determined *ex-post*: the lower is the slope of the coloured line at each damage level, the higher is the difference between the two losses.

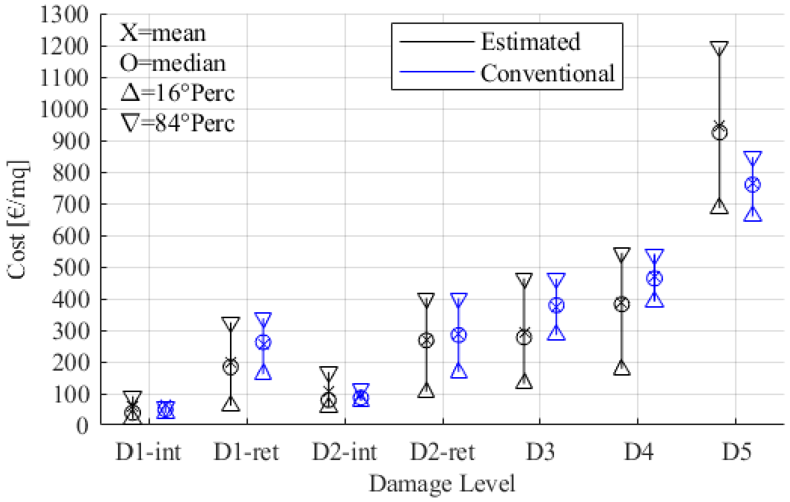

Figure 85. Distributions of the estimated costs (in black) and the conventional costs (in blue) at different damage levels, with indication of mean, median, 16° percentile and 84° percentile of the data.

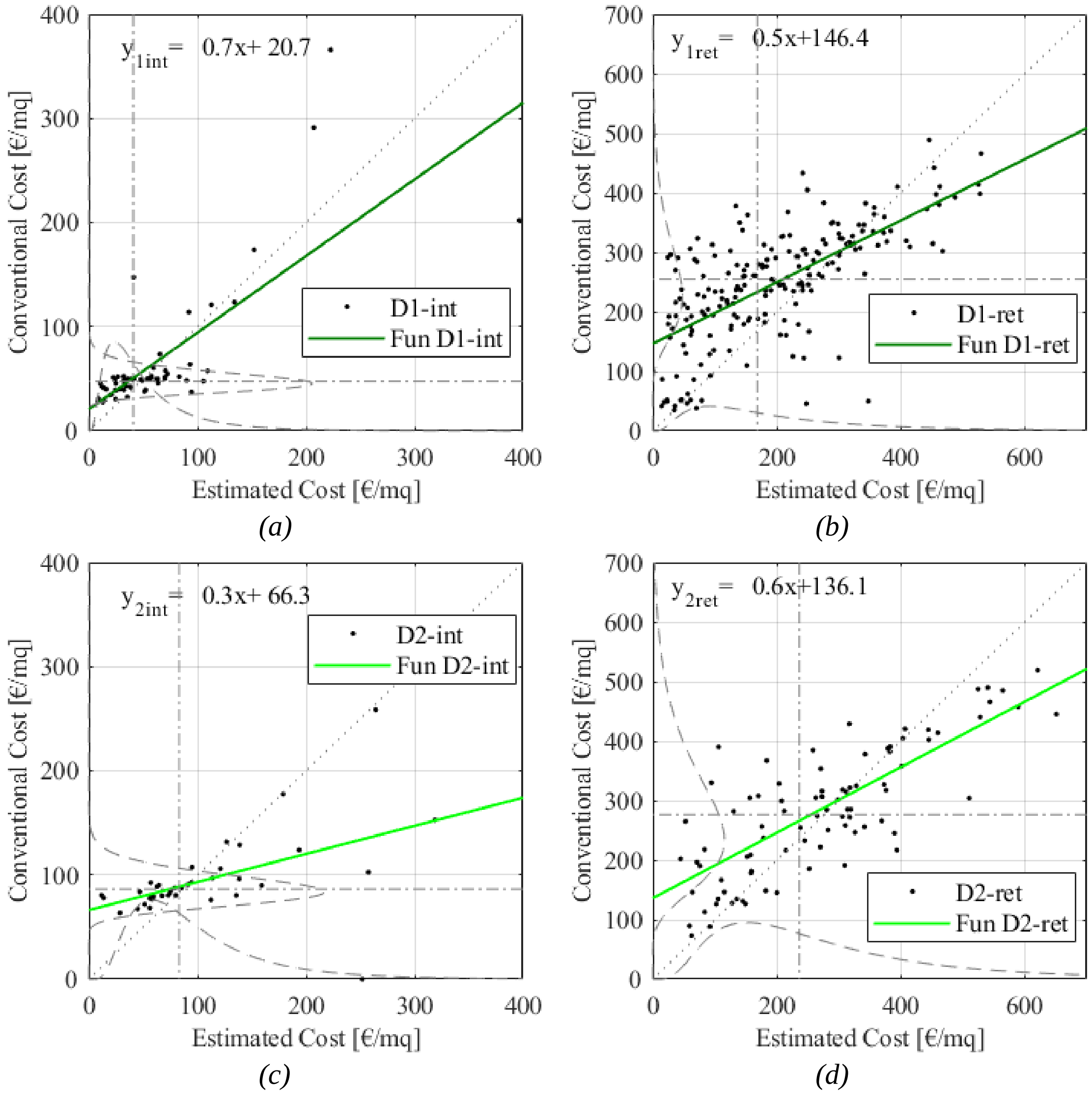

(a) (b)

(c) (d)

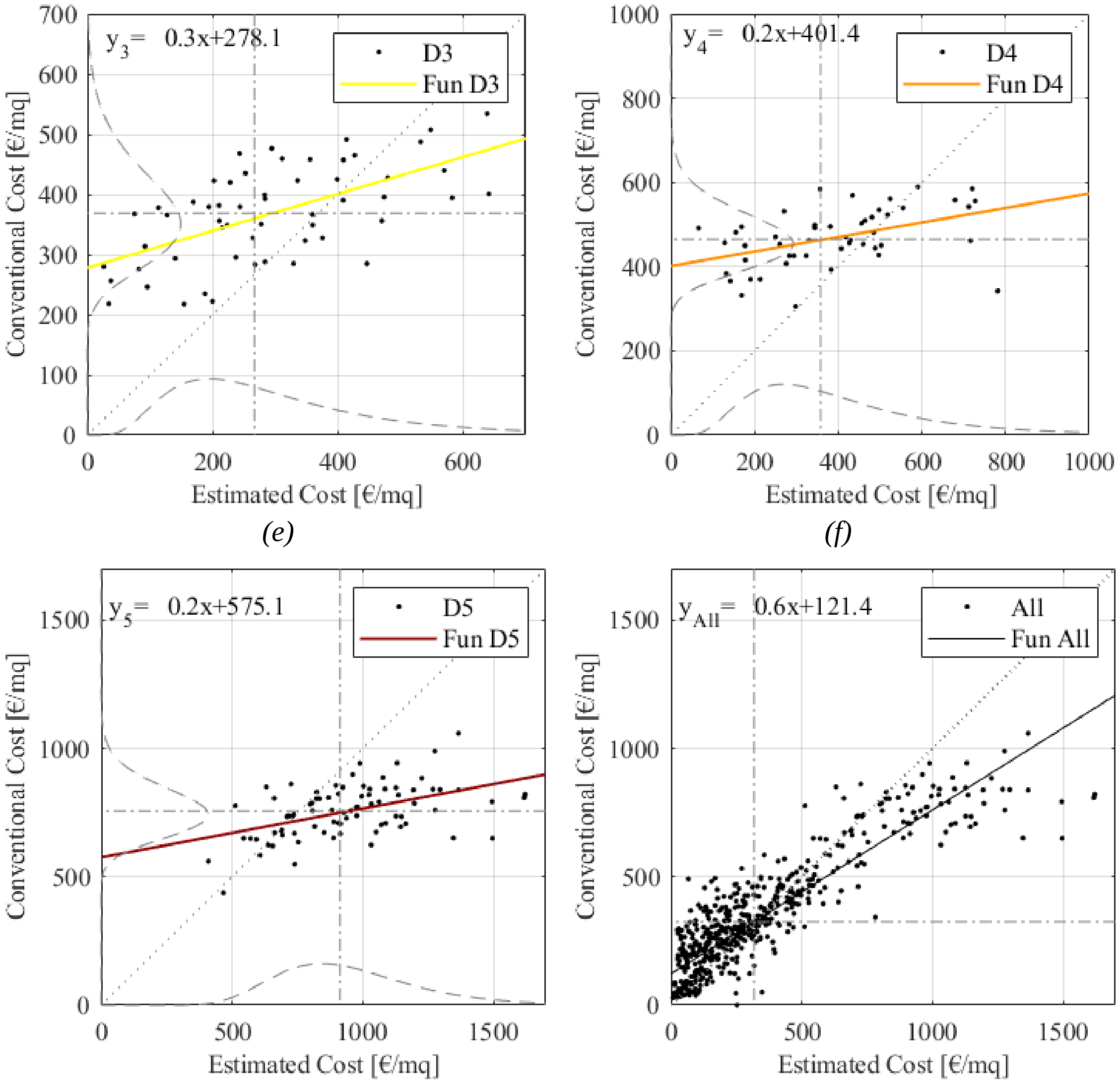

(e) *(f)*

(g) *(h)*

Figure 86. Linear interpolations of the conventional costs against the estimated costs and lognormal fitting curves of the data at: (a) D1 with local interventions; (b) D1 with retrofit; (c) D2 with local interventions; (d) D2 with retrofit; (e) D3; (f) D4; (g) D5; (h) all damage levels together.

4.2.2.4. LOSSES VERSUS SURFACE IN PLAN OF THE BUILDINGS

Both conventional and estimated losses of the precast RC buildings in the database can be analysed based on the variation of some significant structural parameters or seismic-related intensities. Considering the first aspect, the surface in plan of the building in the pre-earthquake condition is a structural data available for all the 600 precast structures. Thus, once considering the five damage levels and once the six structural typologies, the relationship between losses and surface in plan is analysed. In the following analyses, the distinction between local intervention and seismic retrofit at D1 (and D2) is not considered, as well as that between D5 and D5-POST.

In particular, in Figures 87, 88, 89 and 90, a linear interpolation of the total costs against the surface in plan is derived, in the form y=ax+b. It is worth observing that a black dashed line in each graph interpolate all the losses by the surface, and the same function (y_{tot}) is reported in the sub-Figures a and b of each Figure.

All these functions may be adopted to perform an estimate of the expected seismic losses of a precast RC building, whose damage can be described with the damage metric considered in this study. Moreover, average loss estimates may be conducted to assess the seismic losses of a building belonging to a specific structural typology.

Figures 87 and 89 illustrate the relationship between costs in €/mq and surface, while Figures 88 and 90 account for costs in €. The interpolating lines of the costs in €/mq at different damage levels, in general, feature a slightly decreasing slope with the increase of the surface, a part from that at D4, in both conventional and estimated cost. In general, the total relative costs over meter square of a structural intervention in small buildings (i.e., with smaller surfaces in plan) are higher compared to those of large buildings. Indeed, there are some fixed costs of interventions that are amortized if the total amount of work increases, in particular at high damage levels.

On the contrary, the absolute costs in € at different damage levels are expected to increase with the increase of the surface of the buildings. This is evident in Figures 88 and 90, both at the five damage levels and considering the six structural typologies, even if T4 has a completely deviating behaviour due to the lack of data and the presence of outliers (removed in the relative costs, not in the absolute ones). The interpolating lines of both the costs in €/mq and in € of the structural typologies show that the costs of T1 tend to be higher than those of the other typologies, as previously mentioned. The behaviour of the functions is in line with what expect for conventional losses in €/mq, while the expected losses slightly deviate since the data are more scattered, as mentioned.

Concerning the functions of the conventional losses in € at a certain value of the surface, the costs of T1 and T2 are almost twice those of T3. Whereas, the trend of the estimated losses in € of T1 and T2 are nearly three times those of T3. This is because the lines interpolating the total conventional and estimated costs in € of typology T3 are very different. Indeed, all the functions of the conventional costs are prone to the total curve (marked with a black dashed line), while those of the estimated costs diverge from the corresponding total curve.

The trend of the plots defining the costs in € as a function of the surface in plan of the buildings are, on average, in line with the aggregated ones reported in Rossi et al. (2019b) and Agenzia Regionale per la Ricostruzione (2018).

4.2.2.4.1. CONVENTIONAL

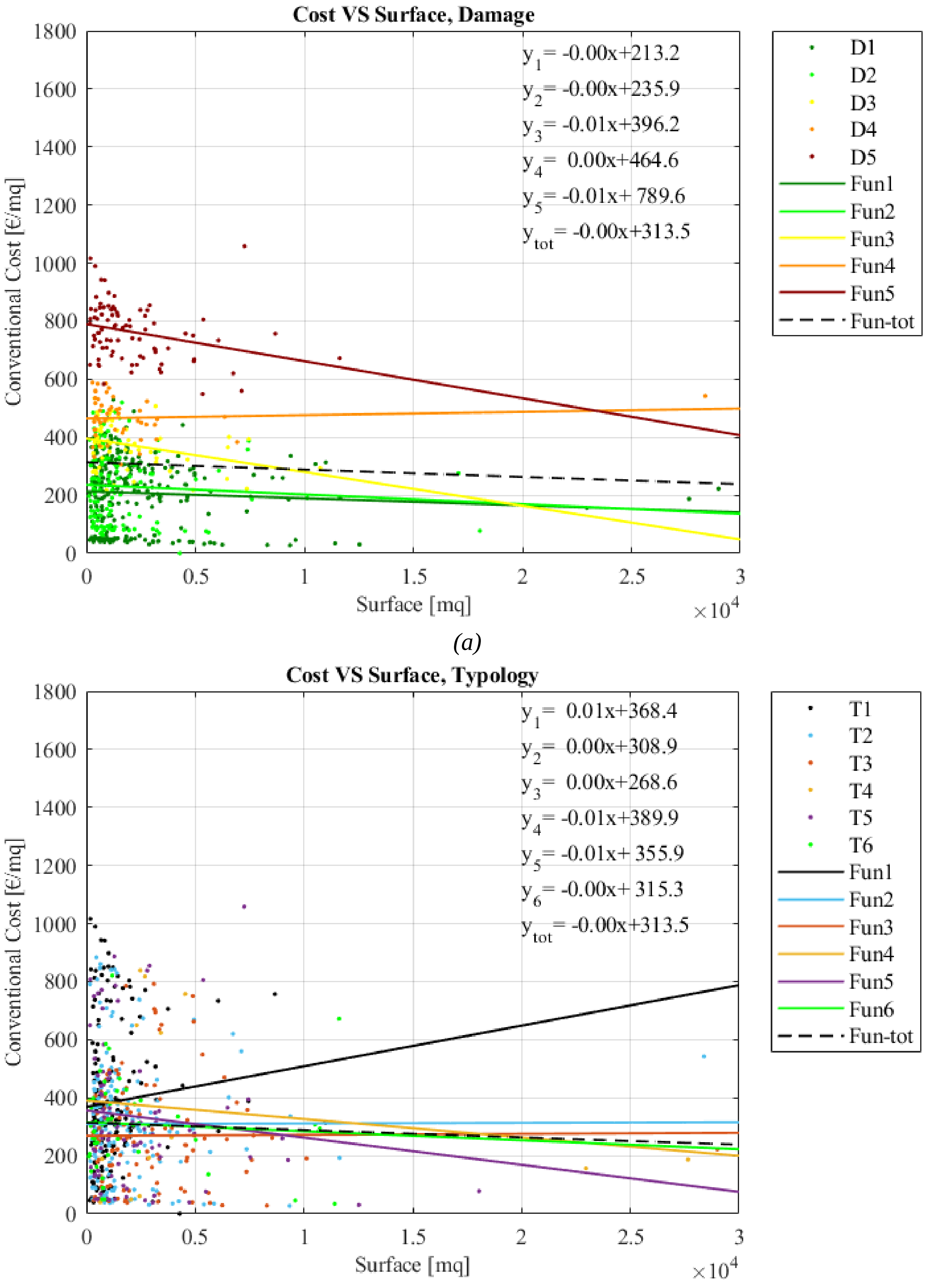

(a)

(b)

Figure 87. Conventional costs in €/mq versus surface in plan and linear interpolations for: (a) five damage levels; (b) six structural typologies.

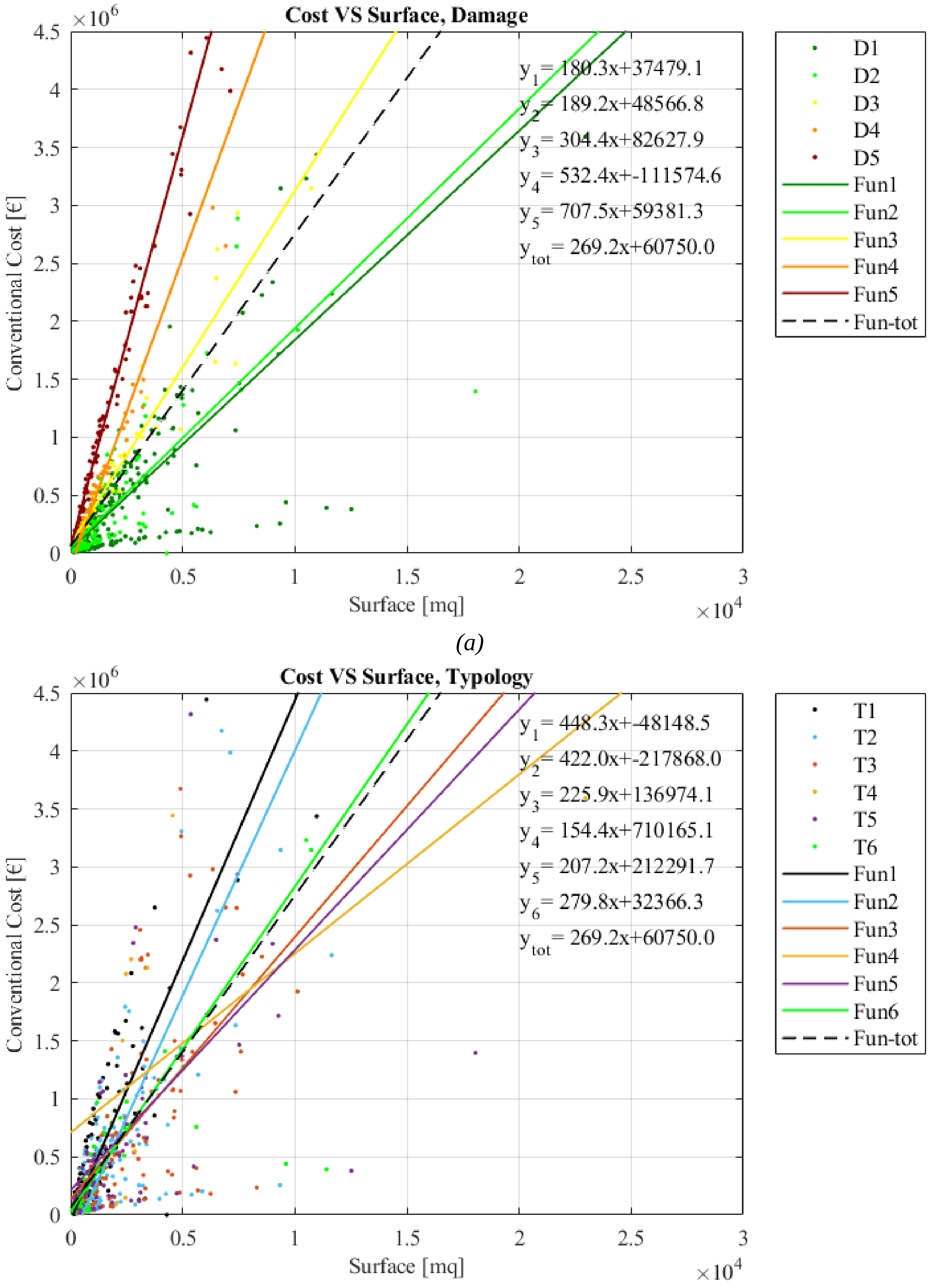

(a)

(b)

Figure 88. Conventional costs in € versus surface in plan and linear interpolations for: (a) five damage levels; (b) six structural typologies.

4.2.2.4.2. ESTIMATED

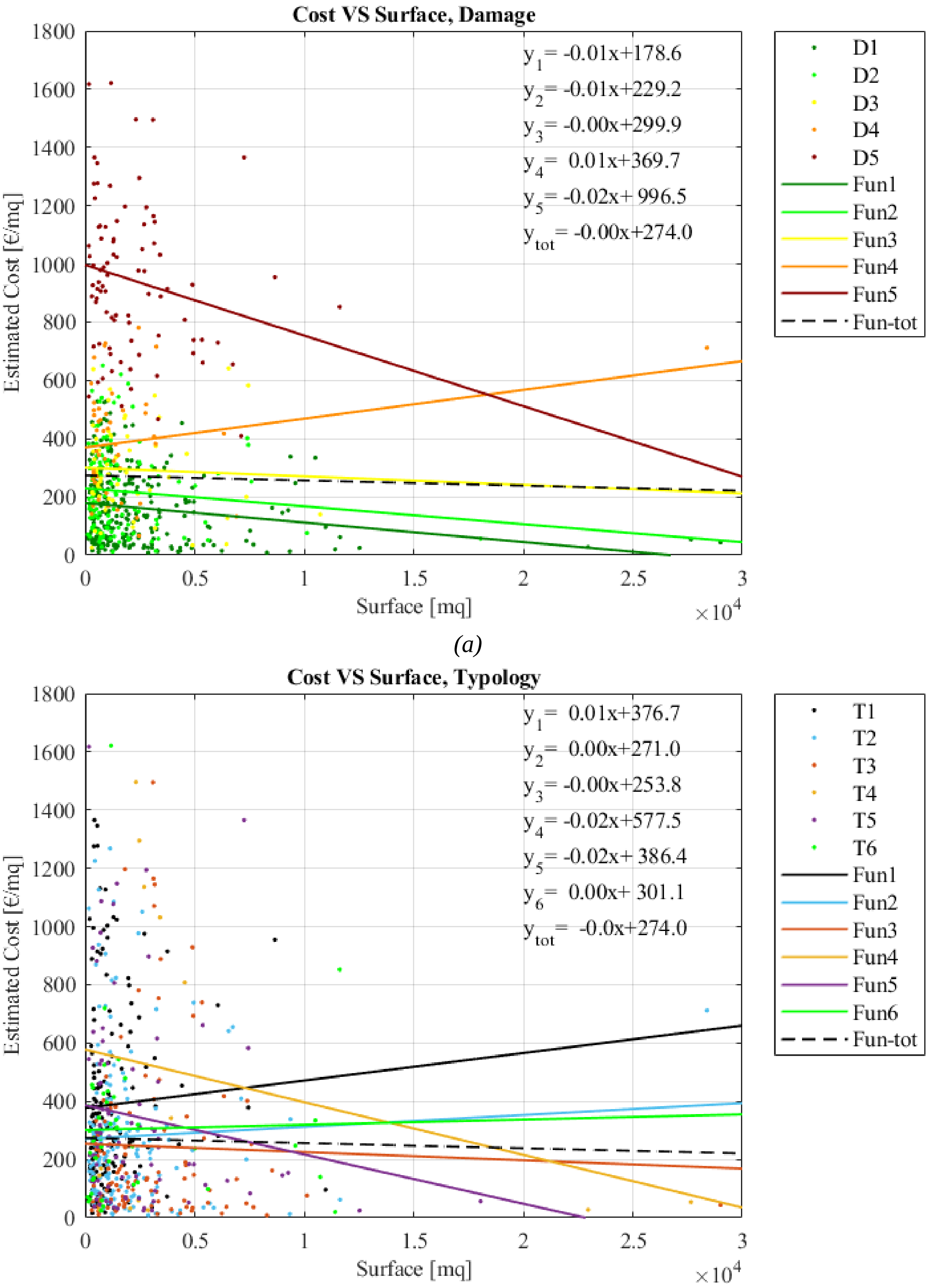

(a)

(b)

Figure 89. Estimated costs in €/mq versus surface in plan and linear interpolations for: (a) five damage levels; (b) six structural typologies.

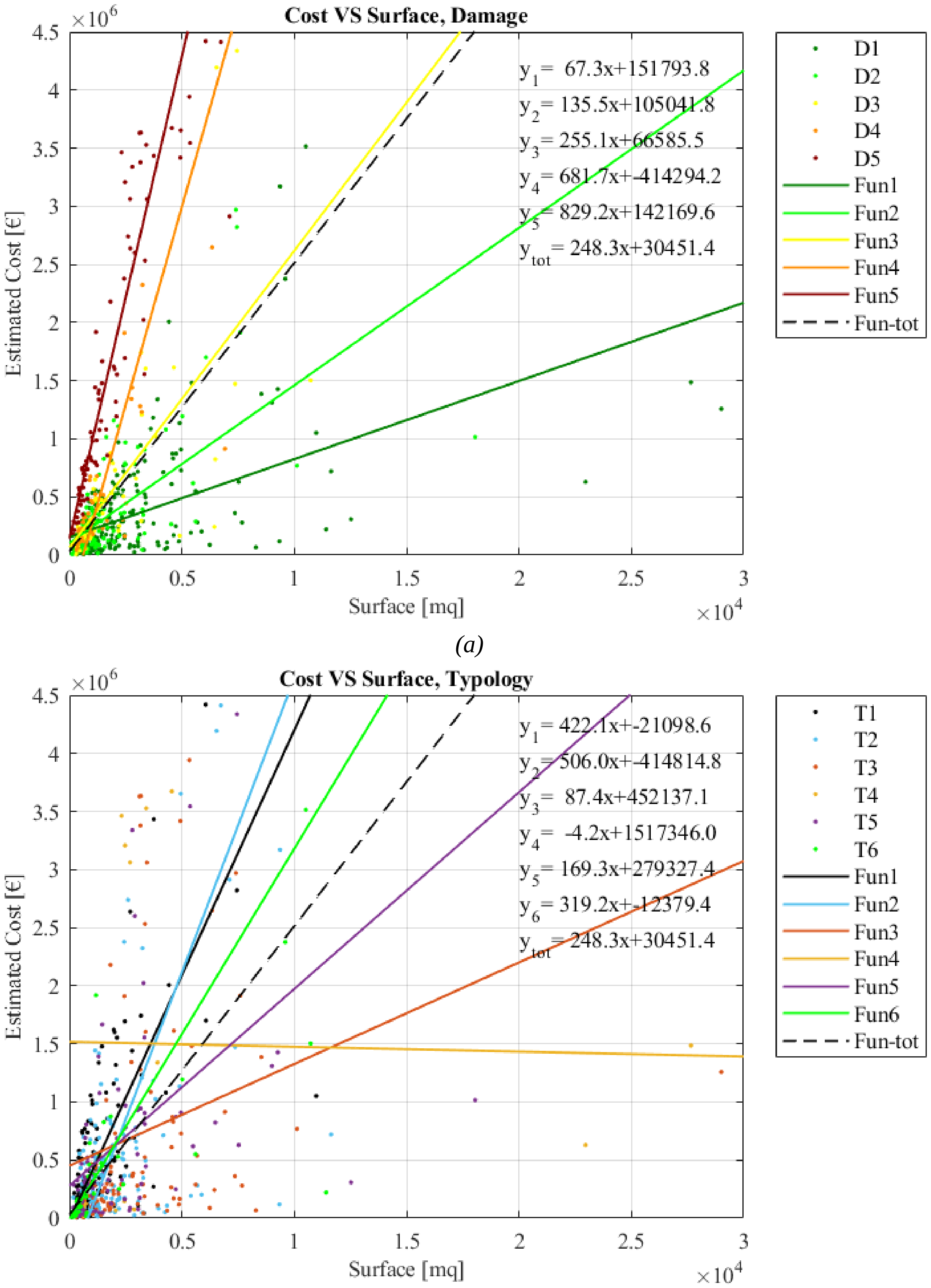

(a)

(b)

Figure 90. Estimated costs in € versus surface in plan and linear interpolations for: (a) five damage levels; (b) six structural typologies.

4.2.2.5. LOSSES VERSUS PGA

Considering the seismic intensity, it is interesting to explore the variability of the losses depending on the values of PGA estimated through the shake-maps (Buratti et al. 2022). This is commonly not provided in loss assessment analyses available in the literature.

The linear interpolations of the losses against the PGA may be adopted to predict the expected seismic losses of a precast RC building, whose damage can be described with the damage metric considered in this study, knowing the peak-ground-acceleration expected to occur. Moreover, average estimates may be conducted to assess the average seismic losses of buildings belonging to a specific structural typology.

Similar to what obtained in Section 4.2.2.4, the relationships are defined through a linear interpolation of the data, both at different damage levels and for different structural typologies. Analogously, the distinction between local intervention and seismic retrofit at D1 (and D2) is not considered here, as well as that between D5 and D5-POST.

Figures 91 and 92 show the lines estimating the total costs in €/mq versus the PGA, in the form $y=ax+b$. The graphs illustrate the relationship between the costs in €/mq and PGA, for conventional and estimated losses, respectively. It is worth observing that a black dashed line in each graph interpolate all the losses versus the PGA, and the same function (y_{tot}) is reported in the sub-Figures a and b of Figure 91 and 92.

The majority of the PGA data are located over 0.3 g, confirming the distributions observed in Figure 57. Moreover, the red data corresponding to D5 are more concentrated to the top right part of graphs 91a and 92a, ranging in the higher PGA and losses as expected, especially those of the estimated costs. Conversely, the dark green dots (D1) are more concentrated in the lower left part.

The interpolating lines of the costs at different damage levels are almost constant as expected for the conventional costs since the PGA are divided per damage state: the average loss in €/mq is expected to be almost constant. Whereas, those of the estimated costs are characterized by a more marked slope in particular at the higher damage states due to the dispersion of the values. Among those, the interpolating line at D5 may be not reliable considering its significantly decreasing slope, due to the presence of lower losses at the highest values of PGA within damage level D5.

The higher dispersion of the estimated losses can be observed also by comparing Figures 91b and 92b: the lines interpolating the conventional losses of the different structural typologies are more densely concentrated around the total loss function (marked with a black dashed line), while those of the estimated costs diverge from the corresponding total loss line. However, the lines of conventional and estimated costs in €/mq of different structural typologies both have a slightly increasing slope, and the costs of T1 tend to be higher than T2 and T3 also in these representations.

4.2.2.5.1. CONVENTIONAL

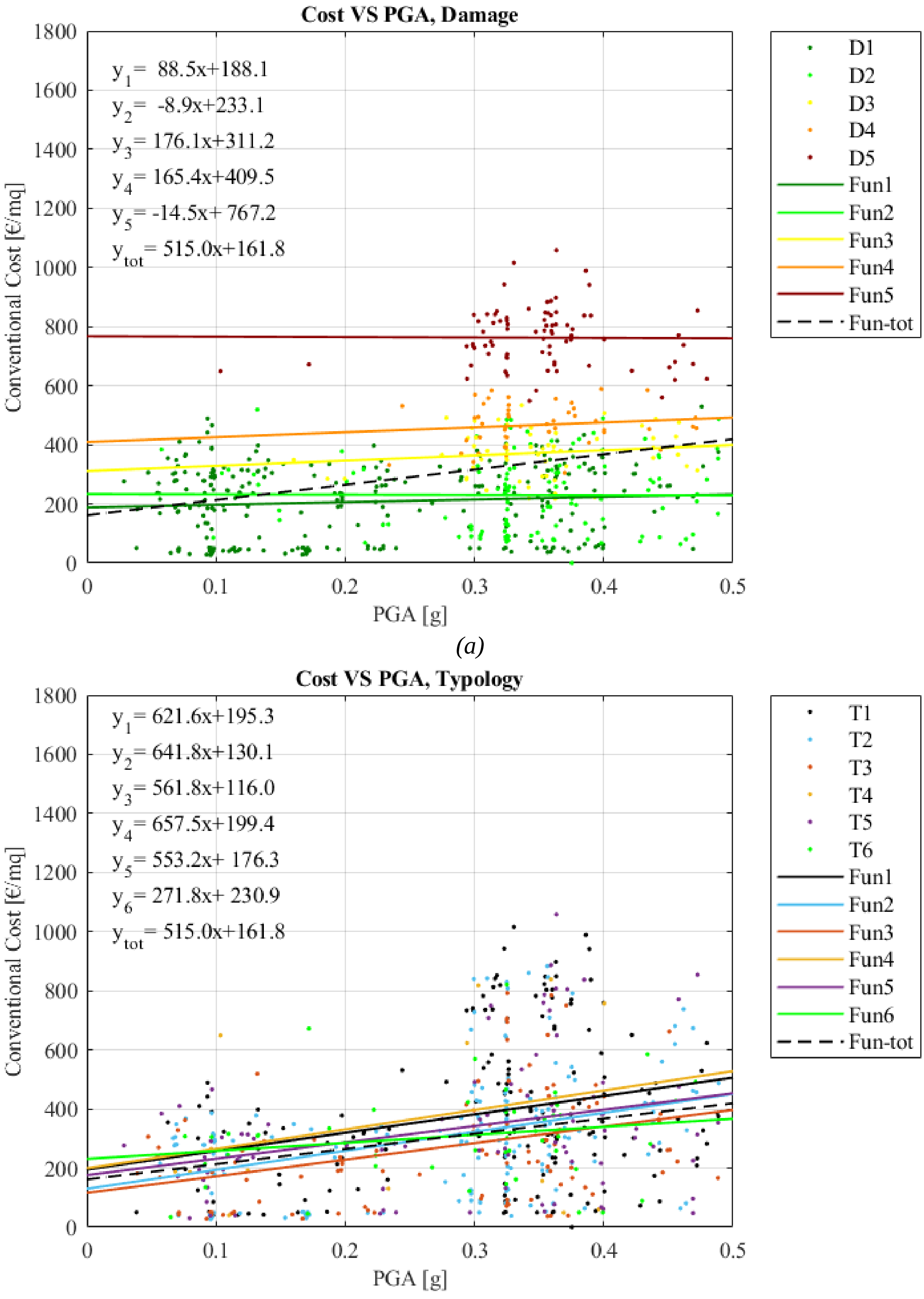

Figure 91. Conventional costs in €/mq versus PGA and linear interpolations for: (a) five damage levels; (b) six structural typologies.

4.2.2.5.2. ESTIMATED

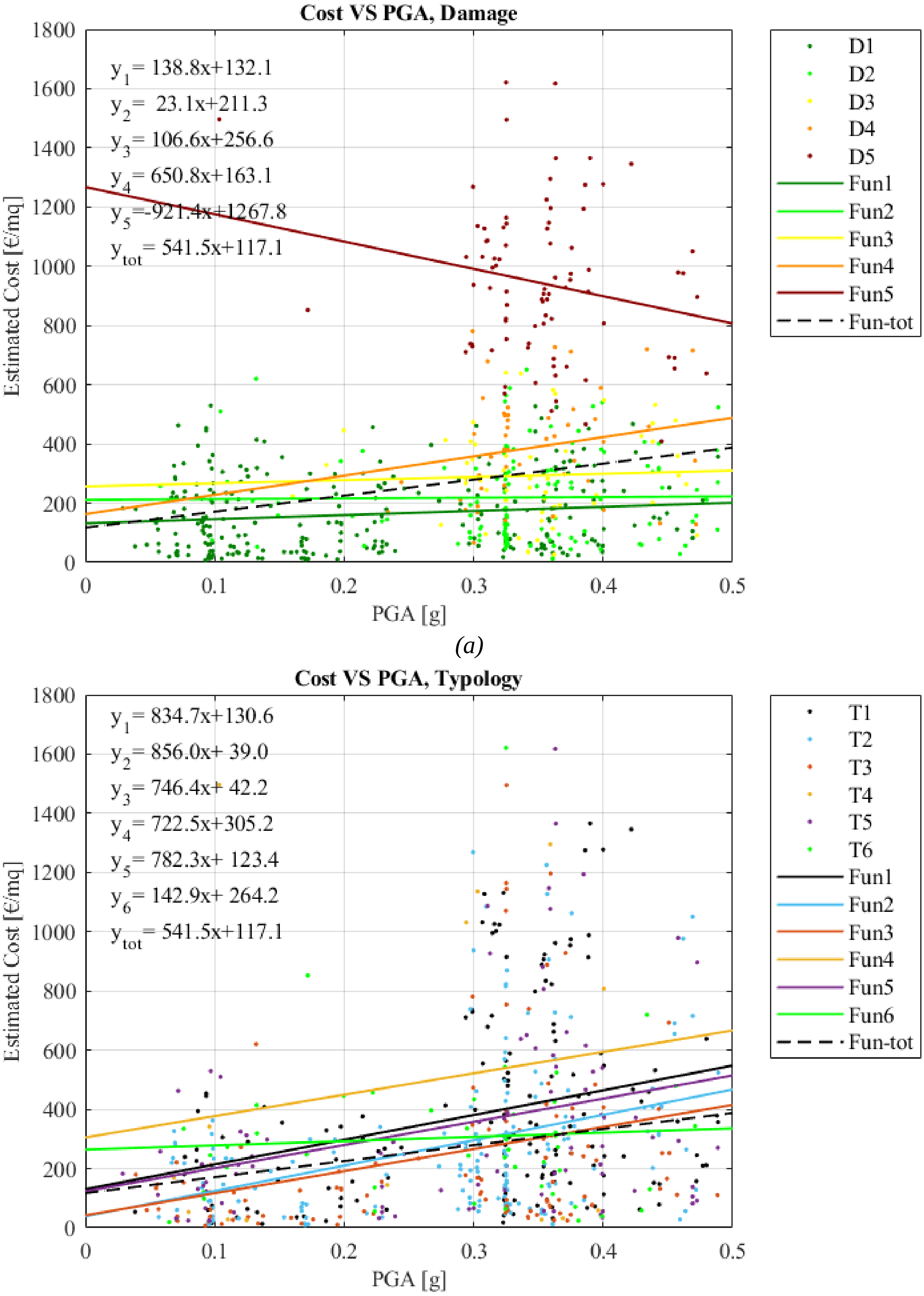

(a)

(b)

Figure 92. Estimated costs in €/mq versus PGA and linear interpolations for: (a) five damage levels; (b) six structural typologies.

4.2.3. ESTIMATED LOSSES OF TYPOLOGIES T1, T2 AND T3

The most significant structural typologies of precast RC buildings in the database are T1, T2 and T3 since these are the most common ones observed in the surveys in the territory, and present in SFINGE (according to Ongaretto et al. 2019).

At this stage of the analysis, only the actual estimated losses are considered. A more in-depth analysis disaggregating the losses into different damage levels is outlined in this Section, considering the structural and the non-structural components.

The outliers have been removed in the total estimated losses at the five damage states, as mentioned in Section 4.2.2. Clearly, the number of data is consistently lower than those analysed in Section 4.2.2.1, because the disaggregation is performed for both damage degree and structural typology.

The statistical analysis of the data is reported in different Tables at the beginning of each Paragraph. It is worth mentioning that only the losses at D5-POST are presented here, neglecting the D5 computed considering the surfaces in the pre-earthquake condition.

In addition, in Section 4.2.3.4 the analysis of the different occupancies of the internal spaces is performed to offer an insight on the partition in plan of the three typologies. Indeed, in the documents presented for the request of regional contributions, the technicians had to indicate the total amount of surface in plan used for the various destinations (both pre- and post- the earthquake). Part of the area of the industrial buildings was used mainly for production, part for the storage of products, but usually there were also smaller parts dedicated to offices or residential units.

The study of the distributions of the losses of the most common precast structures allows defining significant additional tools for loss-assessment evaluations. The functions derived may be adopted to calculate the seismic losses of precast RC buildings belonging to the three typologies, evaluating the influence of the damage occurred to structural and non-structural components. Only the cumulative distributions are reported in the following Sections, for the sake of brevity.

Figures 93a and 93b illustrate the distributions of the actual costs in €/mq and in € at different damage levels, with the indications of the mean and the median of the samples. From the first Figure, it is possible to infer that typology T1 is characterized by higher repair costs than T3, but a lower reconstruction costs (those at damage level D5). Typology T2 is in an intermediate position at the first three damage levels, while it is characterized by the lower losses at D4 and D5. This evidence confirms the same outcomes suggested by previous evaluations.

Since the outliers were removed considering the costs in €/mq, the costs in € appear to be more scattered. Thus, from the second Figure, the behaviour is less clear because the losses are reported in absolute values in €, but it is interesting to observe the total amount of losses spent for each typology. For instance, the reconstruction costs of some buildings of typology T3 have almost reached the amount of 5 billion of Euros. On average, the mean value of the reconstruction costs (D5) of typology T3 is significantly higher compared to those of typologies T1 and T2, confirming the previous outcomes. Indeed, the mean value of T3 is almost three times higher.

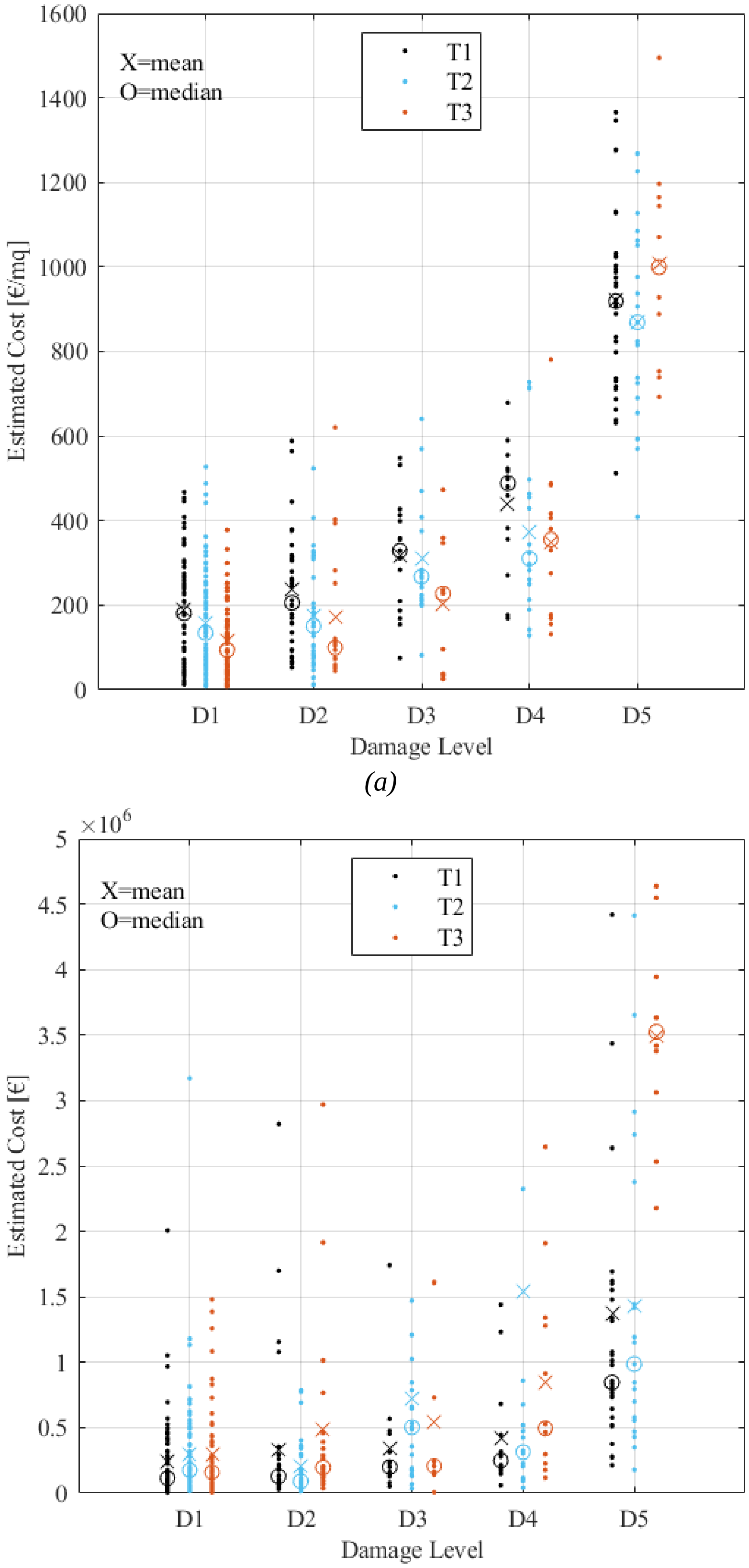

(a)

(b)

Figure 93. Distributions of the estimated costs of typologies T1, T2 and T3 at five damage levels, with indication of the mean and median of the data: (a) costs in €/mq; (b) costs in €.

4.2.3.1. ESTIMATED LOSSES AT DIFFERENT DAMAGE LEVELS

In the following Figures the cumulative distributions of the data are plotted together with the lognormal fitting functions. The total estimated costs in €/mq are analysed individually at each damage state, thus a final image with the cumulative distributions of the data and the fitting functions is proposed for each typology in Figures 96, 99, 102 for comparison. The main descriptors of each function are shown in the cumulative distributions with letters μ and σ, together with the analogous values of mean and the standard deviation of the samples.

The total estimated losses of category T1 at all the damage states are characterized by higher mean and median values compared to those of T2 and T3. It is useful to recall that T1 buildings are the oldest ones and have smaller dimensions compared to the newer T3. In addition, T2 buildings are newer compared to T1, but they are characterized by similar volumes and surfaces, even if they feature different precast elements. The higher estimated costs per square meters of T1 and T2 buildings may be due to the presence of more columns and roof elements per square meters of surface, since they feature smaller span dimensions compared with T3 structures. This is not valid anymore at damage level D5 at which the losses of T3 are higher: this is due to the presence of significantly higher structural costs for the reconstruction of these newer buildings, as shown in the analyses of Section 4.2.3.2.

In general, the cumulative fitting curves have increasing mean values following the order of the damage states. However, in Figure 102 regarding typology T3, there is an overlap between the loss functions at damage state D2 with retrofit, and D3. This is due to the lack of loss data for typology T3 (see the total numbers in Table 34) compared with those available for T1 and T2.

4.2.3.1.1. TYPOLOGY T1

Table 32. Statistical analysis of the estimated losses of typology T1 at different damage levels.

	D1-ret	**D1-int**	**D2-ret**	**D2-int**	**D3**	**D4**	**D5-post**
Mean [€/mq]	224.11	74.64	267.42	142.63	316.92	439.99	866.93
Median [€/mq]	239.57	58.72	253.89	115.25	329.10	488.89	907.38
Max [€/mq]	467.51	207.30	588.83	257.55	547.88	679.01	1426.22
Min [€/mq]	17.84	13.12	52.60	67.29	75.26	169.09	369.94
Standard deviation [€/mq]	132.22	56.83	146.61	78.35	138.18	151.08	241.24
Total number [-]	45	14	24	8	15	14	32
16° percentile [€/mq]	61.04	27.73	129.11	73.92	167.38	246.21	633.65
84° percentile [€/mq]	365.00	138.70	422.06	253.07	437.34	563.81	1062.37
Kurtosis [-]	-1.0	0.8	-0.2	-1.3	-0.7	-0.3	0.1
Skewness [-]	0.1	1.0	0.6	0.6	0.0	-0.5	0.0
CoV [%]	59.0	76.1	54.8	54.9	43.6	34.3	27.8
90% C.I. mean (-) [€/mq]	191.79	49.73	218.34	97.20	258.41	373.77	796.99
90% C.I. mean (+) [€/mq]	256.44	99.55	316.50	188.06	375.44	506.21	936.87

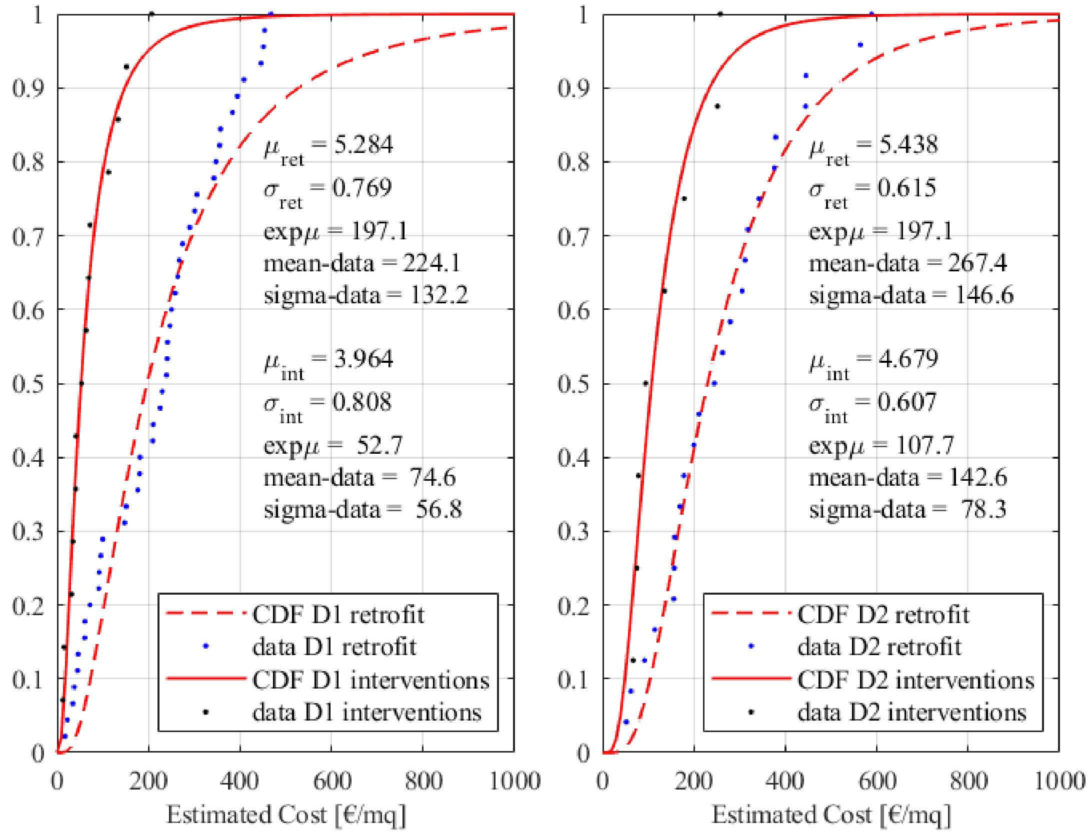

(a) *(b)*

Figure 94. Cumulative distribution of the estimated costs of T1 and lognormal fitting curves: (a) at D1 with local interventions and with retrofit; (b) at D2 with local interventions and with retrofit. Indication of the main descriptors of the function, and the mean and the standard deviation of the data.

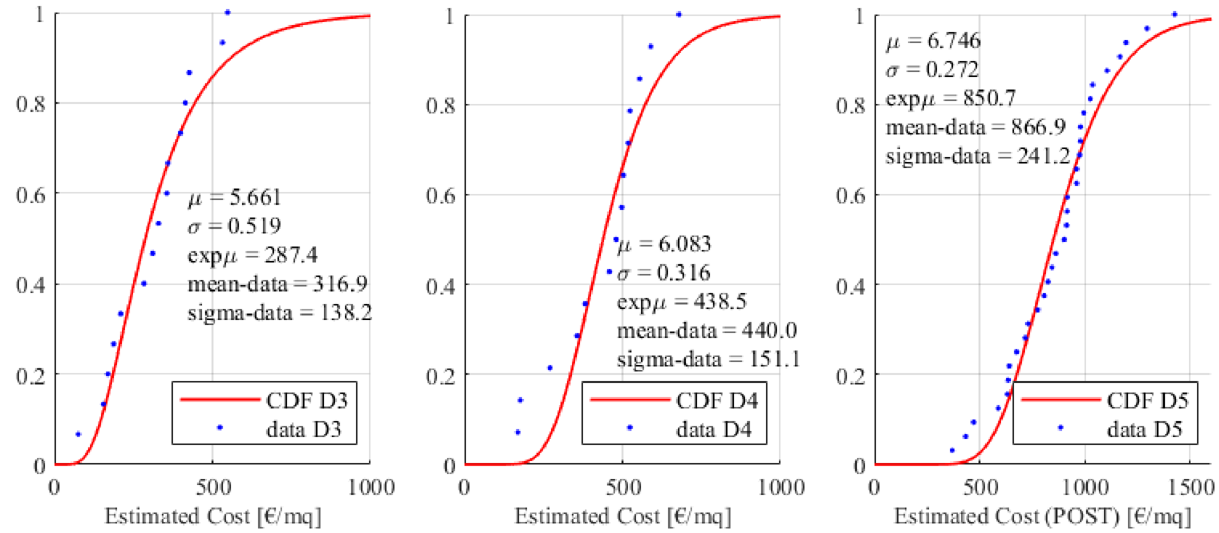

(a) *(b)* *(c)*

Figure 95. Cumulative distribution of the estimated costs of T1 and lognormal fitting curves at: (a) D3; (b) D4; (c) D5-POST. Indication of the main descriptors of the function, and the mean and the standard deviation of the data.

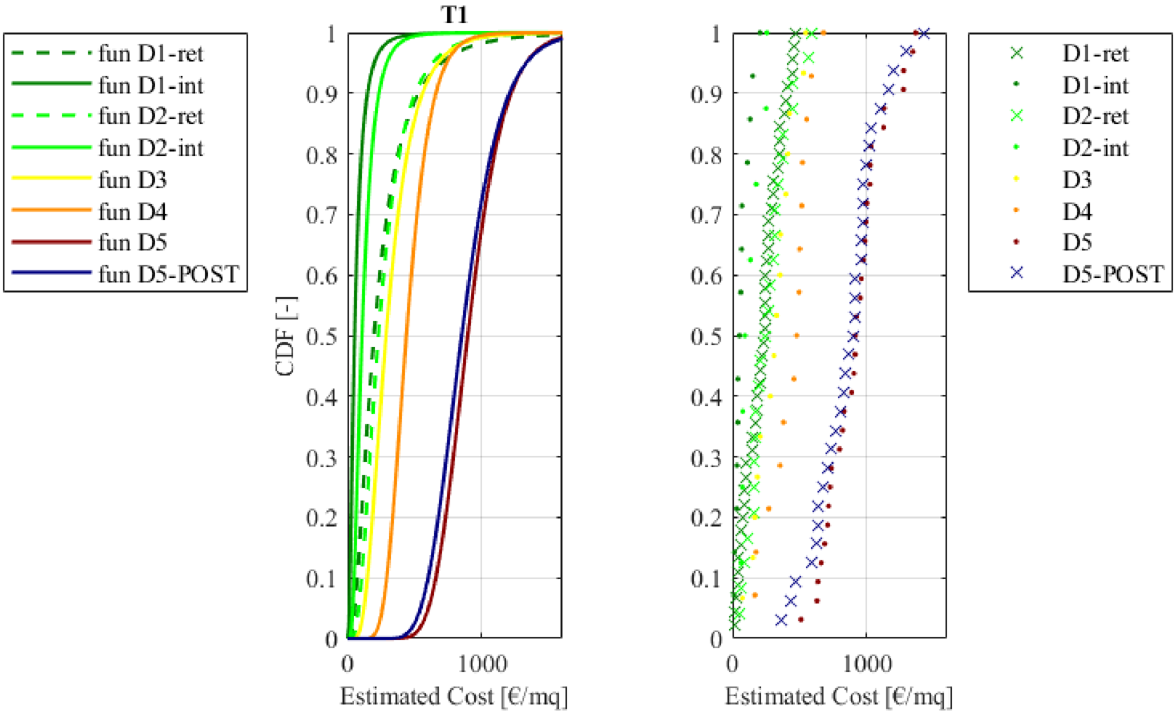

(a) *(b)*

Figure 96. Cumulative distribution of the estimated costs of T1 and lognormal fitting curves at different damage levels: (a) lognormal fitting curves; (b) cumulative representation of the data.

4.2.3.1.2. TYPOLOGY T2

Table 33. Statistical analysis of the estimated losses of typology T2 at different damage levels.

	D1-ret	**D1-int**	**D2-ret**	**D2-int**	**D3**	**D4**	**D5-post**
Mean [€/mq]	199.12	46.43	224.97	91.98	309.37	373.59	870.73
Median [€/mq]	191.23	38.94	183.39	69.51	267.76	310.47	831.91
Max [€/mq]	527.53	93.19	524.16	318.92	641.06	727.27	1355.55
Min [€/mq]	13.99	8.66	83.10	11.67	82.02	128.41	409.06
Standard deviation [€/mq]	121.68	27.62	116.79	82.42	137.99	190.24	243.35
Total number [-]	59	21	24	14	19	18	19
16° percentile [€/mq]	70.53	14.36	105.79	24.71	206.57	198.70	629.09
84° percentile [€/mq]	317.50	84.07	327.16	168.03	437.00	630.22	1099.10
Kurtosis [-]	0.0	-1.0	0.0	3.8	0.9	-0.3	-0.3
Skewness [-]	0.6	0.4	0.7	1.7	0.9	0.7	0.1
CoV [%]	61.1	59.5	51.9	89.6	44.6	50.9	27.9
90% C.I. mean (-) [€/mq]	173.14	36.55	185.87	55.85	257.45	300.05	779.17
90% C.I. mean (+) [€/mq]	225.10	56.32	264.07	128.10	361.29	447.12	962.29

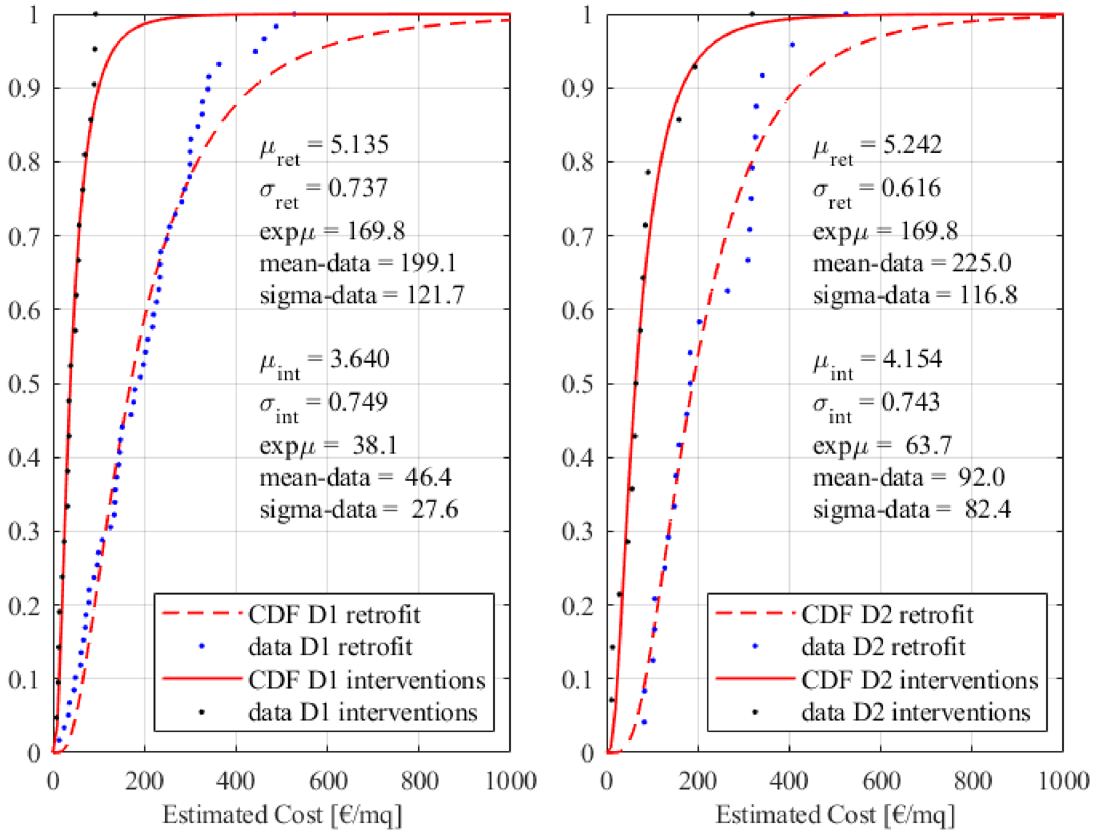

(a) *(b)*

Figure 97. Cumulative distribution of the estimated costs of T2 and lognormal fitting curves: (a) at D1 with local interventions and with retrofit; (b) at D2 with local interventions and with retrofit. Indication of the main descriptors of the function, and the mean and the standard deviation of the data.

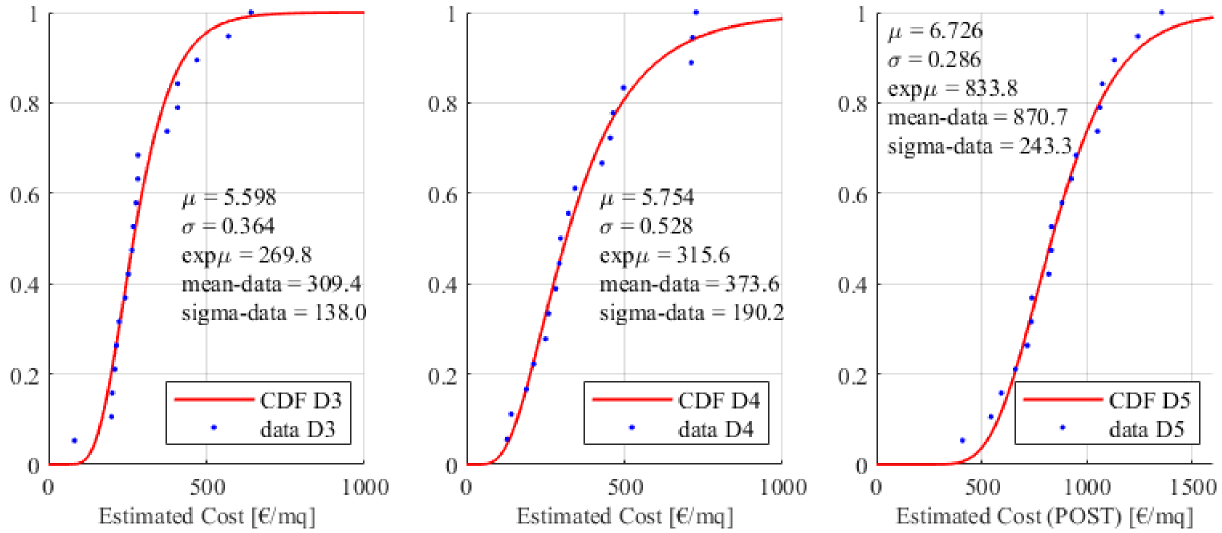

(a) *(b)* *(c)*

Figure 98. Cumulative distribution of the estimated costs of T2 and lognormal fitting curves at: (a) D3; (b) D4; (c) D5-POST. Indication of the main descriptors of the function, and the mean and the standard deviation of the data.

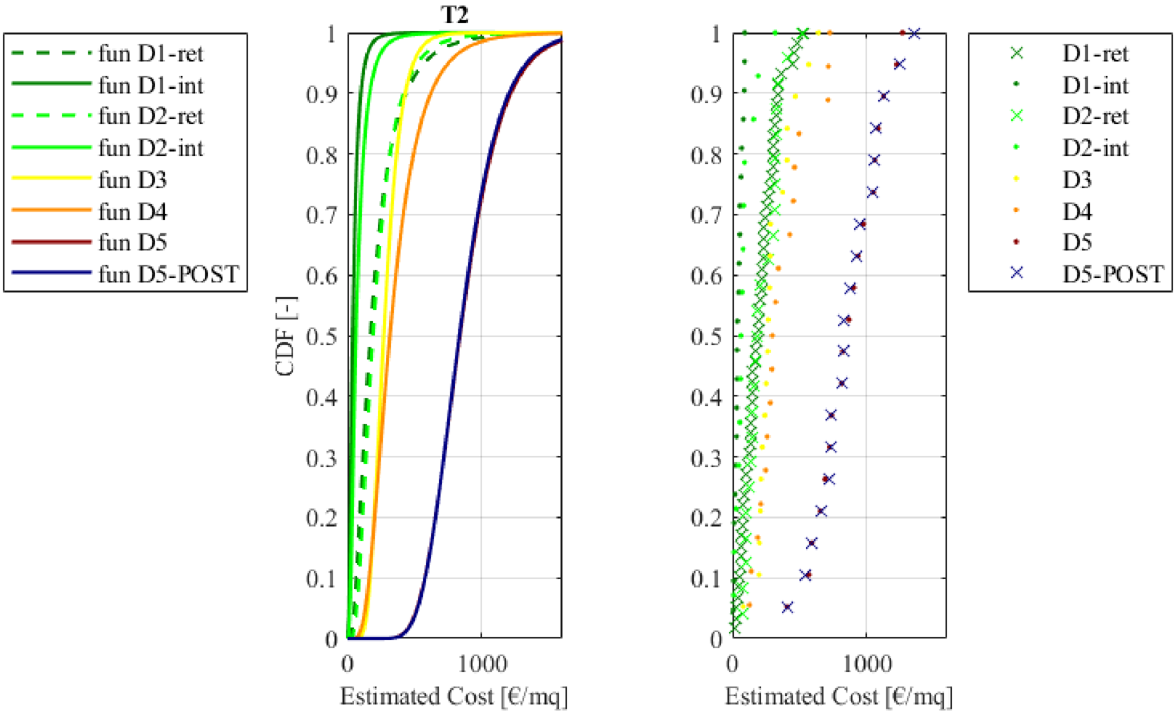

(a) *(b)*

Figure 99. Cumulative distribution of the estimated costs of T2 and lognormal fitting curves at different damage levels: (a) lognormal fitting curves; (b) cumulative representation of the data.

4.2.3.1.3. TYPOLOGY T3

Table 34. Statistical analysis of the estimated losses of typology T3 at different damage levels.

	D1-ret	D1-int	D2-ret	D2-int	D3	D4	D5-post
Mean [€/mq]	142.84	38.72	253.02	76.07	204.30	349.76	998.29
Median [€/mq]	132.85	30.37	252.13	59.47	228.03	355.43	1020.14
Max [€/mq]	377.26	109.28	620.62	121.06	473.58	781.01	1497.55
Min [€/mq]	14.82	8.06	44.65	51.35	25.97	132.13	551.17
Standard deviation [€/mq]	90.81	30.84	185.06	26.84	165.57	187.20	296.99
Total number [-]	41	14	11	9	9	12	10
16° percentile [€/mq]	43.73	12.36	80.65	55.73	33.43	160.81	640.37
84° percentile [€/mq]	241.24	70.47	402.85	114.28	366.61	486.27	1203.24
Kurtosis [-]	-0.2	1.2	-0.4	-0.9	-1.4	1.2	-0.7
Skewness [-]	0.6	1.2	0.6	0.8	0.3	0.8	0.0
CoV [%]	63.6	79.7	73.1	35.3	81.0	53.5	29.7
90% C.I. mean (-) [€/mq]	119.59	25.20	161.51	61.40	113.79	261.14	844.26
90% C.I. mean (+) [€/mq]	166.10	52.23	344.53	90.75	294.81	438.39	1152.31

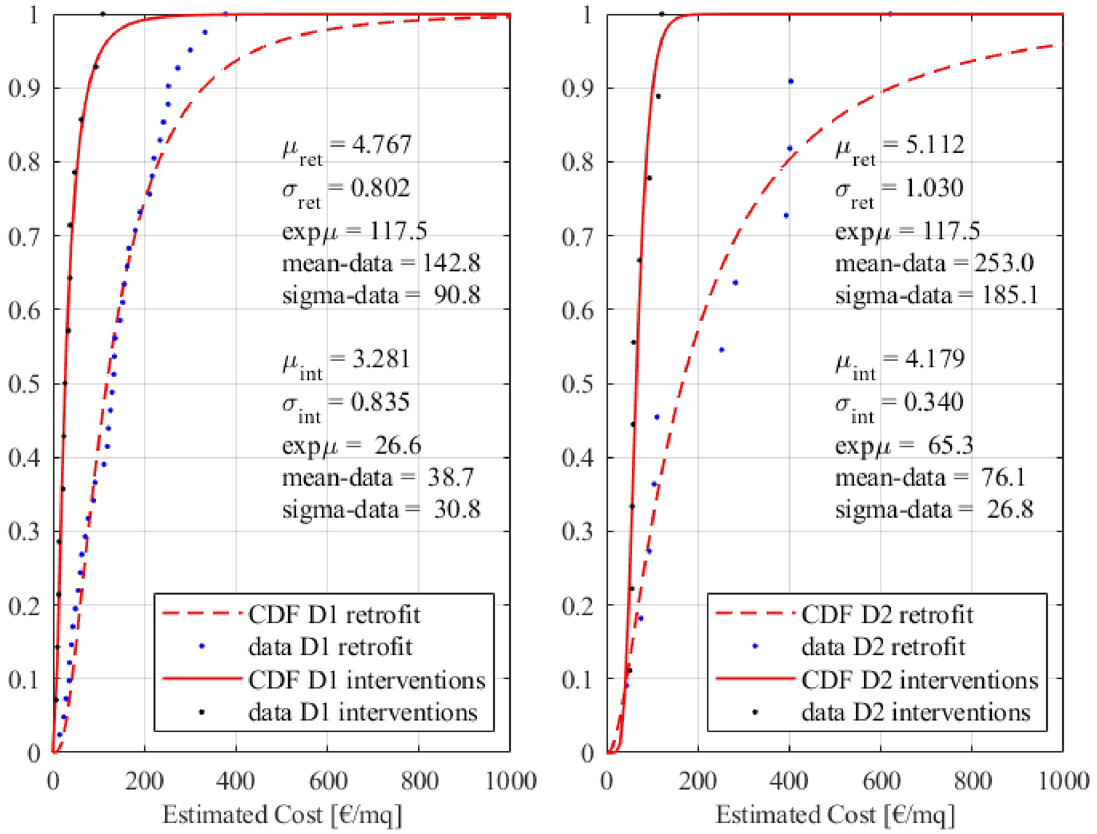

(a) *(b)*

Figure 100. Cumulative distribution of the estimated costs of T3 and lognormal fitting curves: (a) at D1 with local interventions and with retrofit; (b) at D2 with local interventions and with retrofit. Indication of the main descriptors of the function, and the mean and the standard deviation of the data.

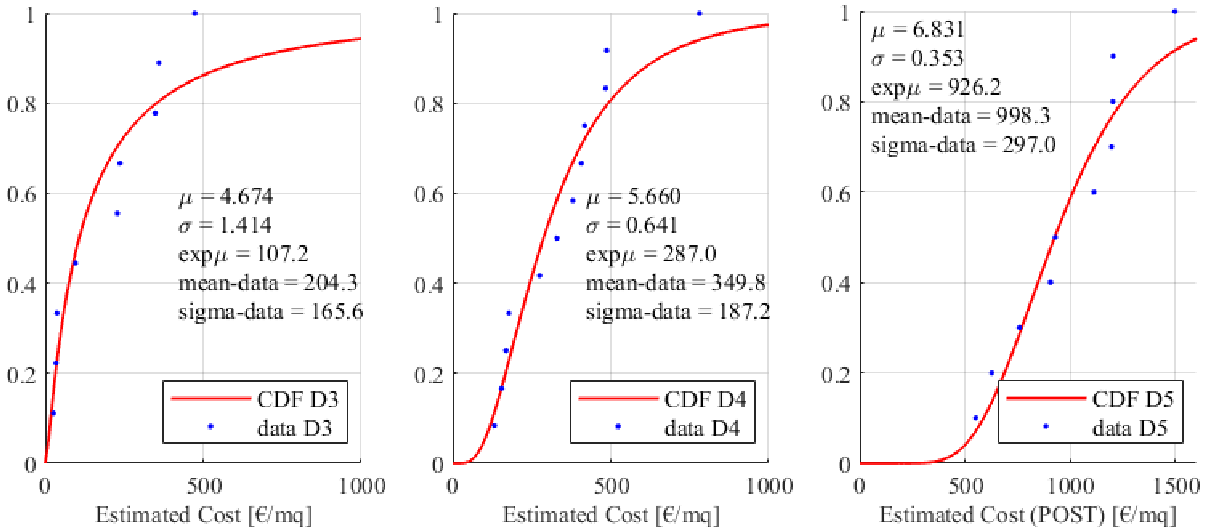

(a) *(b)* *(c)*

Figure 101. Cumulative distribution of the estimated costs of T3 and lognormal fitting curves at: (a) D3; (b) D4; (c) D5-POST. Indication of the main descriptors of the function, and the mean and the standard deviation of the data.

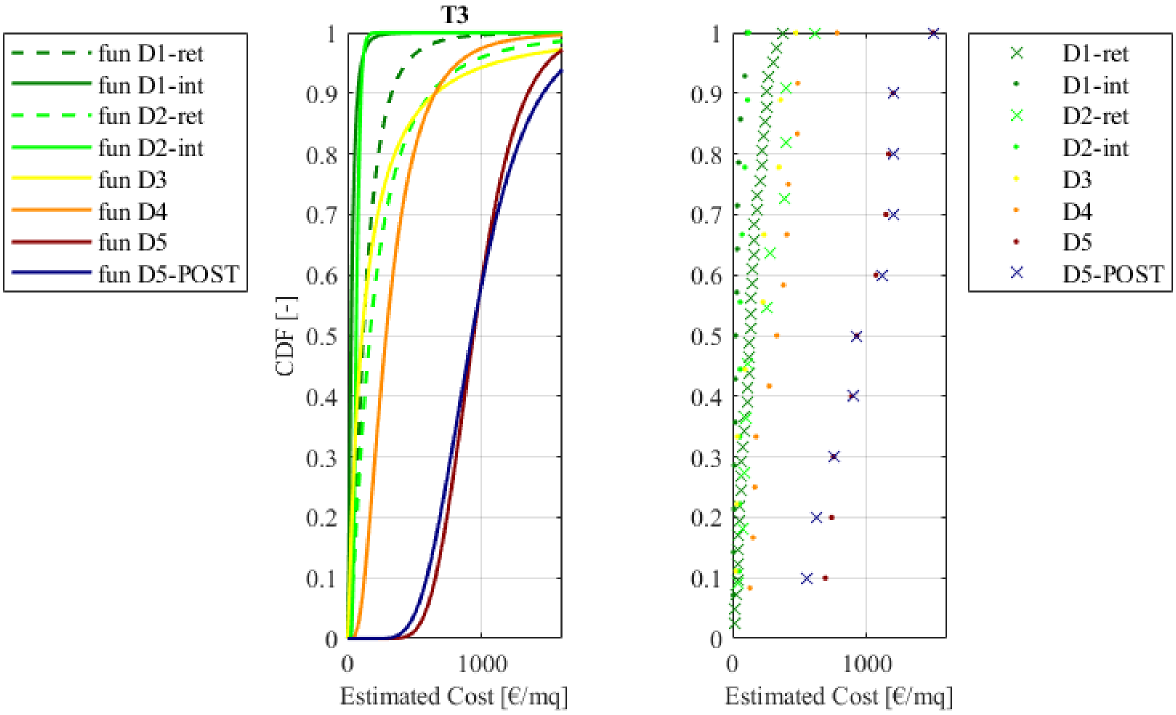

(a) *(b)*

Figure 102. Cumulative distribution of the estimated costs of T3 and lognormal fitting curves at different damage levels: (a) lognormal fitting curves; (b) cumulative representation of the data.

4.2.3.2. STRUCTURAL LOSSES (A)

The structural losses (category A of the estimated costs) are reported in €/mq and are analysed individually at the five damage states, for the three typologies T1, T2 and T3. Thus, a final graph with the cumulative distributions of the data and the fitting functions is proposed in Figures 105, 108, 111 for comparison.

The structural costs included in this category are those spent for the reparation of the buildings, of the structural components and the necessary structural and geotechnical tests, at each damage degree.

The structural losses of category T1 are characterized by higher mean and median values compared to those of T2 and T3, at damage levels D1 to D4, while and opposite trend is detected at damage D5 (i.e., D5-POST). Indeed, at D5 the mean structural costs due to demolition and reconstruction of T3 are almost the 40% higher than those of T1 and T2, confirming the outcomes of previous Sections. This aspect is probably because T3 buildings were built with more recently developed structural roof elements able to cover large span dimensions, with higher prices compared to older solutions. Therefore, the adoption of these elements for the entire reconstruction of the buildings may raise the costs per square meters.

As in the previous Section, the cumulative fitting curves have increasing mean values following the order of the damage states. However, in Figure 111 for typology T3, it is possible to observe an overlap between the loss functions at damage state D1 with retrofit, D2 with retrofit, and D3, due to the lack of loss data at these damage states (around ten samples each, according to Table 37).

4.2.3.2.1. TYPOLOGY T1

Table 35. Statistical analysis of the estimated structural losses of typology T1 at different damage levels.

	D1-ret	**D1-int**	**D2-ret**	**D2-int**	**D3**	**D4**	**D5-post**
Mean [€/mq]	182.36	56.76	207.13	113.98	232.56	349.08	591.40
Median [€/mq]	203.03	41.24	193.58	95.47	203.15	356.85	590.93
Max [€/mq]	424.47	130.16	459.36	204.61	500.77	595.81	899.29
Min [€/mq]	12.75	8.71	40.65	56.38	53.55	118.93	244.22
Standard deviation [€/mq]	108.43	40.41	105.09	59.83	122.16	131.77	141.13
Total number [-]	45	14	24	8	15	14	32
16° percentile [€/mq]	49.21	21.96	110.96	59.41	114.97	218.21	487.23
84° percentile [€/mq]	303.55	104.98	322.92	181.59	341.00	477.33	735.85
Kurtosis [-]	-0.8	-0.5	-0.1	-1.8	0.5	0.0	0.9
Skewness [-]	0.1	0.7	0.5	0.4	0.7	-0.1	-0.4
CoV [%]	59.5	71.2	50.7	52.5	52.5	37.7	23.9
90% C.I. mean (-) [€/mq]	155.85	39.05	171.95	79.29	180.83	291.32	550.48
90% C.I. mean (+) [€/mq]	208.87	74.48	242.31	148.67	284.29	406.83	632.32

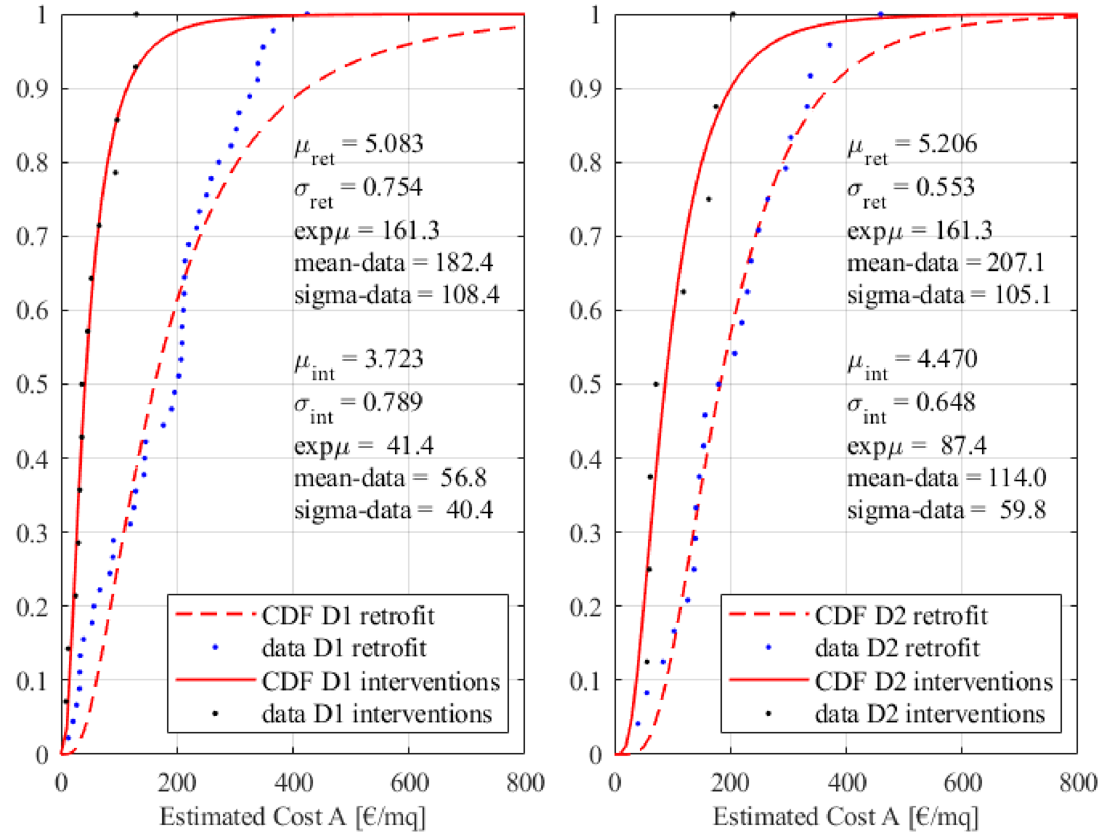

(a) (b)

Figure 103. Cumulative distribution of the estimated structural costs of T1 and lognormal fitting curves: (a) at D1 with local interventions and with retrofit; (b) at D2 with local interventions and with retrofit. Indication of the main descriptors of the function, and the mean and the standard deviation of the data.

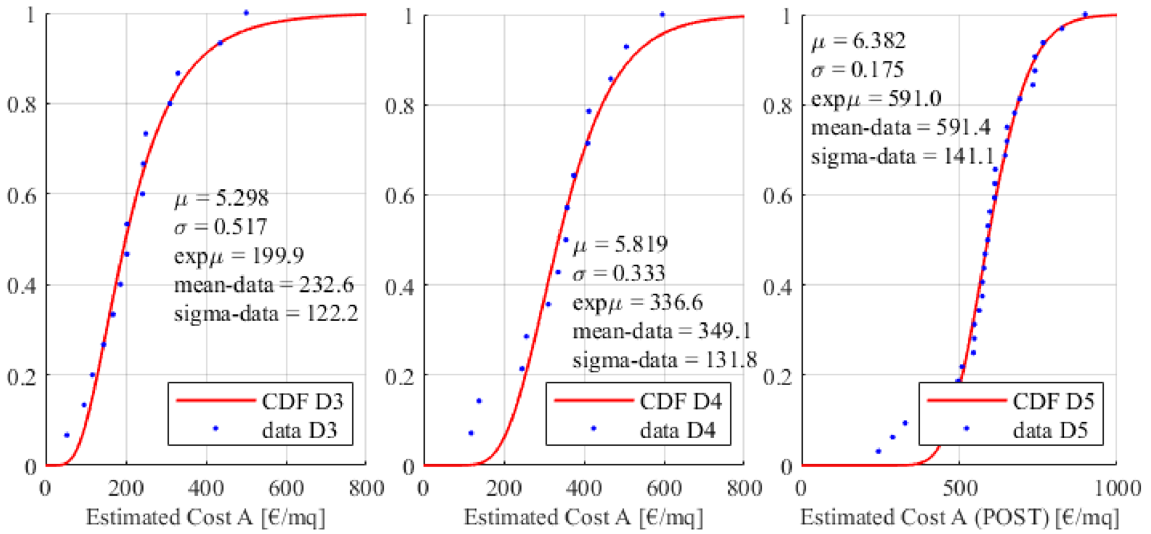

(a) (b) (c)

Figure 104. Cumulative distribution of the estimated structural costs of T1 and lognormal fitting curves at: (a) D3; (b) D4; (c) D5-POST. Indication of the main descriptors of the function, and the mean and the standard deviation of the data.

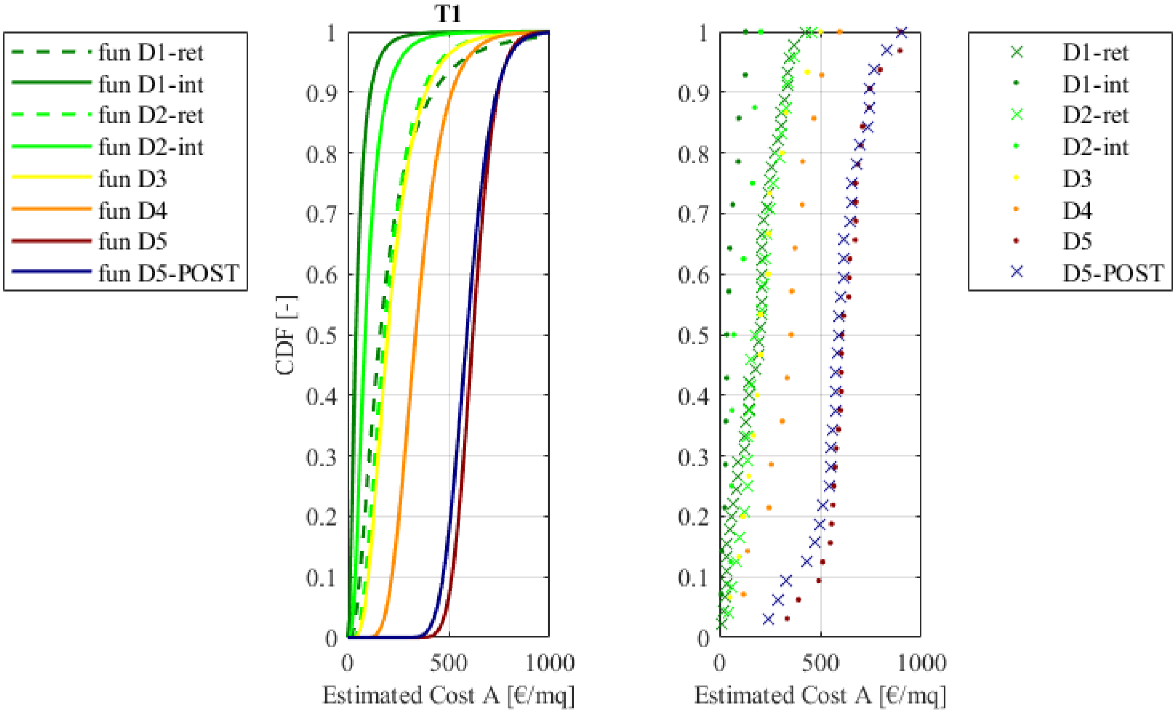

(a) *(b)*

Figure 105. Cumulative distribution of the estimated structural costs of T1 and lognormal fitting curves at different damage levels: (a) lognormal fitting curves; (b) cumulative representation of the data.

4.2.3.2.2. TYPOLOGY T2

Table 36. Statistical analysis of the estimated structural losses of typology T2 at different damage levels.

	D1-ret	**D1-int**	**D2-ret**	**D2-int**	**D3**	**D4**	**D5-post**
Mean [€/mq]	163.59	37.21	181.80	73.76	237.55	311.61	562.64
Median [€/mq]	149.10	31.74	156.30	54.20	215.24	261.02	533.05
Max [€/mq]	473.06	83.62	359.56	240.64	466.95	678.17	997.39
Min [€/mq]	12.47	7.47	70.04	10.26	74.57	109.49	99.65
Standard deviation [€/mq]	104.79	23.02	89.56	66.18	108.96	176.97	236.65
Total number [-]	59	21	24	14	19	18	19
16° percentile [€/mq]	54.27	9.54	94.21	17.81	143.34	155.45	377.46
84° percentile [€/mq]	272.70	60.20	285.23	145.16	382.21	516.42	842.91
Kurtosis [-]	0.4	-0.5	-1.4	2.2	0.1	0.1	-0.2
Skewness [-]	0.8	0.4	0.4	1.4	0.8	0.9	0.2
CoV [%]	64.1	61.9	49.3	89.7	45.9	56.8	42.1
90% C.I. mean (-) [€/mq]	141.22	28.97	151.82	44.75	196.55	243.20	473.60
90% C.I. mean (+) [€/mq]	185.97	45.45	211.78	102.76	278.54	380.02	651.68

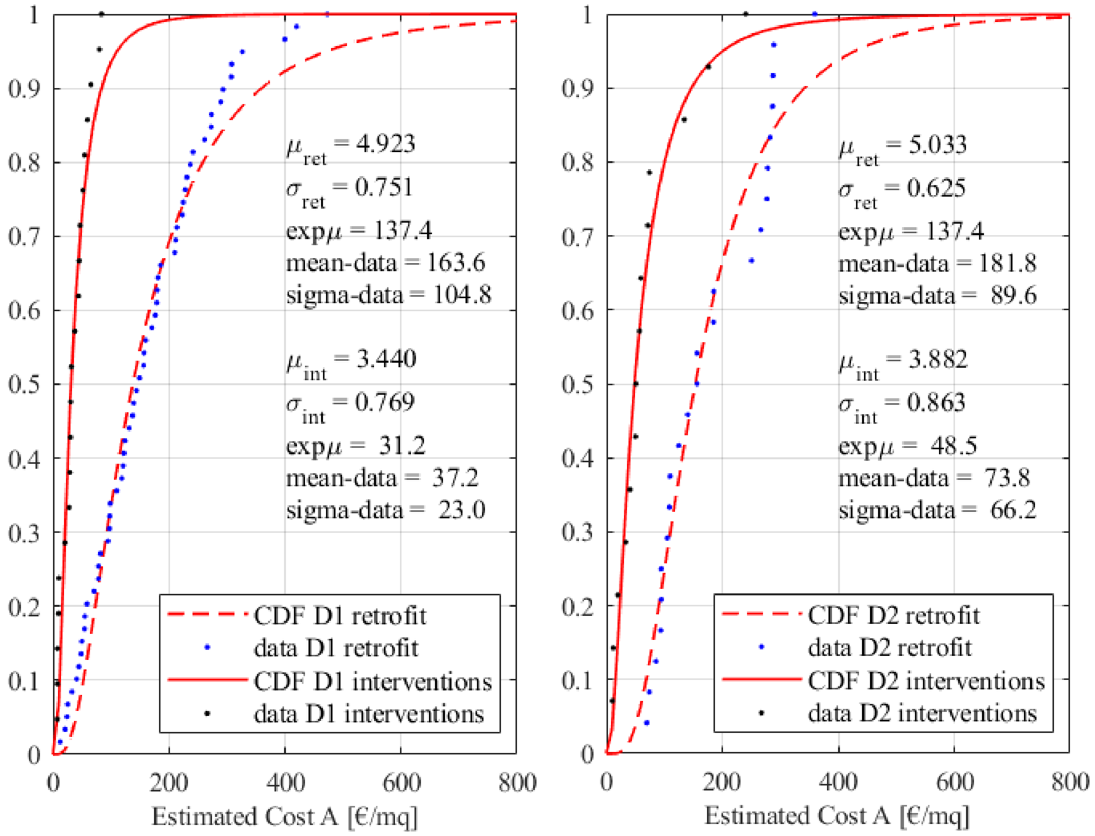

(a) *(b)*

Figure 106. Cumulative distribution of the estimated structural costs of T2 and lognormal fitting curves: (a) at D1 with local interventions and with retrofit; (b) at D2 with local interventions and with retrofit. Indication of the main descriptors of the function, and the mean and the standard deviation of the data.

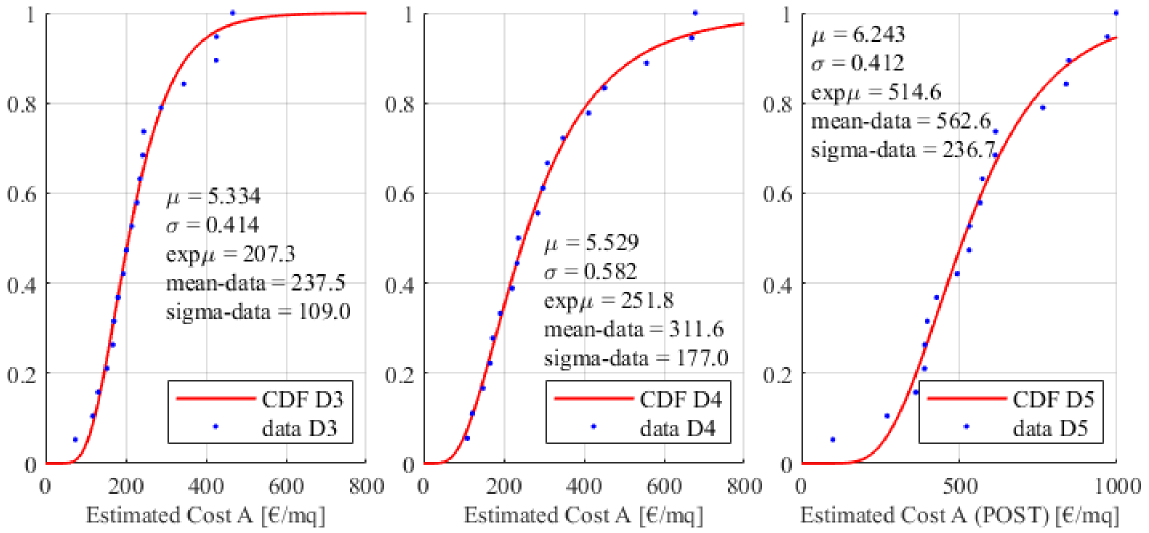

(a) *(b)* *(c)*

Figure 107. Cumulative distribution of the estimated structural costs of T2 and lognormal fitting curves at: (a) D3; (b) D4; (c) D5-POST. Indication of the main descriptors of the function, and the mean and the standard deviation of the data.

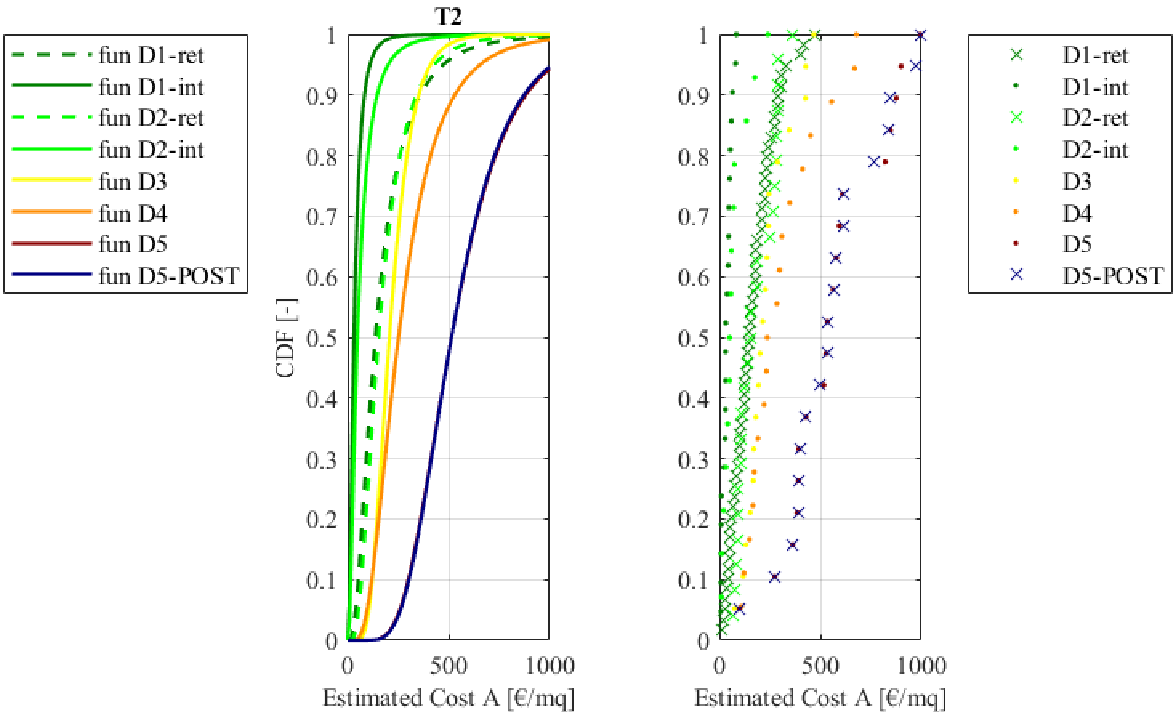

(a) *(b)*

Figure 108. Cumulative distribution of the estimated structural costs of T2 and lognormal fitting curves at different damage levels: (a) lognormal fitting curves; (b) cumulative representation of the data.

4.2.3.2.3. TYPOLOGY T3

Table 37. Statistical analysis of the estimated structural losses of typology T3 at different damage levels.

	D1-ret	**D1-int**	**D2-ret**	**D2-int**	**D3**	**D4**	**D5-post**
Mean [€/mq]	111.96	32.14	213.54	55.73	120.23	269.42	824.26
Median [€/mq]	109.21	25.28	230.66	49.71	86.91	285.02	684.93
Max [€/mq]	289.76	88.16	526.61	114.37	317.35	440.38	1322.32
Min [€/mq]	9.73	5.80	33.15	31.78	19.39	91.30	507.16
Standard deviation [€/mq]	69.95	26.40	165.55	24.74	105.38	126.57	284.72
Total number [-]	41	14	11	9	9	12	10
16° percentile [€/mq]	35.05	10.29	54.04	36.55	28.15	126.98	599.90
84° percentile [€/mq]	194.69	61.30	367.48	67.86	221.42	409.67	1101.62
Kurtosis [-]	-0.2	0.9	-0.8	4.3	-0.4	-1.6	-1.2
Skewness [-]	0.6	1.2	0.5	1.6	0.7	-0.1	0.5
CoV [%]	62.5	82.1	77.5	44.4	87.7	47.0	34.5
90% C.I. mean (-) [€/mq]	94.04	20.57	131.68	42.21	62.62	209.50	676.60
90% C.I. mean (+) [€/mq]	129.88	43.71	295.40	69.26	177.83	329.34	971.92

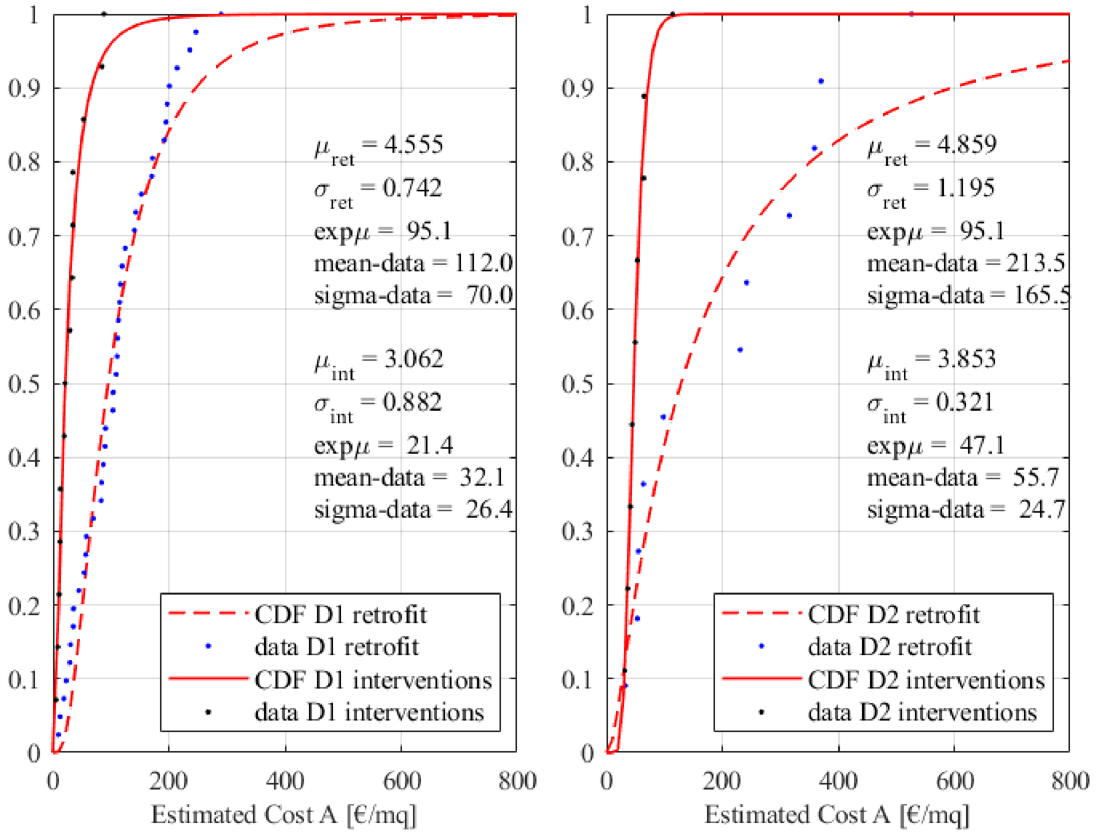

(a) *(b)*

Figure 109. Cumulative distribution of the estimated structural costs of T3 and lognormal fitting curves: (a) at D1 with local interventions and with retrofit; (b) at D2 with local interventions and with retrofit. Indication of the main descriptors of the function, and the mean and the standard deviation of the data.

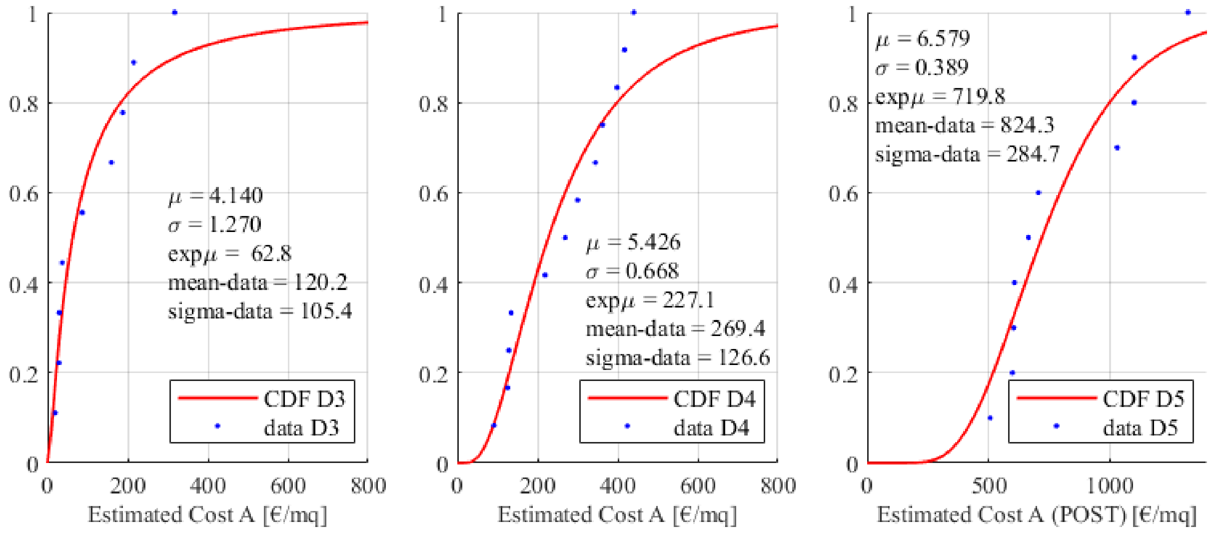

(a) *(b)* *(c)*

Figure 110. Cumulative distribution of the estimated structural costs of T3 and lognormal fitting curves at: (a) D3; (b) D4; (c) D5-POST. Indication of the main descriptors of the function, and the mean and the standard deviation of the data.

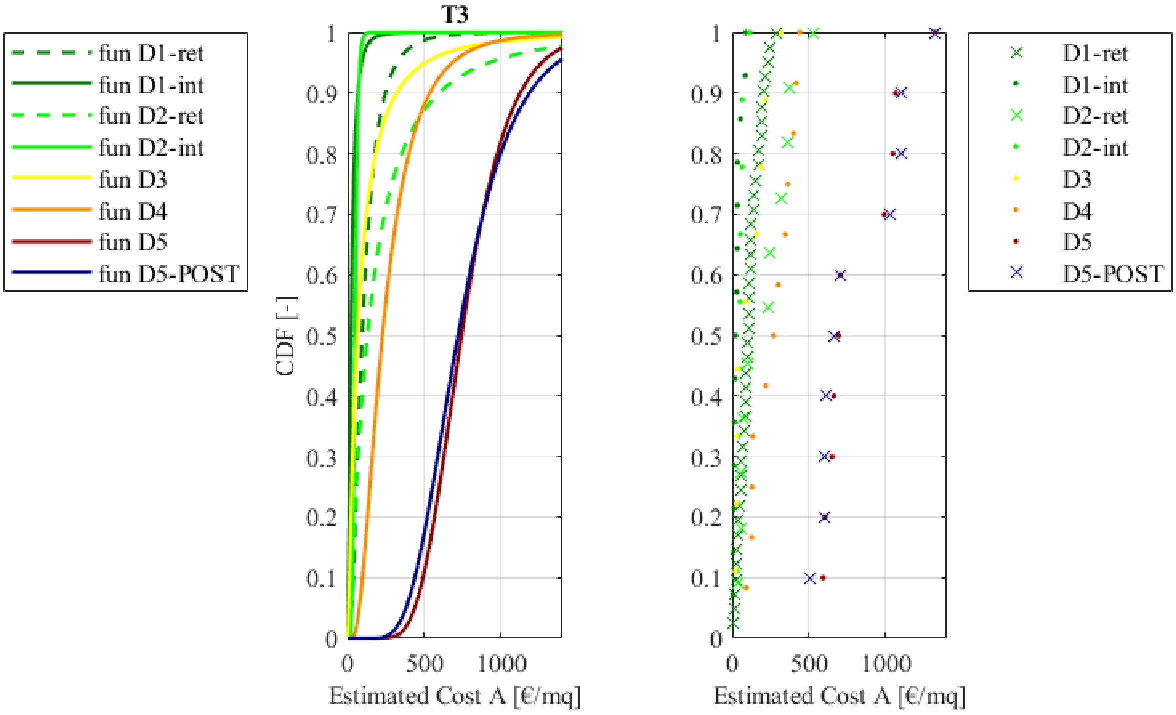

(a) *(b)*

Figure 111. Cumulative distribution of the estimated structural costs of T3 and lognormal fitting curves at different damage levels: (a) lognormal fitting curves; (b) cumulative representation of the data.

4.2.3.3. NON-STRUCTURAL LOSSES (C)

The non-structural estimated losses (category C of the losses) are reported in €/mq for each structural typology. In some cases, the non-structural losses were equal to zero, since the seismic damage only affected the structural elements. Therefore, there are several null values among the losses of all categories that have been neglected in the statistical analysis. The remaining values have been adopted for the analysis of the losses, although the curves presented here are less accurate due to the reduced number of samples available.

It is useful to recall that the non-structural costs are due to the repair of the finishing and the ordinary systems and plants, since other distinct requests for funds were presented for the reparation of the industrial machineries

The final cumulative distributions of the data and the fitting functions of each typology are depicted in Figures 114, 117, 120. The non-structural data of categories T1 and T2 are similar and higher compared to those of T3, apart from those at damage levels D3 and D4. The reason is that, in T3, some values are deviating from the others resulting in a high increase of the mean and the median of the samples. Nevertheless, the fitting functions of T1, T2 and T3 have similar values of μ and σ at the five damage levels.

At damage level D5, the μ obtained for T1 and T2 are four to five times those at D4, while for T3 there is not a significant gap between the values at D4 and D5. It worth noting that the smaller number of data is available once again for typology T3 (see Table 40), leading to less accurate results.

4.2.3.3.1. TYPOLOGY T1

Table 38. Statistical analysis of the estimated non-structural losses of typology T1 at different damage levels.

	D1-ret	**D1-int**	**D2-ret**	**D2-int**	**D3**	**D4**	**D5-post**
Mean [€/mq]	29.15	12.13	46.56	20.96	52.63	58.91	246.74
Median [€/mq]	20.82	5.33	21.31	23.47	52.48	52.84	220.62
Max [€/mq]	78.45	46.47	336.79	44.31	168.23	135.31	566.53
Min [€/mq]	2.91	1.25	1.40	2.12	4.90	8.09	3.01
Standard deviation [€/mq]	21.49	15.04	76.19	16.91	43.19	41.48	155.65
Total number [-]	27	10	18	5	15	11	26
16° percentile [€/mq]	8.85	1.46	8.21	3.63	12.12	10.78	82.03
84° percentile [€/mq]	49.84	27.93	68.68	39.34	77.84	101.13	414.91
Kurtosis [-]	0.0	2.1	14.1	-0.9	2.6	-0.6	-0.7
Skewness [-]	0.9	1.4	3.3	0.2	1.2	0.4	0.3
CoV [%]	73.7	124.0	163.6	80.7	82.1	70.4	63.1
90% C.I. mean (-) [€/mq]	22.37	4.33	17.11	8.56	34.34	38.40	196.67
90% C.I. mean (+) [€/mq]	35.93	19.93	76.01	33.36	70.92	79.42	296.80

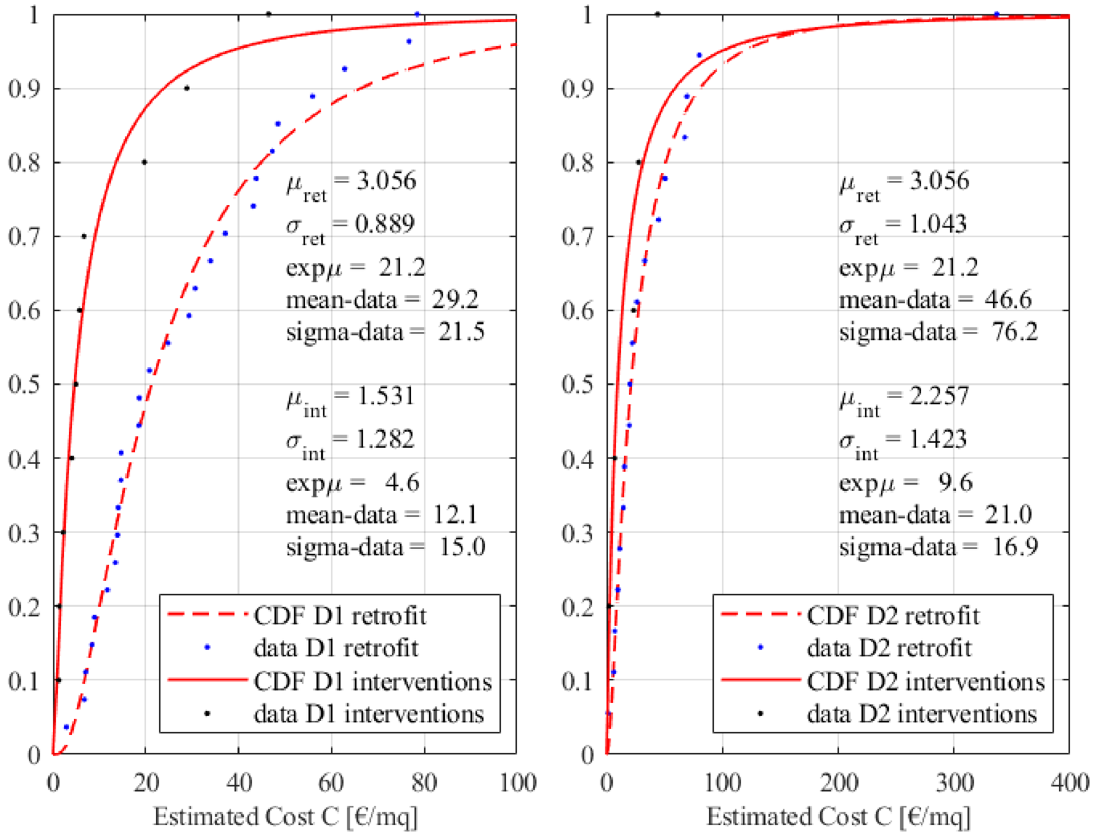

(a) *(b)*

Figure 112. Cumulative distribution of the estimated non-structural costs of T1 and lognormal fitting curves: (a) at D1 with local interventions and with retrofit; (b) at D2 with local interventions and with retrofit. Indication of the main descriptors of the function, and the mean and the standard deviation of the data.

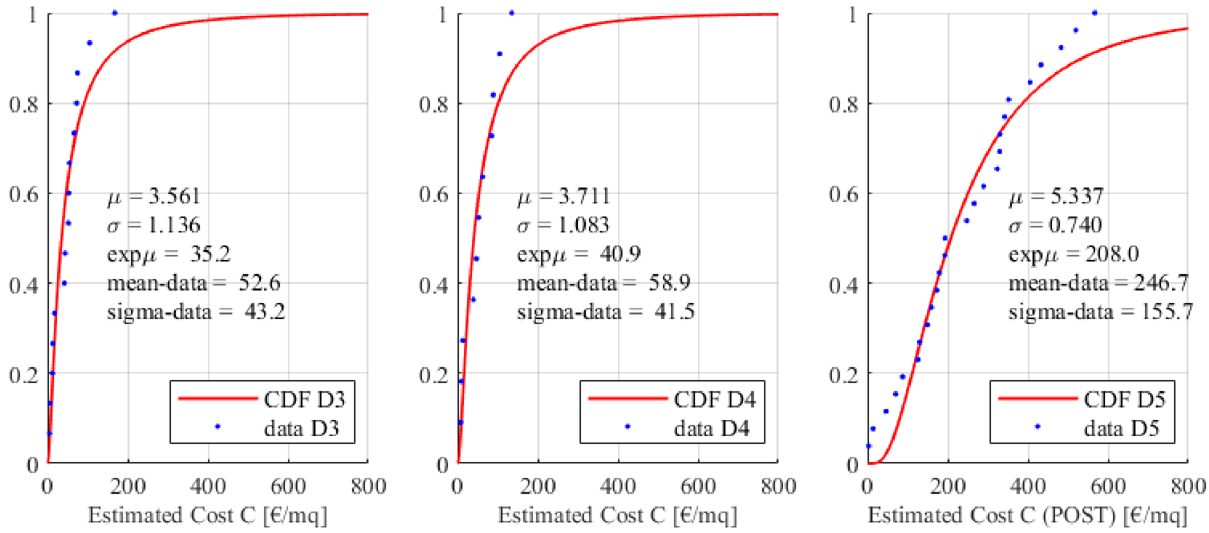

(a) *(b)* *(c)*

Figure 113. Cumulative distribution of the estimated non-structural costs of T1 and lognormal fitting curves at: (a) D3; (b) D4; (c) D5-POST. Indication of the main descriptors of the function, and the mean and the standard deviation of the data.

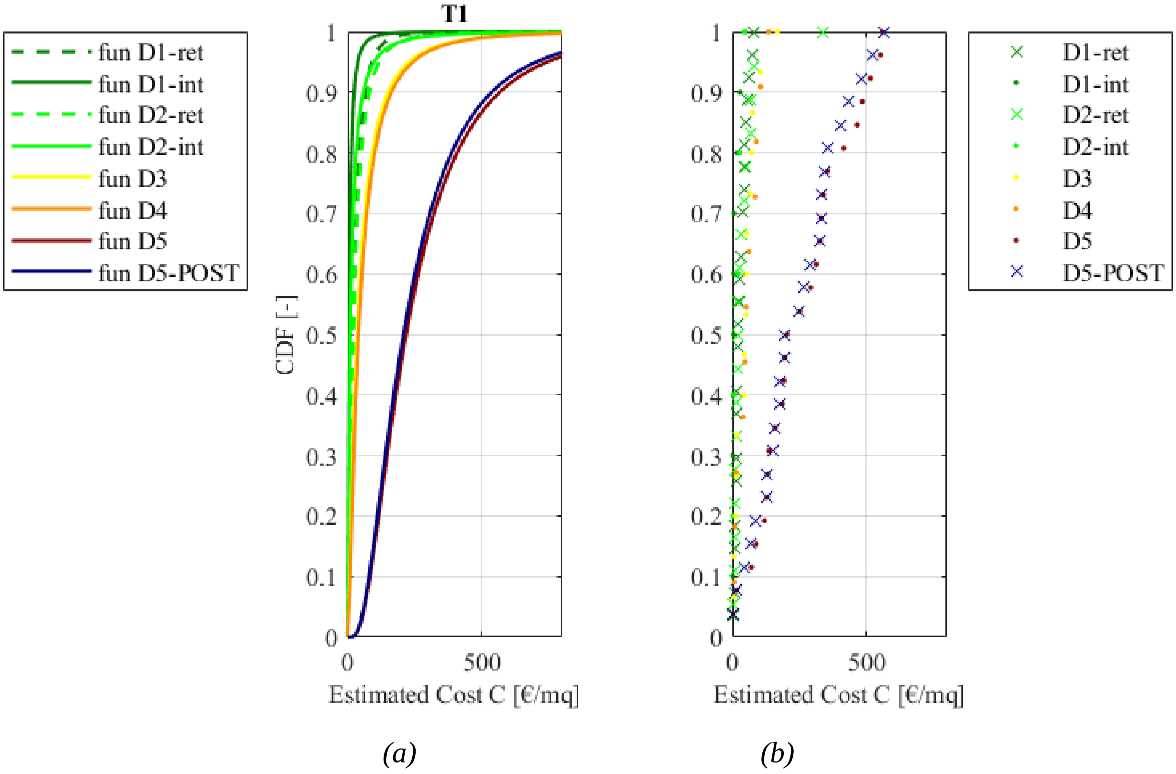

Figure 114. Cumulative distribution of the estimated non-structural costs of T1 and lognormal fitting curves at different damage levels: (a) lognormal fitting curves; (b) cumulative representation of the data.

4.2.3.3.2. TYPOLOGY T2

Table 39. Statistical analysis of the estimated non-structural losses of typology T2 at different damage levels.

	D1-ret	D1-int	D2-ret	D2-int	D3	D4	D5-post
Mean [€/mq]	19.58	5.44	28.85	9.66	52.02	49.95	252.90
Median [€/mq]	15.13	2.85	14.33	7.57	32.36	41.26	238.51
Max [€/mq]	108.34	31.52	110.26	49.29	168.85	115.58	706.49
Min [€/mq]	0.00	0.02	2.96	0.06	9.01	2.65	17.39
Standard deviation [€/mq]	21.21	7.79	31.16	12.40	51.27	44.93	202.67
Total number [-]	45	16	17	13	16	11	14
16° percentile [€/mq]	0.82	0.42	4.63	2.00	11.78	4.81	32.25
84° percentile [€/mq]	35.18	10.50	53.20	10.68	123.02	111.74	442.79
Kurtosis [-]	5.9	9.0	2.1	10.6	0.5	-1.3	0.6
Skewness [-]	2.0	2.5	1.5	2.7	1.2	0.4	0.8
CoV [%]	108.3	143.1	108.0	128.3	98.6	90.0	80.1
90% C.I. mean (-) [€/mq]	14.40	2.25	16.46	4.02	31.00	27.73	164.07
90% C.I. mean (+) [€/mq]	24.77	8.63	41.25	15.30	73.04	72.16	341.73

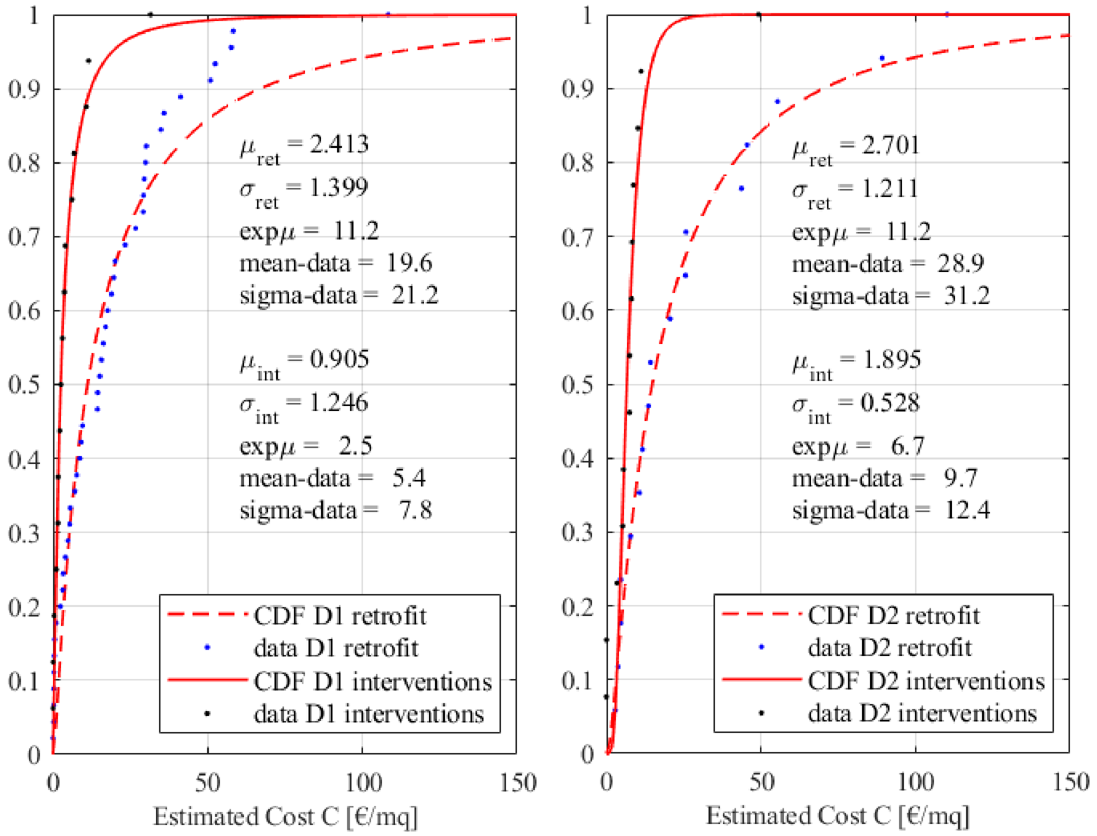

(a) *(b)*

Figure 115. Cumulative distribution of the estimated non-structural costs of T2 and lognormal fitting curves: (a) at D1 with local interventions and with retrofit; (b) at D2 with local interventions and with retrofit. Indication of the main descriptors of the function, and the mean and the standard deviation of the data.

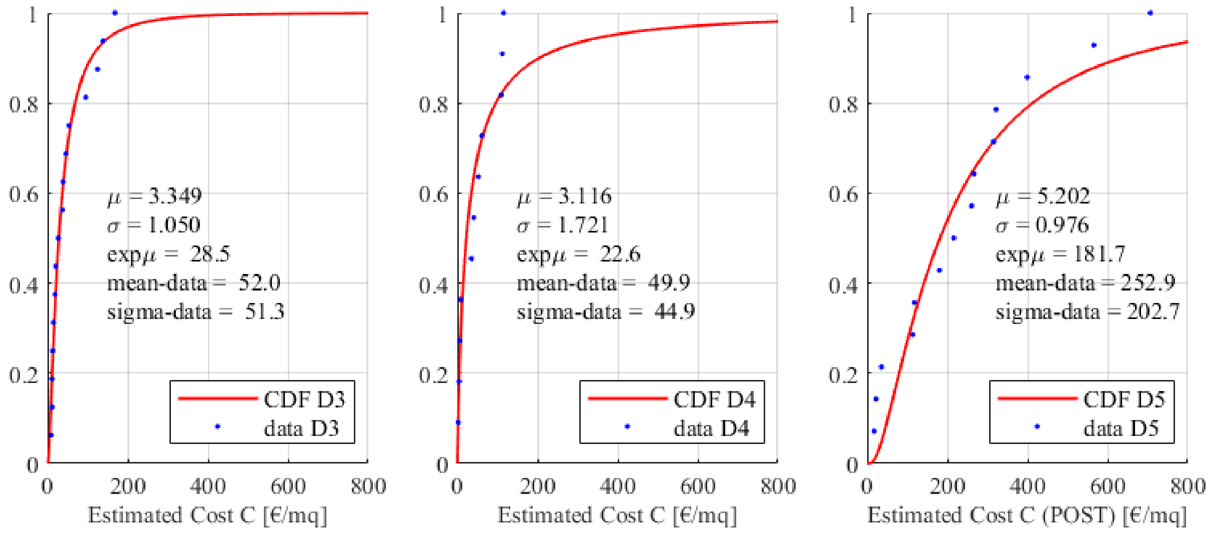

(a) *(b)* *(c)*

Figure 116. Cumulative distribution of the estimated non-structural costs of T2 and lognormal fitting curves at: (a) D3; (b) D4; (c) D5-POST. Indication of the main descriptors of the function, and the mean and the standard deviation of the data.

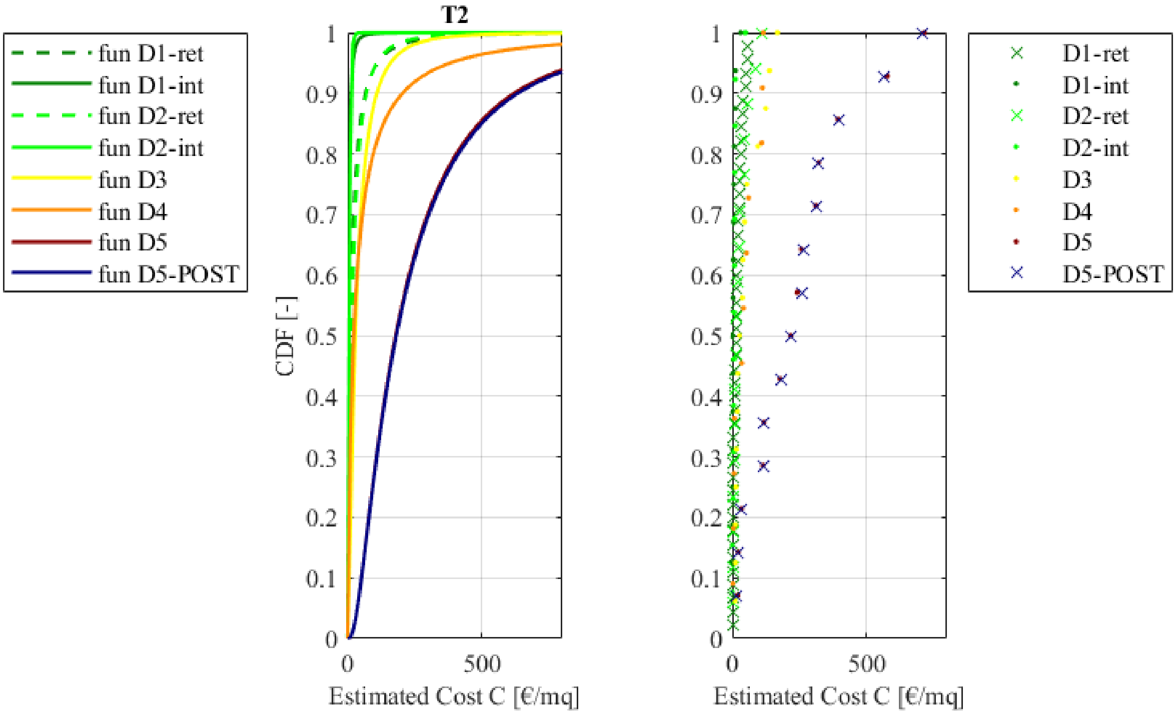

(a) *(b)*

Figure 117. Cumulative distribution of the estimated non-structural costs of T2 and lognormal fitting curves at different damage levels: (a) lognormal fitting curves; (b) cumulative representation of the data.

4.2.3.3.3. TYPOLOGY T3

Table 40. Statistical analysis of the estimated non-structural losses of typology T3 at different damage levels.

	D1-ret	**D1-int**	**D2-ret**	**D2-int**	**D3**	**D4**	**D5-post**
Mean [€/mq]	20.77	3.95	22.51	16.95	122.63	82.14	134.37
Median [€/mq]	14.52	2.41	21.69	18.33	19.43	28.43	83.75
Max [€/mq]	55.33	11.85	44.26	39.02	421.84	445.27	533.17
Min [€/mq]	0.41	0.49	6.33	0.20	2.14	9.64	14.04
Standard deviation [€/mq]	17.66	4.08	15.44	12.78	180.58	148.01	183.03
Total number [-]	33	10	8	7	5	8	7
16° percentile [€/mq]	4.64	0.53	7.26	3.02	2.88	11.33	22.58
84° percentile [€/mq]	45.48	8.53	40.14	28.43	344.83	152.01	301.48
Kurtosis [-]	-0.7	-0.3	-2.0	0.5	2.0	7.6	5.3
Skewness [-]	0.8	0.9	0.2	0.4	1.1	2.2	1.7
CoV [%]	85.1	103.5	68.6	75.4	147.3	180.2	136.2
90% C.I. mean (-) [€/mq]	15.72	1.83	13.56	9.03	-9.81	-3.69	20.91
90% C.I. mean (+) [€/mq]	25.81	6.06	31.46	24.87	255.07	167.96	247.82

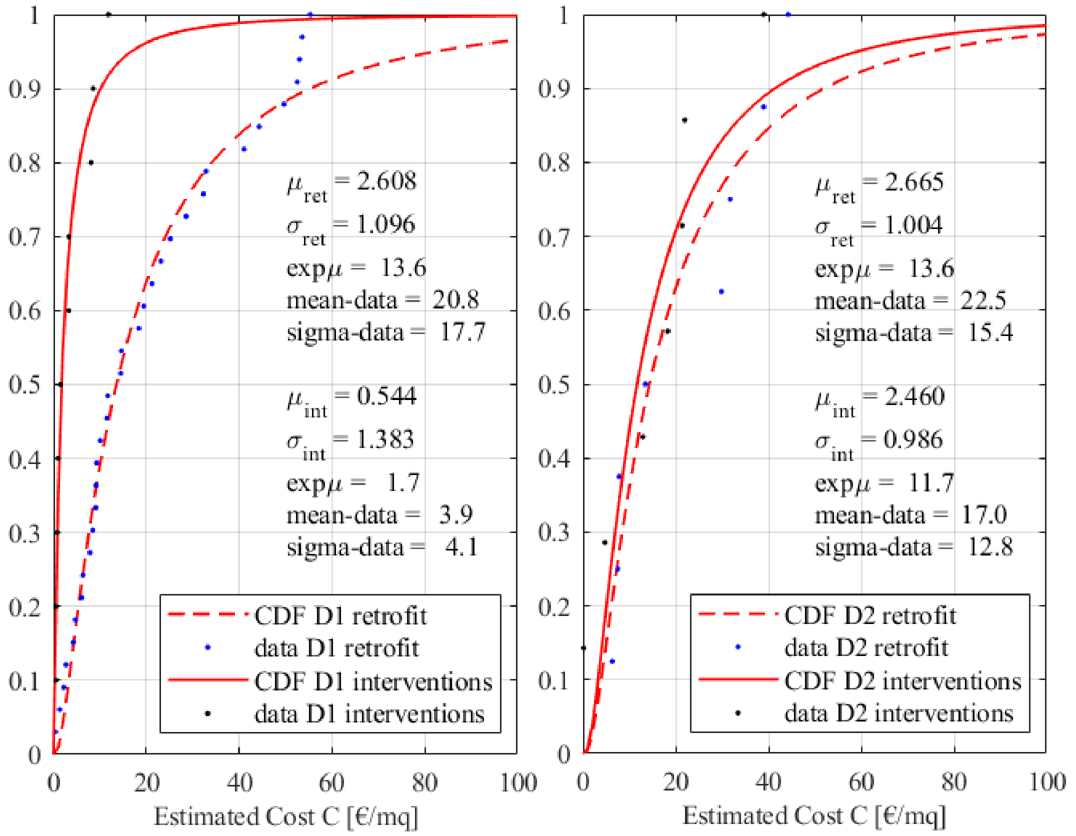

(a) *(b)*

Figure 118. Cumulative distribution of the estimated non-structural costs of T3 and lognormal fitting curves: (a) at D1 with local interventions and with retrofit; (b) at D2 with local interventions and with retrofit. Indication of the main descriptors of the function, and the mean and the standard deviation of the data.

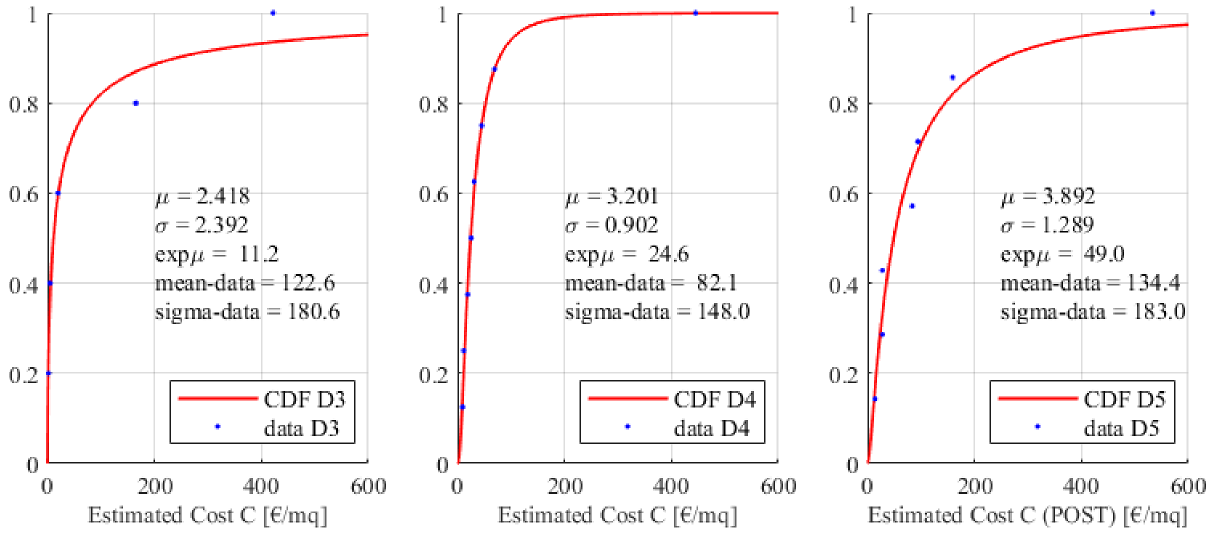

(a) *(b)* *(c)*

Figure 119. Cumulative distribution of the estimated non-structural costs of T3 and lognormal fitting curves at: (a) D3; (b) D4; (c) D5-POST. Indication of the main descriptors of the function, and the mean and the standard deviation of the data.

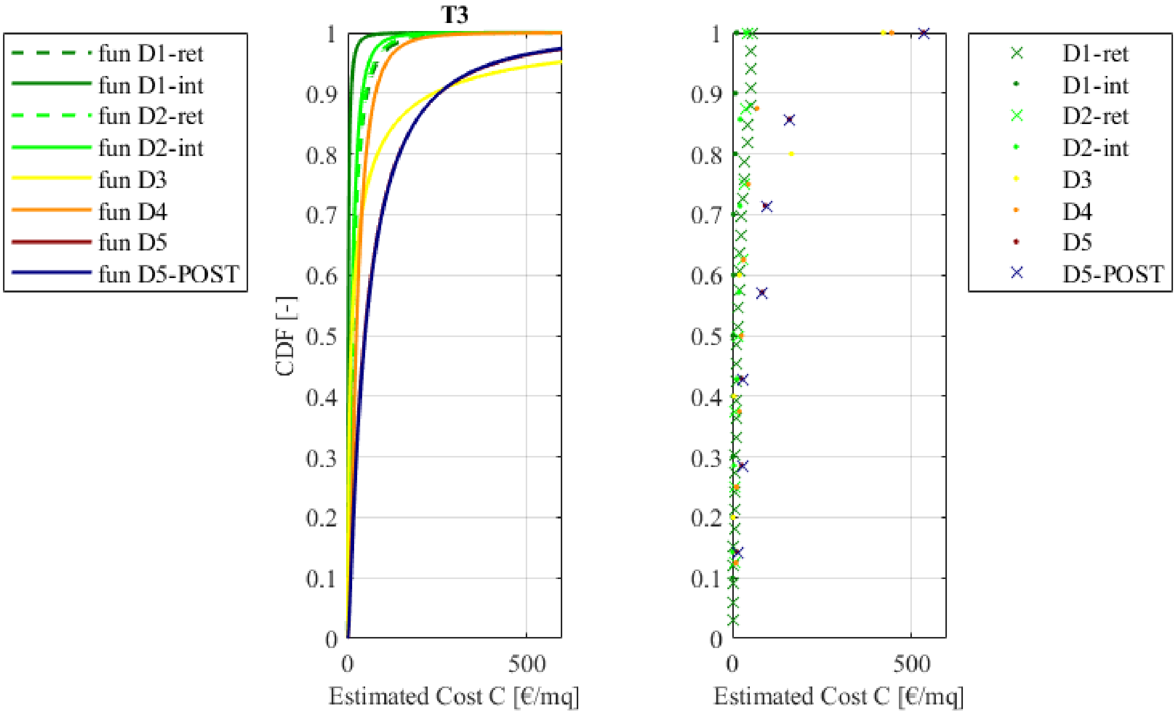

(a) *(b)*

Figure 120. Cumulative distribution of the estimated non-structural costs of T3 and lognormal fitting curves at different damage levels: (a) lognormal fitting curves; (b) cumulative representation of the data.

4.2.3.4. SURFACE IN PLAN

In the documents for the request of regional funds the technicians should indicate the total amount of internal surface in plan in each unit used for the following destinations: production, storage of products, office or residential. The percentage occupation of each part, in the pre-earthquake condition, has been calculated as a fraction of the total surface in plan of the buildings. Figure 121 illustrates the distributions of the percentage occupation in plan for typologies T1, T2 and T3 with indication of the mean values. It is worth saying that the zero values, representing buildings hosting only some of the aforementioned destinations, are neglected.

On average, the part dedicated to production in the precast RC buildings is more than the 80% of the surface. The average percentage occupancy for storage is below the 40% of the surface in T1, while

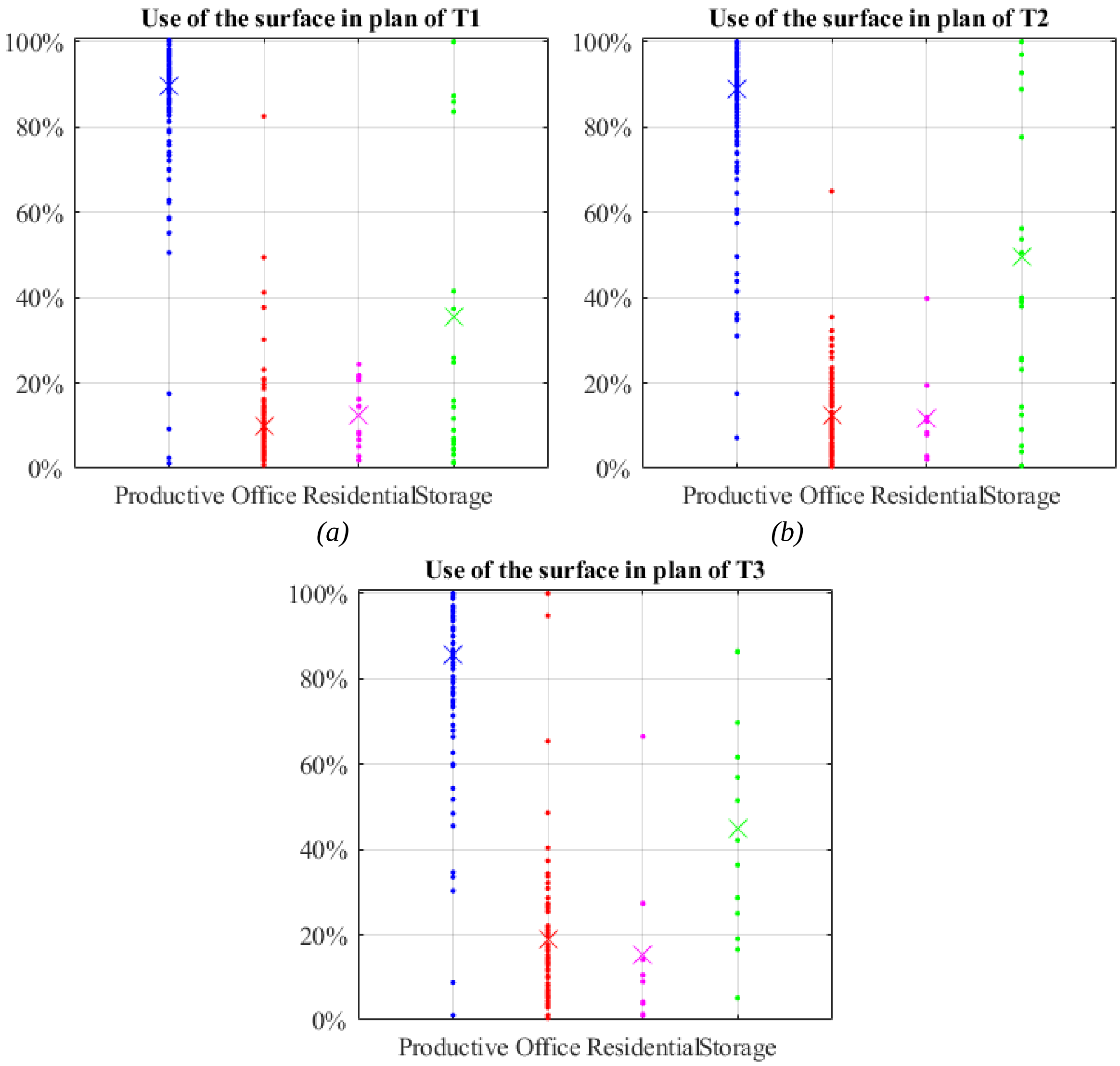

(a) *(b)*

(c)

Figure 121. Distributions of the percentages use of the total area in plan of the buildings for: (a) typology T1; (b) typology T2, (c) typology T3. Indication of the mean values with an x.

it is higher in T2 and mainly T3. The residential use covers about the 10-15% of the surface in all categories, while the office use is higher in modern buildings T3 (around the 20%) compared to T1 and T2 (the 10-15%).

The single dots representing the structures with a high percentage of office or residential surface use are single units, which are part of large estates with many units, each used with a precise unique destination.

The distributions of the actual dimensions of the surface partitions are shown in Figure 122, 123, 124 for each structural typology. The bin-width considered in the histograms is 50 mq for production and storage areas, 25 mq for office and 10 mq for residential areas.

The total number of samples and the amount of zero values (neglected in the analysis) is reported in each Figure. Clearly, the number of observations is significantly lower for residential and storage

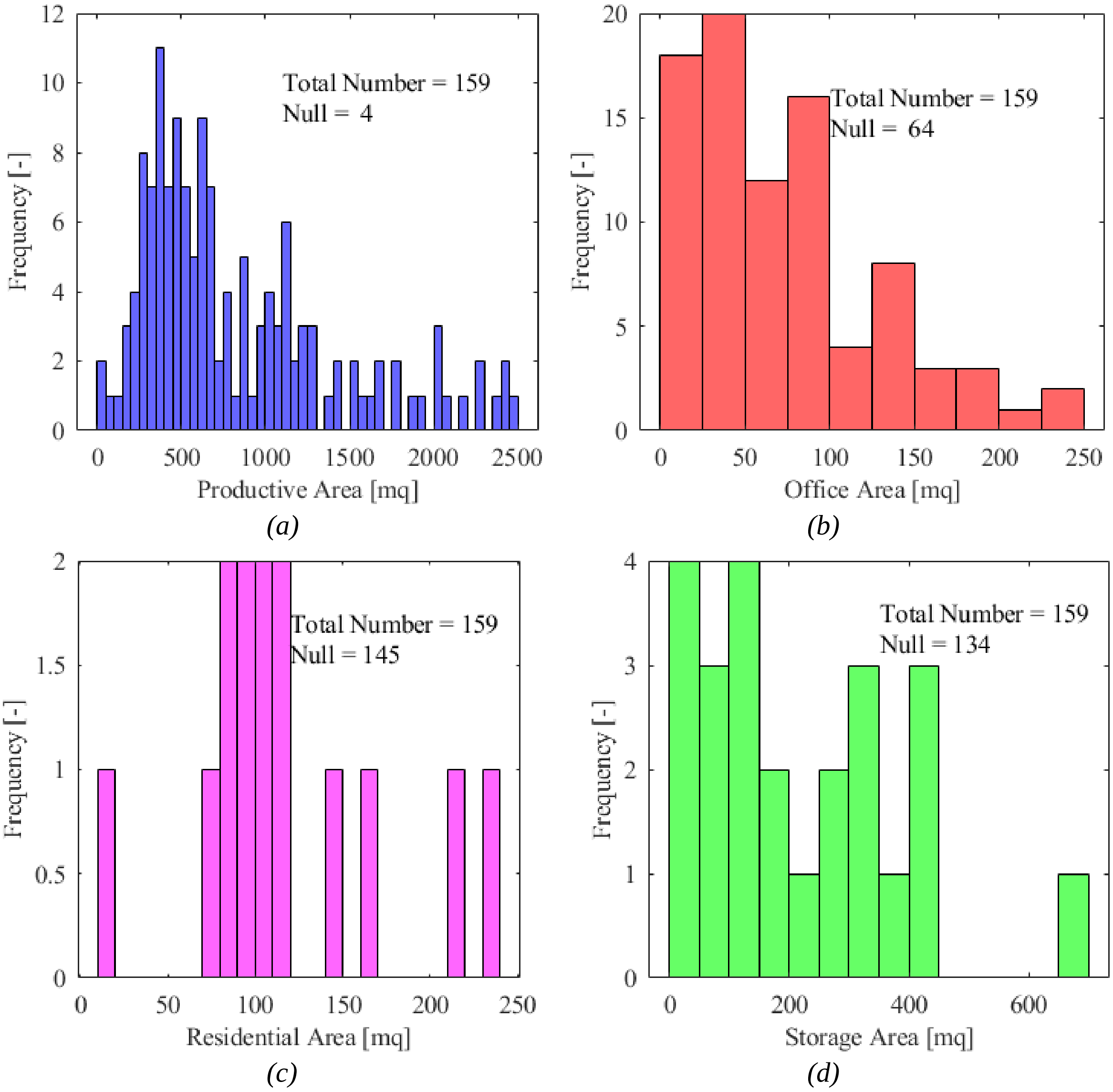

(a) *(b)*

(c) *(d)*

Figure 122. Distributions of the area in plan of buildings T1 used as: (a) productive area; (b) office area, (c) residential area; (d) storage area. Indication of the total number of observations and the zero values.

areas, meaning that the most common uses of the buildings are production and office, as visible from the number of dots in Figure 121.

The areas dedicated to production are the largest ones in all typologies, with increasing dimensions from T1 to T3, as expected considering the main features of the buildings (see the full descriptions in Section 4.1). Indeed, the average dimensions of the production areas in T3 (2205 mq) are almost twice those in T2 (1270 mq) and T1 (828 mq). Hence, there are the storage areas (mean values of 1572 mq in T3, 644 mq in T2, 224 mq in T1), followed by the office (mean values of 325 mq in T3, 164 mq in T2, 73 mq in T1) and the residential areas that are the smallest ones (mean values of 99 mq in T3, 108 mq in T2, 117 mq in T1). Regarding this, there are usually small parts used with residential destination mainly located in the extremities in large precast buildings, or there are small external structural units entirely used with this scope.

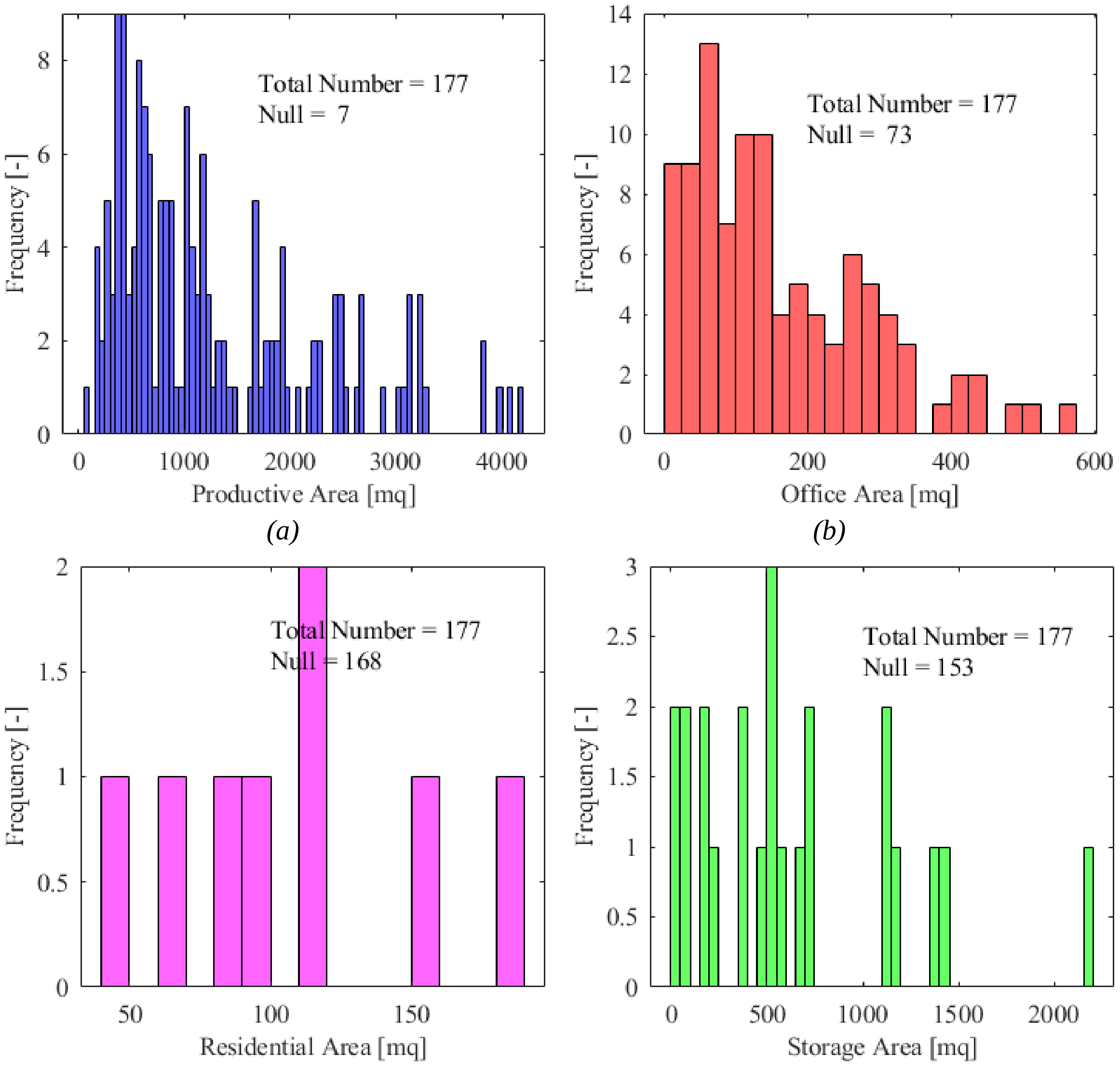

(a) *(b)*

(c) *(d)*

Figure 123. Distributions of the area in plan of buildings T2 used as: (a) productive area; (b) office area, (c) residential area; (d) storage area. Indication of the total number of observations and the zero values.

4.2.4. OTHER LOSS METRICS

In the typological-loss database, other significant quantities can be analysed to explore the variability of the seismic losses. The amount of insurance given (when present) and the final contribution granted are two indicators of the effort sustained by private companies and the Region. Furthermore, the percentage of the different components (A, C, B1 and D) of the estimated losses are provided, together with the statistical distributions of B1 and D, which are the technical fees and the professionals' fees, respectively. Finally, the PGA-based empirical fragility curves are derived at different damage states, providing an insight on the cumulative distributions of the intensity measures considered in the database. In the following analyses, the difference between local interventions and seismic retrofit at D1 (and D2) is not considered, as well as that between D5 and D5-POST.

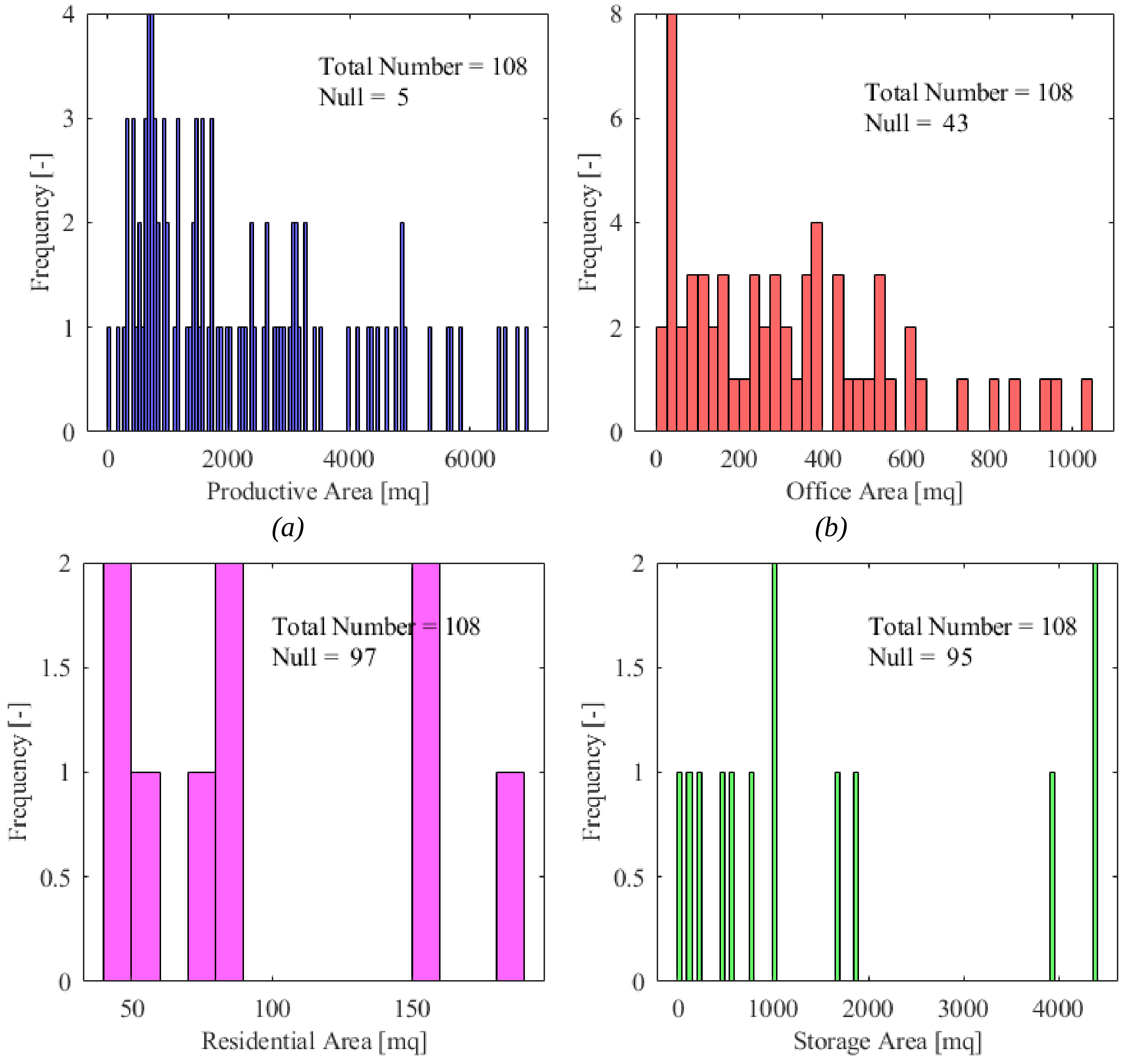

(a) *(b)*

(c) *(d)*

Figure 124. Distributions of the area in plan of buildings T3 used as: (a) productive area; (b) office area, (c) residential area; (d) storage area. Indication of the total number of observations and the zero values.

4.2.4.1. INSURANCE

In this Section, the total amount of insurance refunding in € is analysed including only the buildings with a coverage from private companies, i.e., 153 buildings over 600. No removal of the outliers is applied in this case. The median, the 16° and the 84° percentiles are evaluated at each damage state (Figure 125a) and for the different structural typologies (Figures 126a). Moreover, the percentage ratio of the insurance granted with respect to the total estimated costs has been computed and the median and the 16° and 84° percentiles of the ratios are reported in Figures 125b and 126b.

On average, the insurance granted increases with the increase of the damage level but the percentage ratio decreases, meaning that the amount given by companies could cover nearly the 30% of the total actual loss estimated at D5. Considering the different typologies, the median value of the insurance of T1 is almost twice those of the modern T2 and T3, but the coverage ratio is only slightly higher.

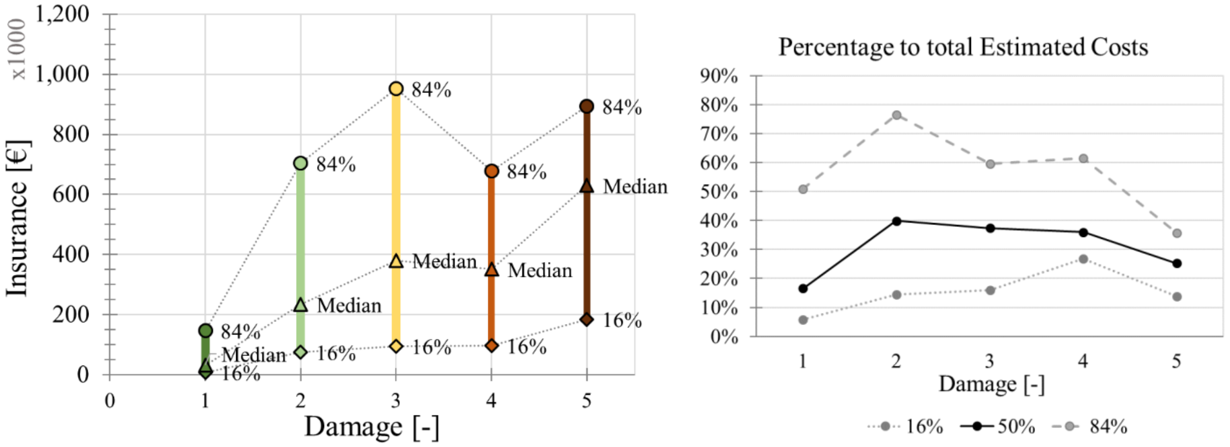

(a) *(b)*

Figure 125. Median value, 16° percentiles and 84° percentiles of: (a) insurance in € at different damage levels; (b) percentage ratio between insurance and total estimated cost at different damage levels.

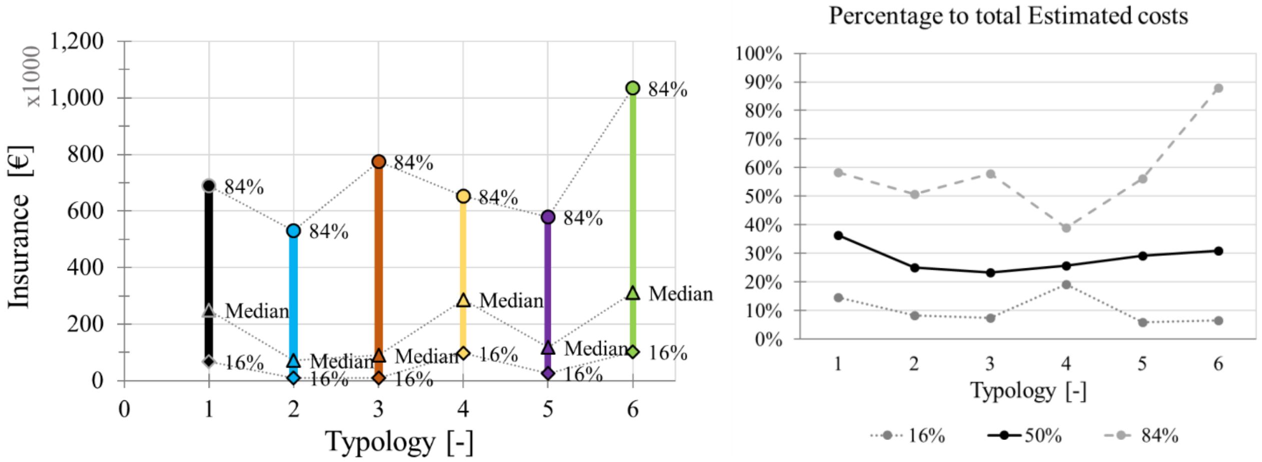

(a) *(b)*

Figure 126. Median value, 16° percentiles and 84° percentiles of: (a) insurance in € of different structural typologies; (b) percentage ratio between insurance and total estimated cost of different structural typologies.

4.2.4.2. REGIONAL CONTRIBUTION GIVEN

The final contribution granted by the Region in € is computed as the lowest value between the Conventional cost and the Estimated cost subtracted by the Insurance, if present. No removal of the outliers is applied in this case.

Figure 127 provides the median, the 16° and the 84° percentiles at each damage states and considering the six different structural typologies. The absolute monetary grant given by the Region has analogous values at the first four damage levels, while is almost three times higher at D5, reaching peaks of more than 2 billion €. Considering the different typologies, the values are similar for all the typologies; apart from T4 (shed buildings) for which there are not enough data to provide a reliable estimate of the losses, as previously mentioned.

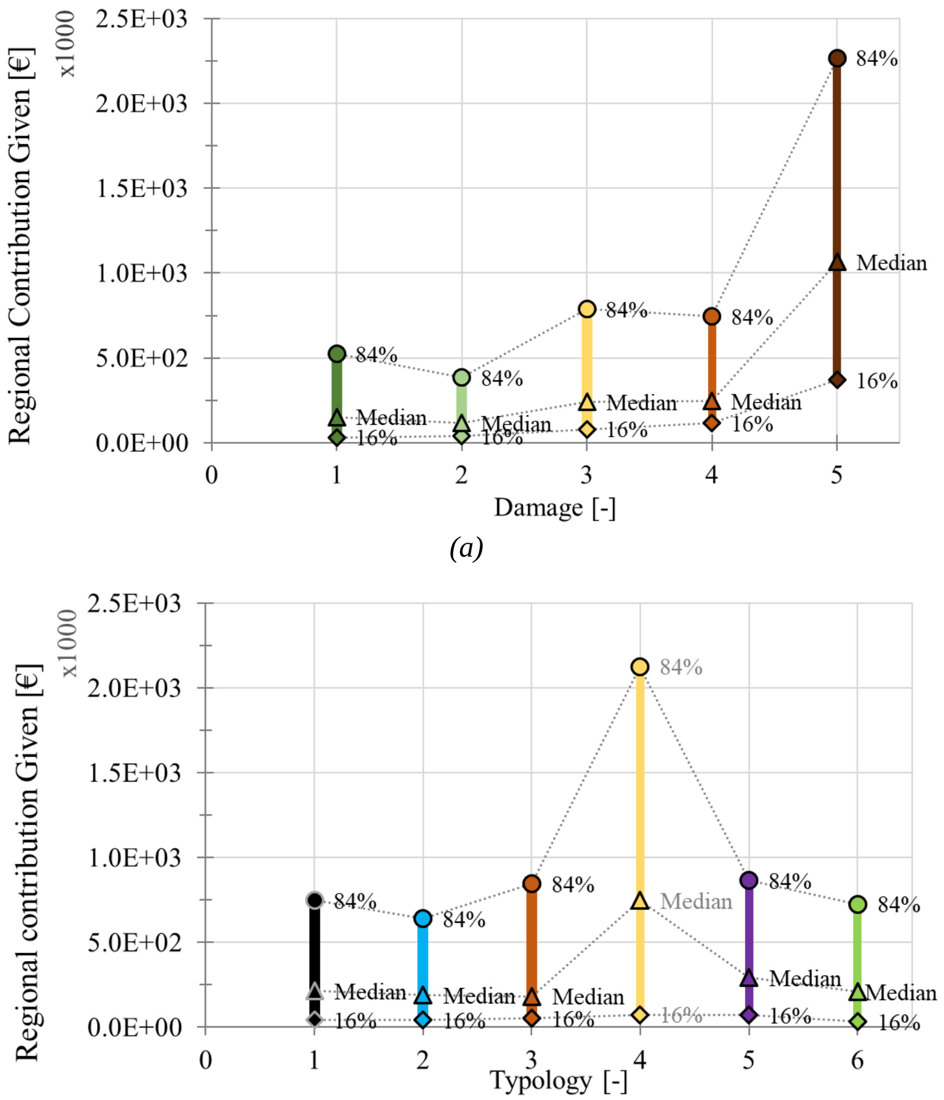

(a)

(b)

Figure 127. Median value, 16° percentiles and 84° percentiles of the regional contribution given in €: (a) at different damage levels; (b) of different structural typologies.

4.2.4.3. PERCENTAGE OF DIFFERENT LOSS COMPONENTS

The estimated losses can be partitioned into four different components: the structural costs for the reparation of buildings (A), the technical fees (B1), the non-structural costs due to the repair of the finishing and the ordinary plants (C), the professionals' fees due to the architectural and structural projects and the direction of the construction site (D). The percentage ratio of each component with respect to the total estimated costs has been computed, and the median, the 16° and the 84° percentiles at different damage levels are shown in Figure 128. Figure 129 reports an insight of the structural and non-structural costs evaluated for typologies T1, T2 and T3. The outliers have not been removed.

Around the 80% of the losses is represented by the structural costs only, while the 15% by the finishing and plants. Components B1 and D constitute a minor fixed percentage of the total losses. On average, it is possible to infer that at damage level D5 (entire reconstruction of the buildings) the percentage of the structural costs decreases, while the percentage of the non-structural costs increases. This effect is evident for all typologies together (Figure 28) and for T1 and T2, but not for T3 (Figure 129).

It is worth mentioning that in this analysis the losses due to the reparation of the industrial equipment and the restoration of damaged products are not considered, and these are expected to be significantly higher. Indeed, additional separate requests were compiled for the recovery of these quantities, but only in some specific cases and cannot be adopted here for an intra-building statistic.

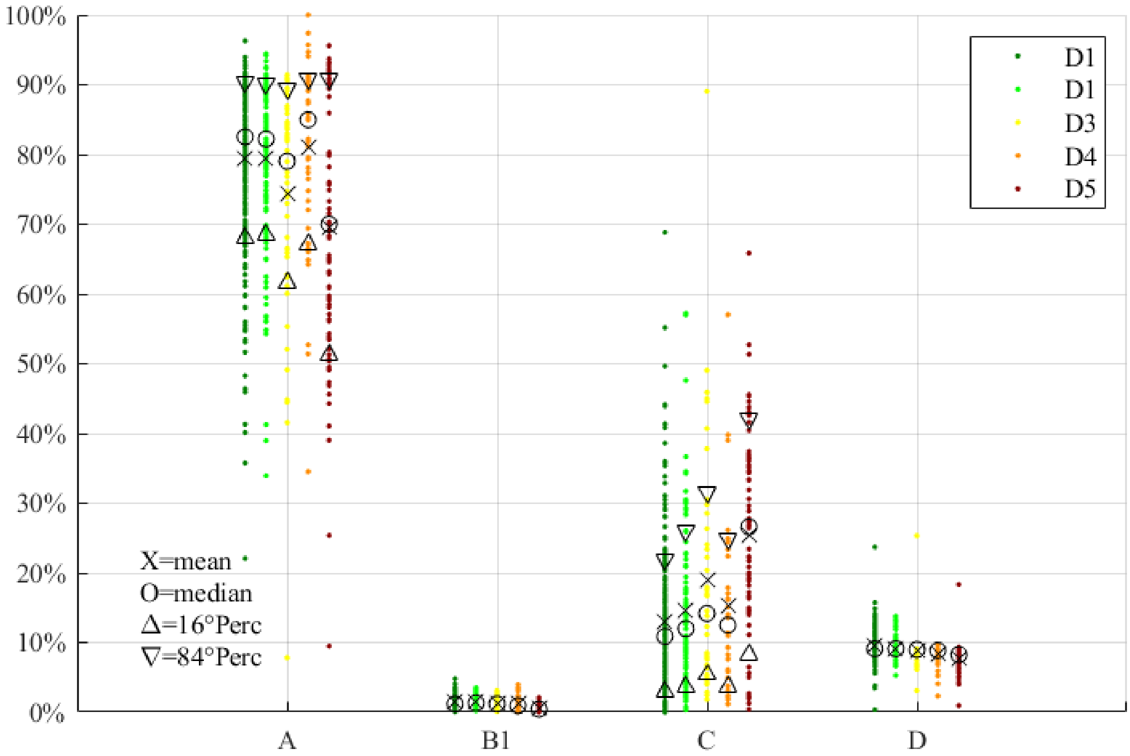

Figure 128. Percentage distribution of the component of estimated losses at different damage levels: A-structural costs, B1-technical fees, C-non-structural costs, D-professionals' fees.

4.2.4.4. TECHNICAL FEES (B1, D)

The technical fees are typically computed as a percentage on the total costs estimated. It is worth recalling that B1 are the technical fees not depending on the typology of intervention, such as the registration in the land-office, the environmental reports and the evaluation of conformity; and D are the professionals' fees.

In Figures 130 and 131 the losses B1 and D are reported in €/mq, respectively. No removal of the outliers is applied. The median and the 16° and 84° percentiles are evaluated at each damage states and for the different structural typologies.

Both technical costs B1 and D increase with the increase of the damage, following the general trend observed for the total estimated losses. The losses of B1 are almost negligible compared to those of category D, in particular at the highest damage degrees. It is worth observing that the median of the B1 losses at the fifth damage states is nearly one tenth of that of the D ones.

Since these technical costs are proportional to the total amount of losses, T1 is more expensive than T3, while T2 is intermediate, in line with the observations presented in Section 4.2.3.

The low values of costs B1 and D with respect to the total losses in €/mq observed in Section 4.2.2 confirm the outcomes presented in the previous paragraph, meaning that these costs weight less than the 10% on the total amount estimated. Thus, with a good approximation these may be neglected in the analyses, since only the structural and the non-structural components of the losses may be examined for production buildings.

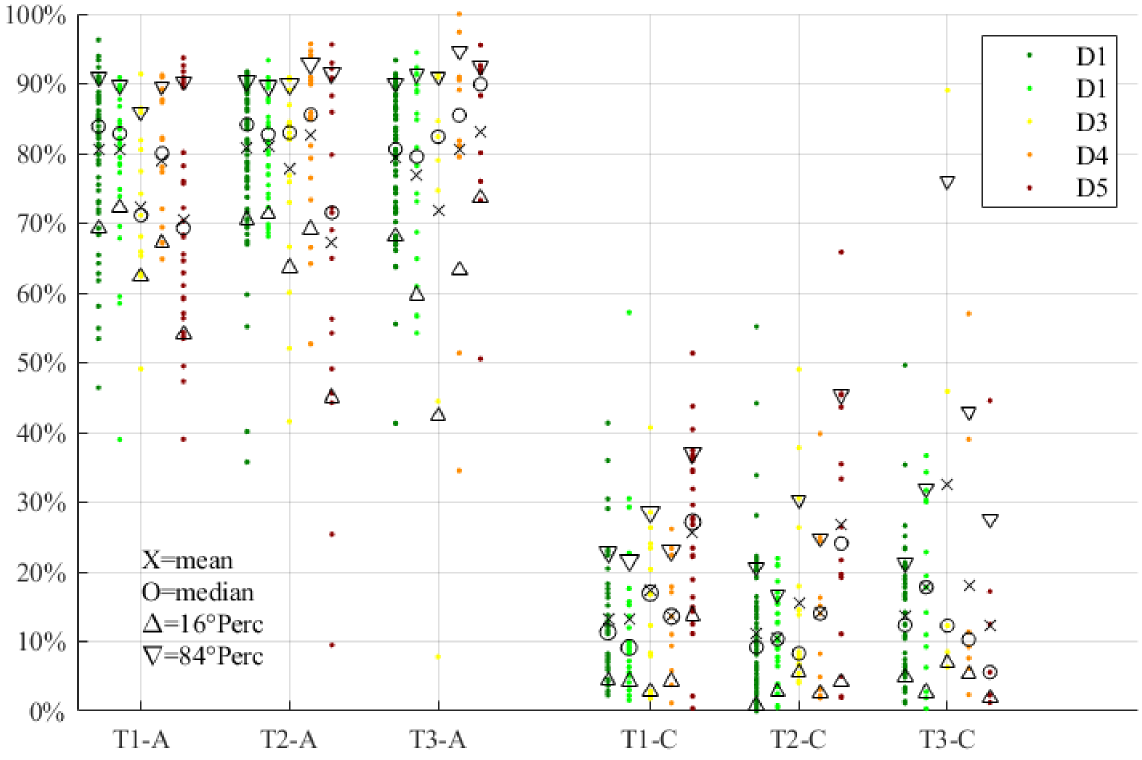

Figure 129. Percentage distribution of structural (A) and non-structural (C) losses of typologies T1, T2 and T3 at different damage levels.

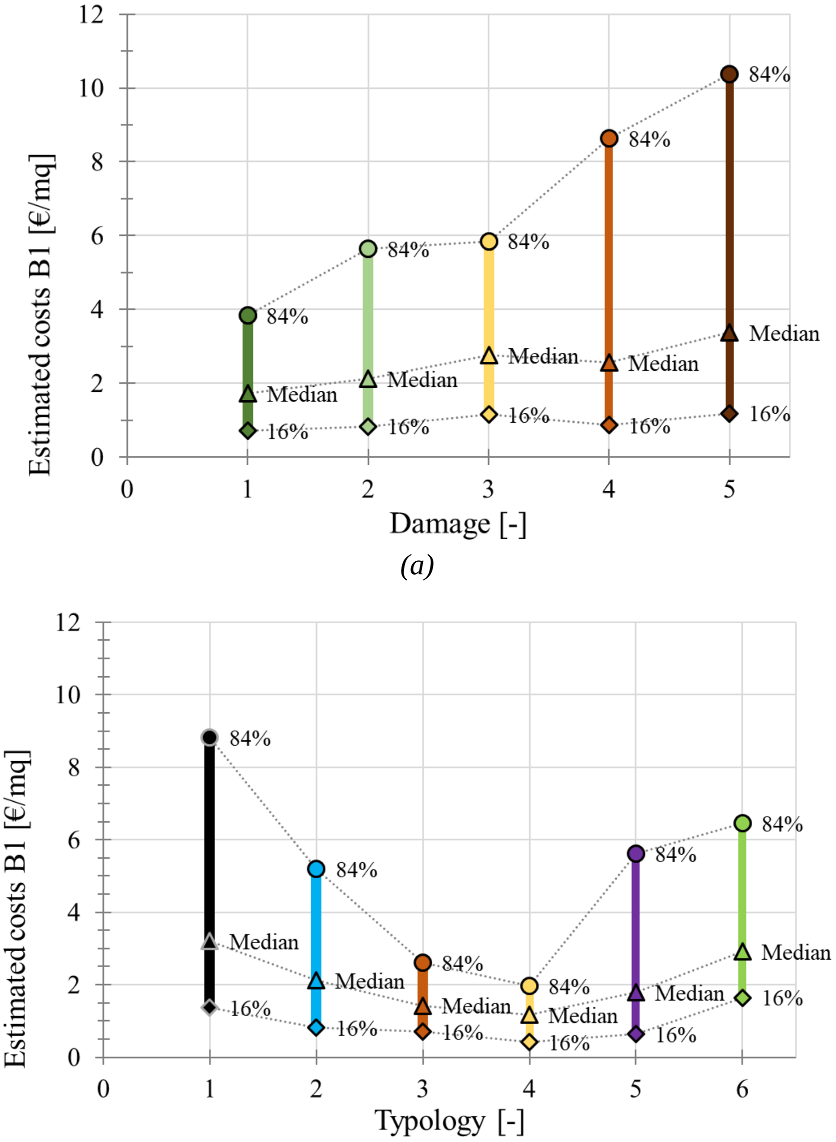

(a)

(b)

Figure 130. Median value, 16° percentiles and 84° percentiles of the technical fees B1 in €/mq: (a) at different damage levels; (b) of different structural typologies.

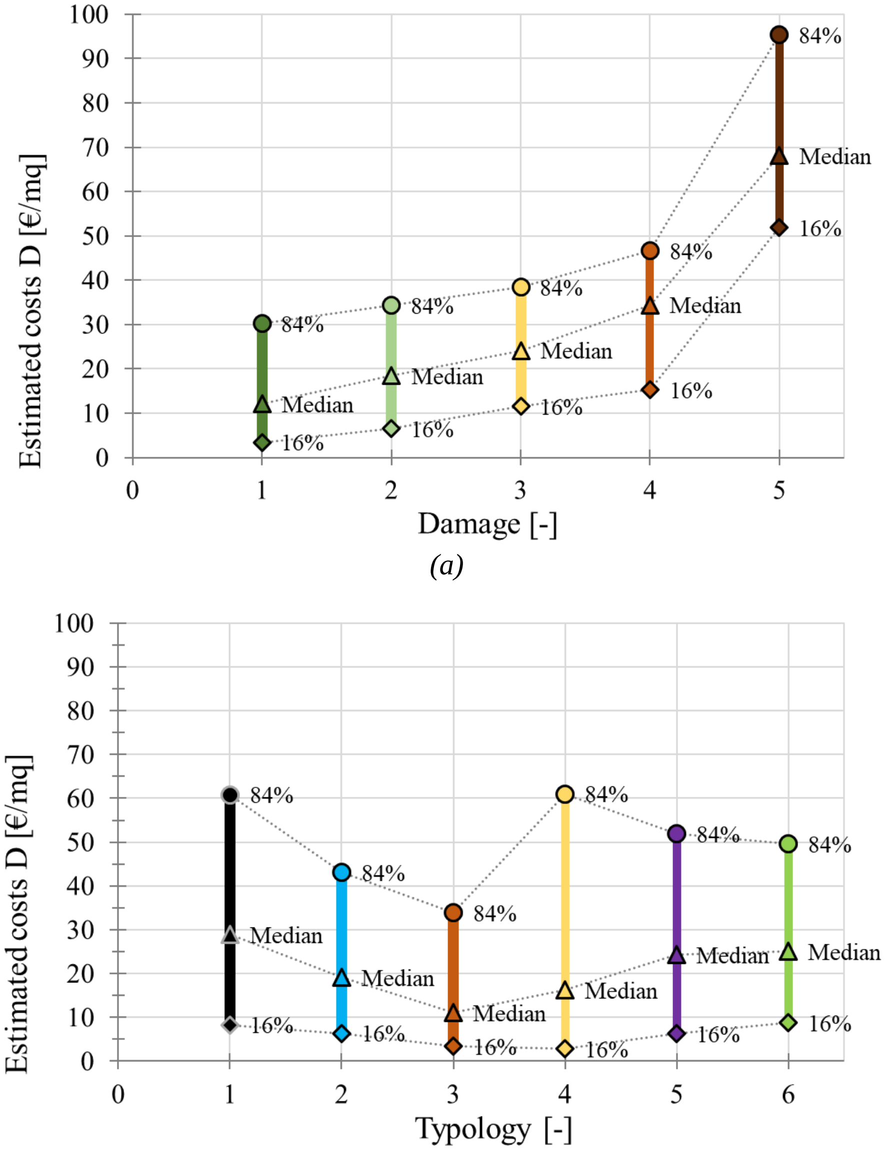

(a)

(b)

Figure 131. Median value, 16° percentiles and 84° percentiles of the technical fees D in €/mq: (a) at different damage levels; (b) of different structural typologies.

4.2.4.5. PGA-BASED FRAGILITY CURVES AT DIFFERENT DAMAGE LEVELS

The maximum PGA occurred in 2012, estimated through the shake-maps at the exact location of the 600 buildings in the database, are analysed to derive the empirical fragility curves at different damage levels. The log-normal fitting functions are proposed in Figure 132 for comparison, thus, the cumulative distributions of the data are shown individually at each damage state in Figure 133. The main descriptors of each function are reported in the cumulative distributions with letters μ and σ, together with the mean and the standard deviation of the samples.

The curve at damage level D1 has a significantly lower mean value compared to that of the others, which are very similar to each other and difficult to distinguish. This is because the lognormal functions at damage levels D2 and D3 are not able to fit appropriately the lower PGA samples (see Figure 133b and 133c), thus they present a high mean value μ. The curves obtained may be compared with those presented in Buratti et al. (2017). The one at D1 presents a similar mean value (around 0.17 g) compared with that reported by the authors, while the other curves presented here have a μ similar to that at the highest damage level.

The differences are due to the use of a lower number of input data, different shake-maps and fitting models. In particular, the possibility to predict the PGA of the buildings located close to the epicentres (and inside the faults) increases considerably the PGA values compared to those officially published by INGV after the Earthquake and adopted in Buratti et al (2017), as emerged in Figure 57. For this reason, the fragility curves obtained should be used with care for stronger ground-motions.

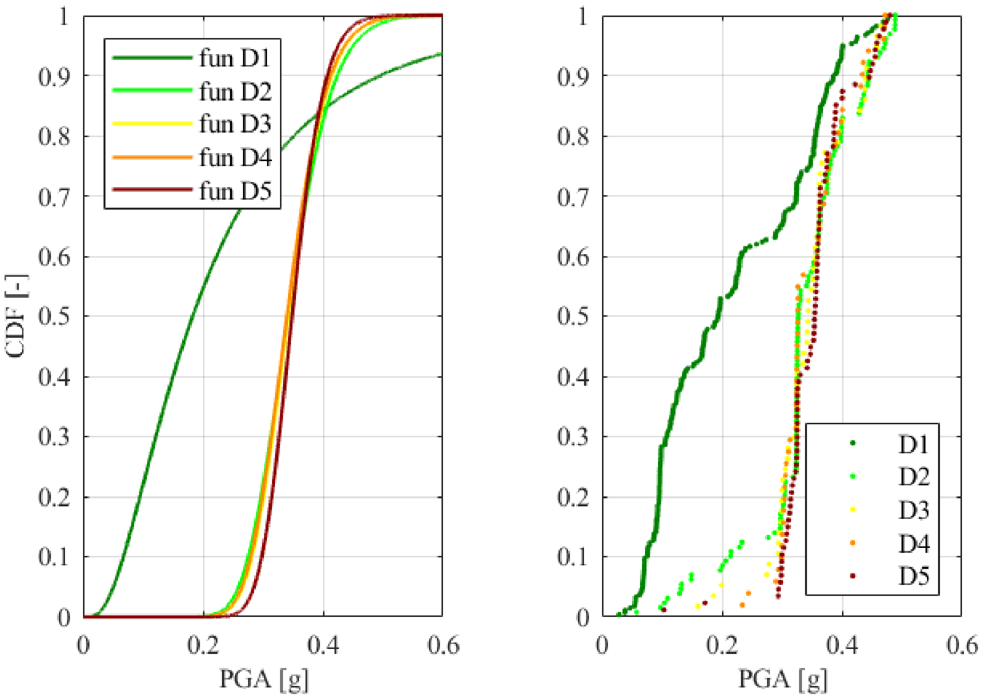

(a) *(b)*

Figure 132. Cumulative distribution of the PGA values and lognormal fitting curves at different damage levels: (a) lognormal fitting curves; (b) cumulative representation of the data.

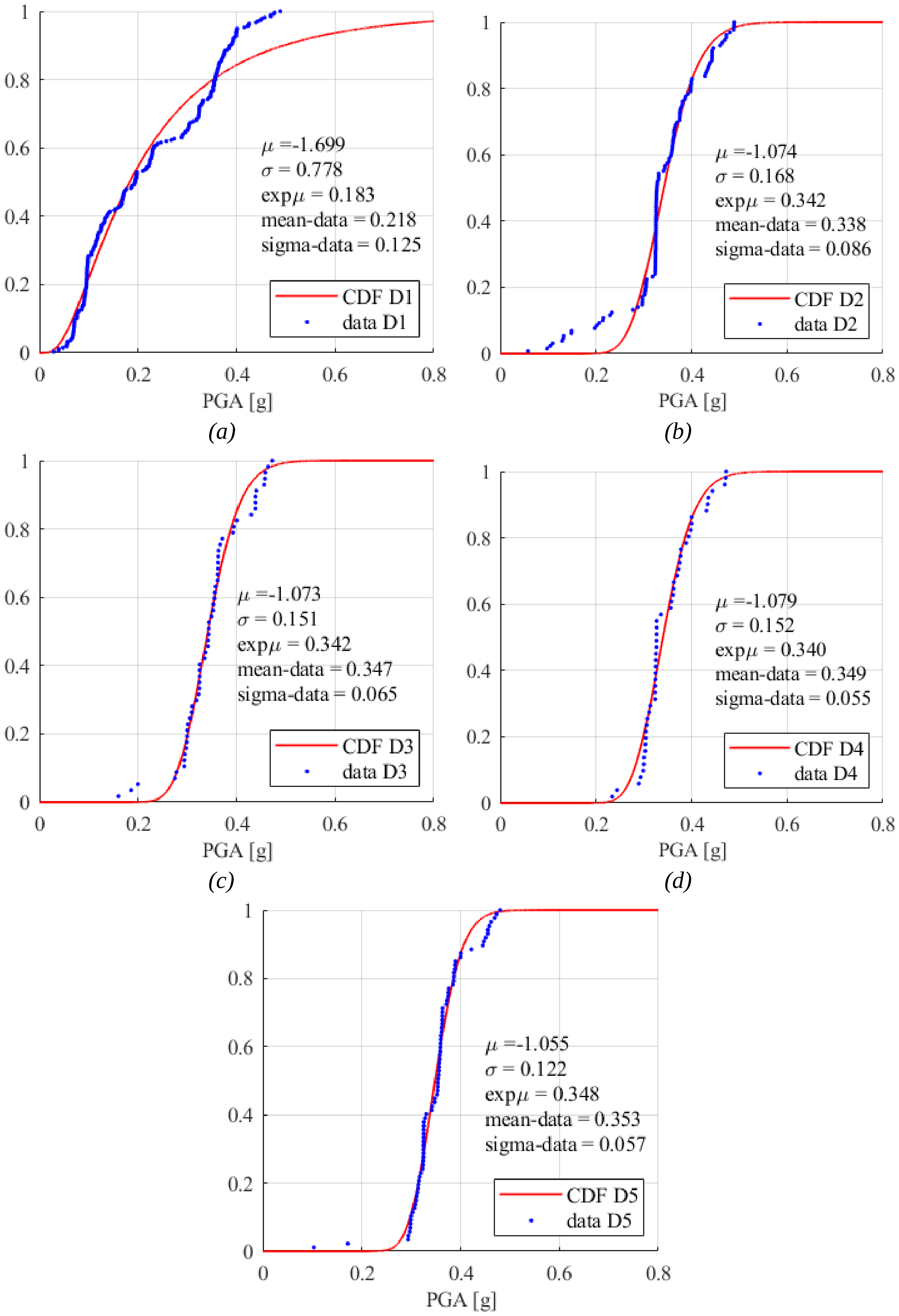

(a) *(b)*

(c) *(d)*

(e)

Figure 133. Empirical fragility curves at different damage levels: (a) D1; (b) D2; (c) D3; (d) D4; (e) D5. Indication of the main descriptors of the functions, and the mean and the standard deviation of the data.

4.3. THE STRUCTURAL-LOSS DATABASE: A SUB-SET OF 150 PRECAST RC BUILDINGS

The structural-loss database is constituted by a sub-set of 150 buildings selected in the typological-loss one, for which a detailed documentation of the structural-geometrical features was available. The buildings selected belong to typologies T1, T2 and T3 only, since these are the most common ones in the seismic area.

The geographical scheme in Figure 134 shows the position of the precast buildings, divided per damage level. The buildings are randomly located in the seismic area, and rather homogenously divided into damage levels, as shown in Figure 135. Indeed, there is a total value of 30 buildings at all damage levels, except 32 buildings at D3. However, there is a slight lower number of buildings for typology T3, i.e., 45 buildings against 54 buildings for T1 and 53 for T2.

Figure 136 illustrates the distribution of the three typologies in the main industrial districts of the area. The highest number of buildings are positioned in the clusters of Mirandola, San Felice sul Panaro, Finale Emilia, Medolla and Cavezzo, which are located close, or inside, the two faults.

In this database, the removal of the outliers of the losses is not applied since the number of observations is significantly lower. Nevertheless, the availability of detailed structural-geometrical data of the precast buildings allows performing additional investigations on the variability of the seismic losses, and classify the structural information of the typologies. In addition, by adopting the shake-maps (Buratti et al. 2022), the maximum PSA between those computed in the events of the 20th and the 29th May 2012 is calculated at the fundamental period of vibration of each structure.

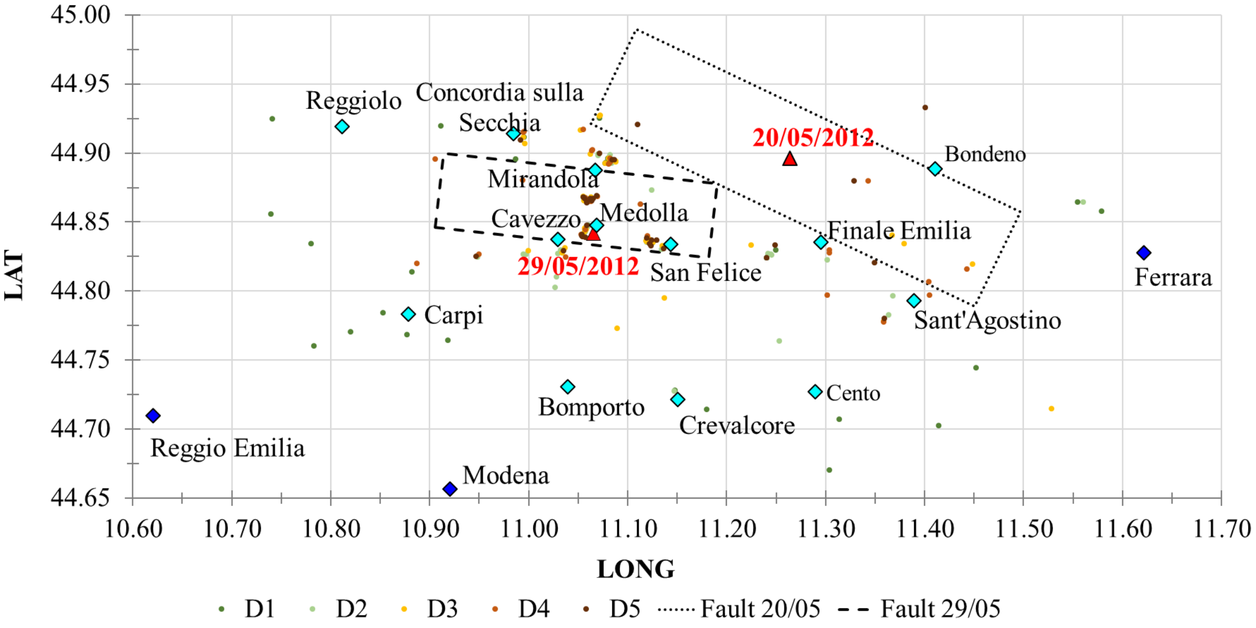

Figure 134. Geographical distribution of the buildings in the structural-loss database at different damage levels; position of the main cities in blue; of the main industrial districts in light-blue; of the epicenters of the main-shocks of 2012 in red, and identification of the faults. Coordinates are in decimal degrees.

4.3.1. FEATURES OF T1, T2 AND T3

The structural features of the buildings in the database are analysed in this Section, together with any additional relevant information derived from the documents. First, the year of construction is schematically illustrated in Figure 137. Figure 137a reports the construction year of the buildings for which an exact information was available. For the remaining buildings, a time interval has been identified considering the similarities with the other units based on the geometrical layout and the structural elements, and reported in Figure 137b. As mentioned previously, the oldest buildings are confirmed to belong to typology T1, while the most recent to T3. Both T2 and T3 buildings are built

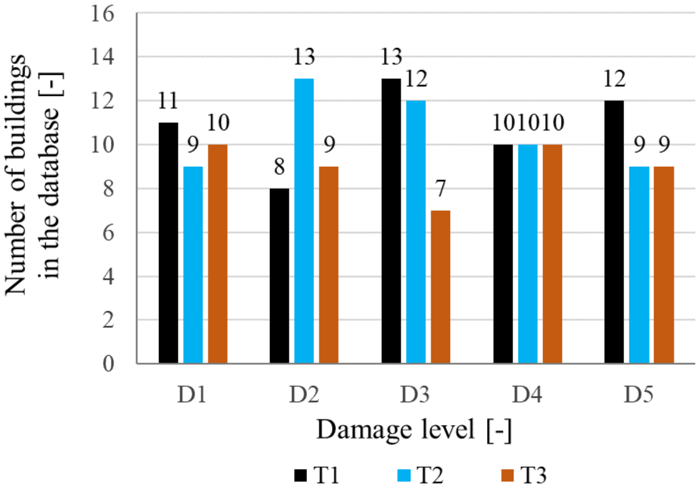

Figure 135. Composition of the structural-loss database: disaggregation of the number of buildings depending on the damage state and the structural typology.

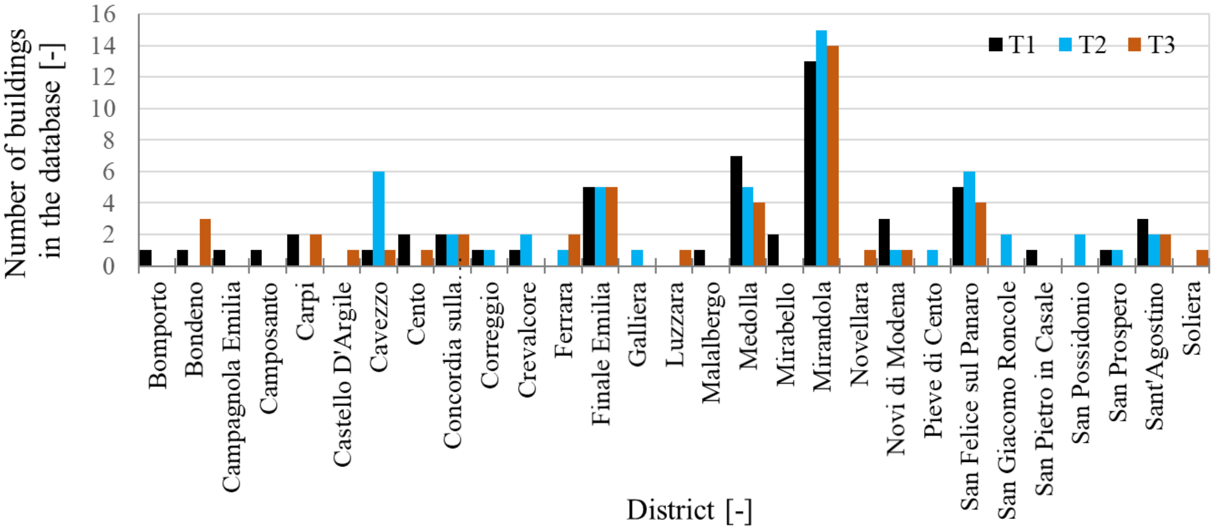

Figure 136. Distribution of buildings T1, T2 and T3 in the database, in different districts.

after the 80’s, as described in Section 4.1, while the construction years of buildings T1 in the database do not overcome year 2000.

Another information reported in the repository is the number of workers registered in the buildings at the time of the earthquake. Due to the lack of information in many units, only the remaining data have been studied. The average number of workers in the buildings was 61 for typology T1, 90 for typology T2, and 100 for T3. The average values reflect the dimensions of the corresponding building typologies, even though they are derived from information available in the 43% of T1 units, the 45% of T2 and the 71% in T3 in the database. This data may be adopted in loss models to forecast possible direct seismic consequences such as the number of injured and the fatalities.

Further information regarding the use of the buildings is given in the cadastral category. The Italian cadastre is divided into categories according to the activities undergoing in the real estate units. The main cadastral categories found in the database are D/7 (33% of the structures) meaning buildings hosting a specific industrial activity, D/8 (11%) meaning commercial activities, and D1 (10%) representing the factories. Other few buildings are marked C/3 (5 units) which is for laboratories of manufacturers, C/2 (3 buildings) meaning small buildings used as storages, D/10 (1 building) for agrifood activities, while for the 40% of the units in the database there is no information.

A more accurate definition of the specific activities is given in the ATECO code, which is available for all the buildings in the database. The ATECO code allows distinguishing the different economic activities classified according to the Italian institute of statistics (Istat 2007) with a series of letters

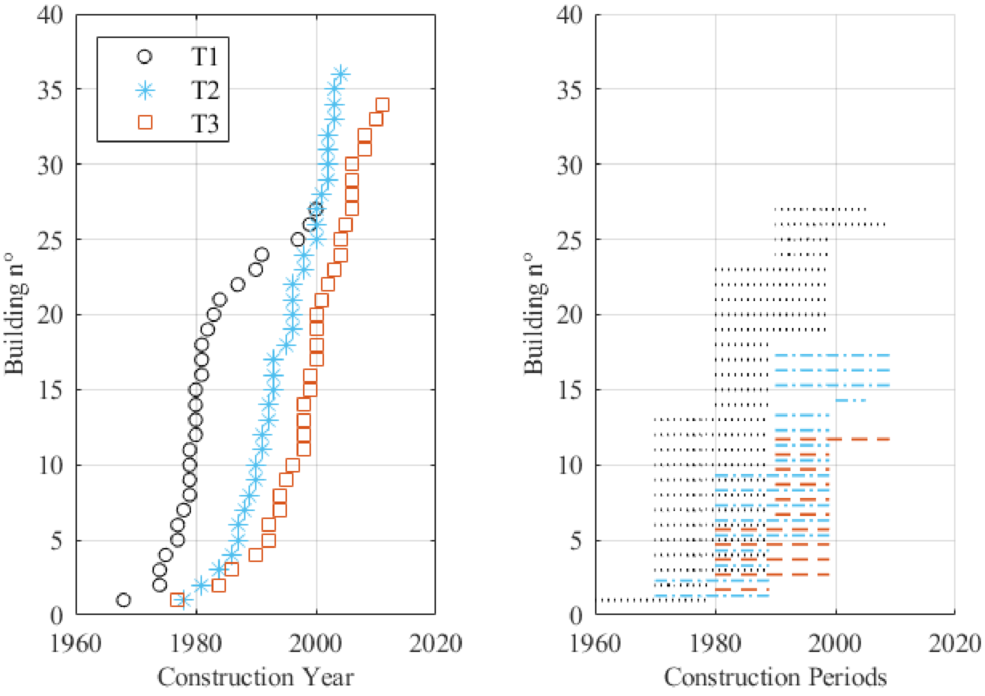

(a) *(b)*

Figure 137. Construction year of buildings T1, T2 and T3 in the database: (a) exact construction year of the buildings; (b) construction period associated to buildings with no indication of the exact year.

and numbers. The predominant activities in the typologies T1, T2 and T3 are the manufacturing activities (section C), whose most recurrent are the production of metal products (C-25), the production of machineries (C-28), and the textile industries (C-23). This is valid for the 60% of buildings T1 and T3, and the 55% of T2 in the database. Others less common activities consist in the commerce and reparation of moto-vehicles (G-45), and the construction and building activities (section F).

Concerning T1, some other relevant categories are the sport activities (R-93), the production of electronic equipment (C-26), and other manufactories (C-32). In typology T2, additional activities concern the meat production (C-10), the textiles (C-14), and the storage of garbage (E-38). In T3, it is also worth mentioning the production of paper (C-17), the refinement of minerals (C-23), the production of furniture (C-31), and the trading of food products (G-46).

It is worth noting that all the buildings in the database have been geo-referenced with the coordinates or the address given in the documents. For each building, the geographical orientation of the main beams with respect to North (0°) has been registered. This is achieved by means of a detailed inspection of the satellite pictures in the pre-earthquake years available in Google Earth (2021).

This information is reported in Figure 138, for the different typologies at each damage level. The majority of the buildings are oriented between 0° and 30°, and between 90° and 120° following the layout of the main streets. It is worth saying that these values are analogue to those observed in the work presented in Section 3.3.2.1: the cluster considered in San Felice has the main average orientations, even if calculated with a different reference system. From Figure 138, it is not possible

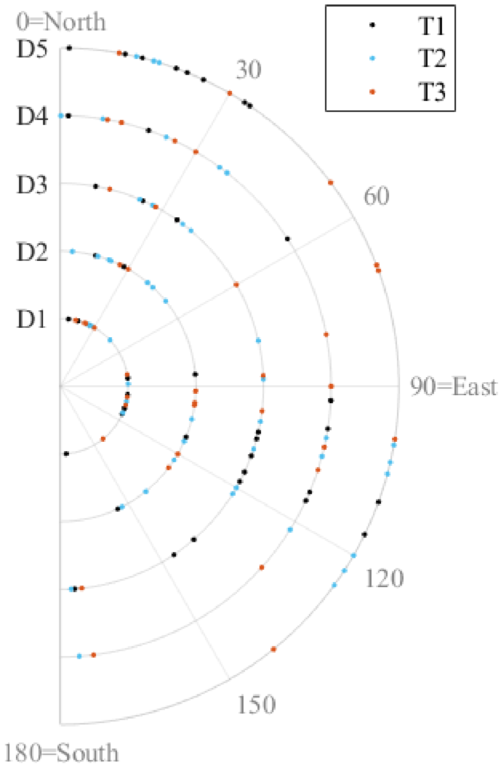

Figure 138. Geographical orientation of the main beams of buildings T1, T2 and T3 in the database, at different damage levels.

to draw conclusions about the effect of the directionality of the ground-motion on the damage states, since the buildings come from different districts. However, this data may be adopted to perform damage scenario assessments of different industrial districts, such as that described in Section 3.3.

Another important aspect is the geometry of the buildings, which is distinctive for each typology. Indeed, different column sections and height characterize the buildings of T1, T2 and T3. Figure 139 illustrates the maximum sectional dimensions found among the columns of each building, for the three typologies, in which 'X' is the direction of the main beams. The smaller spans of buildings T1 lead to lower axial loads on the columns resulting in smaller sections, while those of structures T3 are larger. Indeed, some column sections in the T3 buildings in the database reach width of more than 1 m. Since the points are mainly concentrated along the diagonal of the graph, the majority of the columns have a squared section. From the Figure, it is not possible to infer how many buildings feature the same sectional dimensions of columns. The mean values of the maximum sectional dimensions are (XxY directions): 44.7 cm x 43.5 cm for T1, 49.2 cm x 46.7 cm for T2, 53.4 cm x 52.7 cm for T3.

The height of the columns is in line with what observed previously, since the precast buildings T3 and T2 have higher columns compared to T1 ones. The distributions of the height of the columns, up to the main-beams, can be observed in Figure 140, in which the bin-width of the histograms is 0.5 m. The mean values are: 5.7 m for columns in T1, and 6.3 for both T2 and T3.

Other relevant information concerning the structural layout of the buildings in the database are the presence of local elements that can be source of irregularity or vulnerability, and the typology of precast cladding elements on the perimeter. These are reported in Figure 141a and 141b, respectively. Concerning the first aspect, in the precast RC buildings there may be intermediate mezzanine floors, usually located on one side or corner of the plan, causing a source of irregularity in the seismic

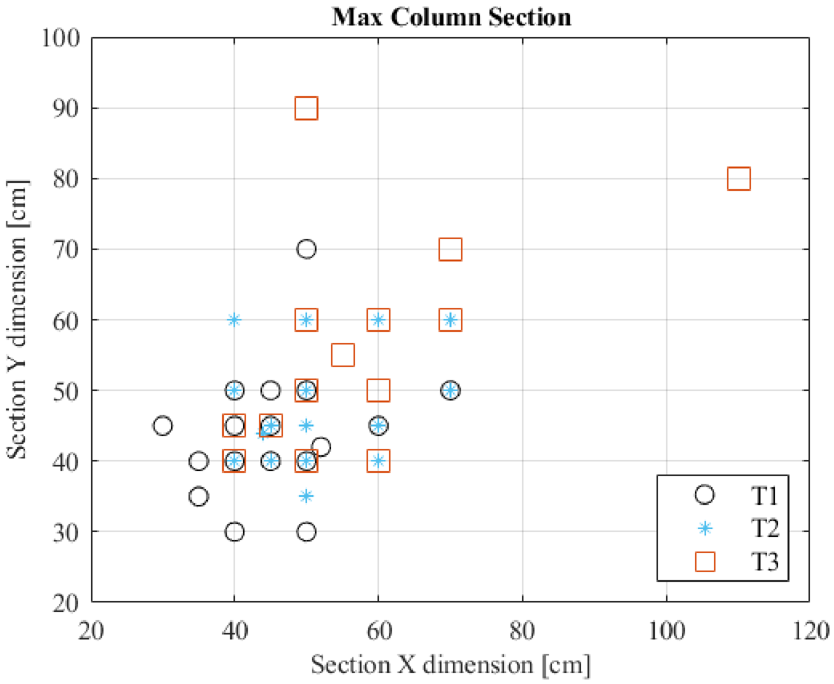

Figure 139. Maximum sectional dimensions of columns in buildings T1, T2 and T3 in the database.

behaviour. This major source of irregularity is constituted by intermediate floors with average surface of: 107 mq in T1 buildings, 155 mq in T2 and 285 mq in T3. The mean height of the intermediate floors is equal to 3 m in all the typologies.

Moreover, there may be local element of vulnerability in the roof due to the presence of shed elements or openings/panels for lighting purposes in few portions, interrupting the continuity of the structural elements. These are present in less than the 10% and almost the 60% of the buildings, respectively.

Finally, the most common source of seismic vulnerability, and one of the most frequent causes of failure (Savoia et al. 2012), is the presence of strip-windows on the facades. This last element of irregularity, at least on a portion of the perimeter of the buildings, has been detected in most of the units in the database, as shown in Figure 141a, and mainly in T1 buildings.

Regarding the typology of external cladding elements on the perimeter, Figure 141b shows the percentage distribution of the most common elements in the three typologies. The majority of T1 buildings has masonry infill walls placed between the external columns, T2 buildings mainly have horizontal precast cladding panels external to columns, and T3 buildings mainly feature horizontal and vertical precast cladding panels external to columns. This information may be adopted to perform large-scale seismic assessments, for instance using the fragility curves of the PRESSAFE-disp methodology (see Section 3.2).

The precast elements located in the roof feature different lengths, but the sections and the geometries are recurrent due to the high standardisation of the structural precast RC elements. Figure 142 illustrates the percentage distribution of different common typologies of main beams and secondary elements.

The T1 buildings mainly have double slope I beams supporting hollow-clay elements, TT secondary elements or box-hollow elements. The majority of T2 buildings feature double slope I beams, with different roof elements, mainly hollow-clay or TT secondary elements. The T3 buildings feature more recently developed solutions to cover larger spans, such as planar inverted-T beam supporting Y-shaped secondary elements, TT elements, or with wing-shaped elements. Indeed, the planar roofs with straight profiles usually characterize the buildings of typology T3.

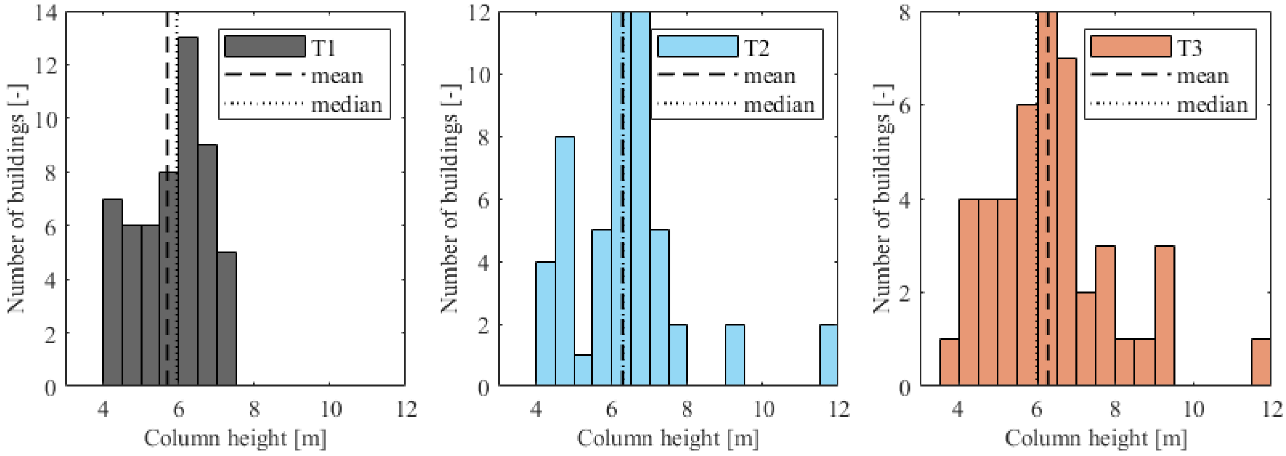

(a) (b) (c)

Figure 140. Distribution of the height of the columns up to the main beams in buildings: (a) T1; (b) T2; (c) T3. Indication of the mean and the median of the data.

Finally, it is worth observing that, in the pre-earthquake condition, the 58% of the buildings in the database have upper pocket supports at the top of columns to host the main-beams, while the 35% feature simply-supported beams with no restraints. For the rest of the units there was no information. In general, it was not possible to detect with precision the presence or absence of steel connectors between the structural elements.

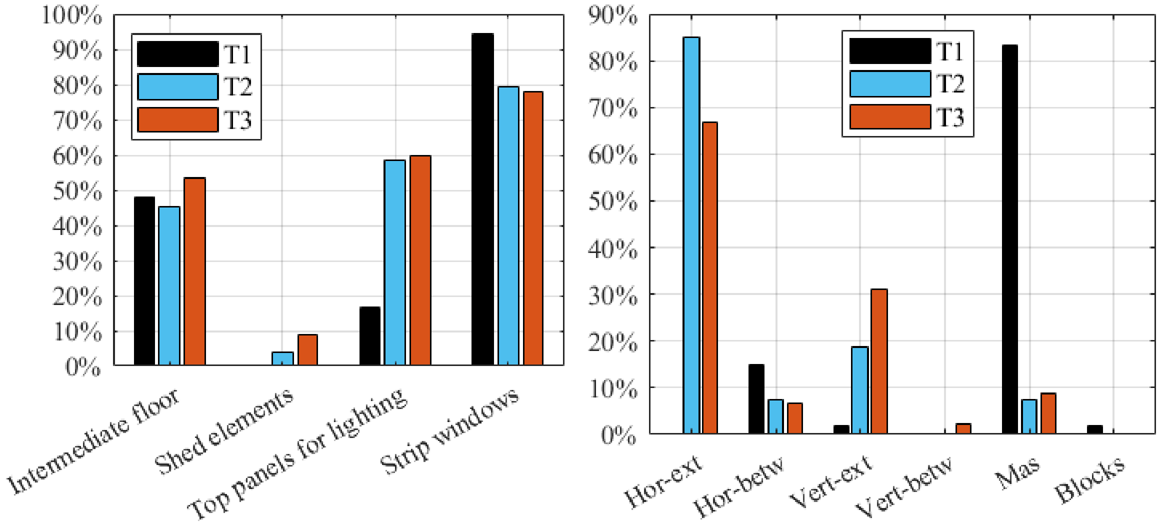

(a) *(b)*

Figure 141. Percentage distribution of specific features of the buildings of T1, T2 and T3: (a) different elements causing local irregularities; (b) different typologies of external cladding elements, in order: horizontal precast cladding panels external to columns; or between columns; vertical precast cladding panels external to columns; or between columns; masonry infill walls; precast RC blocks.

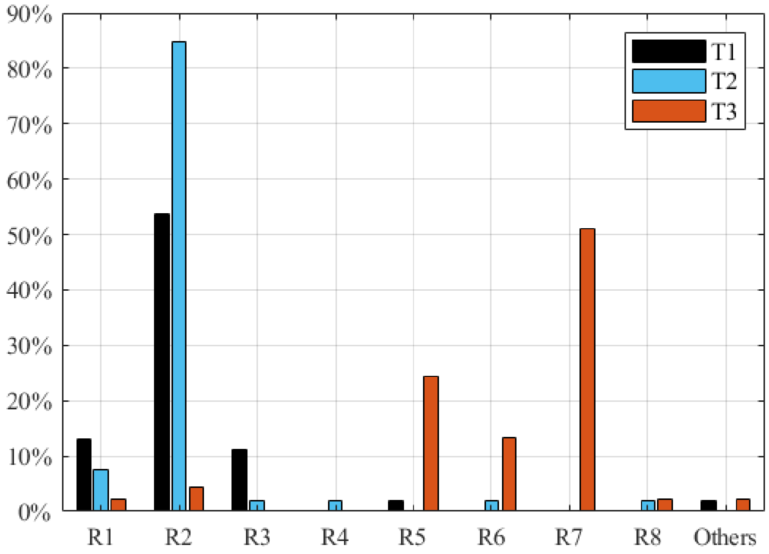

Figure 142. Percentage distribution of different roof typologies in the buildings of T1, T2 and T3. In order: double slope I beams with hollow-clay elements (R1); or with TT elements (R2); or with box-hollow elements (R3); or with W elements (R4); planar inverted-T beam with Y elements (R5); or with TT elements (R6); or with wing-shaped elements (R7); or with double slope secondary elements (R8); others.

4.3.1.1. DIMENSIONS IN PLAN

The three typologies of precast structures in the database are characterized by different arrangements in plan and different span dimensions. The layout in plan of the industrial buildings is usually regular, featuring repetitive spans.
The smaller dimensions of T1 and T2 buildings compared to the T3 ones are confirmed in Figure 143 reporting the total lengths on each side of the perimeter. However, there are few spare data of large T1 and T2 buildings: this is the case of big factories with several adjacent buildings, sharing the same columns in repetitive layouts.
Figure 144 and 145 report the dimensions of main beams and the secondary roof elements, and the number of spans on each side, respectively. The T3 buildings feature shorter main beams compared to the secondary elements, and have a higher number of spans in the direction of the main beams. The buildings of typologies T1 and T2 instead, have longer main beams and shorter secondary elements, with a higher number of spans in the direction of the secondary elements, which often represents the distance between the main frames. The newer T3 buildings feature slender horizontal precast elements able to cover longer spans, in particular the roof elements supported by the main beams.
Figure 146 and 147 illustrate the distributions of the length of the main beams and the secondary elements, respectively, adopting a bin-width of the histograms of 1 m. The aforementioned results are confirmed by the data illustrated and their mean values. Indeed, the beams in T1 are 16.7 m long on average, 17.8 m in T2 and 11.2 m in T3. The mean values of the roof elements lengths are: 7.2 m in T1, 8.7 m in T2 and 18.2m in T3.
The outcomes obtained here are, in general, in line with those presented in the statistical analysis of the precast buildings reported in Bellotti et al. (2014).

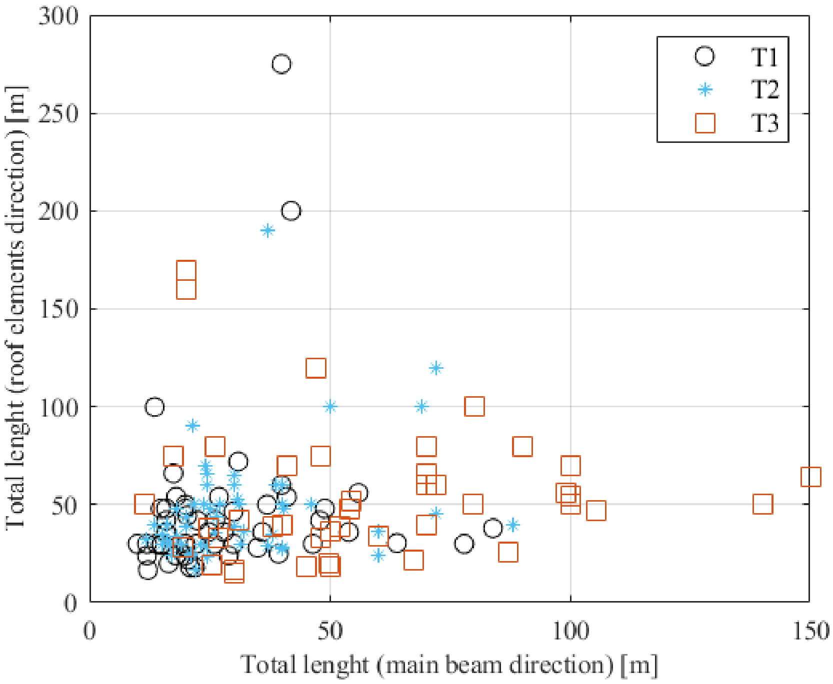

Figure 143. Total lengths of the two dimensions in plan of buildings T1, T2 and T3 in the database.

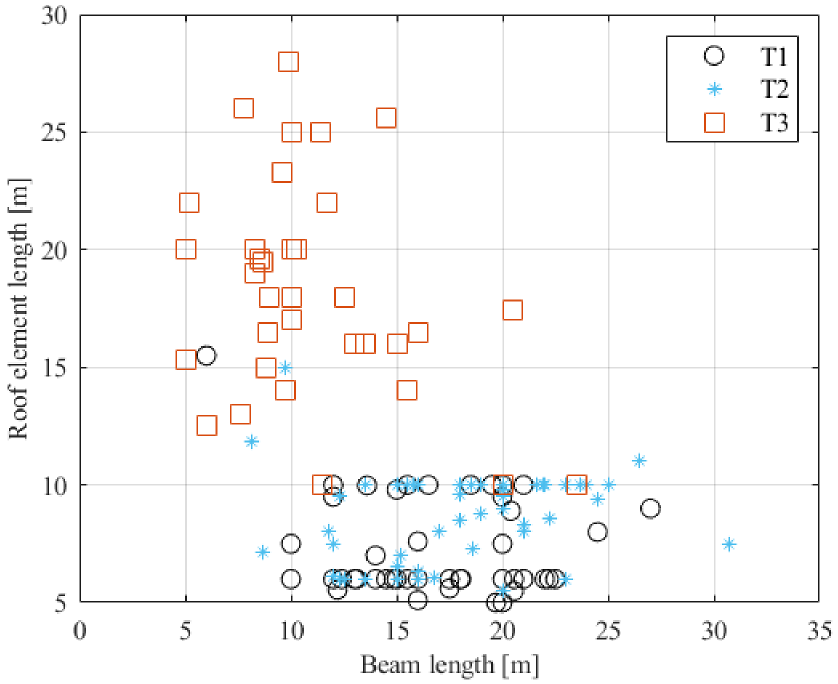

Figure 144. Lengths of main beams and secondary elements in buildings T1, T2 and T3 in the database.

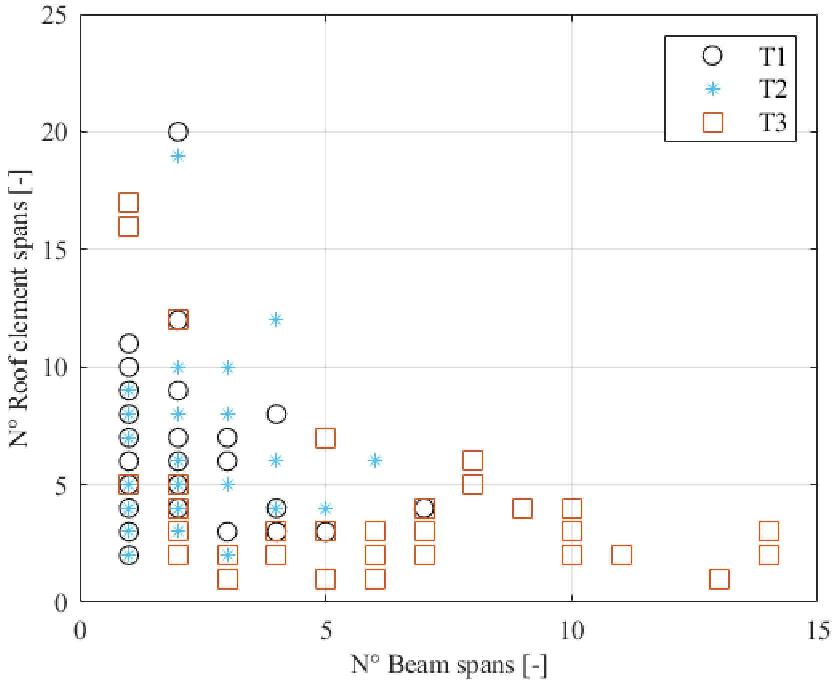

Figure 145. Number of spans in the two directions in plan of buildings T1, T2 and T3 in the database.

4.3.1.2. FIRST PERIOD OF VIBRATION AND SEISMIC DEMAND

Through the analysis of the data available in the documents, it was possible to estimate the fundamental periods of vibration of the industrial buildings. To obtain this, the geometry, the material and the mass have to be known. However, some information required (e.g., the material properties and the loads) were not available or well defined for all the units, and they were obtained from the literature or estimated through expert opinion. The first periods of vibration have been calculated considering the columns acting as cantilevers under the seismic action (see Equation 3.6).

The total mass is the summation of different contributions: the roof load, the self-weight of columns and the load of the cladding panels hung on the structural frames. The load of the main beams (per length) and the roof elements (per square meter) is computed considering the unitary weights given in Bellotti et al. (2014) and Bovo and Savoia (2021) for the most common precast sections.

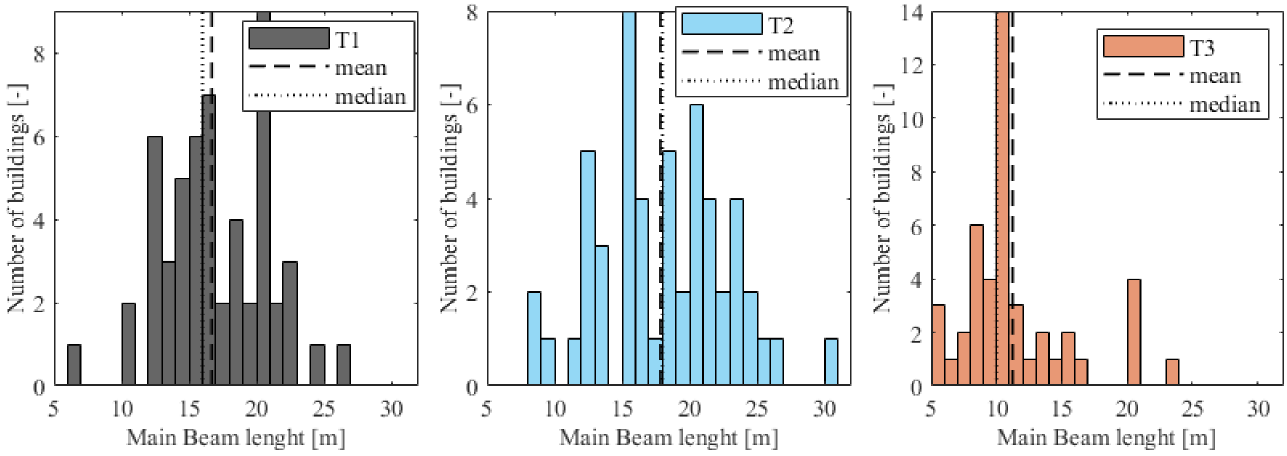

(a) (b) (c)

Figure 146. Distribution of the length of the main beams in buildings: (a) T1; (b) T2; (c) T3. Indication of the mean and the median of the data.

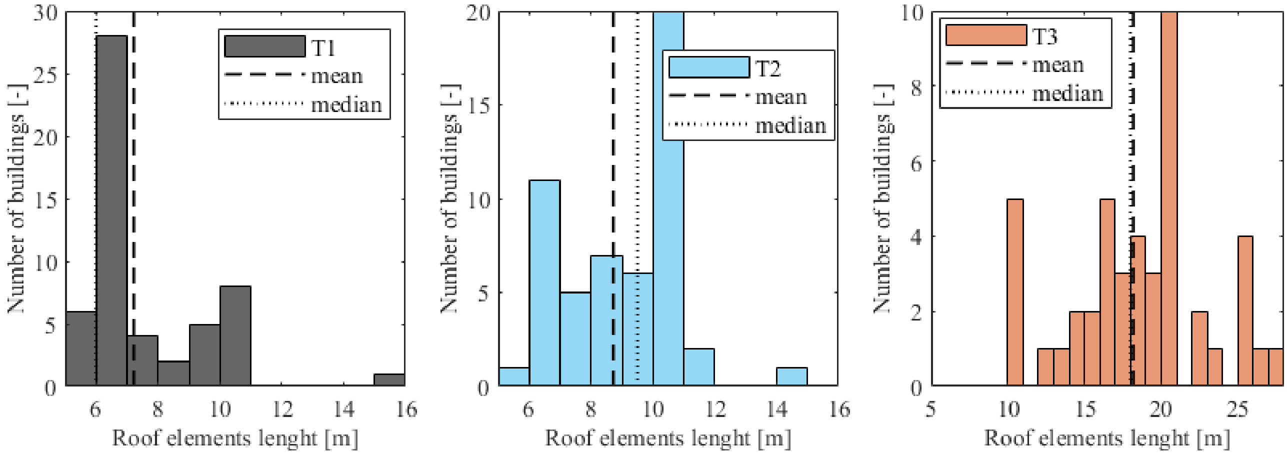

(a) (b) (c)

Figure 147. Distribution of the length of the secondary roof elements in buildings: (a) T1; (b) T2; (c) T3. Indication of the mean and the median of the data.

The exact weight of each element was assessed through a proportion based on the length of each element, in the intervals given by authors. The additional non-structural loads has been also taken into account. Similarly, the entire mass of the external panels was computed and reduced with a coefficient of 0.8 to account for the presence of openings on the perimeter (Colombo et al. 2016). The total seismic mass of each building was evaluated by summing the mass of the horizontal elements (main beams and roof) with the 37% of the mass of the vertical elements (columns and external panels). This is a simplified assumption taking into account that part of the vibrating mass of the vertical elements is carried by the structure, and part releases on the ground. Based on the hypothesis of cantilever columns in one-storey isostatic systems, the percentage mass transferred to the sustaining members is calculated following the suggestions given in Colombo et al. (2016). This assumption is considered acceptable at the scale of a territorial analysis, in which many uncertainties are present, to obtain a first estimation of the periods of vibration. Moreover, it is worth noting that during the seismic events of 2012 the widespread lack of appropriate connectors in the cladding panels caused their collapse before the attainment of the structural capacity of the frames, reducing their interaction with the structural elements (Savoia et al. 2012).

The elastic modulus of the material was calculated considering the average concrete resistance adopted in the classification described in Section 3.2, i.e., R_{ck} equal to 35 for typologies T1 and T2, and R_{ck} equal to 40 for the recent buildings T3. This allowed estimating the first period of vibration of the 150 buildings in the database, whose distributions are reported in Figure 148 for each typology, considering a bin-width of the histograms of 0.05 s.

The mean values of the periods are: 0.788 s for T1, 0.897 s for T2 and 0.887 s for T3. The lower average period of T1 buildings confirms their smaller dimensions, while T3 buildings have a longer mean period featuring higher columns and larger spans. In addition, T2 buildings have a slightly higher mean period of vibration due to the average height of the columns equal to that of T3 buildings (see Figure 140) but the similar plan dimensions of T1, leading to more flexible structures than T1. The values obtained, in general, are analogous with those observed in the analyses of Sousa et al. (2020) and Magliulo et al. (2018).

The availability of the periods of vibration permit the evaluation of the spectral acceleration (PSA) occurred in the seismic events at each building's location. The PSA are calculated through the shake-maps at the fundamental period of each structure, considering the highest value between those computed in the two main events. The distributions of the values obtained for each structural typology are reported in Figure 149, adopting a bin-width of the histograms of 0.05 g. The mean values are comparable, being: 0.448 g for T1, 0.421 g for T2 and 0.423 g for T3. The PSA-based fragility curves at the five damage states cannot be not derived since the periods of vibration of the buildings are all different.

Once the PSA and the periods are known, the spectral displacements PSD is evaluated. Indeed, the relationship between the quantities is straightforward and allows deriving another significant parameter of the seismic demand. The distributions of the values obtained for each structural typology can be observed in Figure 150, adopting a bin-width of the histograms of 1 cm. The mean values are: 6.68 cm for T1, 8.24 cm for T2 and 7.81 cm for T3. It appears that the more slender structures (T2 and T3) were subjected to larger displacements under the seismic action, as expected.

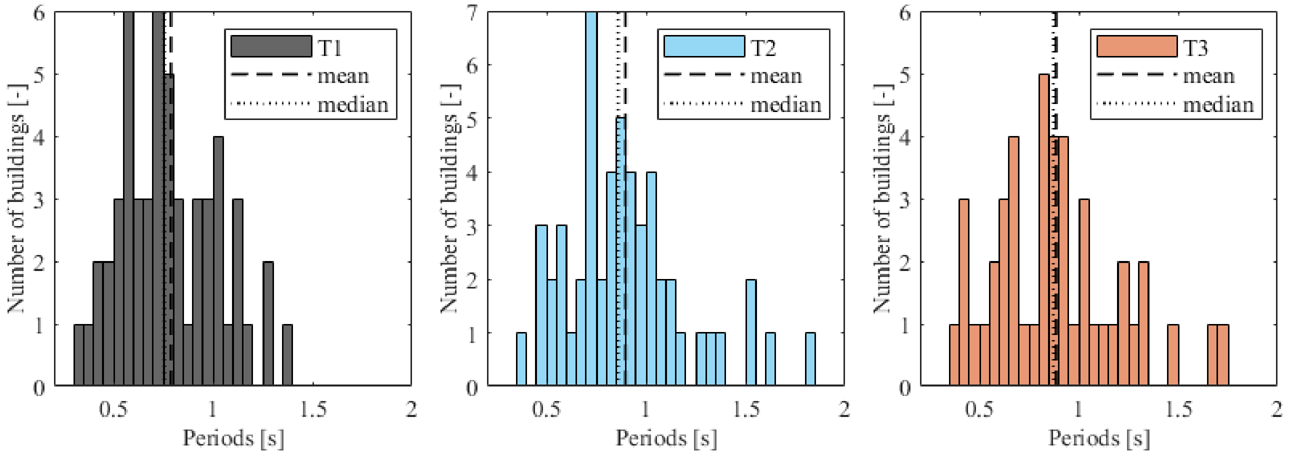

(a) *(b)* *(c)*

Figure 148. Distribution of the main periods of vibration of buildings: (a) T1; (b) T2; (c) T3.

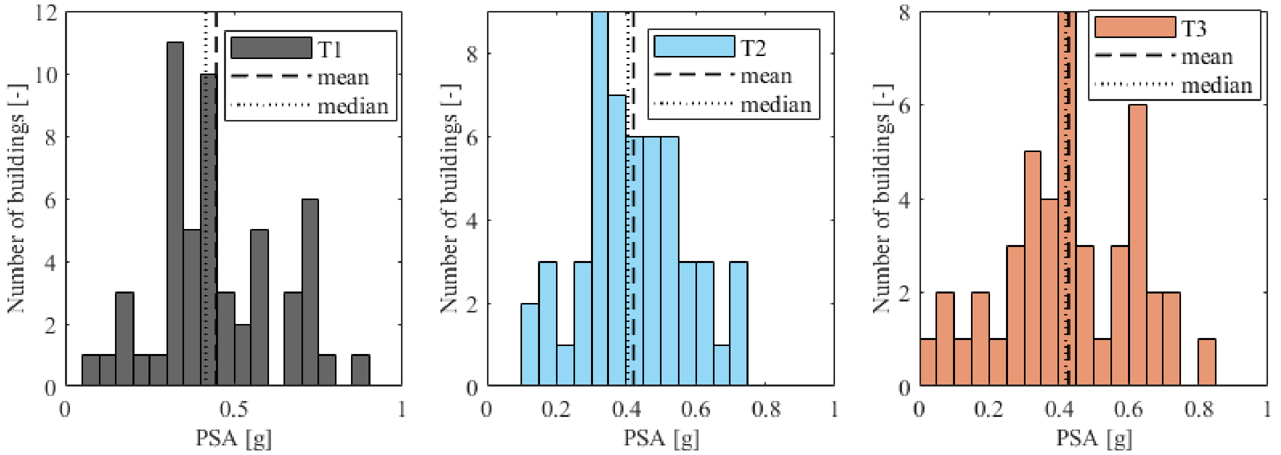

(a) *(b)* *(c)*

Figure 149. Distribution of the spectral accelerations PSA(T_1): (a) T1; (b) T2; (c) T3.

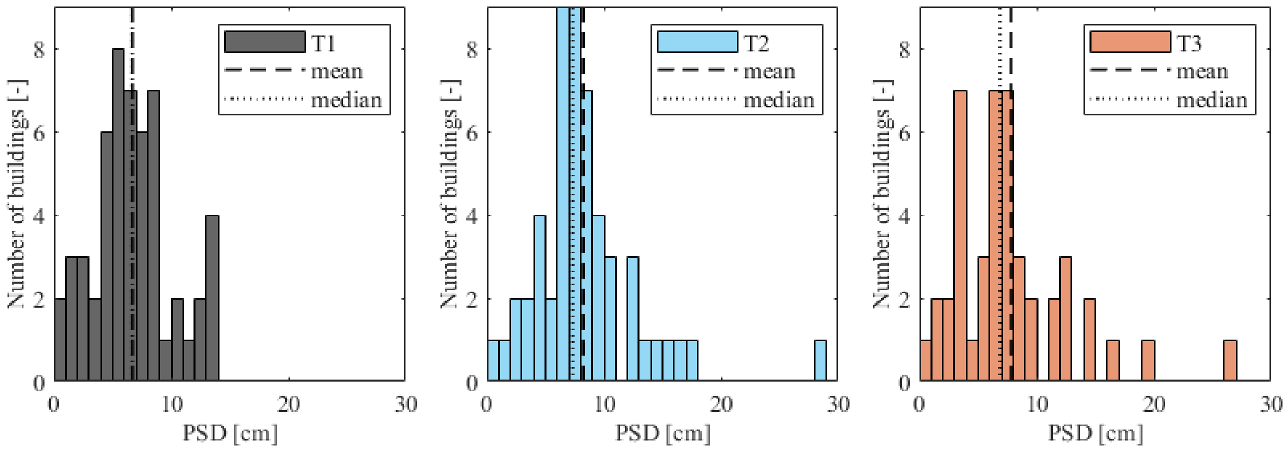

(a) *(b)* *(c)*

Figure 150. Distribution of the spectral displacements PSD(T_1): (a) T1; (b) T2; (c) T3.

4.3.2. ADDITIONAL CONSIDERATIONS ON THE ESTIMATED LOSSES

In this Section, the variability of the actual estimated losses in €/mq is examined considering few significant structural parameters and seismic-related intensities.

Firstly, the spectral acceleration (PSA) is considered. Figure 151a shows the maximum PSA computed at the location of the buildings, classified according to the three typologies and the five damage levels. On average, the PSA required to achieve the higher damage states is higher than that of the first ones, for all the structural typologies, expect for T3 which slightly deviates from this behaviour at D5.

Figure 151b depicts the data of the estimated losses depending on the PSA, and the linear interpolation computed for the three typologies (in the form y=ax+b). Even if there is a high deviation of the data, it is possible to infer that, on average, the losses of the three structural typologies increase with the increase of the spectral acceleration, i.e., the actual seismic demand on each building. Considering the range of PSA adopted in the database, the average losses of T1 are higher compared to T2 and T3, in line with the results discussed previously. The formulas expressed in the Figure may be adopted in loss evaluations to find the average loss expected at a certain value of PSA, for a precast building belonging to one of the three common typologies.

In addition, the same analysis is conducted considering the spectral displacement (PSD) on the buildings of each structural typology. Figure 152a shows that the PSD increases with the increase of the damage state for typologies T1 and T3, while for T2 the behaviour is different due to few high values computed at D2 and D3. By removing the outliers of the PSD values, the trend of T2 would likely become rather similar to that of the other structural typologies.

Figure 152b illustrates the linear interpolation of the estimated losses versus PSD (in the form y=ax+b). The losses of T1 and T3 buildings increase with the increase of the spectral displacement, while T2 has an opposite behaviour due to the aforementioned reason. After a process of refinement, through the calculation of additional data, the functions of the trend lines reported in the Figure may be adopted to estimate the average loss expected at a certain value of PSD.

In order to perform additional investigations, the displacement capacity at yielding of each building has been estimated through the following simplified formula (Priestley et al. 2007):

$$d_c = \chi_y \cdot \frac{h^2}{3} \tag{4.1}$$

$$\chi_y = 2.1 \cdot \frac{\varepsilon_y}{h_{sec}} \tag{4.2}$$

Where: χ_y is the curvature at yielding, h is the height of the column; and ε_y is the strain at yielding of steel, and h_{sec} is the height of the section of columns. In order to evaluate the minimum capacity for each building, the largest sectional dimension among those of its columns has been adopted in the calculation. In this way, the smallest yielding curvature is derived for each unit, thus the smallest displacement capacity d_c.

Thus, the capacities, in terms of maximum displacement at the top of the columns before yielding at the base, are compared with the displacement demand PSD. The ratio between the two values is calculated at different damage levels for the three typologies. The results are illustrated in Figure 153, showing that, in general, the ratio between displacement capacity and demand decreases with the increase of the damage levels.

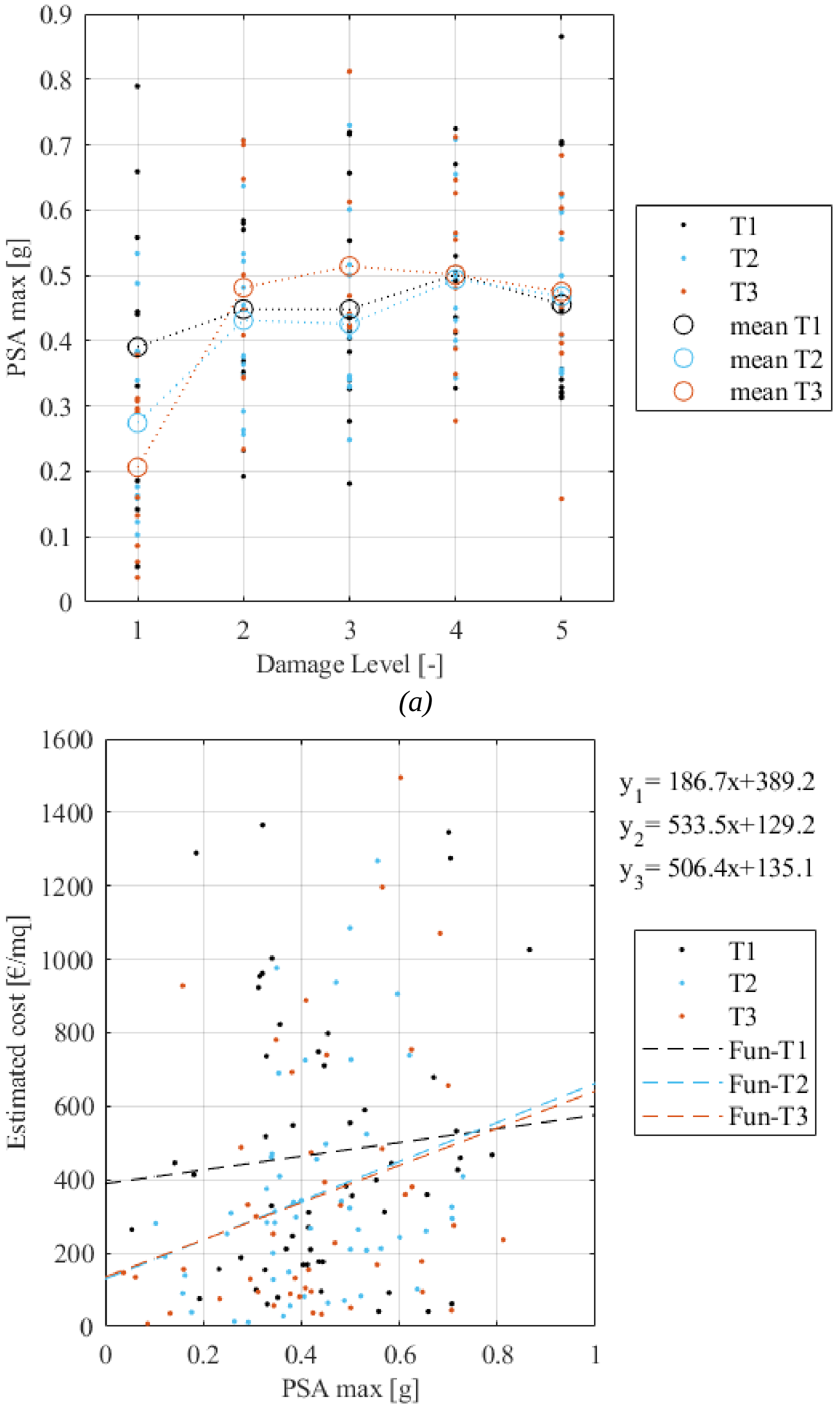

(a)

(b)

Figure 151. PSA max in buildings T1, T2 and T3 in the database: (a) PSA at different damage levels; (b) linear interpolation of estimated cost versus PSA.

This is in accordance with the hypothesis considered, since at higher damage states the columns are more prone to yielding. However, the ratio between the two values is, in most of the cases, higher than one meaning that the seismic displacement demand does not overcome the capacity. Actually, the yielding at the base of some columns was present since damage grade two (see Tables 21 and 22). This outcome may be due to the simplified formulas and the approximations considered.

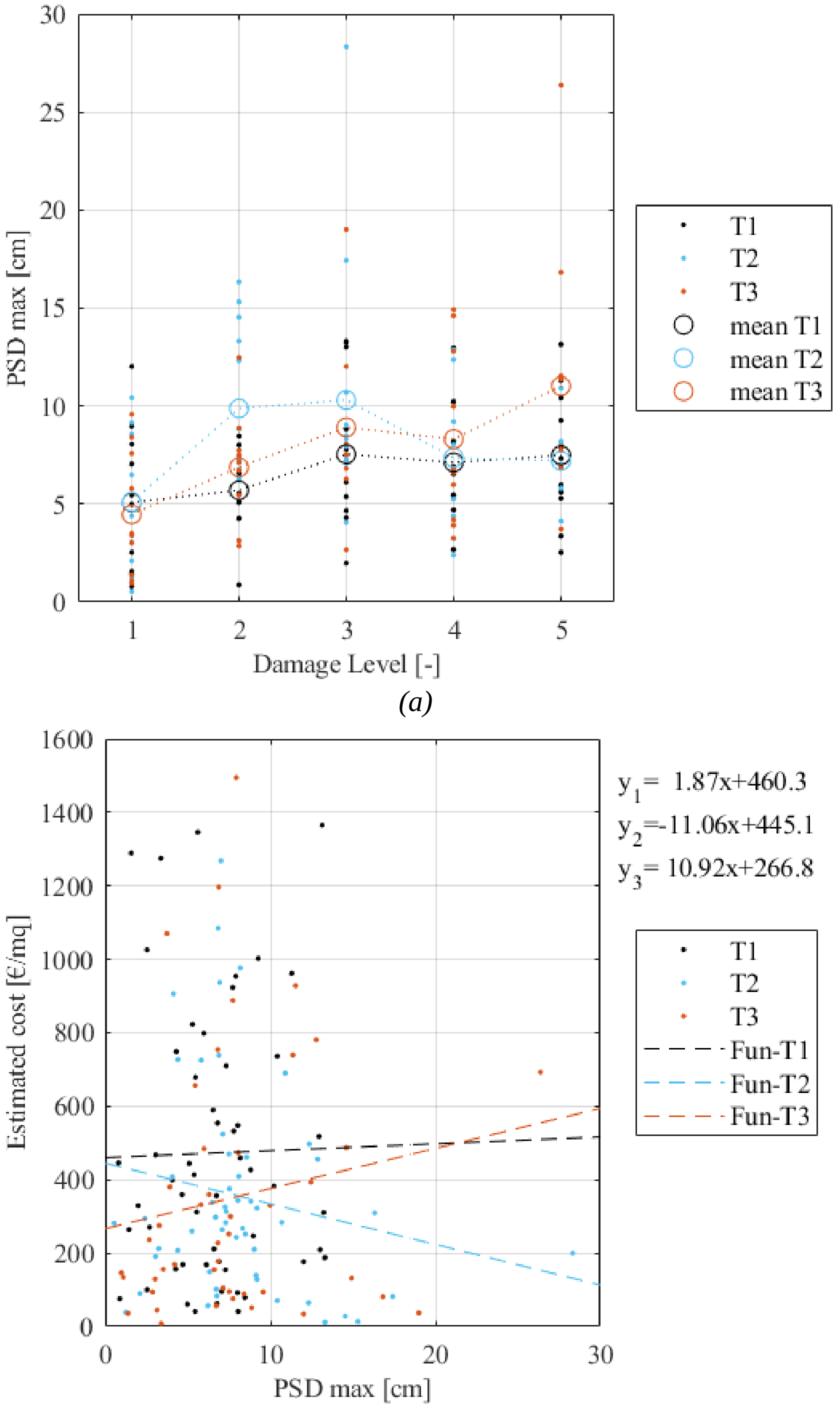

(a)

(b)

Figure 152. PSD max in buildings T1, T2 and T3 in the database: (a) PSD at different damage levels; (b) linear interpolation of estimated cost versus PSD.

However, it is worth noting that the P-Δ effects have not been taken into account and may anticipate the damage of the vertical elements under the seismic action.

Indeed, the P-Δ effects are a cause of concern in the precast RC buildings, due to the significant height of the columns, the high axial loads, and the large displacement demand (Magliulo et al. 2018, Torquati et al. 2018). The second order effects may increase the seismic demand at the base of the

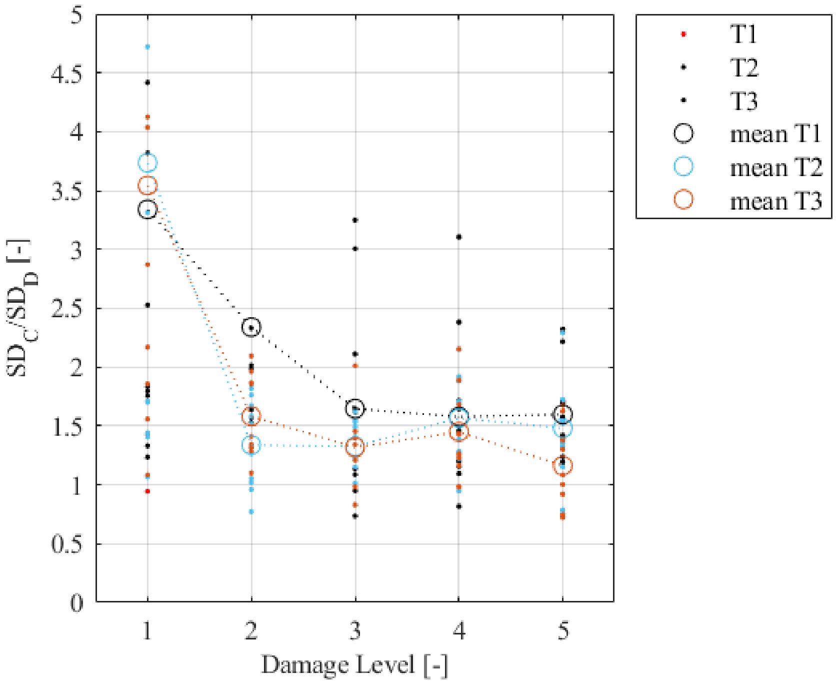

Figure 153. Ratio between displacement capacity and demand in buildings T1, T2 and T3 in the database, at different damage levels.

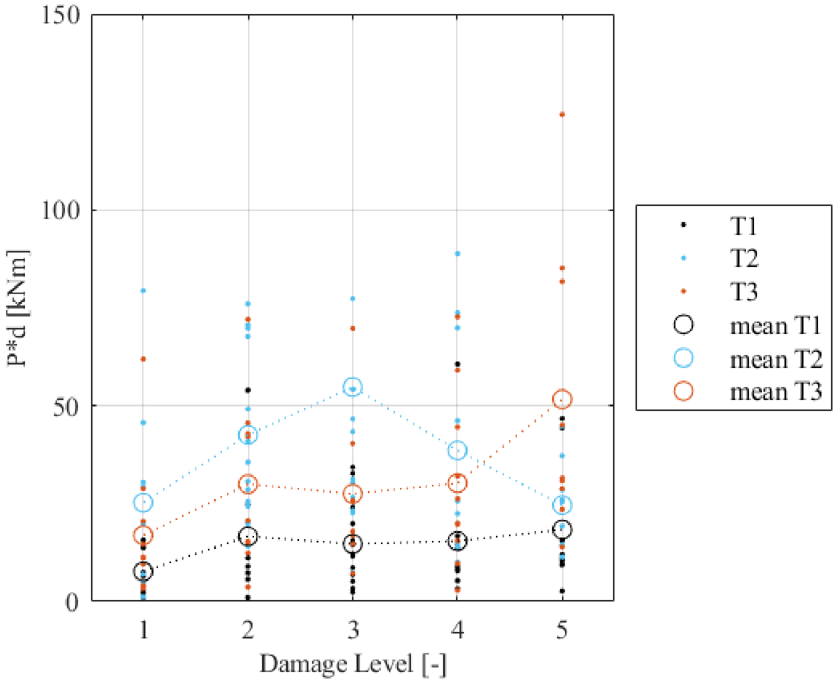

Figure 154. Second order moment in buildings T1, T2 and T3 in the database at different damage levels.

columns (i.e., the bending moment), anticipating the yielding at the base under rather low ground-motions. For this reason, the P-Δ effects may have caused the yielding of the vertical elements anticipating the attainment of their displacement capacities reported in Figure 153. These effects are heavier on high slender columns and buildings with large spans (higher axial loads on columns), i.e., the T3 precast buildings mainly, but also some T2.

To explore this last aspect, the axial force acting on the corner columns was computed for all the units. The corner column was considered representative for this insight to ease the comparison since it is present in all the buildings of the database, while those on the perimeter and the internal ones are not due to the different geometrical layouts and spans. However, it should be noted that the corner column is subjected to lower axial forces compared to those along the perimeter, and mainly to the internal ones. The mean values of axial loads computed for the corner columns of the three structural typologies are: 207 kN for T1, 425 kN for T2 and 369 kN for T3. The T2 buildings have a higher average value due to the presence of heavy roof elements analogous to those in T1, but higher elevations and slightly larger spans compared to T1 (see Section 4.3.1.1).

In addition, the product between the axial force on the corner columns (in kN) and the seismic displacement demand (in m) is calculated to estimate the second order moments. Figure 154 illustrates the variability of the second order moment at the different damage levels, for all the buildings belonging to T1, T2 and T3. In general, considering the mean values at each damage state, there is an increase of the values with the increase of the damage levels for T1 and T3 buildings but not for T2, even if the latter are subjected to the highest moments (until D4). This behaviour is probably due to the presence of the aforementioned high displacement demands in some T2 buildings at D2 and D3.

The values computed are not negligible if compared with the data of flexural capacities of the columns presented in Section 3.2 and in Appendix A, considering that few dots in the Figure are higher than 50 kN. This means that, in some cases, the second order moments alone may activate 1/4 of the resisting capacity of the columns, anticipating the yielding at the base with the increase of seismic displacement. Thus, in general, is it possible to infer that the second order effects play a role in the determination of the damage state in the precast RC buildings, causing secondary moments that should not be neglected. In particular, the highest values are estimated in the buildings of typology T2, which feature tall columns and high axial loads.

4.4. CONCLUDING REMARKS

A repository of seismic loss data of damaged one-storey precast RC buildings was assembled through the detailed examination of the documentation collected after the 2012 Emilia Earthquake. The typological-loss database has been analysed focusing on several aspects of the losses of the 600 buildings considered. Moreover, a structural-loss database of 150 buildings was created to perform additional analyses on the features of the three most common structural typologies.

The study of the databases allowed deriving some general concluding remarks:

- the distributions of several loss terms at different damage levels and for the most common structural typologies have been statistically analysed, obtaining a comprehensive panorama of the repair and the reconstruction costs of the precast RC buildings; the lognormal functions derived are useful tools to adopt in seismic loss assessment of precast RC buildings considering the damage metric used in this study;

- the linear functions associating the losses to the surface in plan and the PGA may be used to perform predictions on the actual expected losses of industrial buildings;
- the parametric conventional costs estimated by the Region were not able to represent the actual variability of the real estimated costs, in particular at the highest damage levels;
- the distributions of the diversified components of the estimated losses have been analysed for the most common structural typologies; the functions derived may be adopted to evaluate the influence of the structural and non-structural components in the loss predictions of industrial buildings, considering the categories analysed in this study;
- the values of other relevant parameters such as the insurance, the regional contribution, the technical fees have been analysed;
- the structural features of the most common precast structural typologies have been classified together with the information on their use and occupancy; these data may be adopted to evaluate additional loss terms in scenario assessments;
- the correlation between the monetary losses and different seismic parameters (PSA, PAD) defines tools not commonly provided, which may adopted to predict the losses based on the probable seismic demands;
- the P-Δ effects are likely to give a significant contribution in the development of the seismic damage in the tall columns of precast RC buildings, as emerged from the analyses of the structural-loss database.

Nevertheless, the definition of some terms may require further refinement. In particular, other continuous functions may be tested to fit the distribution of the losses, since mainly the lognormal one was used. To date, there seems to be not a uniform approach suggested in the literature since different authors adopted diversified fitting curves in recently published works (Buratti et al. 2017, Di Ludovico et al. 2017a and 2017b, Rossi et al. 2019a and 2019b, Del Vecchio et al. 2020).

Moreover, the structural-loss database may be additionally analysed to explore the variability of the estimated losses depending on the use of the buildings, for which several information are available. In addition, it should be furtherly expanded to refine the expressions defining the correlations between the losses and the seismic demand, for the different structural typologies.

Finally, additional considerations on the losses may be obtained from the analysis of few specific requests for the repair of industrial machineries and for the restoration of damaged products, which should be classified in a specific database. This could give relevant information on the losses that distinguish the industrial precast buildings from the ordinary buildings.

5. CONCLUSIONS

The evaluation of the seismic losses is a leading-edge topic in the contemporary scientific research, gradually changing the logics of both the seismic design and the assessment of buildings. To date, the guidelines of Codes aim at avoiding the failure of the structure and postpone the occurrence of the ultimate limit states to guarantee the so-called life-safety of the occupants. However, the latest advancements in the loss assessment suggest that this approach is insufficient. The importance of a single seismic event, even a minor one, changes if possible outcomes such as the repair costs, the reconstruction costs, the injuries, the homeless and the business interruption are considered.

Thus, the assessment of the structural capacity should be integrated with the evaluation of the expected consequences of an earthquake in a synergic procedure, aimed at communicating the multifaceted performance of buildings. The conceptual design performed at preliminary stages and the forecasting of possible future outcomes grow in importance when such tools of evaluation become available.

In this light, the assessment of the seismic losses becomes a fundamental step to attain in order to obtain all the elements that can warn how to avoid severe consequences in future earthquakes. To do so, the decision-making phase need to account for all these ingredients to allow the stakeholders finding the most effective solutions and policies. To acquire rapid results it is not always possible to follow the most robust and sturdy path: the simplified method are introduced to enable the occurrence of prompt outcomes. Indeed, the fast methods of assessment allows a rapid diagnosis of the problem, to guide the more sophisticated models that follow. In many situations, it may not be worthy to achieve the exact measure of a specific parameter, but the focus shifts to the comparative evaluations of different options allowing identifying whether and where to invest the resources. Different parts are concerned in this issue, both looking at the scale of a single structural unit (owners, estate agencies, insurers), both at the territorial scale (companies, governments, Civil Protection).

The outcomes presented in this dissertation include several contributions for the simplified modelling of the seismic losses, and for the collection of empirical loss data to guide the predictions. The streamlined large scale models presented in the first part involve many uncertainties and are clearly approximated but they can be adopted both in the short-term aftermath of a seismic event, to identify the most damaged industrial areas, both in ‘peace time’ to conduct predictions of the consequences in probable earthquakes. The first application presented of the simplified, still fast, large scale methodology paves the way for the development of seismic risk assessments of large building stocks, to give information for the prioritization of the seismic retrofitting of precast RC buildings, for example in Civil Protection or Government plans. In addition, it is worth recalling that the PRESSAFE method is not closed, since it can be easily extended. Due to the parametric nature of the fragility curves, additional analyses following the same approach proposed here, but concerning other structural typologies or damage mechanisms, can be conducted to widen the library of the categories of precast frames. This will be object of future investigations.

Furthermore, the simplified modelling procedure outlined to determine the losses of a single building in a probabilistic framework is developed for the specific purpose of providing information at the decision-making stage of different seismic interventions. As mentioned above, the results have to be consulted for a comparative aim, and raise the attention to the evaluation of the losses at the serviceability limit states since they are not negligible. Further refinements are needed to improve the quality of the results, even though the structure of the framework appears to be quite balanced. Indeed, it would be interesting to include additional failure modes of the structure, and explore the result obtained with the application of other low-damage techniques of intervention. Future developments may be also devoted to the applications and adaptation to other building typologies, in particular to the precast RC buildings.

Lastly, the analysis of the database collecting the seismic losses of damaged precast RC buildings opens the possibility to refine the seismic loss assessment procedures of this structural typology, whose fragility and loss potential is often disregarded with respect to ordinary buildings. The quality of the investigation performed may be improved, even though some interesting results emerged. Indeed, the evaluation of the structural and non-structural components of the losses of different precast structural typologies are of prior importance to calibrate and validate comprehensive loss models. Future research will be devoted to the study of the costs sustained for the repair of particular industrial machineries and the restoration of few products, which have to be analysed with different criteria. Moreover, it would be interesting to develop a similar loss database with the data collected for the ordinary buildings in the reconstruction process issued by the Emilia Region after 2012.

Finally, future works could address the definition of a unique method for the damage and loss evaluation of precast RC buildings at a large scale. This would allow performing a direct comparison between the observed and the predicted losses. By defining the expected number of buildings that undergo a probable damage level with the fragilities of PRESSAFE-disp, the computation of the seismic economic losses, through the consequence functions defined from the database analysis, could allow evaluating the effects of the ground-motion in a multi-criteria performance-based approach.

APPENDIX A

EVALUATION OF THE EFFECTIVENESS OF A SEISMIC RETROFIT INTERVENTION WITH DISSIPATIVE DEVICES IN PRECAST RC FRAMES

This work explores the effectiveness of a seismic intervention with dissipative devices (CWSTs) in an existing precast RC building. The purpose is to reduce the seismic vulnerability of the building with respect to the weaknesses discussed in the dissertation. Non-linear time history analyses have been conducted on two different models of the structure, one with hinged beam-column connections, and on the one with CWSTs. This Appendix discusses the effects of the introduction of the CWSTs in the connections in terms of forces, and proposes equivalent behaviour factors for the two structures. The main findings of this work are reported in Praticò et al. (2021).

A.1 INTRODUCTION

Since the 70's, precast Reinforced Concrete (RC) structures have been widely used in many countries for one-story industrial buildings such as warehouses and factories. The seismic vulnerability of existing precast RC buildings built without seismic-design criteria is a well-known issue nowadays, as highlighted by the 2012 Earthquake. The main source of vulnerability of these structures is the lack of effective mechanical connectors between their structural elements, indeed friction-based connections were widespread (Bournas et al. 2013, Liberatore et al. 2013, Magliulo et al. 2014, Babič et al. 2016, Demartino et al. 2018). Friction-based connections are not able to guarantee an effective shear force transmission, causing loss of support failures and collapses; moreover, the simultaneous effect of the horizontal and vertical components of the seismic action can increase the probability of occurrence of this type of failure (Bovo e Savoia 2019). The vulnerability of structures characterized by these frictional connections has been confirmed by numerous numerical simulations (Biondini et al. 2013b, Magliulo et al. 2014, Ercolino et al. 2016, Bovo e Savoia 2018, Demartino et al. 2018, Titi et al 2018). In addition, the failure of beam-column connections based on friction only, can frequently occur before the development of plastic hinges at the base of columns, causing undesired non-ductile failure modes, as reported in Deyanova et al. (2014).

Given the high vulnerability of friction-based connections and the economic significance of prefabricated RC structures, many strengthening solutions have been proposed in the literature (Bournas et al. 2013, Ligabue et al. 2014, Magliulo et al. 2014, Muciaccia et al. 2014, Nastri et al. 2017). The reduction of damage and collapses due to seismic events for this type of structures, becomes even more strategical since a high economic impact due to industrial business interruption has to be taken in account, in addition to the direct economic losses (Rodrigues et al. 2017, Bosio et al. 2020, Rossi et al. 2020). All the strengthening solutions are typically based on the introduction of steel ties, plates, or cable restraints, to avoid sliding of the beams and therefore unseating failures. Most of these solutions aim only at converting friction-based connections into hinged connections with no focus on energy dissipation, and therefore they often require the strengthening of the base of columns.

Thus, ad hoc solutions based on different energy dissipation mechanisms have been pro-posed. For instance, Dal Lago et al. (2017a, 2017b, 2017c) proposed to concentrate energy dissipation in simple and rather inexpensive elements, such as steel angles connectors. Scotta et al. (2015) focused on the dissipative role of cladding panels acting as shear walls; Belleri et al. (2017) introduced energy dissipation in hinged connection, suggesting a re-centering dissipative device based on rotary friction; Martinelli and Mulas (2010) proposed a similar solution involving the insertion of devices dissipating energy through rotary friction, with no re-centering capacity. Alternative solutions are based on the introduction of dampers, as suggested by Marinini et al. (2011).

In this context, this work refers to a low-damage solution for the retrofit of beam-column connections of existing precast RC structures, proposing the introduction of dissipative fuse devices based on Carbon-Wrapped Steel Tubes (CWST), introduced in Pollini et al. (2014, 2018). Pollini et al. (2021) presented an analytical simplified approach to estimate an equivalent behavior factor to be used in design applications with these devices, validated by comparison with a large number of incremental dynamic analyses (IDAs).

In this work, the evaluation of the improvement in the seismic behavior of an existing precast RC building retrofitted with CWST devices is proposed, through comparative considerations on the behavior factor calculated for the existing structure, and for the one after the intervention. The first part of presents the properties of the dissipative fuse de-vices adopted for the retrofit intervention of the main frame of the building. Thus, the modelling strategies are described in detail, as well as the development of the non-linear time history analyses. Finally, the results in terms of behavior factor quantification, for the cur-rent structure and for the retrofitted one, are proposed and discussed with the aim of evaluating the effects of the CWSTs in the reduction of the seismic vulnerability of the building.

A.2 CWST DISSIPATIVE DEVICES

The dissipative fuse devices based on CWSTs (Pollini et al. 2018, Pollini et al. 2021) have two main purposes: (i) to connect beam-column joints in order to prevent the possible unseating failure of beams, and (ii) to act as dissipative fuses, thus reducing the effects of seismic actions on structural elements. Specific studies in automotive engineering on structural crashworthiness (Song et al. 2000, Lima et al. 2011) showed that metals, combined with composite materials in thin-walled circular tubes, have excellent capacities of energy absorption under axial compressive loads. From these, the CWST devices were developed, and an example of a real application can be seen in Figure A.1a.

It is worth noticing that, since each CWST (Figure A.1b) dissipates energy only under compressive loading, two devices must be positioned at each beam-column joint. A threaded bar is placed through the CWSTs in order to guide their displacement, and also to ease their connection to structural elements. In this way, standard steel anchoring elements can be used to fix the threaded bar to the column. Moreover, the anchorage on the beam is guaranteed by a significantly stiff and strong steel element, able to transfer forces from beams to the CWSTs. The CWST device works firstly in the elastic range, like a fuse restraint avoiding relative displacement between two structural components, below a certain pre-established force threshold. Above this threshold, the plastic deformation of the device begins (plasticization phase), as well as the energy dissipation.

(a) *(b)*

Figure A.1.(a) Example of a beam-column connection provided with coupled CWST dissipative devices; (b) single fuse device made of carbon-wrapped steel tubes.

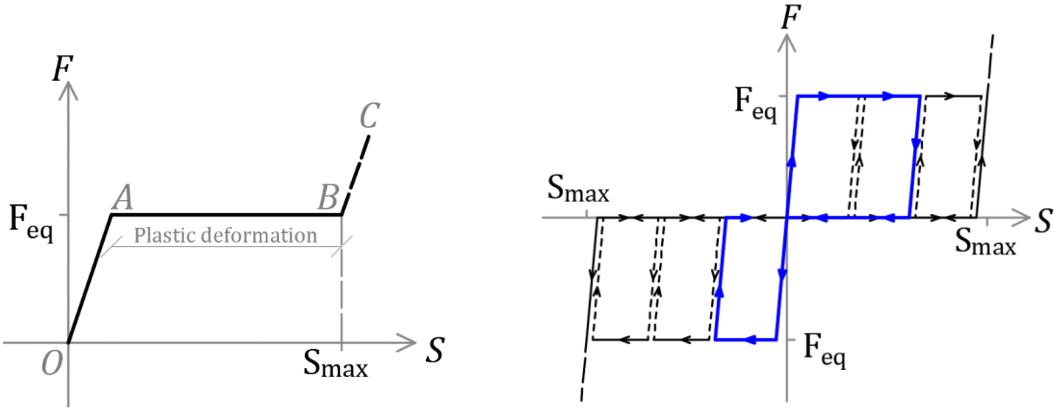

(a) (b)

Figure A.2. Force-deformation behavior of the CWST device: (a) single device behavior under compression; (b) hysteretic behavior of two devices under cyclic loading.

In order to understand the behavior of the devices, in Figure A.2a the force-deformation diagram of a single CWST in compression is proposed (Pollini et al. 2018). In the Figure, F_{eq} is the equivalent plastic force threshold, and S_{max} is the maximum deformation capacity. The behavior of a connection with a CWST device can be described within three main steps. In the initial branch O-A the device remains elastic, and the lateral seismic force is fully taken by the column. As soon as the force overcome F_{eq} (branch A-B of the curve), the device starts to buckle and the plastic deformation develops, while a constant value of the force is transmitted to the column. After point B, when the device attains its maximum deformation capacity, the stiffness boosts significantly. At this step, the device performs as a displacement-limiter between beams and columns, thanks to the aforementioned threaded bar, thus, from this point, the columns fully bears the seismic load and start to deform and yield (typically at the base).

In case of ground motions, and in general under cyclic loading, the two CWSTs positioned in one joint, work alternatively. Figure A.2b represents the force-deformation law of a couple of devices in case of cyclic loads. In the picture, the red path shows that, when a load reversal occurs after entering the plastic branch of one of the devices, the connection slides with no force until the recovery of the entire deformation.

A.3 FEM MODELS OF THE PRECAST RC FRAME

The seismic retrofit with CWST devices is herein applied to an existing precast RC building located in Carpi (MO), in the Emilia Romagna region (Italy). The building was built in the '70, and features double span main frames constituted by I-shaped precast beams, simply supported on rectangular precast columns. After the seismic events of May 2012, the building was subjected to a temporary retrofit solution with steel plates applied at the beam-column joints, aimed to prevent the unseating of the precast elements. It is worth noticing that the retrofit with CWSTs discussed here, has the purpose of improving the seismic behavior of the building with respect to the current condition.

The roof slab is made by simply supported hollow-clay elements, without a rigid concrete slab, thus, the structural scheme lacks structural redundancy, consisting in simply supported beams and cantilever columns (Savoia et al. 2012, Bellotti et al. 2014). Since the building is simple and regular in plan, and there is not a rigid diaphragm at the roof level, the seismic behavior of the entire building can be approximated with the 2D model of one of the internal main frames, in the direction of the beams. In the orthogonal direction, a different retrofit solution was adopted.

In order to evaluate the effects of the retrofit intervention, two different frames are modelled with finite elements, with the software Midas GEN (CSPFEA):

A) main frame of the building with hinged beam-column connections, representing the structure in the current condition with the temporary retrofit solution (Figure A.3a);

B) main frame of the building with CWST devices placed at the beam-column joints, representing the retrofitted structure (Figure A.3b). In this last model, appropriate *link* elements, i.e. nonlinear springs, are used in order to model the behavior of the dissipative devices, as explained in the following sections.

The frames are subjected to seven horizontal recorded ground-motion accelerograms, according to Eurocodes prescriptions for safety verifications of existing buildings with non-linear analyses (CEN 2005, D.M. 2018), as further described in Section A.4.1. The vertical seismic action is not considered in this work.

The main frame illustrated features two spans of 21.8 m, with precast main beams characterized by sections with depth spanning from 0.8 m at their ends to 1.6 m at mid-span. The three columns are 5.5 m high, with a rectangular section of 40 x 54 cm. Mechanical steel connectors are present between beams and columns, allowing to consider a rigid hinged connection between the elements in the existing condition.

The gravity loads are computed in the seismic combination of actions (D.M. 2018) according to the influence area of each element, and transformed into lumped masses for the dynamic analyses. The axial load ratio, computed in the seismic combination of loads, is 0.033 for the two external columns, and 0.063 for the internal. The material properties have been estimated according to in-situ testing reports, showing a concrete class C32/40 and a steel class FeB44k for the column reinforcement.

Since the building was built before the introduction of seismic design criteria in the region, the columns exhibit low seismic detailing and in particular poor transverse reinforcement. Indeed, the columns are reinforced with 4Φ14 ribbed bars with 2.5 cm concrete cover, and 2 additional Φ6 located along the height of the section, confined with transversal stirrups Φ6 spaced 20 cm. The columns are modelled clamped at their base, since, due to the presence of a rigid industrial floor, the interaction with the foundation is not under analysis in this work. At the base of columns, non-linear lumped plastic hinges are modelled adopting trilinear moment-rotation relationships, defined according to Eurocode 8 part 3 formulations for reinforced concrete structures (D.M. 2018, CEN 2005). The shear resistance of the columns is computed following the expression for cyclic shear resistance calculation in Eurocode 8 (CEN 2005), depending on the ductility demand of each element. It is worth noticing that, in all models, beams have a linear behavior since no damage is expected to occur in these elements.

A.3.1. PROPERTIES OF THE PLASTIC HINGES

The non-linear flexural behavior of columns is taken into account by means of plastic hinges at their base. Trilinear moment-rotation rules are implemented, considering the cracking point (θ_{cr}, M_{cr}), the

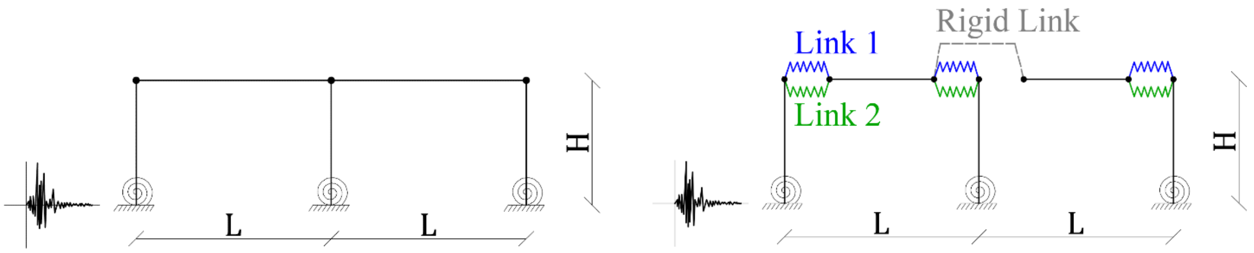

(a) *(b)*

Figure A.3. Structural FEM models adopted in the analyses: a) model A representing the existing structure; b) model B representing the frame retrofitted with CWSTs.

yielding point (θ_y, M_y), and the ultimate point (θ_u, M_u), with a perfectly plastic post-yielding behavior. The hysteresis model considered is a symmetric Takeda rule (Takeda et al. 1970) able to represent the stiffness degradation of the elements, with an exponent in unloading stiffness equal to 0.4, and an inner loop unloading stiffness reduction factor equal to 1.

The value of the chord rotation at cracking is calculated as the ratio between the cracking moment and the elastic stiffness of a cantilever column with a fully reacting section. The yielding and the ultimate rotations at the life safety limit state are defined according to Biskinis and Fardis formulations (2004, 2008) adopted in Part 3 of Eurocode 8. The formulas are reported in Equations (A.1) and (A.2), respectively:

$$\theta_y = \phi_y \frac{L_V}{3} + 0.0013\left(1 + 1.5\frac{h}{L_V}\right) + 0.13\phi_y \frac{d_{bL} f_y}{\sqrt{f_c}} \qquad (A.1)$$

$$\theta_{u,SLV} = \frac{3}{4}\frac{1}{\gamma_{el}} 0.016(0.3^{\nu})\left[\frac{max(0.01;\omega')}{max(0.01;\omega)} f_c\right]^{0.225} \left(\frac{L_V}{h}\right)^{0.35} 25^{\left(\alpha\rho_{sx}\frac{f_{yw}}{f_c}\right)}(1.25^{100\,\rho_d}) \qquad (A.2)$$

Where: ϕ_y is the yield curvature at the end section, L_V is the ratio moment/shear at the end section, h is the depth of the cross-section, d_{bL} is the mean diameter of the tension reinforcement, f_y and f_c are the steel yield stress and the concrete strength, respectively, γ_{el} is equal to 1.5 for primary seismic elements, ν is the axial load ratio, ω and ω' are the mechanical reinforcement ratios of the tension and compression, respectively, longitudinal reinforcements, α is the confinement effectiveness factor, ρ_{sx} is the ratio of transverse steel parallel to the direction of loading, f_{yw} is the stirrup yield strength, ρ_d is the steel ratio of diagonal reinforcement, if any, in each diagonal direction. It is worth noticing that the same materials and sections characterize the three columns, which differ only because of the axial load. Mean values of the material properties are adopted to calculate moments and rotations. Moreover, the shear span L_V is equal to the full column height. The coordinates of the characteristic points of the trilinear plastic hinges are reported in Table A.1.

It is important to highlight that the expression used for the calculation of θ_u is defined for elements with ribbed bars and seismic detailing. The formula can be also adopted for elements that are not conforming to seismic codes, by applying reduction factors. In particular, empirical scaling factors are defined based on whether a member i) does not conform to modern seismic codes (22.9% reduction); ii) is not provided with properly anchored stirrups providing effective confinement (1.6% reduction); iii) has laps of longitudinal bars inside the plastic hinge region (from 15% to 66% reduction). This last factor significantly influences the calculation of the ultimate rotation (Verderame et al. 2010), resulting in a reduction coefficient which increases if the lap is less than 40 diameters (in case of ribbed bars). For the case study frame, the first two empirical reduction coefficients are taken into account for the determination of θ_u. Since the columns are prefabricated, with continuous longitudinal bars, it is not possible to consider the third correcting coefficient. All this enhances the necessity to evaluate other types of significant reduction coefficients to be proposed in this formula for the specific case of existing prefabricated elements not designed with anti-seismic standards, for which additional research may be required (Bovo e Buratti 2019, Magliulo et al. 2019).

In this work, in order to analyse the sensitivity of the results depending on the value of ultimate chord rotation considered, the authors consider the adoption of two alternative values corresponding to 80% and 60% of θ_u. Thus, the dynamic analyses are conducted with three different threshold values of rotations for both the models (i.e. model A and B), in order to evaluate the influence of this parameter on the estimation of the behavior factor. The values calculated for the case study frame are presented in Table A.1.

A.3.2. SHEAR RESISTANCE

The shear in columns is checked at each step of the analysis with respect to the shear resistance, as prescribed by Eurocode 8, avoiding the modelling of non-linear shear hinges. The formula adopted for the verification is given in Eurocode 8, part 3 (CEN 2005). It accounts for the cyclic shear resistance which decreases with the increase of the plastic ductility demand μ_Δ^{pl}. This last parameter is calculated as the plastic part of the chord rotation normalized to the yielding chord rotation θ_y. The adopted shear strength formula is reported in Equation (A.3).

$$V_R = \frac{1}{\gamma_{el}}\left[\frac{h-x}{2L_V} min(N; 0.55A_c f_c) + \left(1 - 0.05\, min\left(5; \mu_\Delta^{pl}\right)\right) \cdot \left[0.16\, max(0.5; 100\rho_{tot})\left(1 - 0.16\, min\left(5; \frac{L_V}{h}\right)\right)\sqrt{f_c}A_c V_W\right]\right] \tag{A.3}$$

Where: γ_{el} is equal to 1.15 for primary seismic elements, h is the depth of the cross-section, x is the compression zone depth, L_V is the ratio moment/shear at the end section, N is the compressive axial force, A_c is the cross-section area, f_c is the concrete strength, μ_Δ^{pl} is the plastic part of the chord rotation normalized to the yielding chord rotation, ρ_{tot} is the total longitudinal reinforcement ratio, V_W is the contribution of transverse reinforcement to shear resistance.

In this formula, mean values of the material properties divided by the partial factors are considered to calculate the shear resistance, in accordance with Eurocode criteria for safety verifications of brittle failure modes. Moreover, the resistance is updated at each step of the analysis depending on the actual ductility demand. In addition, if the ductility demand is lower than 1, the value of shear resistance is calculated with the expression defined for members not requiring shear reinforcement, given in Eurocode 2, part 1-1 (CEN 2004).

Table A.1. Characteristic points of the moment-rotation relationships adopted for the external and the internal columns of the precast frame.

	M_{cr} (kNm)	M_y (kNm)	M_u (kNm)	θ_{cr} (rad)	θ_y (rad)	θ_u (rad)	80% θ_u (rad)	60% θ_u (rad)
External column	70.5	236.6	236.6	0.00074	0.01412	0.03232	0.02586	0.01939
Internal column	70.5	297.5	297.5	0.00074	0.01462	0.03118	0.02495	0.01871

A.3.3. CWSTS DISSIPATIVE DEVICES

The CWST dissipative devices are introduced in frame B (see Figure A.3), i.e. the retrofitted one. The devices are modelled in Midas GEN through the use of two *link* elements working in parallel:

- a non-linear symmetric element with property type *SLIP bilinear* (link 1 element in Figure A.3b) which simulates the cyclic behavior of the devices before the attainment of the maximum deformation capacity. A yielding strength F_{eq} equal to 30 kN and an initial stiffness is 30’000 kN/m are considered. This element works symmetrically in order to represent the presence of two CWSTs equipped at each beam-column node;
- a non-linear symmetric element with *SLIP bilinear* property defined with an initial gap of 7.5 cm (link 2 element in Figure A.3b), which simulates the behavior of the devices after the attainment of the maximum deformation S_{max} capacity. It is modelled with a symmetric behavior in order to consider the maximum displacement of both tubes. The yielding strength and the stiffness of this element are set with significantly high values, so that to model a rigid hinged connection between beams and columns.

A couple of link elements with the aforementioned properties is modelled at the top of each column, connecting beams to columns, to represent a set of seismic devices working in the horizontal direction of the ground-motion. At the top of the internal column, an additional horizontal rigid link is modelled in order to connect the seismic devices to both beam ends, as shown in Figure A.3. It is worth saying that a vertical support is guaranteed for each node of the beams through appropriate settings in the software.

Friction was not implemented in the models because of the uncertainty in the determination of the parameters that control this mechanism, i.e. the definition of the coefficient of friction, the combination of horizontal and vertical components of the seismic action, and the energy dissipation related to friction. Considering a frictional mechanism in the model would imply to admit the benefits of friction energy dissipation that cannot be considered to be constant, and on which it is not always possible to rely because of the variations of the axial load in columns, due to the vertical component of the ground-motion. Furthermore, standard provisions do not allow considering friction in the seismic response of structures. Nevertheless, the contribution of friction in terms of maximum force transferred to columns, has been take into account in the selection of the yielding strength capacity of the dissipative devices adopted in this case study. Indeed, the value of the equivalent force of plasticization F_{eq} (see Section A.2.) for the CWSTs, was selected to be lower than the maximum value of force that could be transferred to the top of the columns without yielding their base sections.

Consequently, the column exhibits a certain degree of overstrength in order to guarantee that the sum of friction threshold force and of forces transmitted by the CWST devices, is lower than the force that would lead to the formation of a plastic hinge at the base. This is in accordance with the design criterion of this retrofit intervention, aimed at having columns performing linear elastic until the devices reach their maximum deformation capacity. Therefore, F_{eq} plus the contribution of frictional forces, has to be lower that the force activating yielding in columns, i.e. about 43 kN in for the external columns, and 54 kN for the central column, for the frame under analysis.

A.4 TIME-HISTORY ANALYSES

The first step of this Section consists in performing linear modal analysis to estimate the first period of vibration of the existing frame. For this purpose, model A is implemented in a linear model without the three plastic hinges at the base of the columns, but considering the cracked stiffness of the columns, following Eurocode 8 part 3 prescriptions (CEN 2005). In particular, a reduction coefficient for the moment of inertia of each column has been evaluated, so that to consider the secant lateral stiffness at yielding of each column. The result of this analysis is a first period of vibration T_1 of 1.561 seconds, for which almost the entire modal mass of the structure is participating. Indeed, precast RC structures are typically simple and strongly dominated by one vibrating mode (Pollini et al. 2018).

A.4.1. SELECTION OF THE RECORDS

The seismic input adopted for the non-linear dynamic analyses is a set of 7 spectrum-compatible ground acceleration time histories. The target spectrum for the selection is the life safety limit state elastic response spectrum, defined by the Italian building code (D.M. 2018) for the site of Carpi (MO) in Italy. This spectrum has a return period of 712 years, corresponding, to a nominal life equal to 50 years and importance class III. Ground type C with no topographic amplification effects is assumed. The 7 accelerograms used in the analyses were selected from the NGA-West database developed by PEER (PEER accessed 2021, Berkeley), with the following *ad hoc* algorithm: i) only earthquakes with moment magnitude between 4 and 6 and recording stations with source-to-site shorter than 30 km are considered; ii) pulse-like ground-motions are excluded; iii) recordings not usable for periods

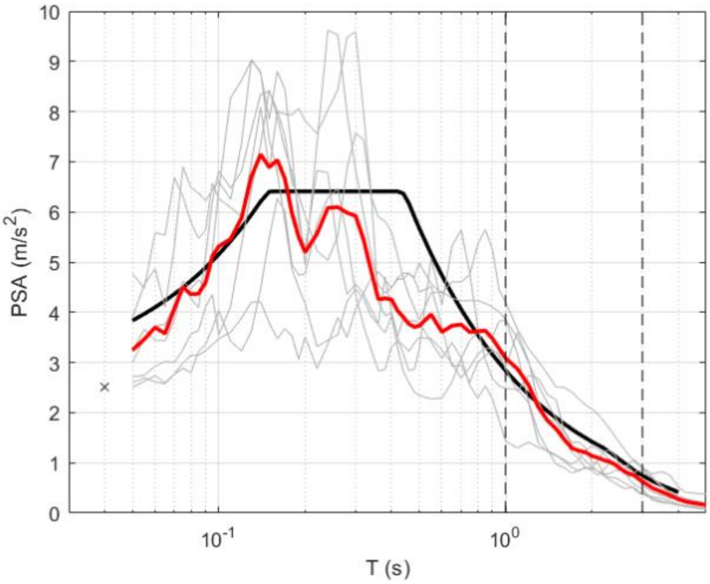

Figure A.4. Scaled response spectra for each of the 7 accelerograms selected (gray lines), average spectrum (red), and target code spectrum for spectral compatibility in the range of periods spanning from 1.0 s to 3.0 s. The PGA is indicated with the symbol ×. All the accelerograms are scaled to the same PGA.

up to 3.0 s are excluded (Boomer and Acevedo, 2004); iv) all spectra of the remaining accelerograms are scaled to the PGA of the target spectrum; v) response spectra with scaling factors higher than 3.0 or lower than 0.4 are excluded; vi) the scaled spectra are sorted based on ascending values of the average root-mean-square deviation of the observed spectrum from the target (DRMS) (Boomer and Acevedo, 2004) in a range of periods from 1.0 s to 3.0 s; vii) all the possible combinations of 7 spectra are considered among the 10 scaled spectra with the lowest DRMS values; viii) for each combination of 7 spectra the DRMS value for the mean spectrum is computed; ix) the 7 spectra with the mean spectrum with the lowest DRMS value are identified.

The selected scaled spectra are plotted in Figure A.4, and the corresponding ground-motion data are reported in Table A.2. In particular, the earthquake name and year are indicated, together with the name of the recording station, the Joyner-Boore source-to-site distance R_{JB}, the moment magnitude (M_w), the direction of the horizontal component with reference to the NGA classification (PEER accessed 2021, Berkeley), the peak ground acceleration PGA, and the scaling factor SF^0.

Following Eurocode 8 recommendations (CEN 2005) when seven ground motions are used, the average result of the response quantities from the analyses is adopted to compute the value of the action effect.

A.4.2. NON-LINEAR ANALYSES

Non-linear time history analyses have been performed on both model A (frame with hinged connections) and model B (frame retrofitted with CWSTs), with the purpose of estimating, for each accelerogram, the scaling factor that leads to the attainment of one of the ultimate conditions of the structure. In particular, each record is gradually scaled until one of these collapse conditions is reached: (i) ultimate chord rotation in one of the three columns; (ii) cyclic shear resistance in one of the three columns. It is worth saying that the scaling of the time-histories is performed with factors SF^1 on the records already scaled with the SF^0 introduced for the spectra compatibility.

Table A. 2. Main parameters of the seven accelerograms selected.

N°	Earthquake name, Year [-]	Station name [-]	R_{JB} Distance [km]	M_w [-]	Component [-]	PGA [m/s^2]	SF^0 [-]
TH1	Chalfant Valley-01, 1986	Bishop - LADWP South St	23.38	5.77	H1	1.270	1.982
TH2	Chalfant Valley-01, 1986	Bishop - LADWP South St	23.38	5.77	H2	0.926	2.717
TH3	Westmorland, 1981	Brawley Airport	15.28	5.90	H1	1.660	1.516
TH4	Westmorland, 1981	Salton Sea Wildlife Refuge	7.57	5.90	H2	1.729	1.455
TH5	Coyote Lake, 1979	Gilroy Array #3	6.75	5.74	H2	2.242	1.122
TH6	San Salvador, 1986	National Geografical Inst	3.71	5.80	H1	3.987	0.631
TH7	Coyote Lake, 1979	Gilroy Array #3	6.75	5.74	H1	2.673	0.941

The scaling factors SF^1 are reported up to the first decimal digit. Therefore, the *i*-th accelerogram is actually scaled by $SF_i = SF_i^0 \cdot SF_i^1$.
The non-linear analyses are carried out with Rayleigh damping, calculated based on the first and the second periods of vibration (see Section A.4.1.), considering 5% damping ratio. P-Delta effects are also taken into account in the analyses, even if not particularly significant for this frame, since the columns are characterized by low axial loads.
For each analysis, the time histories of the following response parameters are evaluated: the shear in columns, the displacements at the top of columns, the chord rotations of columns, the hysteretic behavior of the CWSTs and of the plastic hinges. As mentioned before, the analyses are conducted considering three different values of the ultimate chord rotations:

- Rotation Limit RL1 - Ultimate chord rotations calculated with Equation (A.2);
- Rotation Limit RL2 - 80% of the values of the ultimate chord rotations adopted in RL1;
- Rotation Limit RL3 - 60% of the values of the ultimate chord rotations adopted in RL1.

As an example, some significant results are proposed for models A and B, referring to the accelerogram TH6, for a scaling factor SF^1 equal to 1, for the ultimate chord rotations capacity RL1. Figure A.5 shows moment-rotation plots for the left and the central column of the frame, for the model A (black line) and the model B (red line). In the model A, the rotation in all plastic hinges exceeds the yielding point, while in the model B, all columns remain elastic. Moreover, in model B, one of the CWST devices in each couple at the top of the three columns, reaches the maximum deformation capacity S_{max}. Therefore, the three link 2 elements (see Section A.3.3.) are activated, transferring the full effect of seismic actions from beams to columns. This effect is visible in Figure A.6, which shows the non-linear force-deformation cyclic behaviors of the three devices in model B. The cyclic behavior link 1 elements are shown in Figure A.6a, these have a deformation capacity S_{max} equal to 7.5 cm, then the link 2 elements are activated (Figure A.6b).
With the subsequent increase of the scaling factor SF^1 of time history TH6, the yielding of the plastic hinges of columns gradually occurs also in model B.

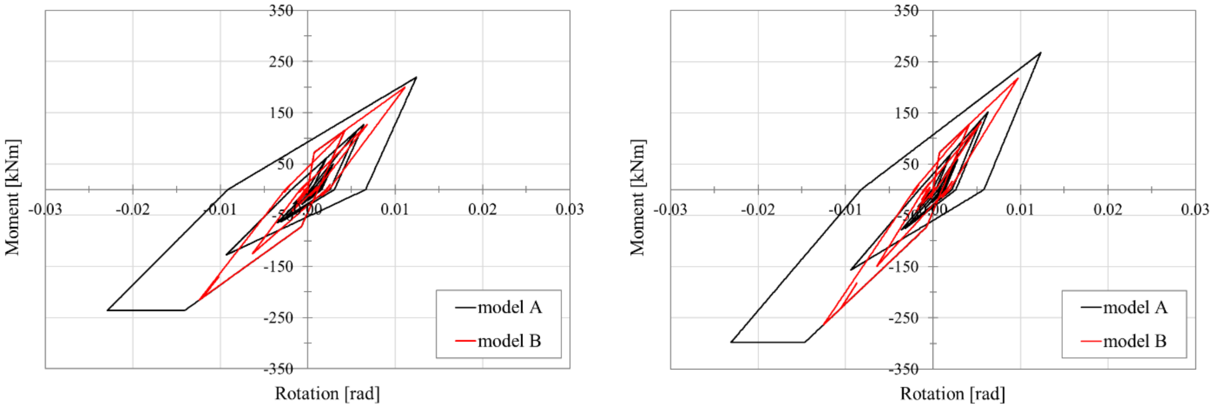

(a) *(b)*

Figure A.5. Cyclic behavior of columns plastic hinges for model A (black line) and model B (red line), for time history TH6 and SF^1 = 1: a) left column the frame; b) central column of the frame.

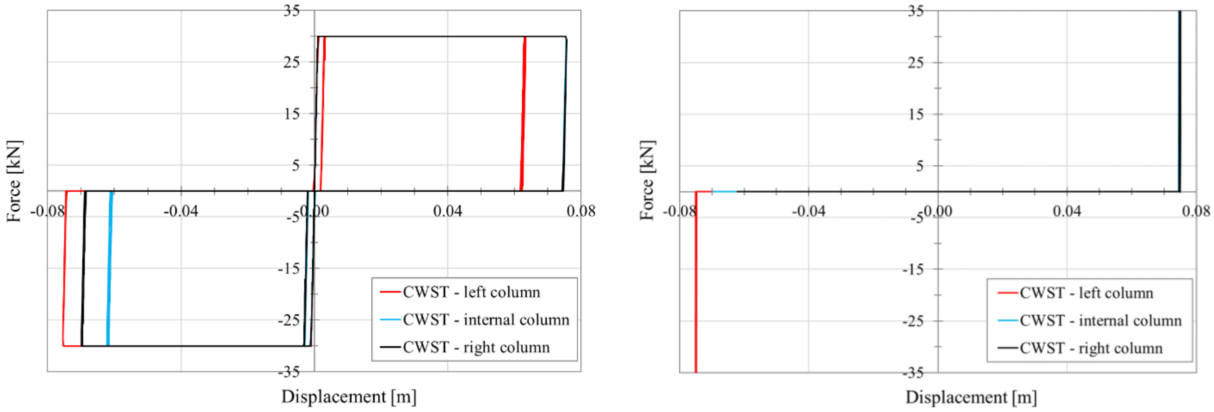

(a) (b)

Figure A.6. Cyclic behavior of the three CWSTs at the beam-column nodes in model B, for time history TH6 and SF^1 *= 1: a) cyclic behavior of link 1 (see Section A.3.3); b) cyclic behavior of link 2 (see Section A.3.3).*

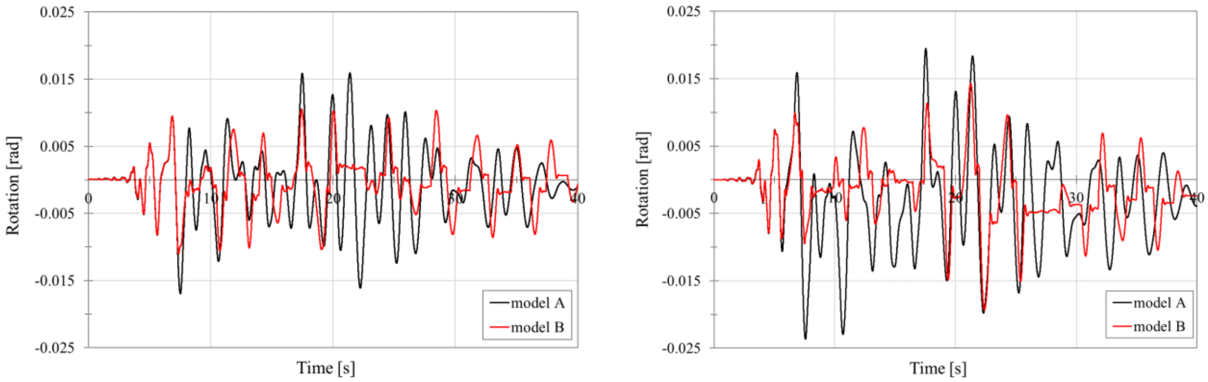

(a) (b)

Figure A.7. Time-histories of the chord rotation of the left column for TH2, for model A (black line) and model B (red line): a) SF^1 *= 1.5; b) SF*^{1} *= 2.0.*

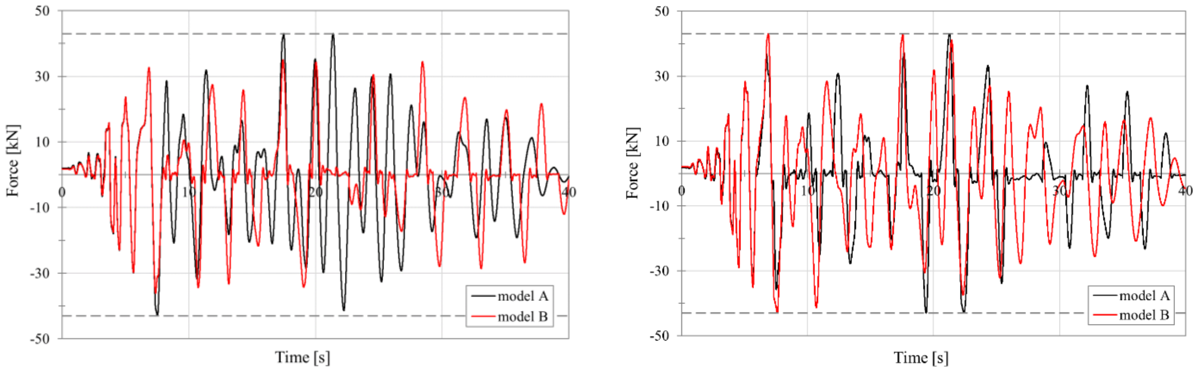

(a) (b)

Figure A.8. Time-histories of the base shear for the left column for TH2, for model A (black line) and model B (red line): a) SF^1 *= 1.5; b) SF*^{1} *= 2.0.*

However, the three columns in model A reach the ultimate rotation values for a SF^1 equal to 1.30, lower than the one corresponding to model B, which is equal to 1.70. Furthermore, for all time histories, it can be observed that the plastic hinges of the columns in model B remain elastic until the CWST devices attain their ultimate deformation capacity. This confirms that the CWSTs in model B, allow to guarantee a higher performance against the ultimate rotation capacity of columns.

In order to further evaluate the influence of the CWSTs, the time-histories of the deformations in the plastic hinge, and the shear in the left column of the frame, are proposed in Figure A.7 and A.8, for the accelerogram TH2 and the rotation limit RL1. Figure A.7a and A.8a refer to a scaling factor SF^1 = 1.5 for both models, while Figure A.7b and A.8b refer to a scaling factor SF^1 = 2. In Figure A.7, the positive effect of the devices can be observed in terms of lower deformations in model B compared to model A. Figure A.8a shows that the left column in model A reaches a value of shear that corresponds to the yielding of the plastic hinge (about 43 kN), while the left column in model B has lower shear values. Indeed, for a scaling factor SF^1 = 1.5, all the columns in model A are yielded, while all the columns in model B are still elastic.

For SF^1 =2, Figure A.8b, it is possible to observe that the left column reaches the yielding force both in model A and B. However, in Figure A.7b it can be noticed that, even if the left column is yielded in both models, the deformation of the plastic hinge in model B is lower than in model A. This is the positive effect of the activation of the CWSTs in the non-linear model B.

As mentioned before, the different values of chord rotations influence also the calculation of the resistance against cyclic shear. For the left column of the frame with SF^1 = 2, that is equal to 82.3 kN for model A and 135.7 kN for model B. Whereas, for SF^1 = 2, they decrease to 80.6 kN and 81.7 kN, respectively. Indeed, due to the fact that the ductility demand is higher in model A, the shear resistance is lower than the one found for model B, for both scaling factors. In any case, the shear strength of columns is always higher than the shear value corresponding to the maximum flexural capacity of the plastic hinges, therefore no shear failure is predicted by the analyses. Therefore, the base shear at the ultimate condition is equal for systems with and without CWSTs, so the verifications depend on the value of chord rotations only.

Table A.3. Scaling factors SF^1 for each of the seven accelerograms adopted in the time-history analyses, for model A and model B, corresponding to the three chord rotation limits considered.

N°	SF^0	RL1: θ_u		RL2: 80% θ_u		RL3: 60% θ_u	
		SF^1 model A	SF^1 model B	SF^1 model A	SF^1 model B	SF^1 model A	SF^1 model B
TH1	1.982	3.20	2.90	2.70	2.80	2.00	2.30
TH2	2.717	2.80	3.20	2.40	2.80	1.60	2.00
TH3	1.516	3.10	3.90	2.70	3.50	2.10	2.30
TH4	1.455	3.80	5.20	3.40	4.40	2.20	3.00
TH5	1.122	1.80	3.10	1.50	2.30	1.10	1.80
TH6	0.631	1.30	1.70	1.10	1.50	0.90	1.30
TH7	0.941	3.60	6.20	3.00	5.10	2.40	3.60

Table A.3 summarizes the scaling factors to be used in models A and B in order to achieve the ultimate rotation of the plastic hinges at the base of columns, considering the three different rotation limits RL defined at the beginning of the present section. The positive effect of the CWSTs is generally visible, since the model B reaches the collapse condition for higher scaling factors compared to model A. However, ground-motion record TH1 has an opposite behavior for the rotation limit RL1. Anyway, this effect is not observed considering all the other cases. This particular behavior can be attributed to the insurgence of dynamic amplifying effects in model B for this specific record, at scaling factors SF^1 higher than 2.8. Indeed, for lower scaling factors, the positive action of the CWSTs is again evident in model B. As expected, the lowest scaling factors for both models A and B among the three thresholds considered, are found for RL3, corresponding to 60% reduction of the ultimate chord rotations.

A.5 BEHAVIOR FACTOR ESTIMATION

The evaluation of the behavior factor for the existing structure (Model A), and for the structure equipped with CWSTs (Model B), is discussed out is this Section. The behavior factor q is calculated as:

$$q = \frac{V_{b,el}}{V_{b,nl}} \tag{A.4}$$

Where $V_{b,nl}$ is the maximum base shear calculated from the non-linear analyses described in Section A.4.2., with a ground-motion scaling factor bringing each model to the ultimate chord rotation, and $V_{b,el}$ is the maximum base shear in an equivalent elastic structure with the same base acceleration. For all the limits of ultimate chord rotation considered, $V_{b,nl}$ is constant and equal to 140 kN while the corresponding scaling factor for each accelerogram is reported in Table A.3, with reference to the three different rotation limits RL. The absolute values of $V_{b,el}$ obtained from the equivalent elastic model are reported Table A.4. This model is similar to model A, but it does not have plastic hinges at the base of columns.

As an example, the time histories of the base shear for the equivalent linear model are reported in Figure A.9, for TH7. In particular, Figure A.9a concerns RL1 and shows with a black line the base shear $V_{b,el}$, calculated with a scaling factor $SF^1 = 3.6$ obtained from model A, and with a red line $V_{b,el}$ calculated with $SF^1 = 6.2$, obtained from model B. The value of $V_{b,nl}$ is also reported with a dashed line. Clearly, since the model is fully linear, the time histories are simply scaled. Figure A.9b illustrates the same results for RL3, corresponding to the 60% reduction of the ultimate chord rotation thresholds. The plots correspond to $SF^1 = 2.4$ for frame A, and $SF^1 = 3.6$ for frame B. In this case, with a lower threshold for the ultimate condition compared to the previously discussed case, the gap between the results of frames A and B is lower. This is probably due to the aforementioned amplifying dynamic effects observed at higher values of the scaling factors.

Table A.5 reports the behavior factor values calculated with Equation (A.4) for each RL, and the corresponding average values in the bottom row. The same values are plotted in Figure A.10, showing the variability of q for the seven accelerograms adopted, for each model. On average, the variability of q is consistent with the values observed for the precast buildings analyzed in Pollini et al. (2021). It is worth noticing that the same behavior factors are obtained for TH5, TH6 and TH7, both for model A for RL1, and for model B for RL3. These results for the two models are not correlated, and they are probably due to the fact the scaling factors SF^1 are calculated up to the first decimal digit. If additional analyses were performed, considering more refined scaling factors, the results would likely differ for the two models.

As expected, the adoption of different ultimate chord rotations in columns affect significantly the results, since in RL2 and RL3 there is a consistent reduction in the behavior factors with respect to RL1. In particular for what concerns the model A, the average behavior factors for RL2 and 3 are 14% and 36% lower than the value obtained for RL1, respectively. Similarly for the model B, the behavior factors are 13% and 34% smaller compared to RL1 results.

Table A.4. Absolute values of the base shear calculated in the time-history analyses of the linear frame model. See Table 3 for the corresponding scaling factors for the accelerograms.

N°	$V_{b,nl}$ [kN]	RL1: θ_u		RL2: 80% θ_u		RL3: 60% θ_u	
		$V_{b,el}$ [kN] model A	$V_{b,el}$ [kN] model B	$V_{b,el}$ [kN] model A	$V_{b,el}$ [kN] model B	$V_{b,el}$ [kN] model A	$V_{b,el}$ [kN] model B
TH1	140	483	441	412	427	309	354
TH2	140	493	558	427	493	289	359
TH3	140	375	466	328	421	257	281
TH4	140	440	591	395	506	258	350
TH5	140	318	528	267	401	197	318
TH6	140	371	471	318	422	263	371
TH7	140	341	543	289	460	234	341

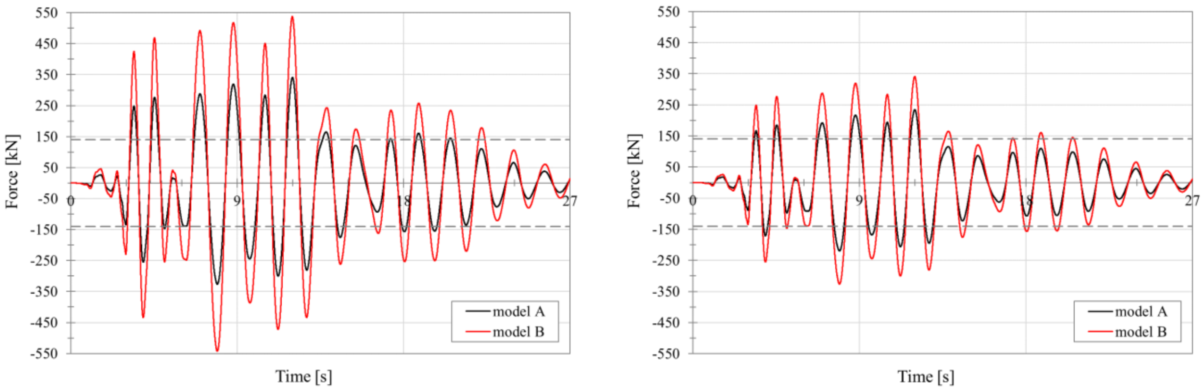

(a) *(b)*

Figure A.9. Time-histories of the base shear $V_{b,el}$ for record TH7, for model A (black line) and model B (red line): a) results for RL1 with threshold θ_u; b) results for RL3 with threshold 60% θ_u.

Eurocode 8 part 1 (CEN 2005), would recommend to adopt a behavior factor lower than 1.5 for a newly designed precast structure without seismic detailing. Moreover, Eurocode 8 part 3 (CEN 2005) suggests to adopt a behavior factor not higher than 1.5 for an existing reinforced concrete structure for which the available ductility is not specifically justified. Since the columns of the existing frame under analysis are characterized by poor transversal reinforcement and are not designed against seismic actions, the average behavior factor of 2.88 obtained for model A is deemed to have a certain degree of overestimation. The result is considered to be more realistic for this case study, when a reduction of the ultimate chord rotation is introduced. In particular, q decreases from 2.88, to 2.49 with a collapse limit 80% of θ_u, and to 1.84 with a collapse limit 60% of θ_u. These results clearly depend on the ultimate rotation limits predicted by Equation (A.2), which are not specific for existing precast columns, therefore, additional research is necessary in order to find more suitable formulations to be applied to this structural typologies, as recognized also by Magliulo et al. (2019).

Table A.5. Behavior factors estimated for model A and model B, for the seven records adopted in the time-history analyses, for the three ultimate Rotation Limits considered.

N°	RL1: θ_u		RL2: 80% θ_u		RL3: 60% θ_u	
	q model A	q model B	q model A	q model B	q model A	q model B
TH1	3.45	3.15	2.94	3.05	2.21	2.53
TH2	3.52	3.98	3.05	3.52	2.06	2.56
TH3	2.68	3.33	2.34	3.01	1.83	2.00
TH4	3.14	4.22	2.82	3.61	1.84	2.50
TH5	2.27	3.77	1.90	2.87	1.41	2.27
TH6	2.65	3.36	2.27	3.01	1.88	2.65
TH7	2.44	3.88	2.06	3.29	1.67	2.44
Average values	**2.88**	**3.67**	**2.49**	**3.19**	**1.84**	**2.42**

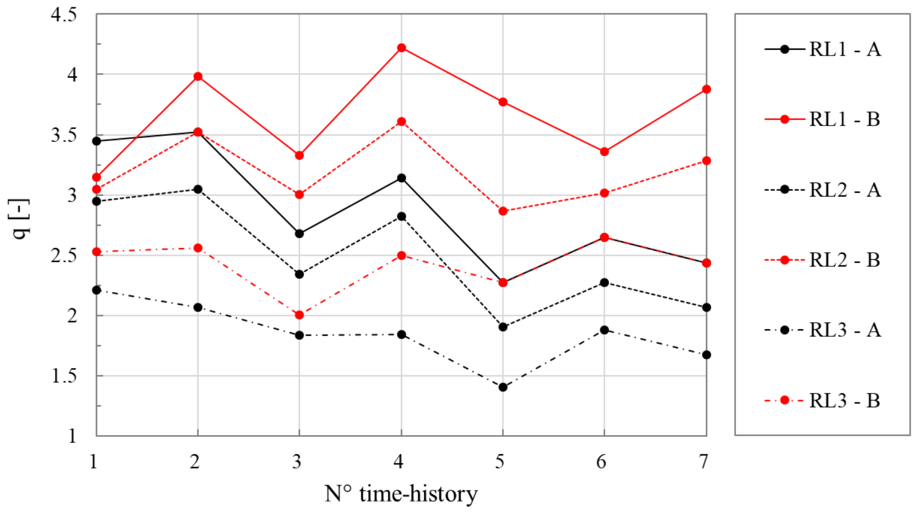

Figure A.10. Behavior factor calculated for model A and B, for the three RL scenarios considered.

A.6 CONCLUSIONS

This work discusses the seismic retrofit of an existing precast RC building equipped with CWSTs at beam-column joints. Non-linear time-history analyses have been conducted on two different models of the main frame of the structure, one with hinged beam-column connections representing the existing condition (model A), and on the one with CWST devices (model B). The effects of the introduction of the CWSTs in the connections is evaluated in terms of chord rotations demand on the columns and base shear forces, and equivalent behavior factors are proposed for the two structures. The sensitivity of the outcomes depending on the ultimate chord rotations of columns is analyzed considering three rotation limits. On the basis of the results of the numerical simulations, the following conclusions can be drawn:

- In general, the maximum chord rotations of columns observed in the frame model with CWSTs are lower than the maximum values observed in the frame model with hinged connections, at the same scaling factor of the records, i.e. under the same seismic action;
- The damage mechanism of columns is in fully agreement with the design criteria adopted for the intervention, since, in all the analyses, the columns in model B do not yield until the attainment of the maximum deformation of the devices;
- Equivalent behavior factors are calculated for model A and model B, for three threshold values of ultimate chord rotations;
- The behavior factors estimated for model B are always higher than the ones estimated for model A, featuring simple hinged connections: the increase of the mean values of behavior factor is about 30% for model B with dissipative devices;
- The behavior factor depends on the ultimate chord rotation of columns considered, showing that the behavior factor significantly decreases with the decrease of θ_u;
- Additional analyses adopting other formulations for the calculation of θ_u are required in order to find realistic results for the specific case of evaluating existing precast columns; moreover, further research may be necessary for the modelling of the non-linear flexural behavior of precast elements;
- CWST devices are deemed to be a good solution for maintaining a low level of stress and deformation in the existing columns of the frame, since frame model B is less vulnerable than frame model A, under the same seismic actions.

LIST OF FIGURES

LIST OF TABLES

REFERENCES

———— A ————

Agenzia regionale per la Ricostruzione – Sisma 2012. (2018) Analisi tecnico-economica della ricostruzione post sisma degli edifici produttivi. Centro Stampa Regione Emilia-Romagna, Bologna. Accessed 13 December 2021 (in Italian). https://www.regione.emilia-romagna.it/terremoto

Andreolli F., Bagolusi P., D’Alpaos C., Faleschini F., Zanini M.A. (2022) An AHP model for multiple-criteria prioritization of seismic retrofit solutions in gravity-designed industrial buildings. *Journal of Building Engineering*, 45-103493. https://doi.org/10.1016/j.jobe.2021.103493

Anglade E., Giatreli A.M., Blyth A., Di Napoli B., Parisse F., Namourah Z., Rodrigues H., Ferreira T.M. (2020) Seismic damage scenarios for the Historic City Center of Leiria, Portugal: analysis of the impact of different seismic retrofitting strategies on emergency planning. *International Journal of Disaster Risk Reduction*, 44:101432. https://doi.org/10.1016/j.ijdrr.2019.101432

Asprone D., Jalayer F., Simonelli S., Acconcia A., Prota A., Manfredi G. (2013) Seismic insurance model for the Italian residential building stock. *Structural Safety*, 44:70-79. https://doi.org/10.1016/j.strusafe.2013.06.001

Asteris P.G., Antoniou S.T., Sophianopoulos D.S., Chrysostomou C.Z. (2011) Mathematical macromodeling of infilled frames: state of the art. *ASCE Journal of Structural Engineering*, 137(12):1508-1517. https://doi.org/10.1061/(ASCE)ST.1943-541X.0000384

ATC - Applied Technology Council. (1989) Procedures for post-earthquake safety evaluation of buildings. ATC20-89: Redwood City, CA.

———— B ————

Babič A., Dolšek M. (2016) Seismic fragility functions of industrial precast building classes. *Engineering Structures*, 118:357-370. https://doi.org/10.1016/j.engstruct.2016.03.069

Basaglia A., Cianchino G., Cocco G., Rapone D., Terrenzi M., Spacone E., Brando G. (2021) An automatic procedure for deriving building portfolios using the Italian “CARTIS” online database. *Structures*, 34:2974-2986. https://doi.org/10.1016/j.istruc.2021.09.054

Batalha N., Rodrigues H., Varum H. (2019) Seismic performance of RC precast industrial buildings-learning with the past earthquakes. *Innovative Infrastructure Solutions*, 4(4):1-13. https://doi.org/10.1007/s41062-018-0191-y

Beetham T. (2013) Simplified displacement based performance assessment of retrofit alternatives for decision making. Dissertation for Master Degree, Università di Pavia.

Belleri A., Brunesi E., Nascimbene R., Pagani M., Riva P. (2014) Seismic performance of precast industrial facilities following major earthquakes in the italian territory. *Journal of Performance of Constructed Facilities*, 29(5):04014135. https://doi.org/10.1061/(ASCE)CF.1943-5509.0000617

Belleri A., Torquati M., Riva P., Nascimbene R. (2015) Vulnerability assessment and retrofit solutions of precast industrial structures. *Earthquake Structures*, 8(3):801-820. http://dx.doi.org/10.12989/eas.2015.8.3.801

Belleri A., Torquati M., Marini A., Riva P. (2016) Horizontal cladding panels: in-plane seismic performance in precast concrete buildings. *Bulletin of Earthquake Engineering*, 14:1103–1129. https://doi.org/10.1007/s10518-015-9861-8

Belleri A., Marini A., Riva P., Nascimbene R. (2017) Dissipating and re-centring devices for portal-frame precast structures. *Engineering Structures*, 150:736-745. https://doi.org/10.1016/j.engstruct.2017.07.072

Belleri A., Cornali F., Passoni C., Marini A., Riva P. (2018) Evaluation of out-of-plane seismic performance of column-to-column precast concrete cladding panels in one-storey industrial buildings. *Earthquake Engineering Structural Dynamics*, 47:397-417. https://doi.org/10.1002/eqe.2956

Belleri A., Dal Lago B., Rodrigues H. (2021) Editorial: Advances in Seismic Performance and Risk Estimation of Precast Concrete Buildings. *Frontiers in Built Environment*, 7:822262. https://doi.org/10.3389/fbuil.2021.822262

Bellotti D., Casotto C., Crowley H., Deyanova M.G., Germagnoli F., Fianchisti G., Lucarelli E., Riva S., Nascimbene R. (2014) Single-storey precast buildings: probabilistic distribution of structural systems and subsystems from the sixties (in Italian). *Progettazione Sismica*, 5(3):41-70. http://dx.medra.org/10.7414/PS.5.3.41-70

Benjamin JR, Cornell CA. (1970) Probability, statistics, and decision for civil engineers. McGraw-Hill Book Company, United States of America.

Biondini F., Dal Lago B., Toniolo G. (2013-a) Role of wall panel connections on the seismic performance of precast structures. *Bulletin of Earthquake Engineering*, 11:1061-1081.

Biondini F., Titi A., Toniolo G. (2013-b) Prestazioni sismiche di strutture prefabbricate con connessioni trave-pilastro ad attrito (in Italian). *Proceedings of the XV Conference of the Italian Association of Seismic Engineering (ANIDIS)*, Padua, Italy, 30 June-4 July.

Biskinis D.E., Fardis M.N. (2004) Cyclic strength and deformation capacity of RC members, including members retrofitted for earthquake resistance. *Proceedings of the 5th International Ph.D Symposium in Civil Engineering*, Delft, Balkema, 1125-1133.

Biskinis D.E., Fardis M.N. (2008) Cyclic deformation capacity, resistance and effective stiffness of RC members with or without retrofitting. *Proceedings of the 14th World conference on Earthquake Engineering*, Beijing, China, 12-17 October.

Boomer J.J., Acevedo A.B. (2004) The use of real earthquake accelerograms as input to dynamic analysis. *Journal of Earthquake Engineering*, 8(1):43-91.

Bonfanti C., Carabellese A., Toniolo G. (2008) Strutture prefabbricate: catalogo delle tipologie esistenti. Assobeton (in Italian). http://www.reluis.it/

Borzi B., Crowley H., Pinho R. (2008a) Simplified pushover-based earthquake loss assessment (SP-BELA) method for masonry buildings. *International Journal of Architectural Heritage*, 2:353-376. https://doi.org/10.1080/15583050701828178

Borzi B., Pinho R., Crowley H. (2008b) Simplified pushover-based vulnerability analysis for large-scale assessment of RC buildings. *Engineering Structures*, 30:804-820. https://doi.org/10.1016/j.engst ruct.2007.05.021

Borzi B., Onida M., Faravelli M., Polli D., Pagano M., Quaroni D., Cantoni A., Speranza E., Moroni C. (2020) IRMA platform for the calculation of damages and risks of residential buildings. *Bulletin of Earthquake Engineering*. https://doi.org/10.1007/s1051 8-020-00924 -x

Borzi B., Faravelli M., Di Meo A. (2021) Application of the SP-BELA methodology to RC residential buildings in Italy to produce seismic risk maps for the national risk assessment. *Bulletin of Earthquake Engineering*, 19:3185:3208. https://doi.org/10.1007/s10518-020-00953-6

Bosio M., Belleri A., Riva P., Marini A. (2020) Displacement-based simplified seismic loss assessment of Italian precast buildings. *Journal of Earthquake Engineering*, 24(1):60-81. https://doi.org /10.1080/13632469.2020.1724215

Bournas D.A., Negro P., Molina F.J. (2013) Pseudodynamic tests on a full-scale 3-storey precast concrete building: behavior of the mechanical connections and floor diaphragms. *Engineering Structures*, 57:609-627.

Bournas D.A., Negro P., Taucer F.F. (2014) Performance of industrial buildings during the Emilia earthquakes in Northern Italy and recommendations for their strengthening. *Bulletin of Earthquake Engineering*, 12:2383-2404. https://doi.org/10.1007/s10518-013-9466-z

Bovo M., Savoia M. (2018) Numerical simulation of seismic-induced failure of a precast structure during the Emilia earthquake. *Journal of Performance of Constructed Facilities*, 32(1):04017119. https://doi.org/10.1061/(ASCE)CF.1943-5509.0001086

Bovo M., Buratti N. (2019) Evaluation of the variability contribution due to epistemic uncertainty on constitutive models in the definition of fragility curves of RC frames. *Engineering Structures*, 188:700-716. https://doi.org/10.1016/j.engstruct.2019.03.064

Bovo M., Savoia M. (2019) Evaluation of force fluctuations induced by vertical seismic component on reinforced concrete precast structures. *Engineering Structures*, 179:70-87. https://doi.org/10.1016/j.engstruct.2018.10.018

Bovo M., Savoia M. (2021) Fast seismic assessment of existing precast structures by means of fragility surfaces: the PRESSAFE methodology. *Journal of Earthquake Engineering*. https://doi.org/10.1080/13632469.2021.1964648

Bovo M., Savoia M., Praticò L. (2021) Seismic Performance Assessment of a Multistorey Building Designed with an Alternative Capacity Design Approach. *Advances in Civil Engineering*, Article ID 5178065. https://doi.org/10.1155/2021/5178065

Bovo M., Praticò L., Savoia M. (2022) PRESSAFE-disp: a method for the fast in-plane seismic assessment of existing precast RC buildings after the Emilia earthquake of May 2012. *Bulletin of Earthquake Engineering*, 20:2751-2794. https://doi.org/10.1007/s10518-022-01318-x

Bradley B.A., Dhakal R.P., Cubrinovski M., MacRae G.A. (2008) Seismic loss estimation for efficient decision making. *Bulletin of the New Zealand Society for Earthquake Engineering*, NSZEE Conference, April 2008.

Bramerini F., Di Pasquale G. (2008) Updated seismic risk maps for Italy. *Ingegneria Sismica*, XXV(2):5-23 (in Italian).

Bressanelli M.E., Bellotti D., Belleri A., Cavalieri F., Riva P., Nascimbene R. (2021) Influence of Modelling Assumptions on the Seismic Risk of Industrial Precast Concrete Structures. *Frontiers in Built Environment*, 7: 629956. https://doi.org/10.3389/fbuil.2021.629956

Brunesi E., Nascimbene R., Bolognini D., Bellotti D. (2015) Experimental investigation of the cyclic response of reinforced precast concrete framed structures. *PCI Journal*, 60(2):57-79.

Brunesi E., Nascimbene R., Peloso S. (2020) Evaluation of the seismic response of precast wall connections: experimental observations and numerical modelling. *Journal of Earthquake Engineering*, 24(7):1057-1082. https://doi.org/10.1080/13632469.2018.1469440

Buratti N., Minghini F., Ongaretto E., Savoia M., Tullini N. (2017) Empirical seismic fragility for the precast RC industrial buildings damaged by the 2012 Emilia (Italy) earthquakes. *Earthquake Engineering & Structural Dynamics*, 46(14):2317-2335. https://doi.org/10.1002/eqe.2906

Buratti N., Simoni E., Mazzotti C. (2022) Shake maps for the 2012 Emilia earthquake in terms of different ground-motion intensity measures. *Submitted for publication*.

———— C ————

Calvi G.M., Pinho R., Magenes G, Bommer J.J., Restrepo-Vélez L.F., Crowley H. (2006) Development of seismic vulnerability assessment methodologies over the past 30 years. *ISET Journal of Earthquake Technology*, 43(3):75-104.

Cardone D., Perrone G. (2015) Developing fragility curves and loss functions for masonry infill walls. *Earthquake and Structures*, 9(1):257-279. https://doi.org/10.12989/eas.2015.9.1.257

Caselli G. (2020) The economic impact of the earthquake. Lecture given in: After the Damages International Summer School, Università di Ferrara. https://www.afterthedamages.com/

Casotto C., Silva V., Crowley H., Nascimbene R., Pinho R. (2015) Seismic fragility of Italian RC precast industrial structures. *Engineering Structures*, 94:122-136.

Celarec D., Ricci P., Dolšek M. (2012) The sensitivity of seismic response parameters to the uncertain modelling variables of masonry infilled reinforced concrete frames. *Engineering Structures*, 35:165-177.

Chiozzi A., Miranda E. (2017) Fragility functions for masonry infill walls with in-plane loading. *Earthquake Engineering and Structural Dynamics*, 46:2831-2850. https://doi.org/10.1002/eqe.2934

Colombo A., Lamperti M., Negro P., Toniolo G. (2016) Design guidelines for wall panel connections. *JRC Technical Reports*. DOI:10.2788/546845

Crisafulli F.J., Carr A.J., Park R. (2000) Analytical modelling of infilled frame structures - a general review. *Bulletin of the New Zealand Society for Earthquake Engineering*, 33(1):30-47. https://doi.org/10.5459/bnzsee.33.1.30-47

Crowley H., Pinho R., Bommer J.J. (2004) A probabilistic displacement-based vulnerability assessment procedure for earthquake loss estimation. *Bulletin of Earthquake Engineering*, 2:173-219.

Crowley H., M. Colombi M., Borzi B., Faravelli M., Onida M., Lopez M., Polli D., Meroni F., Pinho R. (2009) A comparison of seismic risk maps for Italy. *Bulletin of Earthquake Engineering*, 7(1):149–180.

CEN (European Committee for Standardization). (2004) Design of concrete structures – Part 1-1: General rules and rules for buildings. *Eurocode 2 (EC)*, Brussels.

CEN (European Committee for Standardization). (2005) Design of structures for earthquake resistance – Part 1: General rules, seismic actions and rules for building. *Eurocode 8 (EC)*, Brussels.

CEN (European Committee for Standardization). (2005) Design of structures for earthquake resistance – Part 3: Assessment and retrofitting of buildings. *Eurocode 8 (EC)*, Brussels.

Cosenza E., Del Vecchio C., Di Ludovico M., Dolce M., Moroni C., Prota A., Renzi E. (2018) The Italian guidelines for seismic risk classification of constructions: technical principles and validation. *Bulletin of Earthquake Engineering*. https://doi.org/10.1007/s10518-018-0431-8

CSPFEA, Engineering Solutions, Midas GEN. Accessed 21 March 2021. https://www.cspfea.net/prodotti/midas-gen/

——— D ———

D.M. 20/02/2018. (2018) *Norme tecniche per le costruzioni (NTC)*. Decreto ministeriale del Ministero delle Infrastrutture e dei trasporti, Rome.

D'Aragona M.G., Polese M., Di Ludovico., Prota A. (2021) The use of Stick-IT model for the prediction of direct economic losses. *Earthquake Engineering and Structural Dynamics*, 2021:1-24. https://doi.org/10.1002/eqe.3429

da Porto F., Donà M., Rosti A. et al. (2021) Comparative analysis of the fragility curves for Italian residential masonry and RC buildings. *Bulletin of Earthquake Engineering,* 19:3209–3252. https://doi.org/10.1007/s10518-021-01120-1

Dal Lago B., Biondini F., Toniolo G. (2017-a) Friction-based dissipative devices for precast concrete panels. *Engineering Structures*, 147:356-371. https://doi.org/10.1016/J.ENGST RUCT.2017.05.050

Dal Lago B., Biondini F., Toniolo G. (2017-b) Experimental investigation on steel W-shaped folded plate dissipative connectors for horizontal precast concrete cladding panels. *Journal of Earthquake Engineering*, 22(5):778-800. https://doi.org/10.1080/13632469.2016.1264333

Dal Lago B., Toniolo G., Felicetti R., Lamperti Tornaghi M. (2017-c) End support connection of precast roof elements by bolted steel angles. *Structural Concrete*, 18(5):755-767. https://doi.org/10.1002/suco.201600218

Dal Lago B., Ferrara L. (2018) Efficacy of roof-to-beam mechanical connections on the diaphragm behaviour of precast decks with spaced roof elements. *Engineering Structures*, 176:681-696. https://doi.org/10.1016/j.engstruct.2018.09.027

Dal Lago B., Bianchi S., Biondini F. (2019) Diaphragm effectiveness of precast concrete structures with cladding panels under seismic action. *Bulletin of Earthquake Engineering*, 17(1):473-495. https://doi.org/10.1007/s10518-018-0452-3

Daniell J. E., Khazai B., Wenzel F., Vervaeck A. (2011) The CATDAT damaging earthquakes database. *Natural Hazards and Earth System Sciences*, 11:2235–2251. https://doi.org/10.5194/nhess-11-2235-2011

De Martino G., Di Ludovico M., Prota A., Moroni C., Manfredi G., Dolce M. (2016) Estimation of repair costs for RC and masonry residential buildings based on damage data collected by post-earthquake visual inspection. *Bulletin of Earthquake Engineering*. DOI:10.1007/s10518-016-0039-9

De Risi M.T., Del Gaudio C., Verderame G.M. (2020) A component-level methodology to evaluate the seismic repair costs of infills and services for Italian RC buildings. *Bulletin of Earthquake Engineering*, 18:6533-6570. https://doi.org/10.1007/s10518-020-00944-7

Del Gaudio C., Ricci P., Verderame G.M., Manfredi G. (2015) Development and urban-scale application of a simplified method for seismic fragility assessment of RC buildings. *Engineering Structures*, 91:40-57. http://dx.doi.org/10.1016/j.engstruct.2015.01.031

Del Gaudio C., Ricci P., Verderame G.M., Manfredi G. (2016) Observed and predicted earthquake damage scenarios: the case study of Pettino (L'Aquila) after the 6th April 2009 event. *Bulletin of Earthquake Engineering*, 14:2643–2678. DOI:10.1007/s10518-016-9919-2

Del Gaudio C., De Martino G., Di Ludovico M., Ricci P., Verderame G.M. (2017) Empirical fragility curves from damage data on RC buildings after the 2009 L'Aquila earthquake. *Bulletin of Earthquake Engineering*, 15:1425-1450.

Del Monte E., Falsini C., Boschi S., Menichini G., Orlando M. (2019) An innovative cladding panel connection for RC precast buildings. *Bulletin of Earthquake Engineering*, 17:845-865. https://doi.org/10.1007/s10518-018-0470-1

Del Gaudio C., Di Ludovico M., Polese M., Manfredi G., Prota A., Ricci P., Verderame G.M. (2020) Seismic fragility for Italian RC buildings based on damage data of the last 50 years. *Bulletin of Earthquake Engineering*, 18:2023-2059. https://doi.org/10.1007/s10518-019-00762-6

Del Vecchio C., Di Ludovico M., Pampanin S., Prota A. (2018) Repair Costs of Existing RC Buildings Damaged by the L'Aquila Earthquake and Comparison with FEMA P-58 Predictions. *Earthquake Spectra*, 34(1):237-263. DOI:10.1193/122916EQS257M

Del Vecchio C., Di Ludovico M., Prota A. (2020) Repair costs of reinforced concrete building components: from actual data analysis to calibrated consequence functions. *Earthquake Spectra*, 36(1):353-377. DOI:10.1177/8755293019878194

Del Vecchio C., Di Ludovico M., Prota A. (2021) Cost and Effectiveness of Fiber-Reinforced Polymer Solutions for the Large-Scale Mitigation of Seismic Risk in Reinforced Concrete Buildings. *Polymers*, 13:2962. https://doi.org/10.3390/polym13172962

Demartino C., Vanzi I., Monti G. (2017) Probabilistic estimation of seismic economic losses of portal-like precast industrial buildings. *Earthquake Structures*, 13(3):323-335. http://dx.doi.org/10.12989/eas.2017.13.3.323

Demartino C., Vanzi I., Monti G., Sulpizio C. (2018) Precast industrial buildings in Southern Europe: loss of support at frictional beam-to-column connections under seismic actions. *Bulletin of Earthquake Engineering*, 16:259-294. https://doi.org/10.1007/s1051 8-017-0196-5

Deyanova M.G., Pampanin S., Nascimbene R. (2014) Assessment of single-storey precast concrete industrial buildings with hinged beam-column connections with and without dowels. *Second European conference on earthquake engineering and seismology*, Istanbul, Turkey, 25-29 August.

Di Ludovico M., Prota A., Moroni C., Manfredi G., Dolce M. (2017a) Reconstruction process of damaged residential buildings outside historical centres after the L'Aquila earthquake: part I-"light damage" reconstruction. *Bulletin of Earthquake Engineering*, 15(2):667–692. DOI: 10.1007/s10518-016-9877-8

Di Ludovico M., Prota A., Moroni C., Manfredi G., Dolce M. (2017b) Reconstruction process of damaged residential buildings outside historical centres after the L'Aquila earthquake: part II-"heavy damage" reconstruction. *Bulletin of Earthquake Engineering*, 15(2):693–729. DOI: 10.1007/s10518-016-9979-3

Di Ludovico M., Fico R., Provenzano S., Mannella A., De Martino G., Marra A., Speranza E., Prota A., Dolce M. (2020) The reconstruction of residential buildings of historical centres damaged by L'Aquila 2009 Earthquake. In *Proceedings of the 17th World Conference on Earthquake Engineering,* 17WCEE, Sendai, Japan, September 13-18.

Di Ludovico M., De Martino G., Prota A., Manfredi G., Dolce M. (2021) Damage Assessment in Italy, and Experiences After Recent Earthquakes on Reparability and Repair Costs. In: *Advances in Assessment and Modeling of Earthquake Loss*, Springer. https://doi.org/10.1007/978-3-030-68813-4

Dolce M., Masi A., Cappa T., Nigro D., Ferrini M. (2003) Experimental evaluation of effectiveness of local strengthening on columns of R/C existing structures. In *Proceedings of the fib-Symposium Concrete Structures in Earthquake Regions*, Athens, Greece, 6–9 May 2003.

Dolce M., Nicoletti M., Ammirati A., Bianconi R., Filippi L., Gorini A., Marcucci S., Palma F., Zambonelli E., Lavecchia G., et al. (2012) The Ferrara arc thrust earthquakes of May-June 2012 (Northern Italy): strong-motion and geological observations. Mirandola Earthquake Working Group - Report 2. http://www.protezionecivile.gov.it/

Dolce M., Di Bucci D. (2017) Comparing recent Italian earthquakes. *Bulletin of Earthquake Engineering*, 15:497-533. DOI: 10.1007/s10518-015-9773-7

Dolce M., Speranza E., Giordano F., Borzi B., Bocchi F., Conte C., Di Meo A., Faravelli M., Pascale V. (2019) Observed damage database of past Italian earthquakes: the Da.D.O webgis. *Bollettino di Geofisica Teorica e Applicata,* 60(2):141–164. DOI:10.4430/bgta0254

Dolce M., Prota A., Borzi B., da Porto F., Lagomarsino S., Magenes G., Moroni C., Penna A., Polese M., Sper- anza E., Verderame G.M., Zuccaro G. (2020) Seismic risk assessment of residential buildings in Italy. *Bulletin of Earthquake Engineering*. https://doi.org/10.1007/s1051 8-020-01009 -5

Dolce M., Speranza E., De Martino G., Conte C., Giordano F. (2021) The implementation of the Italian National Seismic Prevention Plan: A focus on the seismic upgrading of critical buildings. *International Journal of Disaster Risk Reduction*, 62:102391. https://doi.org/10.1016/j.ijdrr.2021.102391

DPC - Italian Civil Protection Department (2018) National Risk Assessment 2018. Overview of the potential major disasters in Italy. Updated December 2018

——————— E ———————

EMS-98 (1998) European Macroseismic Scale 1998. In: Grünthal G (ed) Cahiers du Centre Européen de Géodynamique et de Séismologie, Vol. 15, Luxemburg.

Ercolino M., Magliulo G., Manfredi G. (2016) Failure of a precast RC building due to Emilia-Romagna earthquakes. *Engineering Structures*, 118:262-273. http://dx.doi.org/10.1016/j.engstruct.2016.03.054

Ercolino M., Bellotti D., Magiulo G., Nascimbene R. (2018a) Vulnerability analysis of industrial RC precast buildings designed according to modern seismic codes. *Engineering Structures*, 158:67-78. https://doi.org/10.1016/j.engstruct.2017.12.005

Ercolino M., Petrone C., Magliulo G., Manfredi G. (2018b) Seismic Design of single-story precast structures for P-Δ effects. *ACI Structural Journal*, 115(4):943-955. DOI:10.14359/51701915

——————— F ———————

Fardis M.N. (1996) Experimental and numerical investigations on the seismic response of RC infilled frames and recommendations for code provisions. LNEC, Lisbon.

FEMA - Federal Emergency Management Agency (1997) FEMA 273, NEHRP Guidelines for the Seismic Rehabilitation of Buildings. Washington, DC.

FEMA - Federal Emergency Management Agency (2000) FEMA 356, Prestandard and Commentary for the Seismic Rehabilitation of Buildings. Washington, DC.

FEMA - Federal Emergency Management Agency (2018) FEMA P-58-1: Seismic performance assessment of buildings: volume 1 – methodology. Second Edition. Washington, DC.

Fisz M. (1963) Probability theory and mathematical statistics. Wiley, New York.

Formisano A., Chieffo N., Mosoarca M. (2017) Probabilistic damage scenario: a case study in Amatrice affected by the 2016 seismic sequence. *Proceedings of 3rd International Conference* PROHITECH, Lisbon.

Formisano A., Chieffo N., Clementi F., Mosoarca M. (2021) Influence of local site effects on the typological fragility curves for class-oriented masonry buildings in aggregate condition. *Open Civil Engineering Journal*, 15(1):149-164. DOI:10.2174/1874149502115010149

——————— G ———————

Gentile R., Del Vecchio C., Pampanin S., Raffaele D., Uva G. (2018) Refinement and validation of the simple lateral mechanism analysis (SLaMA) procedure for RC frames. *Jounal of Earthquake Engineering*. https://doi.org/10.1080/13632469.2018.1560377

Google Earth. Accessed 13 December 2021. https://www.google.it/intl/it/earth/

Grigoriu M. (2002) Stochastic calculus – Applications in Science and Engineering. Birkhäuser, Boston, MA. https://doi.org/10.1007/978-0-8176-8228-6

——————— H ———————

Hofer L., Zanini M.A., Faleschini F., Pellegrino C. (2018) Profitability Analysis for Assessing the Optimal Seismic Retrofit Strategy of Industrial Productive Processes with Business-Interruption Consequences. *Journal of Structural Engineering*, 144(2). https://doi.org/10.1061/(ASCE)ST.1943-541X.0001946

——————— I ———————

INGV, Istituto Nazionale di Geofisica e Vulcanologia. Accessed 13 December 2021. https://www.ingv.it/

Istat, Istituto Nazionale di Statistica (in Italian). Accessed 13 December 2021. https://www.istat.it/it/

Itaca database. Accessed 10 June 2021. http://itaca.mi.ingv.it/ItacaNet_31/#/home

——— K ———

Kurtman B. (2007) A detailed analysis for evaluation of the degradation characteristics of simple structural systems. MS Thesis, Middle East Technical University, Ankara, Turkey.

——— L ———

Lagomarsino S., Cattari S. (2014) Fragility Functions of Masonry Buildings. In: Pitilakis K., Crowley H., Kaynia A. (eds) SYNER-G: *Typology Definition and Fragility Functions for Physical Elements at Seismic Risk*. Geotechnical, Geological and Earthquake Engineering, vol 27. Springer, Dordrecht. https://doi.org/10.1007/978-94-007-7872-6_5

Landi L., Saborio-Romano D., Welch D.P., Sullivan T.J. (2020) Displacement-Based Simplified Seismic Loss Assessment of Post-70s RC Buildings. *Journal of Earthquake Engineering*, 24(S1):114-145. https://doi.org/10.1080/13632469.2020.1735577

Legislative Decree No. 74/2012 of the 6th June (2012) Italian Parliament.

Lestuzzi P., Podestà S., Luchini C., Garofano A., Kazantzidou-Firtinidou D., Bozzano C., Bischof P., Haffter A., Rouiller J.D. (2016) Seismic vulnerability assessment at urban scale for two typical Swiss cities using Risk-UE methodology. *Natural Hazards*, 84:249-269.

Liberatore L., Sorrentino L., Liberatore D., Decanini L.D. (2013) Failure of industrial structures induced by the Emilia (Italy) 2012 earthquakes. *Engineering Failure Analysis*, 34:629-647. https://doi.org/10.1016/j.engfailanal.2013.02.009

Ligabue V., Bovo M., Savoia M. (2014) Connessioni tegolo-trave: studio sperimentale e numerico del comportamento di angolari di collegamento (in Italian). *Proceedings of workshop "Tecniche innovative per il miglioramento sismico di edifici prefabbricati",* Bologna, Italy, 22 October.

Ligabue V. (2015) Cost-effectiveness of alternative retrofit options to support decision making. PhD Thesis, Cicle XXVII, Università di Bologna.

Ligabue V., Buratti N., Savoia M., Pampanin S. (2017) Numerical fragility of typical Italian industrial precast RC frames: effect of geometry and non-structural components. *16th World Conference on Earthquake Engineering*, Paper N° 4531, 16WCEE, January 9th to 13th, Santiago Chile.

Ligabue V., Pampanin S., Savoia M. (2018) Seismic performance of alternative risk-reduction retrofit strategies to support decision making. *Bulletin of Earthquake Engineering*, 16:3001-3030. https://doi.org/10.1007/s10518-017-0291-7

Lima R.M., Ismarrubie Z.N., Zainudin E.S., Tang S.H. (2011) Axial behavior of steel tube wrapped by composite as energy absorber under compressive load, *IEEE Symposium on Business, Engineering and Industrial Applications* (ISBEIA), Langkawi, Malaysia.

Lucantoni A., Bosi V., Bramerini F., De Marco R., Lo Presti T., Naso G., Sabetta F. (2001) Seismic risk in Italy. *Ingegneria Sismica*, XVII(1):5-36 (in Italian).

——— M ———

Magliulo G., Capozzi V., Fabbrocino G., Manfredi G. (2011) Neoprene-concrete friction relationships for seismic assessment of existing precast buildings. *Engineering Structures*, 33:532-538.

Magliulo G., Ercolino M., Petrone C., Coppola O., Manfredi G. (2014) The Emilia earthquake: seismic performance of precast reinforced concrete buildings. *Earthquake Spectra*, 30:891-912. https://doi.org/10.1193/091012EQS285M

Magliulo G., Ercolino M., Cimmino M., Capozzi V., Manfredi G. (2015) Cyclic shear test on a dowel beam-to-column connection of precast buildings. *Earthquake and Structures*, 9(3):541-562.

Magliulo G., Bellotti D., Cimmino M., Nascimbene R. (2018) Modeling and seismic response analysis of RC precast Italian code-conforming buildings. *Journal of Earthquake Engineering,* 22(2):140-167. https://doi.org/10.1080/13632469.2018.1531093

Magliulo G., Bellotti D., Di Salvatore C., Cavalieri F. (2019) RINTC-E project: towards the seismic risk of low and pre-code single-story RC precast buildings in Italy. *Proceedings of the 7th ECCOMAS Thematic Conference on Computational Methods in Structural Dynamics and Earthquake Engineering* (COMPDYN), Crete, Greece, 24-26 June.

Maio R., Ferreira T.M., Vicente R., Estevao J. (2015) Seismic vulnerability assessment of historical urban centres: case study of the old city centre of Faro, Portugal. *Journal of Risk Research*, 19(5):551-580. http://dx.doi.org/10.1080/13669877.2014.988285

Mandelli Contegni M, Palermo A, Toniolo G. (2007) Strutture prefabbricate: schedario dei collegamenti. ReLUIS, Assobeton (in Italian). http://www.reluis.it/

Mandelli Contegni M, Palermo A, Toniolo G. (2008) Strutture prefabbricate: schedario di edifici prefabbricati in C.A. ReLUIS, Assobeton (in Italian). http://www.reluis.it/

Mannela A., Di Ludovico M., Sabino A., Prota A., Dolce M., Manfredi G. (2017) Analysis of the Population Assistance and Returning Home in the Reconstruction Process of the 2009 L'Aquila Earthquake. *Sustainability*, 9,1395. DOI:10.3390/su9081395

Marinini L., Spatti P., Riva P., Nascimbene R. (2011) Strutture prefabbricate: moderni sistemi di protezione antisismica (in Italian). *Progettazione sismica*, 3:23-44.

Martinelli P., Mulas M.G. (2010) An innovative passive control technique for industrial precast frames. *Engineering Structures*, 32:1123-1132. https://doi.org/10.1016/j.engstruct.2009.12.038

Masi A., Chiauzzi L. Santarsiero G., Manfredi V., Biondi S., Spacone E., Del Gaudio C., Ricci P., Manfredi G., Verderame G.M. (2019) Seismic response of RC buildings during the Mw 6.0 August 24, 2016 Central Italy earthquake: the Amatrice case study. *Bulletin of Earthquake Engineering*, 17:5631-5654. https://doi.org/10.1007/s10518-017-0277-5

Masi A., Lagomarsino S., Dolce M., Manfredi V., Ottonelli D. (2021) Towards the updated Italian seismic risk assessment: exposure and vulnerability modelling. *Bulletin of Earthquake Engineering.* https://doi.org/10.1007/s10518-021-01065-5

MathWorks, MATLAB version 2020a. https://www.mathworks.com/products/matlab.html

Mazzotti C., Savoia M., Chinni C., Perri G. (2013) A simplified method for the seismic vulnerability assessment of masonry and reinforced concrete buildings. *Progettazione sismica*, 4(2):95-112 (in Italian). http://dx.medra.org/10.7414/PS.4.2.95-112

Minghini F., Ongaretto E., Ligabue V., Savoia M., Tullini N. (2016) Observational failure analysis of precast buildings after the 2012 Emilia earthquakes. *Earthquake Structures*, 11(2):327-346. https://doi.org/10.12989/eas.2016.11.2.327

Minghini F., Tullini N. (2021) Seismic Retrofitting Solutions for Precast RC Industrial Buildings Struck by the 2012 Earthquakes in Northern Italy. *Frontiers in Built Environment*, 7:631315. https://doi.org/10.3389/fbuil.2021.631315

Miranda E., Aslani H. (2003) Probabilistic Response Assessment for Building-Specific Loss Estimation. PEER Report 2003/03, Berkeley, September.

Moehle J. P. (2003) A framework for performance-based earthquake engineering. *Proceedings, Tenth U.S.-Japan Workshop on Improvement of Building Seismic Design and Construction Practices*, ATC15-9 Report, Applied Technology Council, Redwood City, California.

Muciaccia G., Cervio M., Franzoso M., Veneziano M. (2014) Utilizzo di ancoraggi post-inseriti in interventi di recupero di capannoni industriali in zona sismica (in Italian). *Proceedings of Workshop "Tecniche innovative per il miglioramento sismico di edifici prefabbricati",* Bologna, Italy, 22 October.

——— N ———

Nastri E., Vergato M., Latour M. (2017) Performance evaluation of a seismic retrofitted R.C. precast industrial building. *Earthquake and Structures*, 12(1):13-21. https://doi.org/10.12989/eas.2017.12.1.013

——— O ———

Ongaretto E., Buratti N., Savoia M. (2019) Empirical seismic fragility of different typologies of precast RC industrial buildings. Proceedings of XVIII Convegno Anidis, Ascoli Piceno, Italy.

OpenSees v2.4.0. (2015) Open System for Earthquake Engineering Simulation. Pacific Earthquake Engineering Research Center (PEER).

Ordinanza 57 of the 12 October 2012 of the Emilia Romagna Region, following the Legislative Decree 74/2012. Approvazione delle Linee Guida per la presentazione delle domande e le richieste di erogazione dei contributi (In Italian).

Ottonelli D., Cattari S., Lagomarsino S. (2020) Displacement-Based Simplified Seismic Loss Assessment of Masonry Buildings. *Journal of Earthquake Engineering*, 24:23-59. https://doi.org/10.1080/13632469.2020.1755747

——— P ———

Pampanin S. (2017) Towards the practical implementation of performance-based assessment and retrofit strategies for RC buildings: challenges and solutions. In: SMAR2017- *Fourth conference on Smart Monitoring, Assessment and Rehabilitation of Structures*, Keynote Lecture, 13-15 Sept, Zurich, Switzerland.

PEER, Pacific Earthquake Engineering Research Center. (2013) Final Report of the NGA-West2 Directivity Working Group, PEER Report 2013/09.

PEER, Pacific Earthquake Engineering Research Center, Berkeley. Structural Performance Database PEER Website. Accessed 10 June 2020. http://nisee.berkeley.edu/spd/index.html

PEER, Pacific Earthquake Engineering Research Center, Berkeley. Accessed 21 March 2021. https://peer.berkeley.edu/nga-west

Perrone D., O'Reilly G., Monteiro R., Filiatrault A. (2020) Assessing seismic risk in typical Italian school buildings: From in-situ survey to loss estimation. *International Journal of Disaster Risk Reduction*, 44:101448. https://doi.org/10.1016/j.ijdrr.2019.101448

Petruzzelli F. (2016) Seismic risk assessment of an industrial plant struck by the Emilia 2012 earthquakes. *International Journal of Forensic Engineering*, 3(1-2):146–163.

Polese M., Di Ludovico M., Prota A. (2018) Post-earthquake reconstruction: A study on the factors influencing demolition decisions after 2009 L'Aquila earthquake. *Soil Dynamics and Earthquake Engineering*, 105:139-149. https://doi.org/10.1016/j.soildyn.2017.12.007

Polese M., Di Ludovico M., Gaetani d'Aragona M., Prota A., Manfredi G. (2020) Regional vulnerability and risk assessment accounting for local building typologies. *International Journal of Disaster Risk Reduction*, 43:101400.

Pollini A.V., Buratti N., Mazzotti C. (2014) Effectiveness of a dissipative beam-column connection based on carbon-wrapped steel tubes. *Second European conference on earthquake engineering and seismology*, Istanbul, Turkey, 25-29 August.

Pollini A.V., Buratti N., Mazzotti C. (2018) Experimental and numerical behaviour of dissipative devices based on carbon-wrapped steel tubes for the retrofitting of existing precast RC structures. *Earthquake Engineering & Structural Dynamics*, 1-21. https://doi.org/10.1002/eqe.3017

Pollini A.V., Buratti N., Mazzotti C. (2021) Behavior factor of concrete portal frames with dissipative devices based on carbon-wrapped steel tubes. *Bulletin of Earthquake Engineering*, 19:553-578. https://doi.org/10.1007/s10518-020-00977-y

Porter K.A. (2003) An Overview of PEER's Performance-Based Earthquake Engineering Methodology. *Ninth International Conference on Applications of Statistics and Probability in Civil Engineering* (ICASP9) July 6-9, San Francisco.

Praticò L., Pollini A.V., Sonda D., Buratti N. (2021) Seismic retrofit of existing precast RC buildings with dissipative devices based on Carbon Wrapped Steel Tubes. *ECCOMAS-COMPDYN 2021*, Streamed from Athens, Greece, 27–30 June 2021. DOI:10.7712/120121.8767.19292

Priestley M.J.N., Calvi G.M., Kowalsky M.J. (2007). Displacement-based seismic design of structures, IUSS Press.

Presidente del Consiglio dei Ministri. OPCM 3274/2003 (2003) Primi elementi in materia di criteri generali per la classificazione sismica del territorio nazionale e di normative tecniche per le costruzioni in zona sismica (in Italian).

——— R ———

Ramirez C.M., Miranda E. (2009) Building-specific loss estimation methods & tools for simplified performance-based earthquake engineering. Report No.171. The John A. Blume Earthquake Engineering Center, Stanford.

Ramirez C.M., Miranda E. (2012) Significance of residual drifts in building earthquake loss estimation. *Earthquake Engineering and Structural Dynamics*, 41(11):1477-1493. https://doi.org/10.1002/eqe.2217

Regione Emilia Romagna, Terremoto, La ricostruzione. (in Italian). Accessed 13 December 2021. http://www.regione.emilia-romagna.it/terremoto

ReLUIS (2012) Linee di indirizzo per interventi locali e globali su edifici industriali monopiano non progettati con criteri antisismici. Gruppo di Lavoro Agibilità Sismica dei Capannoni Industriali (in Italian). http://www.reluis.it/

Rodrigues D., Crowley H., Silva V. (2017) Earthquake loss assessment of precast RC industrial structures in Tuscany (Italy). *Bulletin of Earthquake Engineering*, 16:203-228. https://doi.org/10.1007/s10518-017-0195-6

Romano F., Alam M.S., Zucconi M., Faggella M., Barbosa A.R., Ferracuti B. (2021) Seismic demand model class uncertainty in seismic loss analysis for a code-designed URM infilled RC frame building. *Bulletin of Earthquake Engineering*, 19:429-462. https://doi.org/10.1007/s10518-020-00994-x

Rossetto T., D'Ayala D., Ioannou I., Meslem A. (2014) Evaluation of existing fragility curves. SYNER-G: typology definition and fragility functions for physical elements at seismic risk. Springer, Dordrecht, 47-93.

Rossi A., Morandi P., Magenes G. (2021) A novel approach for the evaluation of the economical losses due to seismic actions on RC buildings with masonry infills. *Soil Dynamics and Earthquake Engineering,* 145-106722. https://doi.org/10.1016/j.soildyn.2021.106722

Rossi L., Holtschoppen B., Butenwerg C. (2019a) Official data on the economic consequences of the 2012 Emilia-Romagna earthquake: a first analysis of database SFINGE. *Bulletin of Earthquake Engineering*, 17:4855-4884. https://doi.org/10.1007/s10518-019-00655-8

Rossi L., Parisi D., Casari C., Montanari L., Ruggieri G., Holtschoppen B., Butenwerg C. (2019b) Empirical data about direct economic consequences of Emilia-Romagna 2012 earthquake on long-span-beam buildings. *Earthquake Spectra*, 35(4):1979-2001. DOI: 10.1193/100118EQS224DP

Rossi L., Stupazzini M., Parisi D., Holtschoppen B., Ruggieri G., Butenweg C. (2020) Empirical fragility functions and loss curves for Italian business facilities based on the 2012 Emilia-Romagna earthquake official database. *Bulletin of Earthquake Engineering*, 18:1693-1721. https://doi.org/10.1007/s10518-019-00759-1

Rota M., Penna A., Strobbia C., Magenes G. (2011) Typological seismic risk maps for Italy. *Earthquake Spectra,* 27(3):907-926. https://doi.org/10.1193/1.3609850

Rovida A., Locati M., Camassi R., Lolli B., Gasperini P. (2020) The Italian earthquake catalogue CPTI15. *Bulletin of Earthquake Engineering,* 18(7):2953-2984. https://doi.org/10.1007/s10518-020-00818-y

Rovida A., Locati M., Camassi R., Lolli, B., Gasperini P., Antonucci A. (2021) Catalogo Parametrico dei Terremoti Italiani (CPTI15), versione 3.0. Istituto Nazionale di Geofisica e Vulcanologia (INGV). https://doi.org/10.13127/CPTI/CPTI15.3

——— S ———

Savoia M., Mazzotti C., Buratti N., Ferracuti B., Bovo M., Ligabue V., Vincenzi L. (2012) Damages and collapses in industrial precast buildings after the Emilia earthquake (in Italian). *Ingegneria Sismica*, 29(2):120-131.

Savoia M., Buratti N., Vincenzi L. (2017) Damage and collapses in industrial precast buildings after the 2012 Emilia earthquake. *Engineering Structures,* 137:162-180. https://doi.org/10.1016/j.engst ruct.2017.01.059

Scotta R., De Stefani L., Vitaliani R. (2015) Passive control of precast building response using cladding panels as dissipative shear walls. *Bulletin of Earthquake Engineering*, 13:3527-3552. https://doi.org/10.1007/s10518-015-9763-9

SEAOC (1995). Vision 2000 Report: Performance Based Seismic Engineering of Buildings.

Shabani A., Kioumarsi M., Zucconi M. (2021) State of the art of simplified analytical methods for seismic vulnerability assessment of unreinforced masonry buildings. *Engineering Structures,* 239-112280. https://doi.org/10.1016/j.engstruct.2021.112280

Shinozuka M., Feng M.Q., Kim H., Uzawa T., Ueda T. (2000) Statistical analysis of fragility curves. *Journal of Engineering Mechanics*, 126(12):1224-1231. https://doi.org/10.1061/(ASCE)0733-9399(2000)126:12(1224)

Silva V., Crowley H., Pagani M., Monelli D., Pinho R. (2014) Development of the OpenQuake engine, the Global Earthquake Model's open-source software for seismic risk assessment. *Natural Hazards*, 72:1409–1427. DOI 10.1007/s11069-013-0618-x

Silva V., Akkar S., Baker J., Bazzurro P., Castro J.M., Crowley H., Dolsek M., Galasso C., Lagomarsino S., Monteiro R., Perrone D., Pitilakis K., Vamvatsikos D. (2019) Current challenges and future trends in analytical fragility and vulnerability modelling. *Earthquake Spectra*, 35(4):1927–1952. https://doi.org/10.1193/042418EQS101O

Silva V., Horspool N. (2019) Combining USGS ShakeMaps and the OpenQuake-engine for damage and loss assessment. *Earthquake Engineering Structural Dynamics*, 48:634–652. DOI:10.1002/eqe.3154

Silva V., Bazzurro P., Vamvatsikos D. (2021) Preface to the Special Issue: The evolution of fragility and vulnerability. The origin story of a preface. *Bulletin of Earthquake Engineering*, 19:6269-6270. https://doi.org/10.1007/s10518-021-01261-3

Song H-W., Wan Z-M., Xie Z-M., Du X-W. (2000) Axial impact behavior and energy absorption efficiency of composite wrapped metal tubes. *International Journal of Impact Engineering*, 24(4):385-401. https://doi.org/10.1016/S0734-743X(99)00165-7

Sorace S., Terenzi G., Fuso E. (2021) Local Retrofit of Reinforced Concrete Structures by the ACM System. *Buildings* 2021, 11,575:1-17. https://doi.org/10.3390/buildings11120575

Sousa R., Batalha N., Silva V., Rodrigues H. (2020) Seismic fragility functions for Portuguese RC precast buildings. *Bulletin of Earthquake Engineering*. https://doi.org/10.1007/s10518-020-01007-7

Soydan C., Yuksel E., Irtem E. (2020) Seismic performance improvement of single-storey precast reinforced concrete industrial buildings in use. *Soil Dynamics and Earthquake Engineering*, 135:106167. https://doi.org/10.1016/j.soildyn.2020.106167

Stucchi M., Meletti C., Montaldo V., Crowley H., Calvi G.M., Boschi E. (2011) Seismic hazard assessment (2003–2009) for the Italian building code. *Bulletin of the Seismological Society of America,* 101:1885–1911.

Sullivan T.J., Welch D.P., Calvi G.M. (2014) Simplified seismic performance assessment and implications for seismic design. *Earthquake Engineering and Engineering Vibration*, 13:95–122. https://doi.org/10.1007/s11803-014-0242-0

——— T ———

Takeda T., Sozen M.A., Nielsen N.N. (1970) Reinforced concrete response to simulated earthquake. *Journal of the structural division*, 96(12):2557-2573.

Tapan M., Comert M., Demir C., Sayan Y., Orakcal K., Ilki A. (2013) Failures of structures during the October 23, 2011 Tabanlı (Van) and November 9, 2011 Edremit (Van) earthquakes in Turkey. *Engineering Failure Analysis*, 34:606-628. DOI: 10.1016/j.engfailanal.2013.02.013

Titi A., Biondini F., Toniolo G. (2018) Seismic assessment of existing precast structures with dry-friction beam-to-column joints. *Bulletin of Earthquake Engineering*, 16:2067-2086. https://doi.org/10.1007/s10518-017-0271-y

Tocchi G., Polese M., Di Ludovico M., Prota A. (2021) Regional based exposure models to account for local building typologies. *Bulletin of Earthquake Engineering.* https://doi.org/10.1007/s10518-021-01242-6

Torquati M., Belleri A., Riva P. (2018) Displacement-Based Seismic Assessment for Precast Concrete Frames with Non-Emulative Connections. Journal of Earthquake Engineering, 24(10):1624-1651. https://doi.org/10.1080/13632469.2018.1475311

Tzenov L., Sotirov L., Boncheva P. (1978) Study of some damaged industrial buildings due to Vrancea earthquake. *Proceedings of the 6th European Conference on Earthquake Engineering*, Dubrovnik, Yugoslavia, 18-22 September.

——— V ———

Vamvatsikos D., Cornell CA. (2002) Incremental dynamic analysis. *Earthquake Engineering Structural Dynamics*, 31:491–514. https://doi.org/10.1002/eqe.141

Vamvatsikos D., Fragiadakis M. (2010) Incremental dynamic analysis for estimating seismic performance sensitivity and uncertainty. *Earthquake Engineering Structural Dynamics,* 39:141-63.

Verderame G.M., Ricci P., Manfredi G., Cosenza E. (2010) Ultimate chord rotation of RC columns with smooth bars: some considerations about EC8 prescriptions. *Bulletin of Earthquake Engineering*, 8:1351-1373. https://doi.org/10.1007/s10518-010-9190-x

Villar-Vega M., Silva V., Crowley H., Yepes C., Tarque N., Acevedo A.B., Hube M.A., Coronel G.D., Santa Maria H. (2017) Development of a fragility model for the residential building stock in South America. *Earthquake Spectra*, 33(2):581-604. https://doi.org/10.1193/010716EQS005M

———— Z ————

Zanini M.A., Hofer L., Pellegrino C. (2019) A framework for assessing the seismic risk map of Italy and developing a sustainable risk reduction program. *International Journal of Disaster Risk Reduction*, 33:74-93. https://doi.org/10.1016/j.ijdrr.2018.09.012

Zoubek B., Fischinger M., Isakovic T. (2016) Cyclic response of hammer-head strap cladding-to-structure connections used in RC precast building. *Engineering Structures*, 119:135-148.

Zuccaro G., Dolce M., De Gregorio D., Speranza E., Moroni C., (2015) La scheda CARTIS per la caratterizzazione tipologico- strutturale dei comparti urbani costituiti da edifici ordinari. Valutazione dell’esposizione in analisi di rischio sismico, in *Proceedings of GNGTS 2015* (in Italian).

———— W ————

Welch D.P., Sullivan T.J., Calvi G.M. (2014) Developing Direct Displacement-Based Procedures for Simplified Loss Assessment in Performance-Based Earthquake Engineering. *Journal of Earthquake Engineering*, 18(2):290-322. http://dx.doi.org/10.1080/13632469.2013.851046

RINGRAZIAMENTI

Prima di tutto vorrei esprimere la mia gratitudine verso il Prof. Savoia, che stimo molto, per avermi guidata in questo percorso, e per avermi sempre stimolata a condurre la mia ricerca con curiosità e spirito critico.

Ringrazio particolarmente Marco, per avermi sostenuta e per aver creduto in me fin dal principio, regalandomi tanti aiuti preziosi.
Ringrazio il Prof. Buratti per la sua presenza confortante, per avermi consigliato nei momenti di dubbio aiutandomi a sciogliere tanti nodi.

Ringrazio Andrea e Devis per la collaborazione nata in un periodo particolarmente complesso, per la condivisione di idee e gli insegnamenti che mi hanno trasmesso.

Un grande Grazie a tutti i ragazzi in dipartimento che mi hanno regalato dei momenti indimenticabili, in particolare ai miei compagni di ufficio. Un Grazie a Francesca che è stata per me un riferimento importante sin dall'inizio.
Grazie a Luca, che reputo un grande ingegnere, da cui ho imparato molto. Grazie al Prof Mazzotti per i tanti sorrisi che mi ha regalato, presenza incoraggiante e collante del gruppo.

Grazie a Said, Alessandro e Cristian, per aver condiviso il percorso insieme lasciandomi dei bellissimi ricordi, e a Cesare in particolare, per la compagnia e il sostegno nei nostri lunghi viaggi.
Grazie ad Anto e a Pedro, per aver vissuto insieme dei mesi davvero speciali.

Un grazie gigante è dedicato alla mia famiglia, che è sempre più allargata, e a cui voglio sempre più bene. Il sostegno che mi dà è difficile da descrivere.
Grazie a Tommy per essere con me, per starmi sempre vicino, con Ethan. Non avrei superato i momenti più difficili senza di lui, il mio Fantastic Mr. F.